MODELLING OF GRAIN BOUNDARY SEGREGATION, PRECIPITATION AND PRECIPITATE-FREE ZONES OF HIGH STRENGTH ALUMINIUM ALLOYS

by

Hong JIANG

A Doctoral Thesis

Submitted in partial fulfilment of the requirements for the award of

Doctor of Philosophy

of the

Loughborough University of Technology

March 1994

Acknowledgements

The work described in this thesis could not have been carried out without the help of others, whose support I gratefully acknowledge.

In particular, sincere thanks must go to my supervisor, Professor Roy Faulkner of Loughborough University for his help, advice and encouragement throughout the duration of this work.

Also I am deeply indebted to Mr John Bates, the Senior Laboratory Officer at IPTME for his advice, general instruction and guidance in the techniques for the experimental work and, thanks to Mr Shenghau Song, the Research Student at IPTME for his kindly assistance in the experimental work.

For financial support I am indebted to Loughborough University of Technology for their award of a Overseas Research Student Award and to Alcan International, Banbury Laboratory for their supplementation of a Research Studentship.

Abstract

Aluminium alloys of the 7000 series with their high strength to weight ratio characteristics have been considered as a excellent choice in airframe structure manufacturing. The commercial application of the alloys, however, may be restricted by their poor characteristics such as resistance to stress corrosion cracking which, it is reported, strongly depends on the grain boundary precipitation and the widths of precipitate-free zones. Both of these would be affected by segregation.

It is the main aim of the work described in this thesis to construct a combined model in which the kinetics of the segregation of the solute atoms, the nucleation of the grain boundary precipitates, the precipitate growth and coarsening are taken into account and the model gives the prediction of the state of the grain boundary and its environment as a function of heat treatment. A numerical approach is used to perform the combined analysis.

A combined model has been created which can give the prediction of the influence of the heat treatment on the widths of precipitate-free zones, the growth rate and the dispersions of the precipitates on the grain boundaries during the growth of the precipitates. It can also predict the critical time when the coarsening begins, and, the size and the dispersion of the precipitates on the grain boundaries changing with time during the coarsening.

$MgZn_2$ grain boundary precipitation and the widths of precipitate-free zones in 7150 aluminium alloy after being water quenched from solution treatment temperature to room temperature, then ageing at 160°C and 180°C, are predicted theoretically and measured experimentally. The results of the theoretical prediction are in good agreement with the experimental measurements.

The model predicts that the increase in the grain boundary precipitate size with increase in ageing time is growth kinetics controlled. The higher the ageing temperature is, the faster the growing rate. The growth rate is very sensitive to the mean collector plate area, and the volume diffusion coefficient of the solute in the matrix.

The collector plate area before the growth of the precipitates begins depends on the density of the precipitate nuclei at the grain boundaries. The mean collector plate area is very sensitive to T_{mp}, which is the temperature at which most segregation is considered completed, the concentration of Zn and Mg of the alloy, the temperature at which the nucleation takes place and the grain boundary structures. Within the temperature range of interest here, the higher the temperature and/or, the lower the concentrations of Zn and Mg and/or the smaller the grain boundary energy to the precipitate/matrix interface energy ratio, the fewer are the equilibrium precipitate nuclei and the bigger the mean collector plate area. The changing of the mean collector plate area with time during the growth is caused by the coalescence of the precipitates at the grain boundaries.

The widths of the precipitate-free zones is very sensitive to the quenching rate, the diffusion coefficient of the impurity-vacancy complexes and the ageing temperature. Within the temperature range of interest here, The widths of the precipitate-free zones increases with the increase in ageing temperature and decreases with increases in the ageing time.

The situation where both segregation and precipitation take place, the SCC susceptibility is mainly controlled by the inter-particle spacing of the grain boundary precipitates. The decrease in the inter-particle spacing of grain boundary precipitates promotes the propagation speed of SCC along the GBs, and this induces the decrease in the resistance to stress corrosion cracking.

The slower the quench rate and/or the longer the ageing time at an ageing temperature, T, where $T \geq T_{mp}$, the greater are the widths of both solute concentrated and depleted layers caused by non-equilibrium segregation and the bigger but the fewer incoherent precipitates (η phase). The white zones of welds of Al-Zn-Mg alloy satisfy the above condition. Under such condition, the segregation of magnesium and zinc makes these zones highly reactive and promotes the localised production and diffusion of hydrogen into these areas. Magnesium hydride formation takes place selectively on the incoherent interfaces of grain boundary precipitates and facilitates crack nucleation at these sites. Thus these areas become very sensitive to SCC.

Apart from this main work, successful strategies for effectively using the image analysis system in analysing TEM micrographs have been developed.

CONTENTS

List of symbols

a: lattice parameter of matrix phase

a_b: entropy term for the calculation of the grain-boundary diffusion coefficient of the solute element

a_c: entropy term for the calculation of the diffusion coefficient of the impurity-vacancy complexes

a_I: entropy term for the calculation of the volume diffusion coefficient of the solute atoms

a_s: entropy term for the calculation of the self-diffusion coefficient of the matrix atoms in matrix phase

A : parameter defined by $A = \frac{2}{3}(1 - \frac{\sigma_{\alpha\alpha}}{2\sigma_{\alpha\theta}})$

A_{m0}: mean collector plate area before the onset of the growth of the grain boundary precipitates

A_{mg}: mean collector plate area at the time of the onset of coarsening

A_{mi}: mean collector plate area during the period of time, $i\delta t \sim (i+1)\delta t$ $(1 \le i \le n)$, at the first stage ageing temperature, T, before the onset of coarsening

A_{mj}: mean collector plate area during the period of time, $j\delta t \sim (j+1)\delta t$ $(1 \le j \le n')$, at the second stage ageing temperature, T_2, before the onset of coarsening

$A_{mn'}$: mean collector plate area after ageing for time, t_2 (t_2=n'δt, n' is an integer), at the second stage ageing temperature, T_2, before the onset of coarsening

A_{mn}: mean collector plate area after ageing for time, t (t=nδt, n is an integer) , at the first stage ageing temperature, T, before the onset of coarsening

$A_m(t)$: mean collector plate area after ageing for time, t ($t \ge t_{cc}, t_{cc} = g\delta t$), at ageing temperature, T, after coarsening begins

A_v: area of a collector plate

B: parameter defined by $B = \frac{1}{2}\ln(\frac{1}{f})$

c: entropy-connected term of solute in the solubility product equation

C_b: maximum concentration of the impurity at the grain boundary caused by non-equilibrium segregation

C_c: concentration of the non-rate controlling element (in this case is Zn) participating in the precipitation reaction

C_g: concentration of the impurity in the matrix phase (in this case is Mg)

C'_{gbT}: true interfacial concentration of the impurity after time t at temperature, T, caused by equilibrium segregation

C^{∞}_{gbT}: stable interface concentration of the impurity caused by equilibrium segregation

C_I: concentration of impurities

$C_{I\text{-}v}$: concentration of impurity-vacancy complexes

C_v: concentration of vacancies

c(x,iδt): solute concentration given by newly generated numerical-analytical non-equilibrium segregation model for the position at a distance of x from the interface between the solute concentrated layer the grain interior after time, iδt ($1 \le i \le n$), at ageing temperature, T

c(x,t): solute concentration given by newly generated numerical-analytical non-equilibrium segregation model for the position at a distance of x from the interface between the solute concentrated layer the grain interior after time, t, at ageing temperature, T

$c(x,t_{eff})$: solute concentration given by Xu & Song's non-equilibrium segregation model for the position at a distance of x from the interface between the solute concentrated layer the grain interior after effective time, t_{eff}, at solution treatment temperature, T_i

$c(x,t^{j}_{eff''})$: solute concentration given by newly generated numerical-analytical non-equilibrium segregation model for the position at a distance of x from the interface between the solute concentrated layer the grain interior after effective time, $t^{j}_{eff''}$, at the first stage ageing treatment temperature, T

$c(x, t^{i}_{eff})$: solute concentration given by Xu & Song's non-equilibrium segregation model for the position at a distance of x from the interface between the solute concentrated layer the grain interior after effective time, t^{i}_{eff}, at solution treatment temperature, T_i

$c(x, t^{j}_{eff})$: solute concentration given by Xu & Song's non-equilibrium segregation model for the position at a distance of x from the interface between the solute concentrated layer the grain interior after effective time, t^{j}_{eff}, at solution treatment temperature, T_i

$c(y,i\Delta)$: concentration profile in the solute depleted layer given by newly generated numerical non-equilibrium segregation model for the period of effective time, $i\Delta \sim (i+1)\Delta \ (1 \le i \le l)$, at solution treatment temperature, T_i

$c(y,l'\cdot\Delta)$: concentration profile in the solute depleted layer given by newly generated numerical non-equilibrium segregation model for the period of effective time, $l'\Delta \sim (l'+1)\Delta \quad (l' = t^{i}_{eff}/\Delta)$, at solution treatment temperature, T_i

$c(y,l''\cdot\Delta)$: concentration profile in the solute depleted layer given by newly generated numerical non-equilibrium segregation model for the period of effective time, $l''\Delta \sim (l''+1)\Delta \quad (l' = t^{j}_{eff}/\Delta)$, at solution treatment temperature, T_i

$C(y,i\bullet\Delta)$: solute concentration given by newly generated numerical non-equilibrium segregation model for the position at a distance of y from grain boundary (where y=0) outwards into the interior grain during the

period of effective time, $i\Delta \sim (i+1)\Delta$ $(1 \le i \le l)$, at solution treatment temperature, T_i

$C(y,t_{eff})$: solute concentration given by Faulkner's non-equilibrium segregation model for the position at a distance of y from grain boundary (where y=0) outwards into the interior grain after affective time, t_{eff}, at solution treatment temperature, T_i

$C(y, t^i_{eff})$: solute concentration given by Faulkner's non-equilibrium segregation model for the position at a distance of y from grain boundary (where y=0) outwards into the interior grain after affective time, t^i_{eff}, at solution treatment temperature, T_i

$C(y,t^j_{eff})$: solute concentration given by Faulkner's non-equilibrium segregation model for the position at a distance of y from grain boundary (where y=0) outwards into the interior grain after affective time, t^j_{eff}, at solution treatment temperature, T_i

$C_b(t_{eff})$: solute concentration at the solute concentrated layer given by Xu & Song's non-equilibrium segregation model after affective time, t_{eff}, at solution treatment temperature, T_i

$C_b(t^i_{eff})$: solute concentration at the solute concentrated layer given by Xu & Song's non-equilibrium segregation model after affective time, t^i_{eff}, at solution treatment temperature, T_i

$C_b(t^j_{eff})$: solute concentration at the solute concentrated layer after effective time, t^j_{eff}, at solution treatment temperature, T_i, given by Xu & Song's segregation model

$C_b(t_q)$: segregation concentration in the solute concentrated layer after quenching from solution treatment temperature given by Xu & Song's segregation model

d: mean diameter of the grains, d=5000 nm

d_0: width of grain boundary within which the solute diffusion is grain boundary diffusion controlling, d_0=0.1 nm

d_1: width of the layer where solute is highly concentrated by equilibrium segregation, d_1=0.25 nm

d_2: width of solute concentrated layer given by Xu & Song's non-equilibrium segregation model, d_2=1.0 nm

dh: a distance interval

dL: increase in the precipitate size during the period of time, $i\delta t \sim (i+1)\delta t$ $(1 \leq i \leq n)$, at a given temperature, T

d_v: side length of the constant square collector plate, or, inter-particle spacing of the grain boundary precipitates

D_b: grain boundary diffusion coefficient of the solute atoms at temperature, T

D_{bnuc}: grain boundary diffusion coefficient of the solute atoms at temperature, T_{nuc}

D_c: diffusion coefficient of the vacancy-impurity complexes at temperature, T

D_{ci}: diffusion coefficient of the vacancy-impurity complexes at solution treatment temperature, T_i

D_I: volume diffusion coefficient of the solute atoms at ageing temperature, T

D_{I2}: volume diffusion coefficient of the solute atoms at the second stage ageing temperature, T_2

D_{Ii}: volume diffusion coefficient of the solute atoms at solution treatment temperature, T_i

$D_{\alpha\theta}$: diffusion coefficient of the solute atoms moving along the precipitate/matrix interface

E_{b1}: impurity-grain boundary binding energy

E_b: vacancy-impurity binding energy

E_f: energy needed to form a vacancy

f : fraction of the grain boundary covered with precipitates

$f(\psi)$: morphological factor

g: an integer given by $g = t_{cc}/\delta t$

i: an integer, $1 \le i \le n$

j: an integer, $1 \le j \le n'$

k: Boltzmann's constant

$k_{I\text{-}v}$: a geometrical constant for the calculation of the concentration of impurity-vacancy complexes

k_v: a geometrical constant for the calculation of the concentration of vacancies

k': constant aspect ratio

l: an integer given by $l = t_{eff}/\Delta$

l': an integer given by $l' = t^i_{eff}/\Delta$

l'': an integer given by $l'' = t^j_{eff}/\Delta$

l_q: an integer given by $l_q = t_q/\Delta$

L: precipitate half length

L_g: mean radius of the grain boundary precipitates at the critical time when coarsening begins

L_i: mean radius of the precipitates during the period of time $i\delta t \sim (i+1)\delta t$ $(1 \le i \le n)$ at the first stage ageing before the onset of coarsening

L_j: mean radius of the precipitates during the period of time $j\delta t \sim (j+1)\delta t$ $(1 \le j \le n')$ at the second stage ageing before the onset of coarsening

$L_{n'}$: mean radius of the precipitate after ageing for a time of t_2 (t_2=n'δt, n' is an integer) at the second stage ageing temperature T_2 before the onset of coarsening

L_n: mean radius of the precipitate after ageing for a time of t (t=nδt, n is an integer) at first stage ageing temperature, T, before the onset of coarsening

L(t): mean radius of the grain boundary precipitate after ageing for a time of t after coarsening begins

n: an integer given by $n = \frac{t}{\delta t}$

n' an integer given by $n' = \frac{t_2}{\delta t}$

n'': an integer given by $n'' = \frac{t_{eff}^{n'}}{\Delta}$

n_0: distribution probability density function of the number of the precipitate nuclei, or, the number of the collector plates as the function of the size of collector plates before the onset of the growth

n_i: distribution density function of the number of the precipitates, or, the collector plates as the function of the size of collector plates during the period of time $i\delta t \sim (i+1)\delta t$ $(1 \le i \le n)$ at the first stage ageing before the onset of coarsening

n_j: distribution density function of the number of the precipitates, or, the collector plates as the function of the size of collector plates during the period of time $j\delta t \sim (j+1)\delta t$ $(1 \le j \le n')$ at the second stage ageing before the onset of coarsening

$n_{n'}$: distribution density function of the number of the precipitates, or, the collector plates as the function of the size of collector plates after ageing for a time of t_2 ($t_2 = n\delta t$, n' is an integer) at the second stage ageing temperature, T_2, before the onset of coarsening

n_n: distribution density function of the number of the precipitates, or, the collector plates as the function of the size of collector plates after ageing for a time of t ($t = n\delta t$, n is an integer) at first stage ageing temperature, T, before the onset of coarsening

N: number of atoms per unit area of grain boundary

N_A: Avogadro's constant

N_0: number of critical precipitate nuclei per unit area of grain boundary before the onset of the growth

N_s: number of the precipitates at the time of onset of coarsening

N_i: number of the precipitates in a unit area of a grain boundary during the period of time $i\delta t \sim (i+1)\delta t$ $(1 \le i \le n)$ before the onset of coarsening

N_j: number of the precipitates in a unit area of a grain boundary during the period of time $j\delta t \sim (j+1)\delta t$ $(1 \le j \le n')$ at the second stage ageing before the onset of coarsening

$N_{n'}$: number of the precipitates in a unit area of a grain boundary after ageing for a time of t_2 ($t_2=n'\delta t$, n' is an integer) at the second stage ageing temperature T_2 before the onset of coarsening

N_n: number of the precipitates in a unit area of a grain boundary after ageing for a time of t ($t=n\delta t$, n is an integer) at first stage ageing temperature, T, before the onset of coarsening

N_v: total number of atoms per unit volume

N_{v0}: number of critical precipitate nuclei per unit volume

N(t): number of the precipitates at the grain boundary after coarsening begins and after ageing for a time t ($t \ge t_{cc}, t_{cc} = g\delta t$) at ageing temperature

$N_{A_{min}}^{4L_n^2}$: number of the collector plates whose areas are smaller than $4L_n^2$

p: an integer, $1 \le p \le p'$

p': an integer given by $P' = \frac{10000}{\theta} \ln \frac{T_i - T_0}{T_{mp} - T_0}$

Q_b: activation energy term for the calculation of the grain-boundary diffusion coefficient of the solute atoms

Q_c: activation energy term for the calculation of the diffusion coefficient of the impurity-vacancy complexes

Q_I: activation energy term for the calculation of the volume diffusion coefficient of the solute atoms

Q_s: activation energy term for the calculation of the self-diffusion coefficient of the matrix atoms in matrix phase

r: radius of the curvature of a precipitate at the advancing interface

r_{nuc}: radius of curvature of a precipitate nucleus at the advancing interface

R: gas constant

s: true thickness of a precipitate

s(ψ): morphological factor which depends on the shape of the grain boundary precipitate nuclei

$\bar{s}$: thickness-connected term of the precipitate

S: the amount of diffusional component

S_0: unit area

t ageing time at the first stage ageing temperature, T

t_2: ageing time at the second stage ageing temperature, T_2

t_a: effective ageing time at solution treatment temperature, T_i (for the diffusion of the impurity-vacancy complexes)

t_c: effective critical time at solution treatment temperature, T_i, when the process switches from segregation to de-segregation

t_{cc}: critical time for the onset of coarsening, $t_{cc} = g\delta t$

t_{eff}: the effective time which is the sum of effective quenching time, t_q, and effective ageing time, t_a (for the diffusion of the impurity-vacancy complexes)

t^j_{eff}: effective time at the first stage temperature for sample aged for time, t, at the first stage ageing temperature, T, and then for time, $t = j\delta t$, at the second stage ageing temperature, T_2 (for the diffusion of the impurity atoms)

$t^j_{eff''}$: effective time at the first stage temperature for sample aged for time, t, at the first stage ageing temperature, T, and then for time, $t = j\delta t$, at the second stage ageing temperature, T_2 (for the diffusion of the impurity-vacancy complexes)

t^i_{eff}: the effective time at solution treatment temperature for the sample quenched from solution treatment temperature and then aged at the first ageing temperature, T, for time, $t = i\delta t$ (for the diffusion of the impurity-vacancy complexes)

t_{eff}^{j}: the effective time at solution treatment temperature for the sample quenched from solution treatment temperature and then aged at the first ageing temperature, T, for time, t, and at the second stage ageing temperature, T_2, for time, $t = j\delta t$ (for the diffusion of the impurity-vacancy complexes)

$t_{eff}^{n'}$: the effective time at solution treatment temperature for the sample quenched from solution treatment temperature and then aged at the first ageing temperature, T, for time, t, and at the second stage ageing temperature, T_2, for time, t_2 (for the diffusion of the impurity-vacancy complexes)

$t_{eff''}^{n'}$: effective time at the first stage temperature for sample aged for time, t, at the first stage ageing temperature, T, and then for time, $t = n'\delta t$, at the second stage ageing temperature, T_2 (for the diffusion of the impurity-vacancy complexes)

t_q: effective quenching time (for the diffusion of the impurity-vacancy complexes)

t_q^p: effective time at the solution treatment temperature for the time interval staying at the temperature, T_p (for the diffusion of the impurity-vacancy complexes)

T: the first stage ageing treatment temperature

T_0: temperature of quenching media

T_2: the second stage ageing treatment temperature

T_i: solution treatment temperature

T_m: melting temperature of the alloy

T_{mp}: the temperature at which most segregation will have been completed, $T_{mp} = 0.6T_m$

T_{nuc}: temperature of the environment where nucleation takes place

T_p: temperature given by $T_p = (T_i - T_0)\exp(0.0001 \cdot p \cdot \theta) + T_0$

T_s: solvus temperature of η' phase, T_s=250°C

V: half volume of the a precipitate particle

V_θ: molar volume of the precipitate phase

w_0: width of the solute concentrated layer given by newly generated numerical non-equilibrium segregation model for the time after quenching and before the onset of the growth of the precipitates; in this layer the solute concentration is C_b

w_{0i}: width of the solute concentrated layer given by newly generated numerical non-equilibrium segregation model for the period of effective time, $i\Delta \sim (i+1)\Delta \ (1 \le i \le l)$, at solution treatment temperature, T_i; in this layer the solute concentration is C_b

$w_{0l'}$: width of the solute concentrated layer given by newly generated numerical non-equilibrium segregation model for the period of effective time, $l'\Delta \sim (l'+1)\Delta$ where $l' = t^i_{eff}/\Delta$, at solution treatment temperature, T_i; in this layer the solute concentration is C_b

$w_{0l''}$: width of the solute concentrated layer given by newly generated numerical non-equilibrium segregation model for the period of effective time, $l''\Delta \sim (l''+1)\Delta (l' = t^j_{eff}/\Delta)$, at solution treatment temperature, T_i; in this layer the solute concentration is C_b

w: width of the solute depleted layer given by newly generated numerical non-equilibrium segregation model for the time after quenching and before the onset of the growth of the precipitates

w_i: width of the solute depleted layer given by newly generated numerical non-equilibrium segregation model for the period of effective time, $i\Delta \sim (i+1)\Delta \ (1 \le i \le l)$, at solution treatment temperature, T_i

w_{pfz}: mean width of the precipitate free zones

x: distance from x=0 which is the interface between the grain interior and the solute concentrated layer into the grain interior

x_b: solute (in this is magnesium) concentration at the grain boundary

x_α: solute (in this case is magnesium) concentration in the matrix phase

$x_{\alpha i}$: solute (in this is magnesium) concentration in the vicinity of the grain boundary during the period of time, $i\delta t \sim (i+1)\delta t$ $(1 \le i \le n)$ at the first stage ageing temperature, T

$x_{\alpha j}$: solute (in this is magnesium) concentration in the vicinity of the grain boundary during the period of time, $j\delta t \sim (j+1)\delta t$ $(1 \le j \le n')$ at the second stage ageing temperature, T_2

$x_{\alpha T}^{\alpha\theta}$: solute (in this is magnesium) concentration in equilibrium with the precipitate phase and matrix at temperature, T

$x_{\alpha T_{nuc}}^{\alpha\theta}$: solute (in this is magnesium) concentration in equilibrium with the nucleated precipitate phase and matrix at temperature, T_{nuc}

x_θ: solute (in this is magnesium) concentration in precipitate phase

x_E: number of moles of the other non-rate controlling element (in this case is Zn) participating in the precipitation reaction

X(y,t): composition of the solute at the position at a distance of y from grain boundary outwards into the grain after ageing time, t, at ageing temperature, T

y: distance from the grain boundary, where y=0, into the grain interior

α: a constant, $\alpha = \frac{C_{gbT}^{\bullet\bullet}}{C_g}$

β: average fraction of L which a solute atom diffuses along the α:θ boundary before it joins the θ particle

δ: thickness of the α:θ boundary

δl: diffusion distance of the solute in the matrix within time, $t' = i\delta t$

δt: time interval

Δ: effective time interval

ΔG_v: driving force for the formation of a nucleus of the precipitate phase

ΔG_v^*: Gibbs free energy of critical nucleus formation

ΔH: enthalpy term of solute in the solubility product equation

ΔN_n: number of the precipitates vanished because of coalescence after ageing for a time of t (t=nδt, n is an integer) at ageing temperature, T

γ: a constant given by $\gamma = C_b^{max}/C_g$

θ: the cooling rate parameter

ρ_α: molar density of matrix phase

ρ_θ: molar density of precipitate phase

σ: standard deviation of distribution density function of the grain boundary precipitate nuclei, or, collector plates

$\sigma_{\alpha\alpha}$: grain boundary energy

$\sigma_{\alpha\theta}$: matrix/nucleus interfacial energy

τ: incubation time of the nucleation at temperature T_{nuc}

Ω: molar volume of the matrix phase

ψ: the angle where $\cos\psi = \sigma_{\alpha\alpha}/2\sigma_{\alpha\theta}$

ς: numerical factor

Chapter One

Introduction

1.1 *Development of high strength heat treatable aluminium alloys*

In little more than a century, aluminium has grown from virtually a chemical curiosity to be the world's second most commonly used metal. Aluminium and aluminium alloys have been widely used for a multitude of purposes from thin foil for wrapping to highly technological applications in aeronautics, space exploration and electronics.

Pure aluminium is soft and ductile with a tensile strength of about 46 MPa[1]. It is not suitable for structural engineering applications and in the exploitation of its light weight, the mechanical properties especially the strength have to be improved. The transformation of soft aluminium to be a high strength material can be realised by a lot of metallurgical methods such as: cold working, alloying or a specific method called precipitation hardening. Precipitation hardening is a very important process found by Wilm in Al-Cu alloys during the years 1906-1909[2,3]. Since then, a lot of aluminium alloys have been developed. As a result, many kinds of aluminium alloys are available for many applications.

Aluminium alloys have been produced as castings or wrought forms or by powder metallurgical processes. The standard reference for wrought forms is given by the International Alloy Designation System (IADS) which uses the 4 digits system to distinguish the types of alloys. The first digit in the designation indicates the major alloying element in that group. The second digit indicates a close relationship of the alloys within the same group differing only slightly in composition. The third and the fourth digits are a serial number. The designations for wrought aluminium alloys with the major alloying elements are as follows[3]:

alloy type	2xxx	3xxx	4xxx	5xxx	6xxx	7xxx	8xxx
main alloying element	Cu	Mn	Si	Mg	Si & Mg	Zn	others

In certain alloys, the required properties can be obtain by controlling the process of heat treatment or by a combination of strain hardening and heat treatment. The temper properties of alloys are indicated by a system of letters and digits, assigned by the Aluminium Association. Temper designation for heat treatable alloys is outlined in Table 1.1.1[3].

Table 1.1.1: Temper designation for heat treatable alloys.

T1	cooled from an elevated temperature shaping process and naturally aged to a substantially stable condition
T2	cooled from an elevated temperature shaping process, cold worked, and naturally aged to a substantially stable condition
T3	solution heat treated, cold worked, and naturally aged to a substantially stable condition
T4	solution heat treated and naturally aged to a substantially stable condition
T5	cooled from an elevated temperature shaping process and then artificially aged
T6	solution heat treated and then artificially aged
T7	solution heat treated and stabilised
T8	solution heat treated, cold worked, and then artificially aged
T9	solution heat treated, artificially aged and then cold worked
T10	cooled from an elevated temperature shaping process, cold worked and then artificially aged
T73	solution heat treated and then artificially aged in two stages
T76	solution heat treated and then artificially aged in two stages (different from T73)
T51	stress relieved by controlled stretching. This applies directly to plate.
T510	stress relieved by controlled stretching. This applies directly to extrusions that receive no further straightening after stretching
T511	stress relieved by controlled stretching. This applies directly to extrusions that may receive minor straightening after stretching to comply with tolerances
T351	solution heat treated, cold worked, controlled stretched and naturally aged
T651	solution heat treated, cold worked, controlled stretched, and artificially aged
T7351	solution heat treated, controlled stretched and artificially aged in two stages to provide optimum stress corrosion resistance, but with 10-15% lower tensile properties than T6
T7651	solution heat treated, controlled stretched and artificially aged in two stages to provide optimum exfoliation corrosion resistance, but with about 10% lower properties than T6
T52	stressed by compressing
T54	stress relieved by combined stretching and compressing
T42	test specimens solution heat treated from the O (annealed, soft) or F (as manufactured) temper, and naturally aged to a substantially stable condition by supplier to demonstrate response to heat treatment
T62	test specimens solution heat treated from the O (annealed, soft) or F (as manufactured) temper, and artificially aged by supplier to demonstrate response to heat treatment

High strength heat treatable aluminium alloys have been the materials of choice for aircraft structures since the beginning of the aircraft industry. Their development was almost simultaneous with the development of the aircraft industry as it stimulated the need for aluminium alloys with improved performance. Aluminium alloys with the highest possible strength to weight ratio were specified. However, they also needed to meet other specifications of the economic, corrosion resistance, and damage tolerance type. These factors have been key influences on the development of the higher strength alloys.

The earliest use of aluminium alloys in aircraft structures in the 1920s and '30s, was Al-Cu-Mg 2xxx series alloys 2017-T4 and 2024-T3, which had strengths among the highest known at that time[4,5]. As aircraft design progressed, and increased aircraft performance was sought, the need for materials with higher strength also increased. This need spurred further research in developing stronger aluminium alloys.

In the 1940s, researchers discovered that aluminium alloys containing Zn and Mg could develop substantially higher strengths than the 2xxx series alloys. This discovery led to the development of Al-Zn-Mg-Cu 7075-T6 alloy which was first used for the B-299 bomber[4,5].

After World War II, even higher-strength 7xxx series alloys were sought for introduction in commercial transport aeroplanes. This resulted in the 7178-T651 aluminium alloy which was used in the Boeing 707 and 737 aircraft. The approach used in developing this alloy was to evaluate higher levels of Zn, Mg, and Cu than those used in the aluminium alloy 7075. However, the higher strength of this alloy was accompanied by reduced fracture toughness levels and, during the development of the Boeing 747 aircraft, the lower-strength 7075-T651 alloy was specified because of damage tolerance considerations. Another concern which accompanied these high-strength 7xxx series alloys was corrosion resistance, especially in the

peak-aged condition. This led to the development of the T7651 temper for the improved corrosion resistance required by some aircraft manufacturers. However, this corrosion resistance improvement was achieved at some expense of strength. This particular alloy and temper, 7075-T7651, was first used in the Lockheed L1011 aeroplane. For many years, these alloys were the materials of choice for upper wing structures. The development of the Boeing 757/767 aircraft stimulated the need for an aluminium alloy with improved performance over these alloys. Through compositional modifications of 7050 aluminium alloy, which was developed for thick section applications, the 7150-T651 alloy was introduced. This alloy possessed strength which was comparable to the 7178-T651 alloy but had acceptable levels of fracture toughness. The T6151 temper was developed to provide a slightly higher degree of corrosion resistance than 7150-T651 at the same strength level. This temper was used on the airbus A310 and the McDonnel Douglas MD-11 aircraft for the upper wing structure[4,5].

The development of Al-Li alloys and the rapid-solidification processing is a subject of recent research because they offer the prospect of significant weight savings and better corrosion resistance. However, much work remains to be done to optimise composition and processing so as to improve properties such as fracture toughness. Short-term needs, can be met by improved versions of traditional, ingot-based 2xxx- and 7xxx-series alloys. The advances resulting from this approach can provide more cost-effective solutions to the challenges posed by enhanced performance requirements[4,5].

The bulk of research has been on the ways and means to develop the 7xxx series aluminium alloys that combine higher strength/weight ratio and higher stress corrosion cracking (SCC) resistance. Two different approaches have been taken towards this objective. One is called Final Thermo-mechanical Treatment (FTMT), which employs deformation and ageing[6,7]. The other is called Retrogression and

Reageing (RRA), which involves starting with a T6 temper and then ageing at an intermediate temperature (200-260°C) for a few seconds to a few minutes and subsequently an isothermal T6 ageing treatment[8,9]. FIMT is based on the theory that dislocation strengthening could make up for the strength lost while overageing to obtain a more corrosion-resistant microstructure. For RRA, the intermediate temperature step initially results in a decrease in strength due to retrogression of the strengthening precipitates. When a subsequent T6 treatment applies (re-ageing), the microstructure achieves a favourable combination of strength and corrosion resistance. The mechanism for achieving this result has not been understood. Neither the FTMT nor RRA concept has been used in commercial production[4,5]. Even though the susceptibility to stress corrosion cracking is under control for the alloys now being produced, the full capability of the alloys is not yet exploited. Until complete understanding of the process of stress corrosion is obtained, the battle is not won.

Table 1.1.2: The tensile strength, the resistance to stress-corrosion cracking of selected heat treatable aluminium alloys[4,5].

alloy series	alloy type	condition	tensile yield strength MPa	resistance to SCC rating		
				high	mod.	low
2xxx	2017	T4	275			x
	2024	T3	345			x
7xxx	7075	T6	460-505			x
	7075	T651	460			x
	7178	T651	540			x
	7178	T7651	505		x	
	7150	T651	570			x
	7150	T6151, T7751	570		x	

1.2 *7xxx aluminium alloys*

The Al-Zn-Mg system (7xxx series) offers the greatest potential of all aluminium alloys for ageing hardening[10]. In the alloys of this series, zinc and magnesium control the ageing process and develop the strength potential, especially in the range of 3 to 7.5% zinc. Zinc and magnesium form metastable $MgZn_2$ precipitates at temperatures below 250°C[11] which responds considerably to heat treatment. The addition of magnesium in excess (100 and 200%) of that required to form $MgZn_2$ further increases tensile strength. On the negative side, increasing additions of both zinc and magnesium decreases the overall corrosion resistance of aluminium[12].

The very high strength alloys of this series always contain quaternary additions of copper to improve their resistance to stress corrosion cracking[10]. The addition of copper together with small but important amounts of chromium and manganese, results in the highest strength aluminium-based alloys commercially available. The effect of copper is to increase the ageing rate by increasing the degree of supersaturation and perhaps through nucleation of $CuMgAl_2$ phase. Copper also increases quenching sensitivity upon heat treatment. In general, copper reduces the resistance to general corrosion of aluminium-zinc-magnesium alloys, but increases the resistance to stress corrosion cracking. Copper catalyses hydride formation and is expected to make cracking worse in the early stages of ageing. But copper also promotes grain boundary precipitation and bubble formation so hydrogen discharge is achieved sooner which enables high resistance to be developed at higher strength levels compared to copper-free alloys. The minor alloy additions, such as chromium and zirconium, have effects on mechanical properties and corrosion resistance. Zirconium additions in the range 0.1 to 0.3% are used to form a fine precipitate of intermetallic particle that inhibits recovery or recrystallization. Zirconium also improves weldability[12].

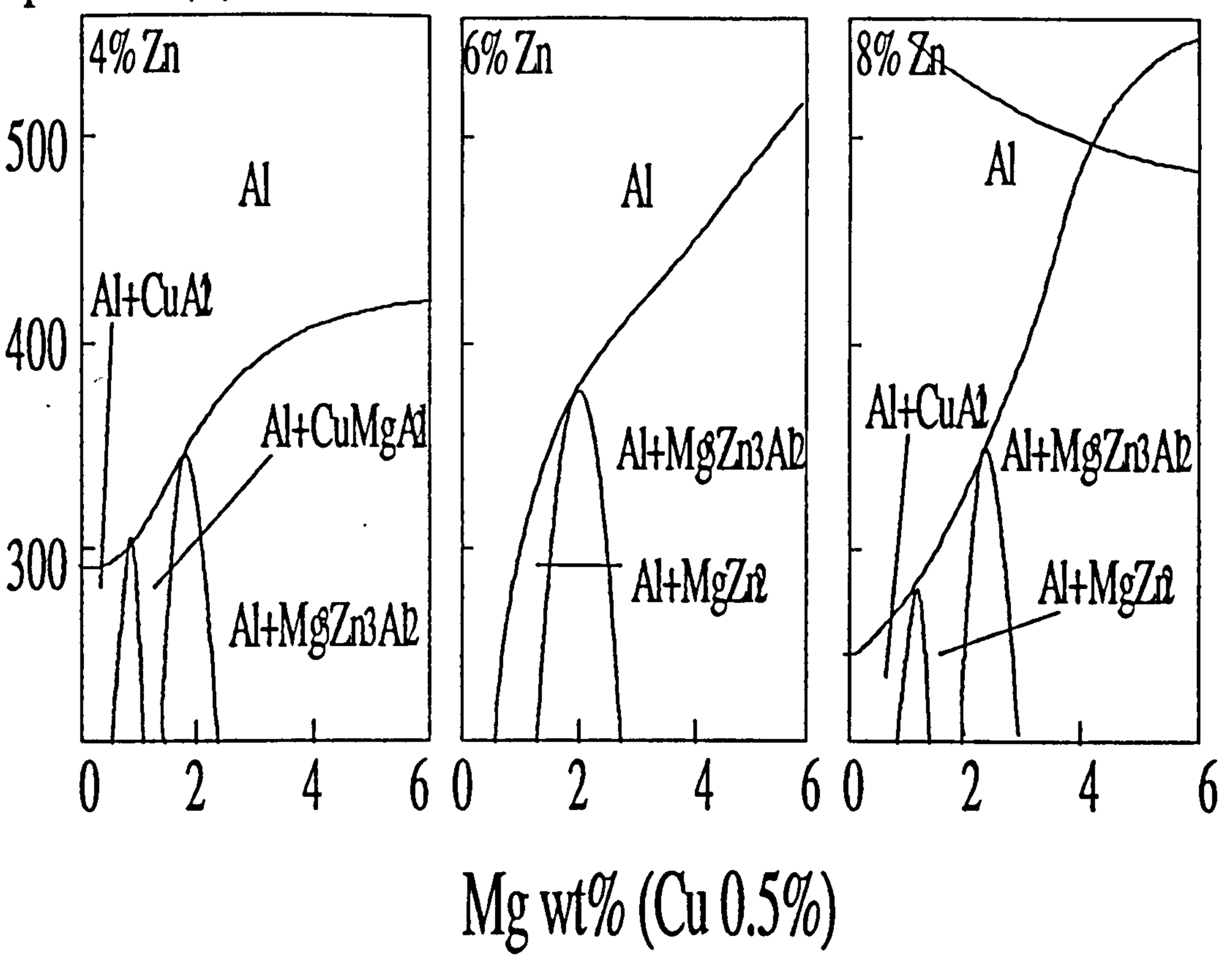

Fig 1.2.1. Sections at 4,6,8% zinc and 0.5% and 1% copper[13].

The typical heat treatment process for 7xxx alloys includes solution treatment, quenching and artificial ageing at one, or more than one, intermediate temperatures, with solution treatment at a relatively high temperature within the single phase region to dissolve the alloying elements; rapid cooling or quenching, usually to a lower temperature to obtain a supersaturated solid solution (SSS) of these elements in aluminium; artificial ageing to control the decomposition of SSS to form finely dispersed precipitates.

Strength and stress corrosion cracking susceptibility of 7xxx alloys are related to the precipitation reactions accompanying heat treatment which normally involves:

(i) Solution treatment at a relatively high temperature within the single phase region to dissolve the alloying elements.

(ii) Rapid cooling or quenching, usually to room temperature, to obtain a supersaturated solid solution (SSS) of these elements in aluminium.

(iii) cold work and controlled stretching to relieve stress.

(iv) Controlled decomposition of SSS to form a finely dispersed precipitate, usually by ageing for convenient times at one and sometimes a few intermediate temperatures.

Generally precipitation occurs in the following sequence:

$$SSS \Rightarrow \text{guinier preston(GP) zones} \Rightarrow \eta' (MgZn_2) \Rightarrow \eta (MgZn_2)$$

at temperatures below 190C°;

and

$$SSS \Rightarrow \text{GP zones} \Rightarrow \eta'(MgZn_2) \Rightarrow \eta (MgZn_2), T [(Al,Zn)_{49}Mg_{32}]$$

at temperature above 190C°.

In terms of stability,

$$T > \eta > \eta' > \text{GP zones}$$

The addition of copper promotes the development of η' from GP zones and stabilises both the η' and η phases[14].

A summary of the precipitates and their characteristics is given in Table 1.2.1[11]

Table 1.2.1: Characteristics of the precipitates.

	GP zones	η'	η	T
stoichiometry	-	$MgZn_2$	$MgZn_2$	$(Al,Zn)_{49}Mg_{32}$
shape	spherical	platelets	rods, plates	irregular
structure	alternate layers of Mg, Zn on (100)	HCP a=4.996A° c=8.68A°	HCP a=5.21A° c=8.60A°	BCC a=14.16A°
coherency	yes	semi	no	no
stability	metastable	metastable	pseudostable	equilibrium
size	35A°	200-A° long 50-A° wide	500A°	-
transition temp. (C)	120-150	120	200-250	190
solvus temp.(C)	150	250	370	190

The strength of the alloys is controlled by the interaction of moving dislocations with precipitates. A structure with a matrix of fine coherent GP zones, some η' particles and closely spaced grain boundary η precipitates is responsible for a high strength and poor resistance to stress corrosion cracking. Nevertheless, a structure with a matrix of incoherent η, η' and a coarse distribution of GP zones and a lower density of larger size grain boundary precipitates is responsible for a poor strength and good resistance to SCC[6,11,15-22].

Improvements in resistance to stress corrosion cracking have come through control of both composition and heat treatment procedures. With respect to composition, it is well known that both tensile strength and susceptibility to cracking increase as the

Zn+Mg content is raised and it is necessary to seek a compromise when selecting an alloy for a particular application. It is generally accepted that Zn+Mg content should be less than 6% in order for a weldable alloy to have a satisfactory resistance to cracking[10]. Zn/Mg ratio is also important and there is experimental evidence which suggests that maximum resistance to stress-corrosion cracking occurs if this ratio is between 2.7 to 2.9[23]. Although alloys containing little or no copper have the advantage of being readily weldable, small amounts of copper and, more particularly, silver have been shown to increase resistance to SCC[10,24].

Two changes in heat treatment procedures have led to a marked reduction in susceptibility to SCC in weldable alloys. One has been the use of slower quench rates, e.g. air-cooling, from solution treatment temperature which both minimises residual stresses and decreases differences in electrode potentials throughout the microstructure[10].

1.3 *7150 aluminium alloy*

The material used in the work described in this thesis is 7150 aluminium alloy.

7150 aluminium alloys was developed in the 1980's through compositional modifications of 7050 aluminium alloy, which was developed for thick section applications. This alloy possesses strength which is comparable to the 7178-T651 alloy but has acceptable levels of fracture toughness. However, like other 7xxx-series alloys this alloy has poor resistance to stress corrosion cracking especially in the peak-aged condition.

The composition of 7150 aluminium alloy consists essentially of 5.9 - 6.9wt% zinc, 2.0 -2.7wt% magnesium, 1.9 - 2.5wt% copper, 0.08 -0.15wt% zirconium, and the

balance of aluminium and trace elements. Of the trace elements present, the maximum wt% of iron allowable is 0.15%, of silicon allowable is 0.12%, of manganese allowable is 0.10%, of chromium allowable is 0.04%, and of titanium allowable is 0.06%. Any other remaining trace elements have maximum limits of 0.05%[25].

Fig. 1.3.1 shows the comparison of the properties of 7150 with other 7xxx series alloys[25].

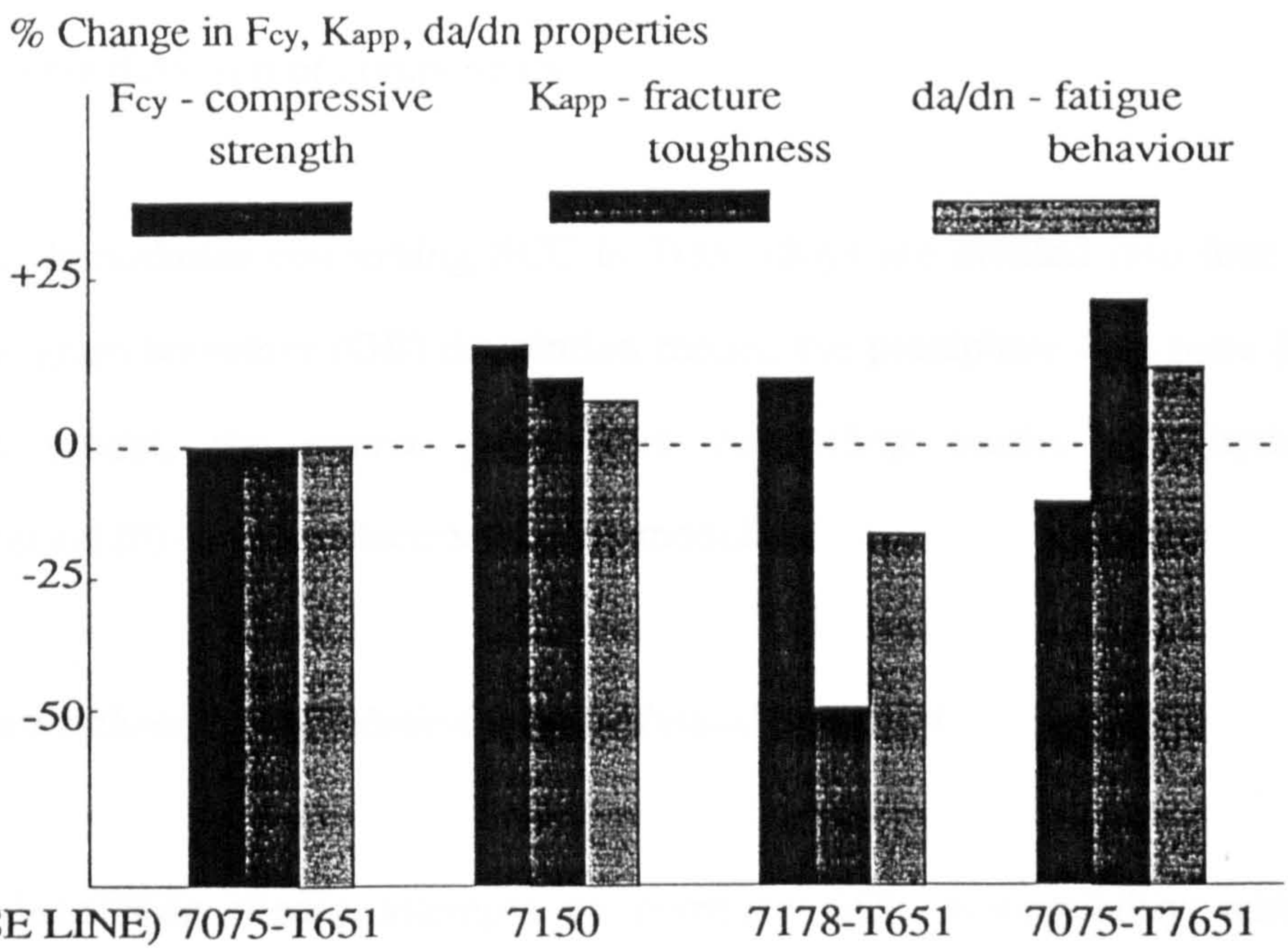

Fig. 1.3.1.The comparison of the properties of 7150 with other 7xxx series alloys.

1.4 *The nature of stress corrosion cracking*

Stress corrosion cracking is known as a material failure, induced suddenly by the simultaneous effects of mechanical and chemical surface attack. It is characterised by the sudden occurrence of failure following previous microcrack formation and propagation without any evidence of corrosion attack. Hence the failure time for

SCC is composed of crack incubation, formation, and propagation periods which run either successively or simultaneously. During the first period, chemical and /or electrochemical processes take place under the influence of chemical attack alone. The second period, crack formation, and the third, crack propagation, periods are mainly associated with physical processes under combined chemical and mechanical action. Either the first and second period together or the third period can be rate controlling in the total SCC process[26]. SCC in aluminium alloys always takes place along grain boundaries and maximum susceptibility occurs in the recrystallized condition and the condition if stressing is normal to the grain direction, i.e. in the short transverse direction of components.

The various hypotheses concerning SCC in 7xxx alloys are divided into four main groups: the grain boundary (GB) dissolution model, the precipitate-free zone (PFZ) dissolution model, the matrix precipitates controlling model and hydrogen embrittlement (HE)-assisted electrochemical model[26].

1.4.1 *Electrochemical dissolution of grain boundary model*

The GB dissolution theory attempts to correlate SCC susceptibility with the microstructure (the inter-particle spacing between GB ppts). According to this theory, stress corrosion cracks form due to the electrochemical dissolution of anodic grain boundary precipitates (ppts) and then propagate along the GB due to the presence of stress concentrations at GBs[27,28]. Stress crack propagation is discontinuous. This indicates that crack propagation between anodic ppts at GBs is brittle in nature and thus takes place very quickly. The brittle fracture is caused by the collapse of microvoids grown during the plastic deformation[27,28]. The stress crack propagation along the GB is delayed by the increase in inter-particle spacing at GB and increase in grain boundary precipitate spacing that occurs during ageing renders the alloys more resistant to stress corrosion attack[6,11,15-22].

There are two limitations for this theory:

(a). The electrochemical dissolution process at the crack tip doesn't explain the fact of very fast rate of SCC propagation proved by both experimental measurement and theoretical calculation[29,30].

(b). The view-point that the brittle fracture between GB ppts is caused by the collapse of microvoids has no experimental evidence. Furthermore, the average value of the mechanical step between GB ppts in the crack propagation was found to be larger than the inter- particle spacing[31].

1.4.2 *Precipitate -free zone (PFZ) dissolution model*

According to this theory, stress cracks follow the PFZ adjacent to GBs. There are two different groups of hypotheses on the formation of the PFZ along the GBs. The PFZ forms (a) due to the suppression of ppt nucleation in the absence of vacancies, and (b) due to the diffusion of solute atoms to GBs and, hence, the removal from a region adjacent to GBs[32-37]. The latter suggestion is widely accepted. The width of PFZ increases with the decrease of cooling rate from solution treatment temperature[38,40].

It has been proposed that the distribution of vacancies near a grain boundary can take the form shown schematically in Fig. 1.4.1[32] (curve A) and that a critical concentration C_1 is needed before nucleation of the precipitate can occur at temperature T_1. The width of the PFZ can be altered by heat treatment conditions; the zones are narrower for higher solution treatment temperatures and faster quenching rates, both of which increase the excess vacancy content (e.g. curve B in Fig. 1.4.1), and for lower ageing temperatures. This latter effect has been attributed to a higher concentration of solute which means that smaller nuclei will be stable, thereby reducing the critical vacancy concentration required for nucleation to occur

(C_2 in Fig. 1.4.1). However, the vacancy depleted part of a PFZ may be absent in some alloys aged at temperatures below the GP zone solvus as GP zones can form homogeneously without the need of vacancies[32].

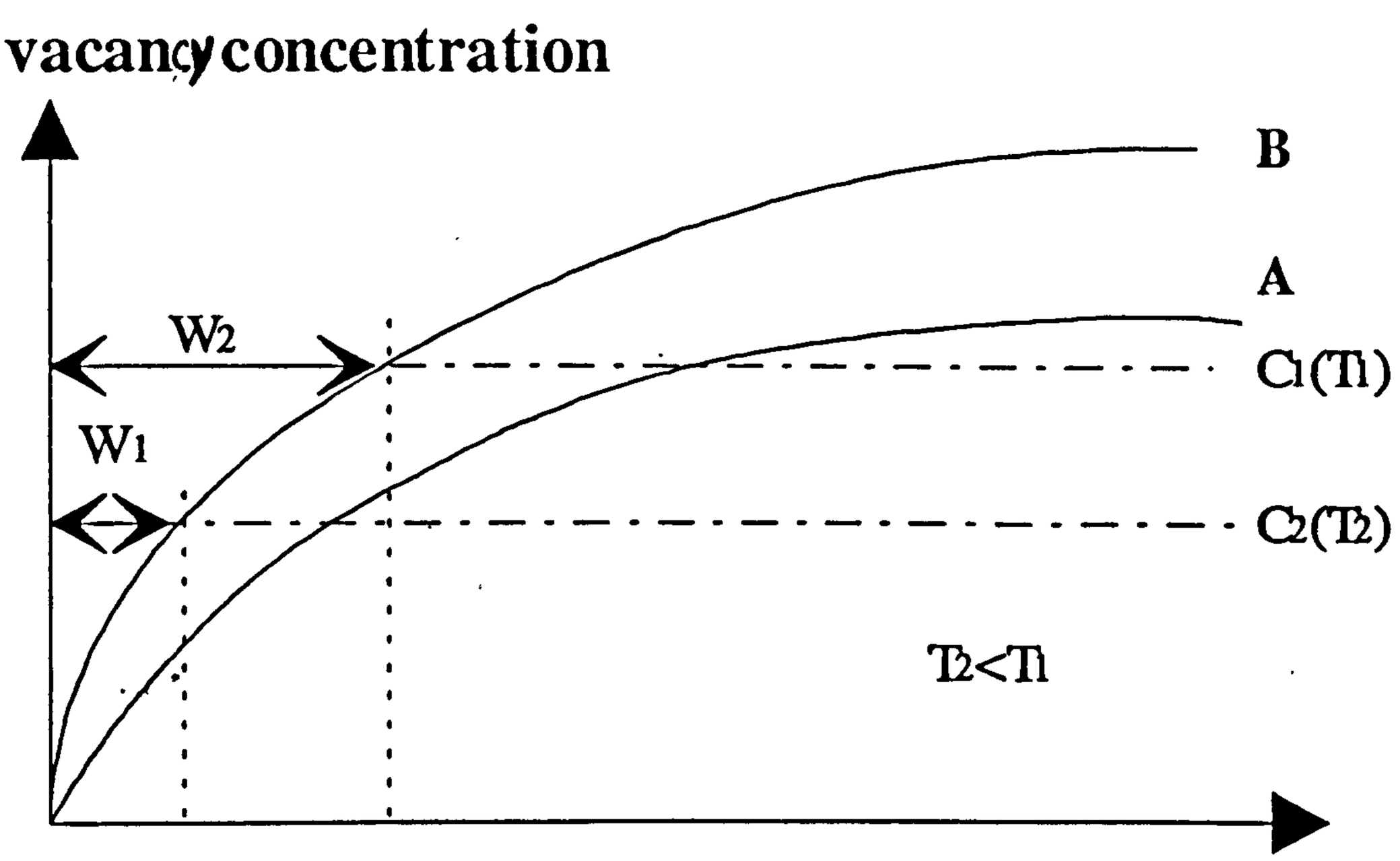

w1 and w2 widths of precipitate-free zones for vacancy concentrations C1 and C2

Fig. 1.4.1: PFZ caused by the depletion of vacancy concentration in the area adjacent to the grain boundaries.

During ageing, the width of PFZ

(a) increases slowly with the increase of ageing time if ageing temperature, T, is lower than the solvus temperature of GP zones[38,39,41],

(b) initially decreases with the increase of ageing time until it reaches a minimum and then, in a later stage increases, if ageing temperature, T, is higher than the soluvs temperature of GP zones and lower the that of η' phase[38,39,41].

Two groups of the PFZ models of SCC are compatible. The first proposes that a marked correlation exists between SCC susceptibility and the width of the PFZ[15,41-

49]. The second requires that SCC susceptibility is not associated with the width of PFZ[16,17,23,50-61].

The explanation for the SCC following the PFZ is that the PFZ flows preferentially because of the absence of the ppts and hence acts as an anodic site relative to an undeformed matrix phase. The wider the width of PFZ, the longer SCC life is because of the relieving of stress applied to grain boundary[15,41-49].

It is still open to question whether it is justifiable to explain the effect of ageing on SCC susceptibility in terms of this PFZ hypothesis because (a) both the width of PFZ and the coherency of ppts in the grain alter as ageing proceeds, and (b) even though the width of the PFZ increases slightly as ageing proceeds at temperatures lower than 150°C, there exists a critical time which corresponds to maximum susceptibility to SCC[15,38-49,52]. This may explain why the SCC is not associated with the width of PFZ.

1.4.3 *Matrix precipitates controlling model*

According to this theory, maximum susceptibility to cracking occurs in alloys when GP zones are present. In this case, deformation tends to be concentrated in discrete slip bands. It is considered that stress is generated where these bands impinge upon grain boundaries which can contribute to intercrystalline cracking under stress-corrosion conditions[23,26,41].

1.4.4 *Hydrogen embrittlement (HE) -assisted electrochemical model*

According to this model, pure SCC is not controlled by electrochemical dissolution, but rather by crack propagation in the presence of hydrogen[29,30,53-62]. It is only when a certain level of grain boundary precipitation has occurred that cracks due to

hydrogen embrittlement can be nucleated and the microstructure becomes stress corrosion susceptible.

1.5 *SCC/Segregation correlation*

Segregation is the highly localised change in concentration achieved during the solid-state thermal redistribution of species between the matrix and interfaces. Segregation can be divided into two categories -equilibrium segregation and non-equilibrium segregation.

Equilibrium segregation occurs at interfaces such as grain boundaries and surfaces. It is caused by impurity atoms moving to interfaces and, as a result, reducing their free energy[63-66].

Non-equilibrium segregation relies on the formation of sufficient quantities of vacancy-impurity complexes and the diffusion of the complexes. When the material is quickly cooled through a large temperature range the equilibrium concentration of vacancies, and thus complexes, is reduced. This true equilibrium concentration cannot be realised during fast cooling conditions except at vacancy sinks. Such sinks are interfaces like grain boundaries and surfaces. Thus vacancy concentration gradients are formed in quickly-cooled materials and there is a net flow of vacancies towards the vacancy sinks. The vacancy-impurity complexes are also carried down these gradients and impurity atoms are thus deposited at the sink. Impurity segregation then accumulates near the relevant interface. Non-equilibrium segregation is dependent on the binding energy of the impurity atom to a vacancy[67-71].

For 7150 aluminium alloy, both equilibrium and non-equilibrium segregation result mainly in the accumulation of magnesium on the grain boundaries since magnesium has a higher binding energy compared with zinc and copper[72,73].

The effect of segregation on the susceptibility of SCC has been studied by Scamans et al[73]. The conclusion of their work is as follows[73]:

1. There is strong correlation between non-equilibrium segregation of zinc and magnesium and susceptibility to stress corrosion cracking in white zones of welded specimens[73-76].
2. Equilibrium magnesium segregation promotes grain boundary reactivity and localised production and entry of hydrogen into grain boundaries. However, magnesium segregation in itself does not induce grain boundary stress corrosion cracking[77-79].
3. Stress corrosion cracking only occurs when cracks can be nucleated on grain boundary precipitates which may be due to the formation of magnesium hydride. In overaged or stabilised microstructures the grain boundary precipitates discharge hydrogen rather than promoting hydride formation[78,80].

During a heat treatment where segregation takes place, segregation strongly affects the grain boundary precipitate nucleation, growth and the width of PFZ and through this affects the susceptibility *to* SCC.

During a heat treatment, the equilibrium and non-equilibrium segregation induces the accumulation of magnesium atoms at the grain boundaries of 7150 aluminium alloy. Precipitation also takes place at the boundaries. The accumulation of the solute atoms influences precipitation nucleation by altering the driving force for the nucleation. The nucleation has a strong effect on the density of grain boundary precipitates. Besides, such accumulation of the solute atoms can effect the

precipitate growth rate by introducing an additional flux of solute atoms. Segregation and precipitation make the PFZ widths change with time because they vary the solute concentration in the area adjacent to the grain boundaries. Differences in solute levels that arise from segregation during heat treatments are thought to modify local electrochemical potentials. Moreover, the high magnesium content in this region results in an adjacent oxide layer with an increased MgO content which, in turn, is a less effective barrier against environmental influences[81].

1.6 *The main aim of this work*

It is getting more and more important to understand the relationship of the strength and SCC with the microstructural features such as the nature of the matrix precipitate, interface segregation, grain boundary precipitation, precipitate-free zones (PFZs) and to predict the influence of heat treatments on such microstructural features of aluminium alloys. This work may provide a guide for the temper designing of alloys to improve their properties. Shercliff and Ashby have put forward the process modelling techniques to describe the changes in yield strength due to age hardening of heat-treatable aluminium alloys[82]. It is the main aim of the work described in this thesis to construct a combined model which can predict the influence of heat treatments on combined segregation, grain boundary precipitation and precipitate-free zones (PFZs) formation in high strength heat treatable aluminium 7xxx series alloys. This work can help us in controlling stress corrosion cracking of the alloys by choosing right heat treatments to control the microstructural features. Put in detail, the model is constructed to give the following predictions :

- **the mean size of the grain boundary precipitates as a function of ageing time at a given ageing temperature after being quenched from solution treatment temperature into quenching media.**
- **the mean collector plate area, which is defined as an area of a plate on the centre of which there is a precipitate nucleus and by which the grain boundary is filled up, as a function of ageing time at a given ageing temperature after the sample is quenched from solution treatment temperature into quenching media; thus inter-precipitate spacing.**
- **the width of precipitate-free zone as a function of ageing time at a given ageing temperature after the sample is quenched from solution treatment temperature into quenching media.**

In order to approach this aim, a good understanding of the segregation, the grain boundary precipitation nucleation and growth and the formation of precipitate-free zones (PFZs) is very important. The existed theories of the segregation, the nucleation and precipitation is reviewed in **chapter 2.** The new developments of the theories of the segregation, the nucleation, the precipitation and the formation of the PFZ are described in **chapter 3.** It is based on these theories that the combined model is constructed.

Chapter Two

Theory (I)

- Previous Theories of Grain Boundary Segregation, Nucleation And Precipitation

2.1 *Segregation*

Segregation is the highly localised change in concentration achieved during the solid-state thermal redistribution of species between the matrix and interfaces. Segregation to defect sinks, such as grain boundaries is possible by one or both of two distinct mechanisms: equilibrium and non-equilibrium segregation.

2.1.1 *Equilibrium segregation*

The phenomenon of the equilibrium segregation of dilute solutes to interfaces has been recognised for some time since the work of Gibbs[63]. The analysis of the kinetics of equilibrium segregation by McLean[64], and further refinement by Seah and Hondros[65,66] has led to a well-quantified understanding.

Equilibrium segregation occurs at interfaces such as grain boundaries and surfaces. It is caused by impurity atoms moving to interfaces and, as a result, reducing their free energy. The lower the temperature is, the greater the equilibrium concentration of a solute at an interface, but also the longer the time required for equilibrium to be achieved. The spatial distribution of equilibrium segregation concentration is confined to the atomic layer immediately adjacent to the interface; this is where solute strain energy relief occurs.

2.1.1.1 *McLean's equilibrium segregation model[64]*

Mclean's equilibrium segregation model gives a good description of the thermodynamics and kinetics of the grain boundary segregation. Mclean's model states that for an impurity with binding energy to the lattice, E_{b1}, at any temperature, T, there will be an increased concentration of that impurity in a monolayer on boundaries and interfaces, C^{∞}_{gbT}. The driving force for this is the reduction of energy, E_{b1}, of the impurity on placing it in a strain-free environment on the grain boundary.

C^{∞}_{gbT} is given by :

$$C^{\infty}_{gbT} = \frac{C_g \exp(\frac{E_{b1}}{kT})}{1 + C_g \exp(\frac{E_{b1}}{kT})} \qquad (2.1.1)$$

where C_g is the concentration of impurity in the matrix alloy and k is Boltzmann's constant.

C^{∞}_{gbT} is the interfacial concentration of equilibrium segregation when full equilibrium has been reached. The true interfacial concentration will be diffusion-controlled and hence will vary with time. It is governed by the equation:

$$\frac{C^{t}_{gbT} - C_g}{C^{\infty}_{gbT} - C_g} = 1 - \exp(\frac{4D_I t}{\alpha^2 d_1^2}) erfc(\sqrt{\frac{4D_I t}{\alpha^2 d_1^2}}) \qquad (2.1.2)$$

where C^{t}_{gbT} is the true interfacial concentration of the impurity after time t at temperature T; D_I is the diffusion coefficient of the impurity at this temperature; d_1 is the width of the layer where solute is highly concentrated by equilibrium segregation; d_1=0.25nm; α is given by

$$\alpha = \frac{C^{\infty}_{gbT}}{C_g} \qquad (2.1.3)$$

Equation (2.1.2) is derived from the solution of Fick's second law:

$$\frac{\partial C}{\partial t} = D_I \frac{\partial^2 C}{\partial x^2} \qquad (2.1.a)$$

with condition:

$$C|_{t=0} = C_g \qquad (2.1.b)$$

and condition:

$$D_I \frac{\partial C}{\partial x}|_{x=0} = \frac{1}{2} d_1 \frac{\partial C'_{gbT}}{\partial t} = \frac{1}{2} d_1 \alpha \frac{\partial C}{\partial t}|_{x=0} \qquad (2.1.c)$$

where x is the distance from the interface between the solute concentrated layer at the grain boundary and interior grain into interior grain; at the interface, x=0.

It is supposed that equilibrium between crystal interior and crystal boundary is reached at a temperature T_1 and that ratio of concentrations $\frac{C''_{gbT_1}}{C_g} = \alpha_1$; the alloy is very quickly cooled from T_1 to a temperature T at which the equilibrium concentration ratio is α where $\alpha > \alpha_1$. Cooling is supposed to be too rapid for the change to take place before T is reached and the alloy is then held at T; diffusion of impurities towards the grain boundary takes place until the equilibrium value of grain boundary concentration $C''_{gbT} = \alpha C_g$ is reached.

The following is the procedure of the derivation of Equation (2.1.2):

using the Laplace transform; putting

$$\overline{C} = \int_0^{\infty} e^{-pt} C \, dt \qquad (2.1.d)$$

into Laplace transform of Equations (2.1.a), and (2.1.c) , gives:

$$\overline{C} = M \exp(-\sqrt{\frac{p}{D_I}} x) + \frac{C_s}{p} \qquad (2.1.e)$$

$$D_I (\frac{\partial \overline{C}}{\partial x})_{x=0} = \frac{\alpha d_1}{2} (p\overline{C} - \frac{\alpha_1}{\alpha} C_s) \qquad (2.2.f)$$

where $\frac{\alpha_1}{\alpha} C_s$ is the crystal concentration at x=0 immediately after quenching.

Inserting Equation (2.1.e) into Equation (2.1.f) to get M and then replacing M in Equation (2.1.e) gives

$$\overline{C} = \frac{C_s (\frac{\alpha_1}{\alpha} - 1) \exp(-\sqrt{\frac{p}{D_I}} x)}{D_I \sqrt{\frac{p}{D_I}} (\sqrt{\frac{p}{D_I}} + \frac{2}{\alpha d_1})} + \frac{C_s}{p} \qquad (2.1.g)$$

from Tables of Laplace transforms,

$$C = C_s - C_s (1 - \frac{\alpha_1}{\alpha}) \exp(\frac{2x}{\alpha d_1} + \frac{4 D_I t}{\alpha^2 d_1^2}) erfc(\frac{x}{2\sqrt{D_I t}} + \frac{2\sqrt{D_I t}}{\alpha d_1}) \qquad (2.1.h)$$

Putting x=0 gives the crystal concentration in contact with the boundary and on multiplying by α yields Equation (2.1.2).

Equations (2.1.1) and (2.1.2) give the thermodynamic relationship and kinetic relationship of equilibrium segregation. The lower the temperature is, the greater the equilibrium concentration of a solute at an interface, but also the longer the time required for equilibrium to be achieved. Consequently, equilibrium segregation tends to be of most concern at intermediate temperatures. The spatial distribution of

equilibrium segregation is confined to the atomic layer immediately adjacent to the interface; that is where solute strain energy relief can occur.

2.1.2 *Non-equilibrium segregation*

Non-equilibrium segregation has only more recently come to attention. It was first inferred by Westbrook[67] from grain boundary hardness measurements. The theory of non-equilibrium segregation was established by Aust et al[68] and Anthony[69].

Non-equilibrium segregation relies on the formation of sufficient quantities of vacancy-impurity complexes and the diffusion of the complexes. When the material is quickly cooled through a large temperature range the equilibrium concentration of vacancies, and thus complexes, is reduced. This true equilibrium concentration can not be realised during fast cooling conditions except at vacancy sinks. Such sinks are interfaces like grain boundaries and surfaces. Thus vacancy concentration gradients are formed in quickly-cooled materials and there is a net flow of vacancies towards the vacancy sinks. The vacancy-impurity complexes are also carried down these gradients and impurity atoms are thus deposited at the sink. Impurity segregation then accumulates near the relevant interface. Non-equilibrium segregation is dependent on the binding energy of the impurity atom to a vacancy. In contrast to equilibrium segregation, non-equilibrium segregation becomes greater with increasing temperature; the spatial extent of the segregant solute redistribution may extend to hundreds of atomic layers. Thermal ageing will eventually homogenise non-equilibrium segregation, since by definition it is non-equilibrium; whereas ageing increases equilibrium segregation as the system approaches equilibrium.

The work of quantification analysis of non-equilibrium segregation at grain boundaries has been reported by Faulkner[70] and further by Xu & Song[71].

2.1.2.1 *Faulkner's non-equilibrium segregation model*[70]

Faulkner's non-equilibrium segregation model quantifies the magnitude of non-equilibrium segregation at the grain boundary and its extent by predicting the concentration profile shape near to the grain boundary as a function of time and temperature.

(1). Magnitude of non-equilibrium segregation

In Faulkner's treatment, the magnitude of non-equilibrium segregation is indicated by the ratio of the excess impurity concentration at the sink to that at the grain centre.

The excess impurity concentration is represented as the inverse of the ratio C_{I-v}/C_I, where is C_I is the concentration of impurities, C_{I-v} is the concentration of complexes.

At temperature, T, C_{I-v} is given by

$$C_{I-v} = k_{I-v} C_v C_I \exp(\frac{E_b}{kT}) \qquad (2.1.4)$$

where E_b is vacancy-impurity binding energy, k_{I-v} is a geometrical constant, C_v is the concentration of vacancies given by

$$C_v = k_v \exp(\frac{-E_f}{kT}) \qquad (2.1.5)$$

where k_v is a geometrical constant.

Inserting Equation (2.1.5) into (2.1.4) gives

$$C_{I-v} = k_{I-v} k_v C_I \exp(\frac{E_b - E_f}{kT}) \qquad (2.1.6)$$

The change in concentration brought about at the vacancy sink such as a grain boundary is calculated during cooling from temperature T_i to T_{mp}, where T_i is the solution treatment temperature and T_{mp} is the temperature at which most segregation will have been completed, $T_{mp} = 0.6T_m$ where T_m is the melting point of the alloy. The temperature, T_{mp}, is chosen in this way because it is assumed that very little diffusion will occur below T_{mp}.

It is assumed that the alloy is cooled from T_i to T_{mp} in a time sufficiently short that the isolated impurity atoms cannot move. At the sink the ratio $C_{I\text{-}v}/C_I$ will decrease whereas this ratio will remain roughly constant in the grain centres where no vacancy sinks exist. The complexes will diffuse down the concentration gradients between the grain centres and grain boundaries in an effort to keep the concentration of complexes equal at all points. Therefore, an excess of impurities will be established at the grain boundaries.

When the sample is cooled from temperature T_i to T_{mp}, an equilibrium is instantaneously established, appropriate to T_{mp} on the grain boundary and appropriate to T_i at the grain centre. The excess impurity concentration can be represented as the inverse of the ratio of $C_{I\text{-}v}/C_I$ predicted from equation (2.1.6) for the sink that is at T_{mp}, and for the grain centre that is at T_i. Therefore, the ratio of the excess impurity concentration at the sink, i.e. at T_{mp}, to the excess impurity concentration at the grain centre, i.e. at T_i, is

$$\frac{(C_i/C_{i\text{-}v})_{T_{mp}}}{(C_i/C_{i\text{-}v})_{T_i}} = \exp\left[\frac{(E_b - E_f)}{kT_i} - \frac{(E_b - E_f)}{kT_{mp}}\right] \qquad (2.1.7)$$

The magnitude of non-equilibrium segregation, C_b/C_g:

$$\frac{C_b}{C_g} = \exp\left(\frac{E_b - E_f}{kT_i} - \frac{E_b - E_f}{kT_{mp}}\right)\frac{E_b}{E_f} \qquad (2.1.8)$$

(2). The extent of non-equilibrium segregation

In Faulkner's model, the extent of non-equilibrium segregation is quantified for a process that occurs on cooling from T_i to T_{mp}, followed by an isothermal step in the heat-treatment at a temperature T for a time, t.

In Faulkner's model all treatments of the kinetic aspects of non-equilibrium segregation relate the non-equilibrium segregation process to the diffusion constant at one single temperature which is taken as solution-treatment temperature, T_i. So the non-equilibrium segregation for a process that occurs on cooling from T_i to T_{mp}, followed by an isothermal step in the heat-treatment at a temperature T for a time, t, can be equally expressed as that for an isothermal step in the heat-treatment at temperature T_i for an effective time, t_{eff}, which is given by

$$t_{eff} = t_q + t_a \tag{2.1.9}$$

where t_a is the effective ageing time given by

$$t_a = t \exp[\frac{-Q_c(T_i - T)}{kT_iT}] \tag{2.1.10}$$

and t_q is effective quenching time.

Numerical approach is used for the calculation of t_q. The following is the deduction of the calculation.

Fig. 2.1.1 is an illustration of a cooling process in which the curve MN is the variation of temperature with time given by Flewitt's formula[83]. As shown in Fig. 2.1.1, when steps formed by horizontal and vertical segments are chosen small enough, the cooling curve MN will be practically equal to the stepped curve.

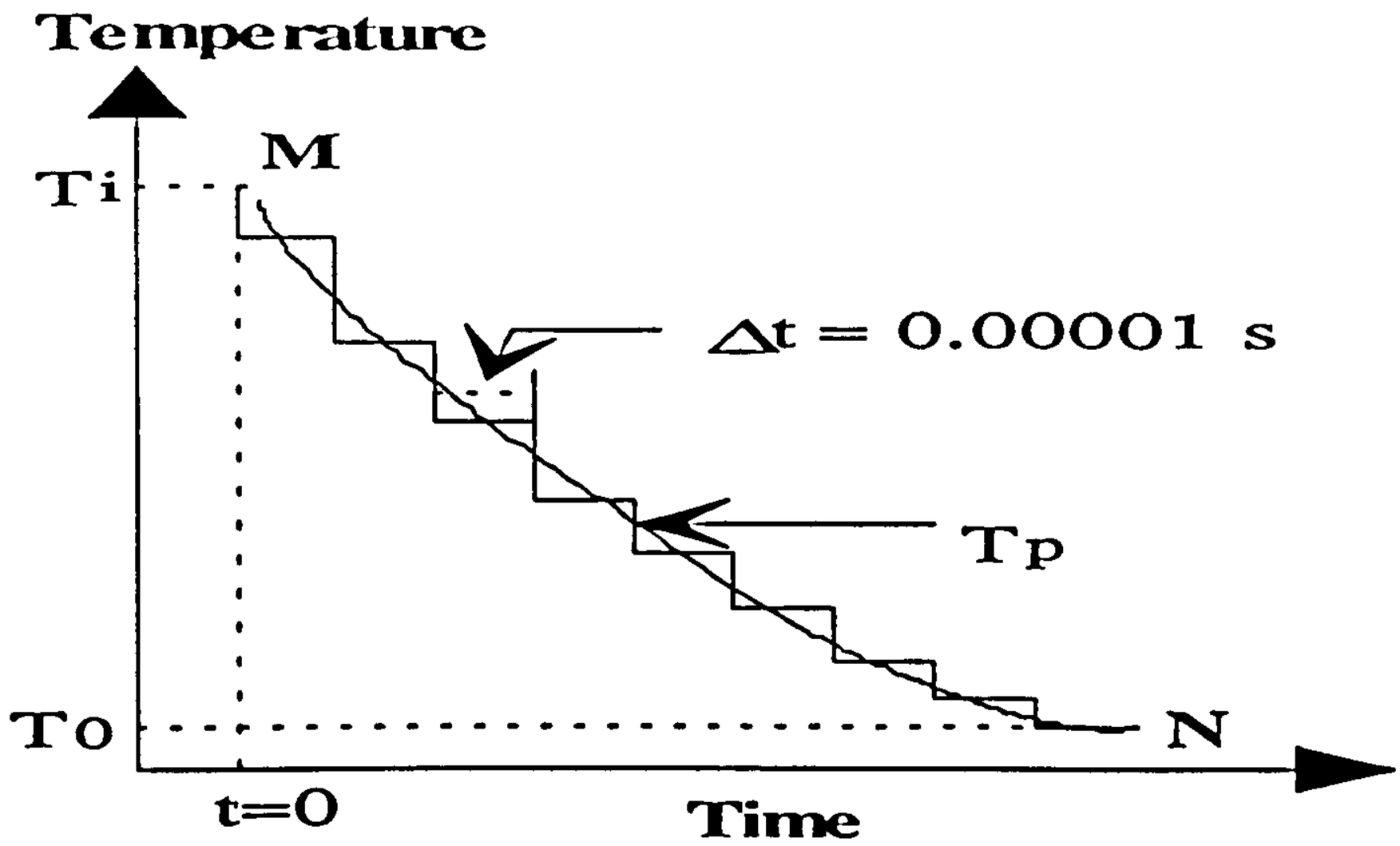

Fig. 2.1.1: Actual cooling curve MN and its approximate stepped curve.

The step length of time is set to 0.0001 second. Using Flewitt's formula[83], the temperature after time, t = 0.0001p, where p is a integer, is

$$T_p = (T_i - T_0)\exp(-0.0001 \cdot \theta \cdot p) + T_0 \qquad (2.1.11)$$

where T_0 is the temperature of quenching media and θ is the cooling rate parameter.

The effective time of the time interval staying at this temperature is:

$$t_q^p = 0.0001 \cdot \exp[-\frac{Q_c(T_i - T_p)}{kT_iT_p}] \qquad (2.1.12)$$

and the effective quenching time, t_q is

$$t_q = \sum_{p=1}^{p'} t_q^p$$

or (2.1.13)

$$t_q = \sum_{p=1}^{p'} 0.0001 \cdot \exp[-\frac{Q_c(T_i - T_p)}{kT_iT_p}]$$

where Q_c is the activation energy for diffusion of complexes, T_p is the temperature given by equation (2.1.11) and p' is an integer given by

$$p' = 10000 \ln\left(\frac{T_i - T_0}{T_{mp} - T_0}\right) \div \theta \qquad (2.1.14)$$

During non-equilibrium segregation two distinct processes are occurring. These are segregation and de-segregation. Firstly, impurities are drawn from the grain centres to the boundaries by the motion of the complexes. The ratio of concentration of impurities, C_b, resulting on the boundaries relative to the matrix concentration, C_g, can never exceed that predicted by equation (2.1.8). Thus, any accumulation of impurities must occur near to the grain boundary in a zone which extends outwards to an extent proportional to the amount of segregation taking place. Secondly, de-segregation occurs when the time under the heat treatment exceeds a critical time, t_c, and the dominant effect is back diffusion, or de-segregation, of the impurity down the concentration gradient, towards the centre of the grain. The rate-determining step in this process is D_{Ii}, which is the impurity diffusion coefficient at temperature, T_i.

(a). Segregation

During segregation, the impurity concentration profile, $C(y, t_{eff})$ varies with time and is governed by

$$\frac{C(y,t_{eff}) - C_g}{C_b - C_g} = erfc\frac{y}{2\sqrt{D_{ci}t_{eff}}} \qquad (2.1.15)$$

where D_{ci} is the complex diffusion coefficient at temperature T_i and y is the distance from the grain boundary, where y=0, into the grain interior.

Equation (2.1.15) is the solution of the Fick's second law,

$$\frac{\partial C(y,t_{eff})}{\partial t_{eff}} = D_{ci}\frac{\partial^2 C(y,t_{eff})}{\partial y^2} \qquad (2.1.i)$$

and it satisfies the condition,

$$C(y,t_{eff})|_{t_{eff}=0} = C_g \qquad (2.1.j)$$

and condition,

$$C(y,t_{eff})|_{y=0} = C_b \qquad (2.1.k)$$

The following is the procedure of the derivation of Equation (2.1.15):

using the Laplace transform; putting

$$\overline{C} = \int_0^{\infty} e^{-p t_{eff}} C(y, t_{eff})\, dt_{eff} \qquad (2.1.l)$$

into Laplace transform of Equation (2.1.i), gives:

$$\overline{C} = M \exp(-\sqrt{\frac{p}{D_{ci}}}y) + \frac{C_g}{p} \qquad (2.1.m)$$

Combining Equation (2.1.m) with the Laplace transform of Equation (2.1.k) gives

$$\overline{C} = \frac{(C_b - C_g)\exp(-\sqrt{\frac{p}{D_{ci}}}y)}{p} + \frac{C_g}{p} \qquad (2.1.n)$$

from a Table of Laplace transforms, we then obtain Equation (2.1.15).

(b). De-segregation

When the effective time, t_{eff}, exceeds a critical time, t_c, the dominant effect is back diffusion, or de-segregation, of the impurity down the concentration gradient, towards the centre of the grain.

t_c is governed by the relative diffusion rates of the complexes towards the grain boundary and the diffusion rates of impurities away from the grain boundary and is given by

$$t_c = \frac{\varsigma d^2 \ln(\frac{D_{ci}}{D_{li}})}{4(D_{ci} - D_{li})} \qquad (2.1.16)$$

where ς is a numerical factor and d is the grain size.

The concentration of impurity, $C(y, t_{eff})$, at a distance, y, from the grain boundaries after time, t_{eff} (where $t_{eff} > t_c$) is given by

$$\frac{C(y, t_{eff}) - C_g}{C_b - C_g} = (\frac{D_{ci} t_c}{D_{li} t_{eff}})^{\frac{1}{2}} \exp(\frac{-y^2}{4 D_{li} t_{eff}}) \qquad (2.1.17)$$

The details of the derivation of equation (2.1.16) and (2.1.17) are given in Faulkner's paper[70].

To summarise, Faulkner's model makes it very clear that non-equilibrium segregation is kinetically driven by the diffusion of vacancy-impurity complexes formed when the material is quickly cooled from high temperature. The magnitude of the segregation is affected by the vacancy-impurity binding energy and the vacancy formation energy. The spatial extent of the segregant solute redistribution may extend to hundreds of atomic layers depending on the amount of segregation taking place. Non-equilibrium segregation becomes greater with increasing temperature, in contrast to equilibrium segregation.

2.1.2.2 *Xu & Song's non-equilibrium segregation model*[71]

Using Faulkner's thermodynamic relationship of the non-equilibrium segregation[70] and the Mclean's kinetics of equilibrium segregation[64], Xu and Song created a non-equilibrium segregation model which gave a relationship of time-depend non-equilibrium segregation concentration during the segregation process of non-equilibrium segregation[71].

In Xu and Song's treatment, a solute concentrated layer is defined. The width of it, d_2, is assumed to be of a value of the width of three atomic layers; $d_2 = 1$ nm .

During segregation process which is when $t_{eff} \leq t_c$, the true solute concentration at the solute concentrated layer after effective time t_{eff}, $C_b(t_{eff})$ is given by

$$C_b(t_{eff}) = C_b^{max} - C_g(\gamma - 1)\exp(\frac{4D_{ci}t_{eff}}{\gamma^2 d_2^2})erfc(\frac{2\sqrt{D_{ci}t_{eff}}}{\gamma d_2}) \qquad (2.1.18)$$

where C_b^{max} is the maximum solute concentration of the non-equilibrium segregation for the sample cooled from temperature T_i to T_{mp}, and then aged at temperature, T.

$$C_b^{max} = \exp(\frac{E_b - E_f}{kT_i} - \frac{E_b - E_f}{kT_{mp}})\frac{E_b}{E_f} \qquad (2.1.19)$$

γ is given by

$$\gamma = \frac{C_b^{max}}{C_g} \qquad (2.1.20)$$

Equation (2.1.18) is Xu and Song's kinetic relationship of the solute concentration at the grain boundary during the segregation process of non-equilibrium segregation.

Equation (2.1.18) is derived from the solution of Fick's second law:

$$\frac{\partial c(x,t_{eff})}{\partial t_{eff}} = D_{ci}\frac{\partial^2 c(x,t_{eff})}{\partial x^2} \qquad (2.1.21)$$

with condition:

$$c(x,t_{eff})|_{t_{eff}=0} = C_g \qquad (2.1.22)$$

and condition:

$$D_{ci}\frac{\partial c(x,t_{eff})}{\partial x}|_{x=0} = \frac{1}{2}d_2\frac{\partial C_b(t_{eff})}{\partial t_{eff}} = \frac{1}{2}d_2\gamma\frac{\partial c(x,t_{eff})}{\partial t_{eff}}|_{x=0} \qquad (2.1.23)$$

where $c(x,t_{eff})$ is the solute concentration at position x and effective time t_{eff}, x is the distance from x=0 which is the interface between the grain interior and the solute concentrated layer into the grain interior.

$$c(x,t_{eff}) = C_g - C_g(1-\frac{1}{\gamma})\exp(\frac{2x}{\gamma d_2}+\frac{4D_{ci}t_{eff}}{\gamma^2 d_2^2})erfc(\frac{x}{2\sqrt{D_{ci}t_{eff}}}+\frac{2\sqrt{D_{ci}t_{eff}}}{\gamma d_2}) \qquad (2.1.24)$$

Equation (2.1.24) is the solution of the diffusion equation (2.1.21) and it satisfies the conditions given by Equations (2.1.22) and (2.1.23). Making x=0 in Equation (2.1.24) and multiplying both sides with factor γ yields equation (2.1.18).

The illustrations of the comparison of the segregation concentration profiles given by Faulkner, Xu & Song's models for segregation process of non-equilibrium segregation are shown by Figs. 2.1.2a-b.

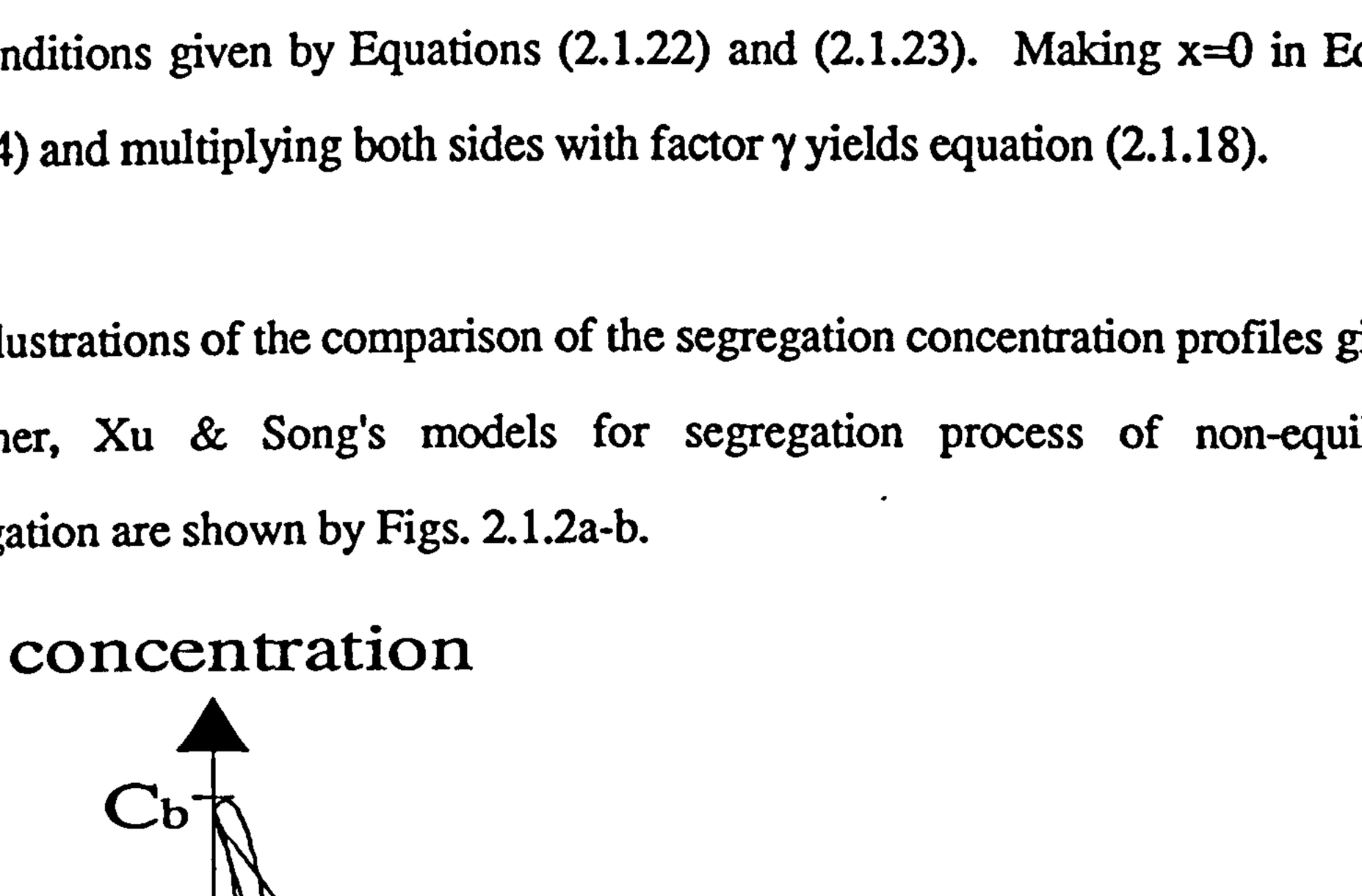

Fig. 2.1.2a: The illustration of the segregation concentration profiles given by Faulkner's non-equilibrium segregation model during segregation process.

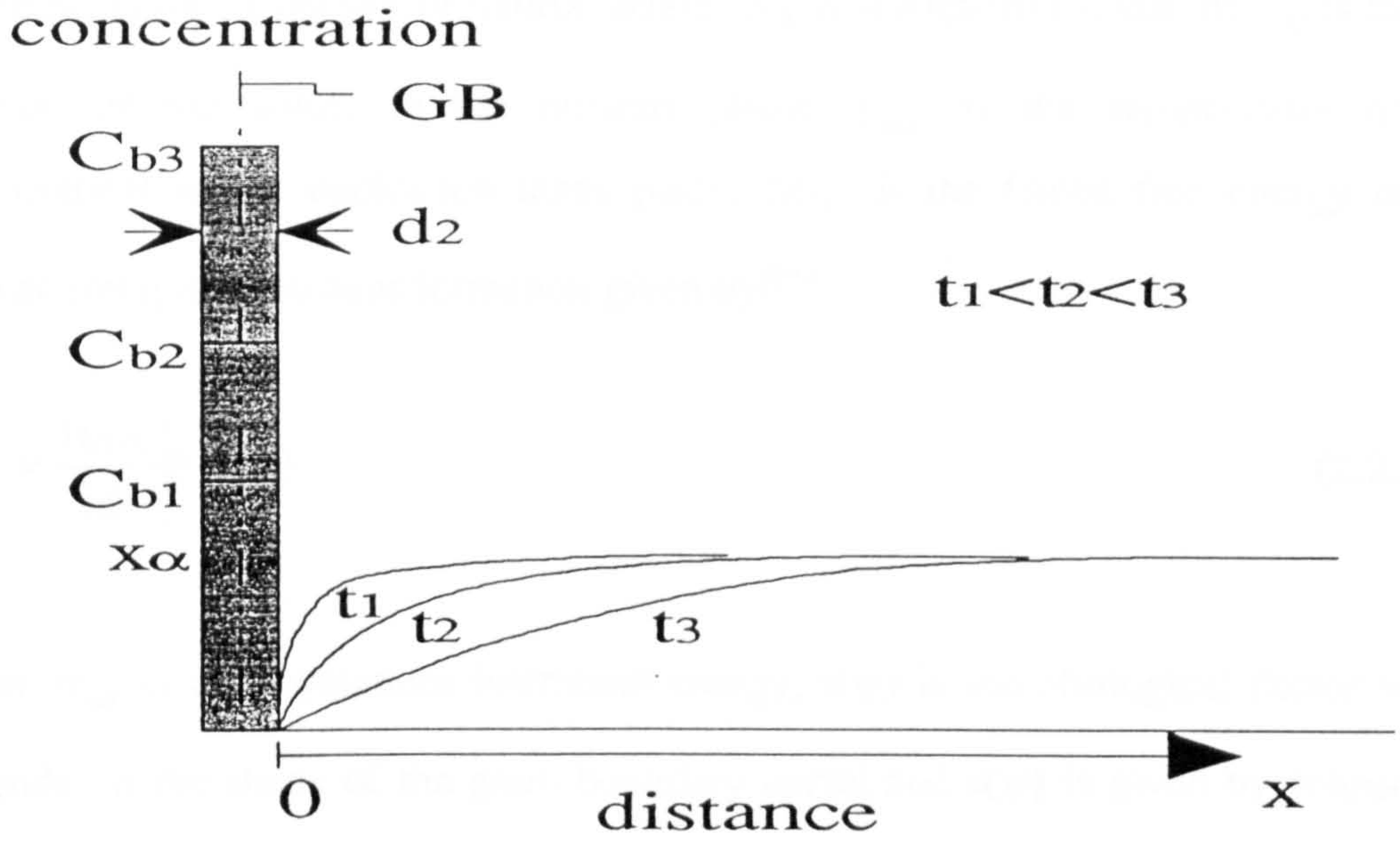

Fig. 2.1.2b: The illustration of the segregation concentration profiles given by Xu & Song's non-equilibrium segregation model during segregation process.

2.2 *Nucleation*

There are several reviews of the theory of nucleation kinetics at grain boundaries[84-89]. The work of other researchers[90, 91, 92] is adopted to analyse the nucleation of $MgZn_2$ grain boundary precipitates in 7150 aluminium alloy.

2.2.1 *The number of critical precipitate nuclei*

In 1969, Russell put forward an equation which gives the relationship of the number of critical precipitate nuclei per unit volume, N_{v0}, in terms of temperature[90].

$$N_{v0} = \frac{N_v}{x_\theta} \exp\left(-\frac{\Delta G_v^*}{kT_{nuc}}\right) \qquad (2.2.1)$$

where N_v is total number of atoms per unit volume taken as

$$N_v = \rho_\alpha N_A \qquad (2.2.2)$$

where ρ_α is molar density of matrix phase; N_A is Avogadro's constant; x_θ is atomic fraction of the solute in the nucleus phase, T_{nuc} is the temperature of the environment where nucleation takes place, ΔG_v^* is the Gibbs free energy of the critical precipitate nucleus formation given by[91]

$$\Delta G^* = \frac{16\pi\sigma_{\alpha\theta}^3}{3\Delta G_v^2} s(\psi) \qquad (2.2.3)$$

where $\sigma_{\alpha\theta}$ is matrix/nucleus interfacial energy, $s(\psi)$ is morphological factor which depends on the shape of the grain boundary nuclei and $s(\psi)$ is given by Johnson et al[91]. For cap shape particle as shown in Fig. 2.2.1 $s(\psi)$ is

$$s(\psi) = \frac{2 - 3\cos\psi + \cos^3\psi}{2} \qquad (2.2.4)$$

where

$$\cos(\psi) = \frac{\sigma_{\alpha\alpha}}{2\sigma_{\alpha\theta}} \qquad (2.2.5)$$

ΔG_v is the driving force for the formation of a nucleus of the precipitate phase. For $MgZn_2$ precipitate ΔG_v is given by

$$\Delta G_v = \frac{RT_{nuc}}{2V_\theta} \ln\left(\frac{x_b}{x_{\alpha T_{nuc}}^{\alpha\theta}}\right) \qquad (2.2.6)$$

where $x_{\alpha T_{nuc}}^{\alpha\theta}$ is the concentration of rate controlling element (Mg) in equilibrium with the nucleated precipitate phase and matrix at temperature T_{nuc}; x_b is the solute concentration at the grain boundary; V_θ is the molar volume of the precipitate phase and R is gas constant.

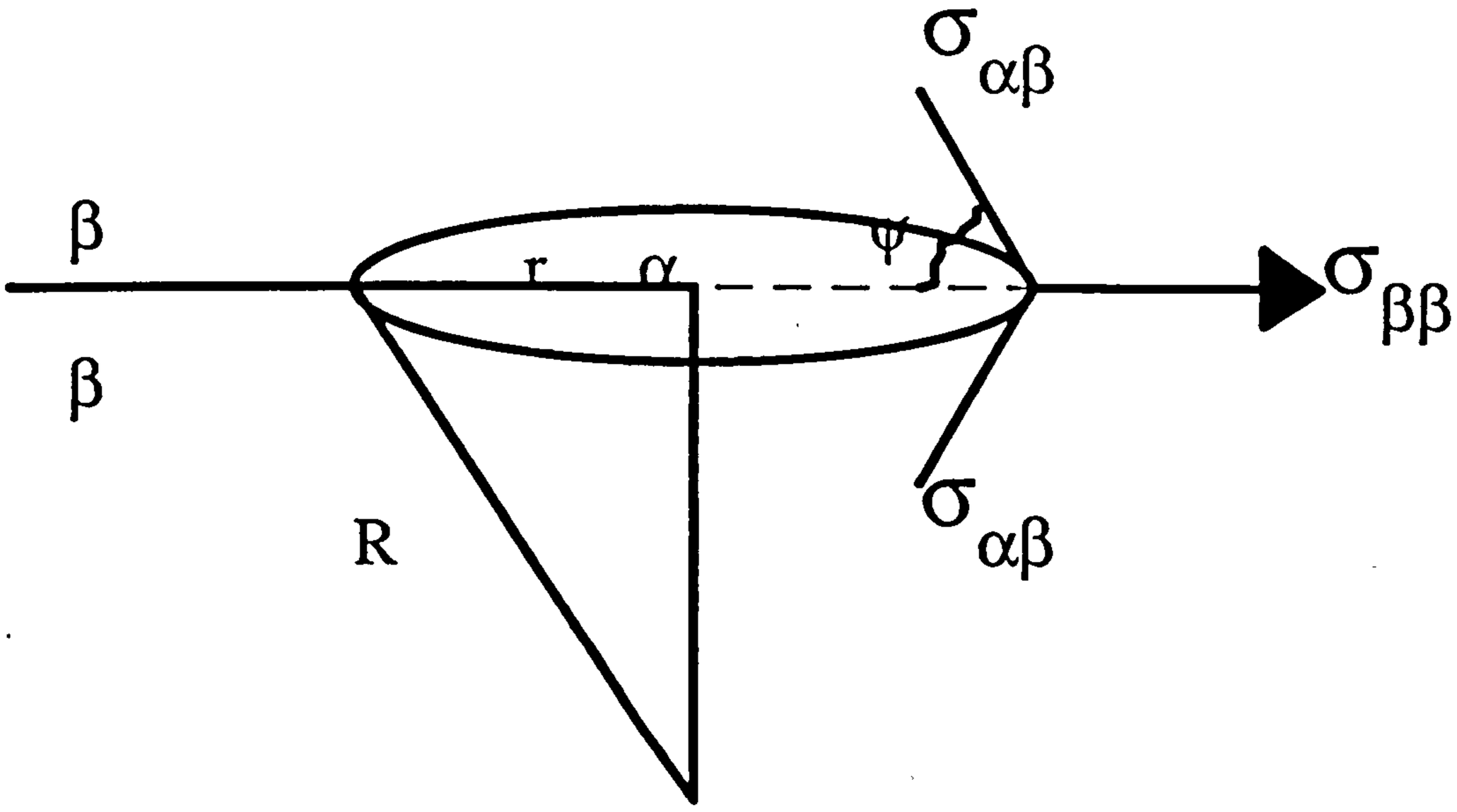

Fig. 2.2.1: Cap shape nucleus morphology.

3.2.2 *Nucleation time of grain boundary precipitates*

Nucleation time is taken as the incubation time according to Russell's theory.

In 1968, Russell first used linked flux analysis to define homogeneous nucleation[93]. The results of the linked flux analysis were then adapted to heterogeneous grain boundary precipitation[90]. Russell et al then made a more detailed and realistic approach to the effects of precipitate morphology on nucleation[91]. This last approach produced a general equation for incubation time that incorporated morphological factors.'' This general equation for incubation time was further modified by replacing the volume diffusivity and the interfacial area of the nucleus available for atomic attachment in the expression for the incubation time with the grain boundary diffusivity and the product of the grain boundary width and the circumference of the nucleus in the plane of the boundary[92]. The modified equation of incubation time[92] is used to predict nucleation time.

The incubation time, τ, of the nucleation at temperature T_{nuc} is then given by

$$\tau = \frac{32kT_{nuc}a^4\sigma_{\alpha\theta}^2 N_A^2}{D_{bnuc}d_0 x_b V_\theta^2 \Delta G_v^3 \sin\psi} \qquad (2.2.7)$$

where D_{bnuc} is grain boundary diffusion coefficient of the solute atom at temperature T_{nuc}, a is the lattice parameter of matrix phase, d_0 is the width of grain boundary within which the solute diffusion is interfacial diffusion controlling, d_0=0.1 nm, ψ is an angle.

2.3 *Growth kinetics of grain boundary precipitates*

In 1949 Zener put forward a growth kinetics theory of grain boundary precipitation and created the first model of the grain boundary precipitation[94]. By equating the mass transfer of solute to the precipitate particle as given by Fick's first law of diffusion to the increase in mass per unit area as the precipitate grew, Zener produced a model which represented the size of the ellipsoidal precipitate particle as a function of time and temperature. This model was successfully applied to carbon diffusion controlled growth of proeutectoid ferrite from austenite in steels. Based on this model Hillert developed a model to describe the lengthening rate of an oblate ellipsoidal particle in 1957[95]. In 1961, by considering lengthening and thickening simultaneously, Horvay and Cahn produced a model which gave lengthening and thickening rates[96]. Horvay and Cahn assumed precipitate shape was preserved as it grew. Length could be related to thickness via a constant known as the constant aspect ratio. Such an assumption was adapted for growth by Faulkner and Caisley(1977)[97]. The model of Horvay and Cahn was applied to the work on Al-Ag alloys.

In 1968, Aaron and Aaronson developed a collector plate model to apply specifically to grain boundaries[98]. This took into account the role of grain boundary short

circuit diffusion using a collector plate mechanism. The model was used to analyse the precipitation of Al-Cu alloys. Based on the Aaron and Aaronson collector plate idea, a simplified model was put forward by Faulkner and Caisley (1977)[97]. They assumed a constant aspect ratio throughout the early stages of precipitate growth and this treatment led to an assessment of overall precipitate size as a function of temperature and time, assuming a constant morphology. Further development, including variable collector plate size and precipitate morphology were considered by Carolan and Faulkner(1988)[99]. Both Faulkner and Caisley's and Carolan and Faulkner's models were applied successfully to carbide precipitation in steels.

The above gives a brief review of the history of development of the growth kinetics of grain boundary precipitation. Following is the introduction in more detail of Aaron and Aaronson's model[98], Faulkner and Caisley's model[97], Carolan and Faulkner's model[99].

2.3.1 *Aaron & Aaronson's model[98]*

In all growth models the dimension L is the precipitate half length.

Aaron and Aaronson were the first to deal with observations that growth rates of grain boundary precipitates were higher than those predicted by models using a simple bulk diffusion mechanism only. They considered using the high diffusivity path of the grain boundary for solute transport. The basis for the model is illustrated in Fig. 2.3.1. Aaron and Aaronson considered each grain boundary was completely filled by a set of square collector plates which was taken to be centred on a single precipitate and had a side length which was inter-particle spacing, d_v and of area A_v ($A_v = d_v^2$). The growing precipitates drew solute from their own collector plates controlled by grain boundary diffusion. The collector plates in turn obtained their solute from the areas of the grains adjacent to the boundaries by bulk diffusion.

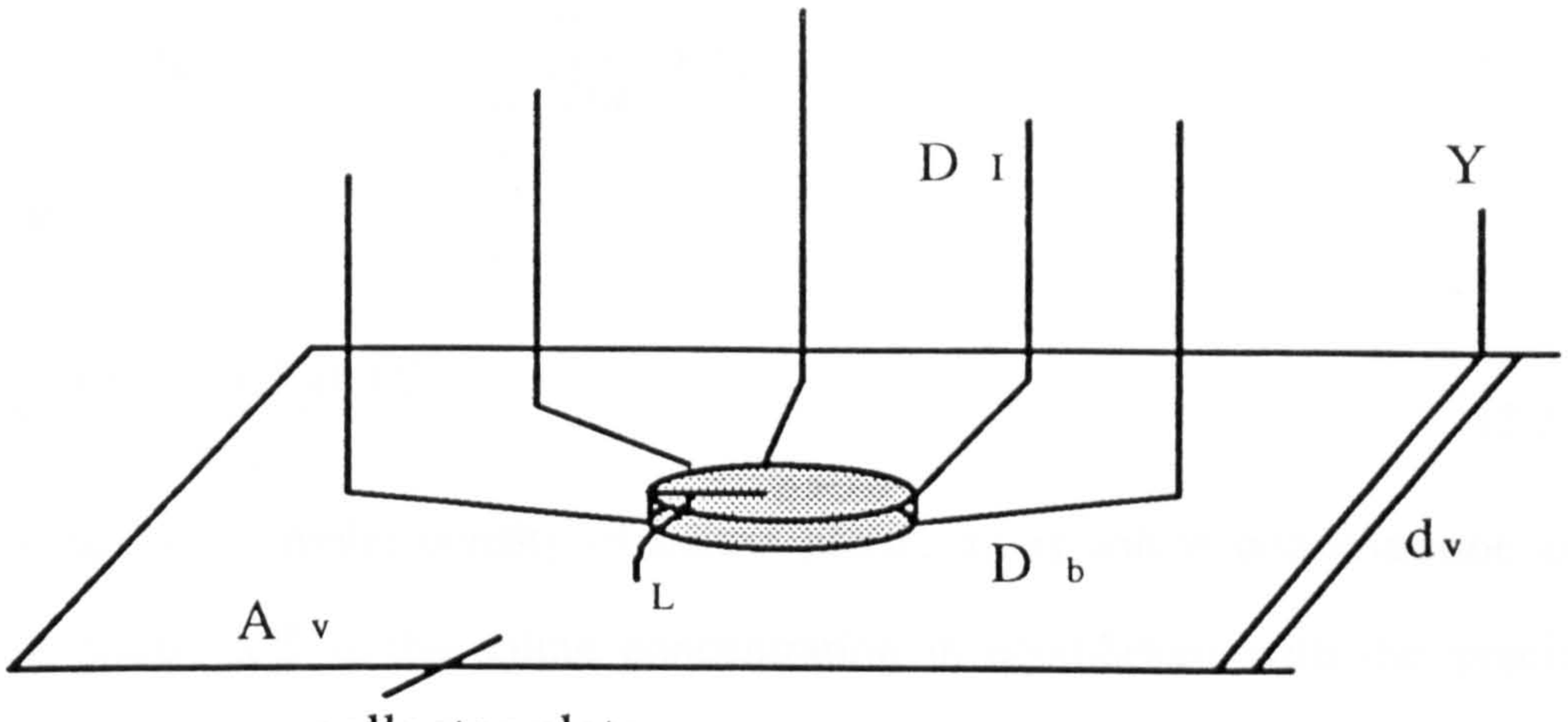

Fig. 2.3.1: Illustration of precipitate growth process by combined volume and boundary diffusion processes.

(a). The lengthening kinetics

This assumed that the grain boundary diffusion process to carry solutes within the collector plates to the precipitates sites was much faster compared with the volume diffusion process to carry solutes to the collector plate. The precipitate growth rate was therefore controlled by the process of the solute from the grains diffusing to the collector plates through volume diffusion.

By Fick's first law, the solute supply for the growth of a grain boundary precipitate, $\frac{dm}{dt}$, is given by:

$$\frac{dm}{dt} = A_v D_I \frac{\partial}{\partial y}[X(y,t)]_{y=0} \qquad (2.3.1)$$

where A_v is the area of constant square collector plate, D_I is the volume diffusion coefficient for the solute in the matrix at ageing temperature, T, y is distance from grain boundary outwards into the grain, t is the ageing time, X(y,t) is the composition of the solute.

Using an error function solution of Fick's second law for X(y,t), which is

$$X(y,t) = (x_\alpha - x_{\alpha T}^{\alpha\theta})\rho_\alpha erf(\frac{y}{2\sqrt{D_l t}}) + x_{\alpha T}^{\alpha\theta}\rho_\alpha \qquad (2.3.2)$$

in Equation (2.3.1):

$$\frac{dm}{dt} = \frac{A_v(x_\alpha - x_{\alpha T}^{\alpha\theta})\rho_\alpha D_l^{\frac{1}{2}}}{\pi^{\frac{1}{2}} t^{\frac{1}{2}}} \qquad (2.3.3)$$

where ρ_α is the molar density of matrix phase, x_α is solute concentration of the matrix phase, $x_{\alpha T}^{\alpha\theta}$ is the solute concentration in equilibrium with the precipitate phase and matrix at temperature, T.

The amount of new precipitate phase, into which this flux converted is given by

$$\frac{dm}{dt} = \frac{dm}{dV}\frac{dV}{dt} \qquad (2.3.4)$$

where

$$\frac{dm}{dV} = (x_\theta - x_{\alpha T}^{\alpha\theta})\rho_\theta \qquad (2.3.5)$$

where V is the half volume of the newly created precipitate phase, ρ_θ is the molar density of precipitate phase, x_θ is the solute concentration in precipitate phase.

The increase in half-volume of a disc-shape precipitate particle, $\frac{dV}{dt}$, is:

$$\frac{dV}{dt} = 2\bar{s}\pi L\frac{dL}{dt} \qquad (2.3.6)$$

where $\bar{s}$ is the thickness-connected term of the precipitate.

Substituting Equations (2.3.5) and (2.3.6) into Equation (2.3.4) yields

$$\frac{dm}{dt} = 2(x_\theta - x_{\alpha T}^{\alpha\theta})\rho_\theta \bar{s}\pi L\frac{dL}{dt} \qquad (2.3.7)$$

Equating Equation (2.3.3) and (2.3.7) yields

$$\frac{dL}{dt}=\frac{A_v D_l^{\frac{1}{2}}(x_\alpha - x_{\alpha T}^{\alpha\theta})\rho_\alpha}{2\pi^{\frac{1}{2}}(x_\theta - x_{\alpha T}^{\alpha\theta})\bar{s}\rho_\theta L t^{\frac{1}{2}}} \qquad (2.3.8)$$

In order to integrate Equation (2.3.8), one needs to know the time dependence of $\bar{s}$. Two limiting cases exist, $\bar{s}$ =constant and, $\bar{s}$ =s, where s is the true thickness of the precipitate; the latter makes the equation complicated with no improvement in accuracy. The former assumptions permit immediate integration of Equation (2.3.8). This assumption was considered in Aaron and Aaronson's treatment and $\bar{s}$ assumed to be equal to the radius of curvature, r. Therefore the integration of Equation (2.3.8) yields

$$L = k_1 t^{\frac{1}{2}} \qquad (2.3.9)$$

where

$$k_1 = [\frac{2A_v D_l^{\frac{1}{2}}(x_\alpha - x_{\alpha T}^{\alpha\theta})\rho_\alpha}{\pi^{\frac{1}{2}}(x_\theta - x_{\alpha T}^{\alpha\theta})\rho_\theta r}]^{\frac{1}{2}} \qquad (2.3.10)$$

Equations (2.3.9) and (2.3.10) together give the lengthening rate of Aaron and Aaronson's model.

Aaron and Aaronson compared the results given by Equations (2.3.9) and (2.3.10) with observations for $CuAl_2$ precipitation in Al-Cu alloys, and found the index of t to be 0.22 - 0.34 experimentally while theoretically it was 0.25.

(b). Thickening kinetics

The solute concentration in matrix at the edge of a precipitate is denoted by $x_{\alpha T}^{\alpha\theta}$. Assume the broad face of a precipitate to be exactly flat only at its centre, where the mole fraction is $x_{\alpha T}^{\alpha\theta}|_{r=\infty}$ and $x_{\alpha T}^{\alpha\theta} > x_{\alpha T}^{\alpha\theta}|_{r=\infty}$. There is thus a driving force for the diffusion of the solute across the broad face of a precipitate. The thickening rate is then controlled by the diffusion of solute over the broad face of a growing

precipitate through interfacial diffusion. The cross-sectional area through which the solute can diffuse from the edges toward the centre of one face of disc-shaped precipitate is $2\pi L\delta$, where δ is the thickness of the α:θ boundary.

By Fick's First law, the rate of mass transport along this face is

$$\frac{dm}{dt} = (2\pi L\delta) D_{\alpha\theta} \frac{\partial x}{\partial L} \qquad (2.3.11)$$

where $D_{\alpha\theta}$ is the diffusivity of solute moving along the precipitate/matrix interface, or in other words the interfacial diffusion coefficient.

The average value of $\frac{\partial x}{\partial L}$ is

$$\overline{\frac{\partial x}{\partial L}} = \frac{(x_{\alpha T}^{\alpha\theta} - x_{\alpha T}^{\alpha\theta}|_{r=\infty})}{\beta L} \rho_{\alpha} \qquad (2.3.12)$$

where β is the average fraction of L which a solute atom diffuses along the α:θ boundary before it joins the θ particle; thus $0<\beta<1$. β is estimated by equating the area between L=0 and L=(1-β)L to the area between L=(1-β)L and L=L. So β is

$$\beta = 1 - \frac{\sqrt{2}}{2} \qquad (2.3.13)$$

Substituting Equation (2.3.12) into Equation (2.3.11) yields

$$\frac{dm}{dt} = 2\pi L\delta D_{\alpha\theta} \frac{(x_{\alpha T}^{\alpha\theta} - x_{\alpha T}^{\alpha\theta}|_{r=\infty})}{\beta L} \rho_{\alpha} \qquad (2.3.14)$$

This equation gives the mass flow of solute through the α:θ boundary. The amount of θ into which this flow is converted is determined by recalling that

$$\frac{dm}{dt} = \frac{dm}{dV}\frac{dV}{dt} \qquad (2.3.4)$$

where

$$\frac{dm}{dV} = (x_\theta - x_{\alpha T}^{\alpha\theta})\rho_\theta \tag{2.3.5}$$

and

$$V = \pi L^2 s \tag{2.3.15}$$

Since

$$\frac{dV}{dt} = \frac{dV}{ds} \bullet \frac{ds}{dt} \tag{2.3.16}$$

one may immediately obtain

$$\frac{dV}{dt} = \pi L^2 \frac{ds}{dt} \tag{2.3.17}$$

Substituting Equations (2.3.5) and (2.3.17) into Equation (2.3.4) yields

$$\frac{dm}{dt} = \pi L^2 (x_\theta - x_{\alpha T}^{\alpha\theta})\rho_\theta \frac{ds}{dt} \tag{2.3.18}$$

Equating the two expressions for $\frac{dm}{dt}$ (i.e. Equation (2.3.14) and (2.3.18)) yields

$$\frac{ds}{dt} = \frac{2\delta D_{\alpha\theta}(x_{\alpha T}^{\alpha\theta} - x_{\alpha T}^{\alpha\theta}|_{r=\infty})\rho_\alpha}{\beta L^2 (x_\theta - x_{\alpha T}^{\alpha\theta})\rho_\theta} \tag{2.3.19}$$

The integration of Equation (2.3.19) (where $L = k_1 t^{\frac{1}{2}}$) yields:

$$s = k_2 t^{\frac{1}{2}} \tag{2.3.20}$$

where

$$k_2 = \frac{4\delta D_{\alpha\theta}(x_{\alpha T}^{\alpha\theta} - x_{\alpha T}^{\alpha\theta}|_{r=\infty})\rho_\alpha}{\beta k_1^2 (x_\theta - x_{\alpha T}^{\alpha\theta})\rho_\theta} \tag{2.3.21}$$

Equation (2.3.20) is the thickening rate.

2.3.2 *Faulkner & Caisley 's model*[97]

Faulkner and Caisley's model is a development of Aaron and Aaronson's model by making use of the fact that the aspect ratio of small grain-boundary precipitates remains constant.

By bringing in such a constant aspect ratio, k', Faulkner and Caisley gave the description of the length of a disc-shape precipitate as L=k's and the half volume of a precipitate as

$$V = \pi k'^2 s^3 \tag{2.3.22}$$

and

$$\frac{dV}{dt} = 3\pi k'^2 s^2 \frac{ds}{dt} \tag{2.3.23}$$

Faulkner and Caisley considered in their treatment that the rate-determining step was either the rate of solute atom arrival from the adjacent grain to the collector plate or diffusion associated with transferring solute along the α:θ interface. If the former of these possibilities is true, then Equation (2.3.3) can be used to describe the rates of solute atom supply for both thickening and lengthening. The amount of θ phase formed as a result of the transformation of solute atom supply rate is given by Equation (2.3.4). Bringing Equations (2.3.5) and (2.3.23) into (2.3.4), gives:

$$\frac{dm}{dt} = 3\pi k'^2 s^2 (x_\theta - x_{\alpha T}^{\alpha\theta})\rho_\theta \frac{ds}{dt} \tag{2.3.24}$$

Equating Equations(2.3.3) and (2.3.24) yields

$$\frac{ds}{dt}=\frac{A_v D_l^{\frac{1}{2}}(x_\alpha - x_{\alpha T}^{\alpha\theta})t^{-\frac{1}{2}}\rho_\alpha}{3\pi^{\frac{1}{2}}k'^2 s^2(x_\theta - x_{\alpha T}^{\alpha\theta})\rho_\theta} \tag{2.3.25}$$

integrating Equation (2.3.25) yields

$$s=[\frac{4A_v^2 D_l(x_\alpha - x_{\alpha T}^{\alpha\theta})^2\rho_\alpha^2}{\pi^3 k'^4(x_\theta - x_{\alpha T}^{\alpha\theta})^2\rho_\theta^2}]^{\frac{1}{6}}t^{\frac{1}{6}} \tag{2.3.26}$$

and

$$L=[\frac{4A_v^2 D_l k'^2(x_\alpha - x_{\alpha T}^{\alpha\theta})^2\rho_\alpha^2}{\pi^3(x_\theta - x_{\alpha T}^{\alpha\theta})^2\rho_\theta^2}]^{\frac{1}{6}}t^{\frac{1}{6}} \tag{2.3.27}$$

Alternatively, if it is assumed that the rate-controlling solute atom transfer mechanism is the diffusion of the solute along the interface rather than the arrival of solute at the rim of the particle from the collector plate, then Equation (2.3.14) must equated to Equation (2.3.24) and

$$\frac{ds}{dt}=\frac{2\delta D_{\alpha\theta}(x_{\alpha T}^{\alpha\theta} - x_{\alpha T}^{\alpha\theta}|_{r=\infty})\rho_\alpha}{3\beta(k's)^2(x_\theta - x_{\alpha T}^{\alpha\theta})\rho_\theta} \tag{2.3.28}$$

integrating Equation (2.3.28) gives

$$s=[\frac{2\delta D_{\alpha\theta}(x_{\alpha T}^{\alpha\theta} - x_{\alpha T}^{\alpha\theta}|_{r=\infty})\rho_\alpha}{\beta k'^2(x_\theta - x_{\alpha T}^{\alpha\theta})\rho_\theta}]^{\frac{1}{3}}t^{\frac{1}{3}} \tag{2.3.29}$$

and

$$L=[\frac{2\delta D_{\alpha\theta}k'(x_{\alpha T}^{\alpha\theta} - x_{\alpha T}^{\alpha\theta}|_{r=\infty})\rho_\alpha}{\beta(x_\theta - x_{\alpha T}^{\alpha\theta})\rho_\theta}]^{\frac{1}{3}}t^{\frac{1}{3}} \tag{2.3.30}$$

The conclusion of Caisley and Faulkner's model is that the linear dimension of a precipitate is proportional to $(time)^{\frac{1}{3}}$ for collector plate diffusion control and it is proportional to $(time)^{\frac{1}{2}}$ for interface diffusion control.

2.3.3 *Carolan & Faulkner's model*[99]

In their work on carbide precipitation in Alloy 800, Carolan and Faulkner discovered that the Aaron and Aaronson's collector plate growth model for grain boundary precipitation was inadequate to fully explain growth at early stages (up to particle diameters of 100nm). Further analysis of the model found that the maximum boundary diffusion distance for Cr in Alloy 800 is three orders of magnitude smaller than the experimentally measured mean collector plate size. This is a fundamental inadequacy of the constant area collector plate model. Carolan and Faulkner developed a new precipitate growth theory in which they introduced the concept of a time dependent collector plate area (i.e. variable collector plate area) to overcome inadequacies of the Aaron and Aaronson's model. Different precipitate morphologies (disc, cap, faceted, and conical) were considered in Carolan and Faulkner's treatment.

Considering different precipitate morphologies, Carolan and Faulkner expressed the half volume of a precipitate as

$$V = f(\psi)\pi L^3 \qquad (2.3.31)$$

where $f(\psi)$ is a morphological factor.

The definitions of $f(\psi)$ for disc, cap, faceted and conical morphologies are given in Table 2.3.1[99].

Table 2.3.1: Morphological factor and profile view of morphology.

morphology	$f(\psi)$	Profile view
Disc	$(\frac{1}{k'})$	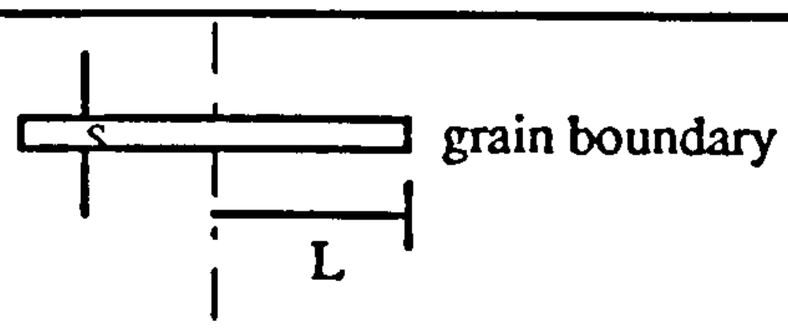
Cap	$\frac{2-3\cos\psi+\cos^3\psi}{3\sin^3\psi}$	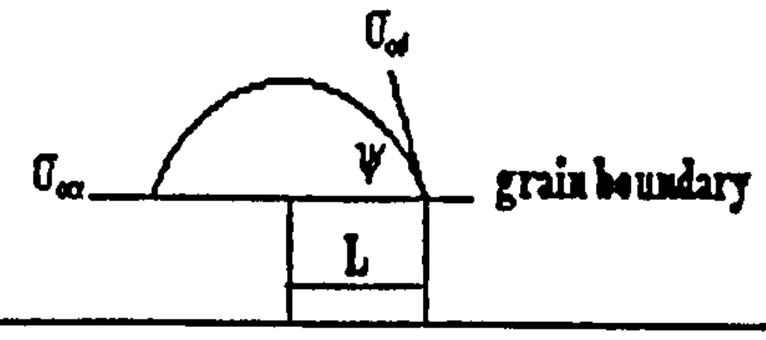
Facet	$\frac{3\cos\phi-3\cos\psi-\cos^3\phi+\cos^3\psi}{3\sin^3\psi}$	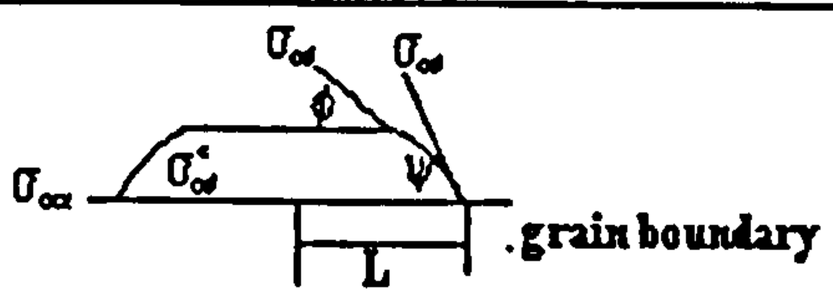
conical	$\frac{\tan\theta}{3}$	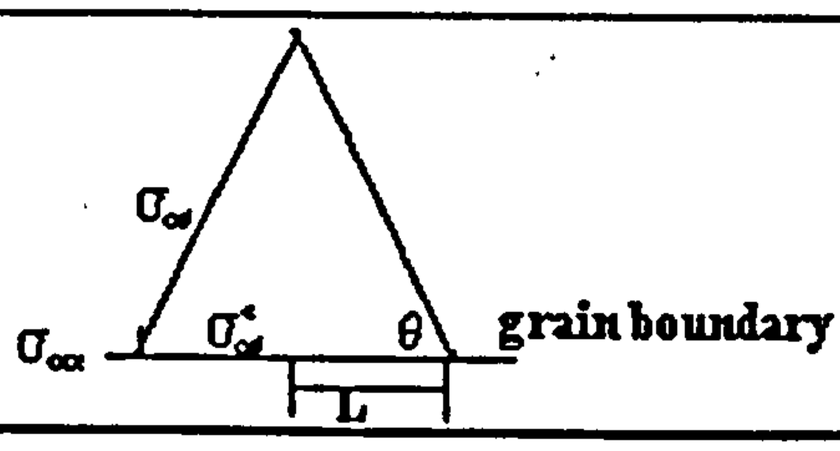

Bringing Equations (2.3.31) and (2.3.5) into Equation (2.3.4) yields

$$\frac{dm}{dt}=3\pi\rho_\theta(x_\theta-x_{\alpha T}^{\alpha\theta})L^2f(\psi)\frac{dL}{dt} \qquad (2.3.32)$$

Equating equations(2.3.32) and (2.3.3) yields

$$t^{-\frac{1}{2}}dt=\frac{3\pi^{\frac{1}{2}}\rho_\theta(x_\theta-x_{\alpha T}^{\alpha\theta})L^2f(\psi)}{(x_\alpha-x_{\alpha T}^{\alpha\theta})A_vD_l^{\frac{1}{2}}\rho_\alpha}dL \qquad (2.3.33)$$

This equation can be integrated to yield a solution for precipitate size (L) in terms of ageing time (t) or vice versa after bringing in the definition of A_v.

Carolan and Faulkner introduced a time dependent collector plate area (A_v) for circular and square shape. The maximum value of A_v at any time, t, is defined as follows.

For circular variable collector plate:

$$A_v = 4\pi D_b t \qquad (2.3.34)$$

where D_b is the boundary diffusion coefficient at temperature, T. An illustration of this kind of collector plate model is given in Fig. 2.3.2

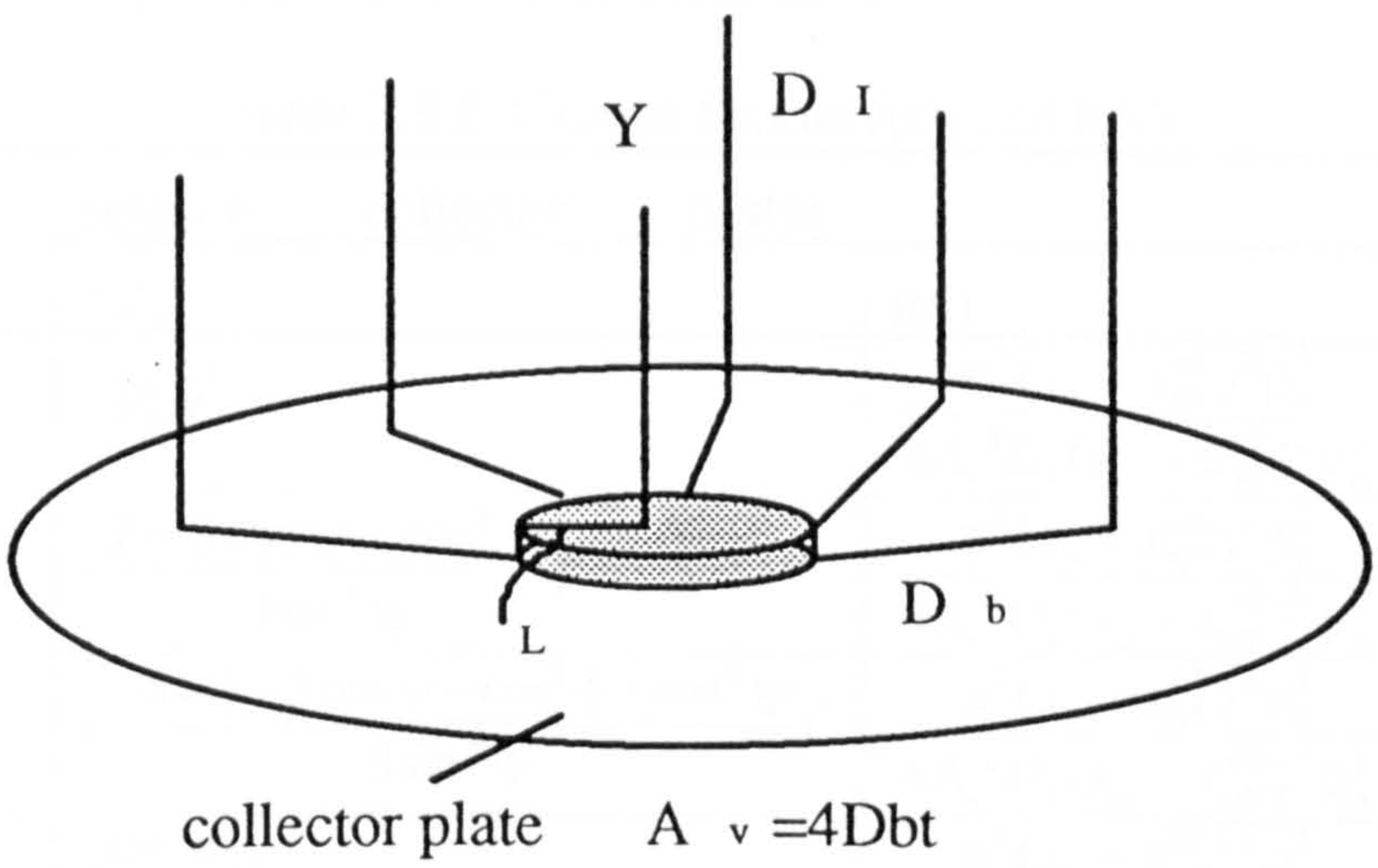

Fig. 2.3.2: Illustration of precipitate growth process by combined volume and boundary diffusion processes through a variable circular collector plate.

For square variable collector plate:

$$A_v = 16 D_b t \qquad (2.3.35)$$

The value of A_v both constant and defined by Equation (2.3.34) are substituted into Equation (2.3.33) and integrated to give the prediction of time, t in terms of L for the constant square and variable circular collector plates respectively

$$t = \frac{\pi^3 \rho_\theta^2 (x_\theta - x_{\alpha T}^{\alpha\theta})^2 L^6 f^2(\psi)}{4(x_\alpha - x_{\alpha T}^{\alpha\theta})^2 A_v^{\,2} D_I \rho_\alpha^2} \qquad \text{(for constant square collector plate)} \quad (2.3.36)$$

$$t = \left[\frac{3\pi^{\frac{1}{2}} \rho_\theta (x_\theta - x_{\alpha T}^{\alpha\theta}) L^3 f(\psi)}{8(x_\alpha - x_{\alpha T}^{\alpha\theta}) D_b D_I^{\frac{1}{2}} \rho_\alpha}\right]^{\frac{2}{3}} \qquad \text{(for variable circular collector plate)} \quad (2.3.37)$$

As a summary, Carolan and Faulkner's precipitate growth theory is:

$$t = f(D)f(X)L^6 \qquad \text{(for constant square collector plate)} \qquad (2.3.38)$$

$$t = f(D)f(X)L^2 \qquad \text{(for variable circular collector plate)} \qquad (2.3.39)$$

The value of f(D) and f(X) are tabulated for all combinations of collector plate and precipitation morphology variations in Table 2.3.2.

Table 2.3.2: Growth factors f(D) and f(X).

constant	**square**	**collector**	**plate:**
morphology	**f(X)**		**f(D)**
Disc	$(1/k')^2$		$\frac{\pi^3(x_\theta - x_{\alpha T}^{\alpha\theta})^2\rho_\theta^2}{4A_v^2 D_l (x_\alpha - x_{\alpha T}^{\alpha\theta})^2\rho_\alpha^2}$
Cap	$(\frac{2-3\cos\psi+\cos^3\psi}{3\sin^3\psi})^2$		$\frac{\pi^3(x_\theta - x_{\alpha T}^{\alpha\theta})^2\rho_\theta^2}{4A_v^2 D_l (x_\alpha - x_{\alpha T}^{\alpha\theta})^2\rho_\alpha^2}$
Facet	$(\frac{3\cos\phi-3\cos\psi-\cos^3\phi+\cos^3\psi}{3\sin^3\psi})^2$		$\frac{\pi^3(x_\theta - x_{\alpha T}^{\alpha\theta})^2\rho_\theta^2}{4A_v^2 D_l (x_\alpha - x_{\alpha T}^{\alpha\theta})^2\rho_\alpha^2}$
conical	$(\frac{\tan\theta}{3})^2$		$\frac{\pi^3(x_\theta - x_{\alpha T}^{\alpha\theta})^2\rho_\theta^2}{4A_v^2 D_l (x_\alpha - x_{\alpha T}^{\alpha\theta})^2\rho_\alpha^2}$
variable	**circular collector**	**plate:**	
morphology	**f(X)**		**f(D)**
Disc	$(1/k')^{\frac{3}{2}}$		$[\frac{3\pi^{\frac{1}{2}}(x_\theta - x_{\alpha T}^{\alpha\theta})\rho_\theta}{8D_l^{\frac{1}{2}}D_b(x_\alpha - x_{\alpha T}^{\alpha\theta})\rho_\alpha}]^{\frac{2}{3}}$
Cap	$(\frac{2-3\cos\psi+\cos^3\psi}{3\sin^3\psi})^{\frac{3}{2}}$		$[\frac{3\pi^{\frac{1}{2}}(x_\theta - x_{\alpha T}^{\alpha\theta})\rho_\theta}{8D_l^{\frac{1}{2}}D_b(x_\alpha - x_{\alpha T}^{\alpha\theta})\rho_\alpha}]^{\frac{2}{3}}$
Facet	$(\frac{3\cos\phi-3\cos\psi-\cos^3\phi+\cos^3\psi}{3\sin^3\psi})^{\frac{2}{3}}$		$[\frac{3\pi^{\frac{1}{2}}(x_\theta - x_{\alpha T}^{\alpha\theta})\rho_\theta}{8D_l^{\frac{1}{2}}D_b(x_\alpha - x_{\alpha T}^{\alpha\theta})\rho_\alpha}]^{\frac{2}{3}}$
conical	$(\frac{\tan\theta}{3})^{\frac{2}{3}}$		$[\frac{3\pi^{\frac{1}{2}}(x_\theta - x_{\alpha T}^{\alpha\theta})\rho_\theta}{8D_l^{\frac{1}{2}}D_b(x_\alpha - x_{\alpha T}^{\alpha\theta})\rho_\alpha}]^{\frac{2}{3}}$
variable	**square**	**collector**	**plate:**
morphology	**f(X)**		**f(D)**
Disc	$(1/k')^{\frac{3}{2}}$		$[\frac{3\pi(x_\theta - x_{\alpha T}^{\alpha\theta})\rho_\theta}{8D_l^{\frac{1}{2}}D_b(x_\alpha - x_{\alpha T}^{\alpha\theta})\rho_\alpha}]^{\frac{2}{3}}$
Cap	$(\frac{2-3\cos\psi+\cos^3\psi}{3\sin^3\psi})^{\frac{3}{2}}$		$[\frac{3\pi(x_\theta - x_{\alpha T}^{\alpha\theta})\rho_\theta}{8D_l^{\frac{1}{2}}D_b(x_\alpha - x_{\alpha T}^{\alpha\theta})\rho_\alpha}]^{\frac{2}{3}}$
Facet	$(\frac{3\cos\phi-3\cos\psi-\cos^3\phi+\cos^3\psi}{3\sin^3\psi})^{\frac{2}{3}}$		$[\frac{3\pi(x_\theta - x_{\alpha T}^{\alpha\theta})\rho_\theta}{8D_l^{\frac{1}{2}}D_b(x_\alpha - x_{\alpha T}^{\alpha\theta})\rho_\alpha}]^{\frac{2}{3}}$
conical	$(\frac{\tan\theta}{3})^{\frac{2}{3}}$		$[\frac{3\pi(x_\theta - x_{\alpha T}^{\alpha\theta})\rho_\theta}{8D_l^{\frac{1}{2}}D_b(x_\alpha - x_{\alpha T}^{\alpha\theta})\rho_\alpha}]^{\frac{2}{3}}$

2.4 *The coarsening kinetics of grain boundary precipitates*

When the growth of the precipitates from supersaturated solid solution is complete, further ageing leads to precipitate coarsening driven by the interfacial free energy between the precipitate and the matrix - the process known as Ostwald ripening. The physical process by which the microstructure coarsens and releases its excess surface energy is due to the higher solubility of small particles, since these have a larger ratio of surface area to volume. The larger particles thus grow at the expense of the smaller ones. The relationship of the radius of the grain boundary precipitate with ageing time, L(t), during coarsening is given as follows according to Kirchner's theory(1971)[100]:

$$L(t)=[\frac{9d_0D_b\sigma_{\alpha\theta}x_{\alpha T}^{\alpha\theta}V_\theta(t-t_{cc})}{32ABRT}+L_g^4]^{\frac{1}{4}} \qquad (2.4.1)$$

where L_g is the mean radius of the grain boundary precipitates before the start of coarsening; t_{cc} is the critical time of the onset of coarsening; d_0 is the grain-boundary thickness; T is the ageing temperature; t is the ageing time at temperature, T; D_b is the grain boundary diffusion coefficient; $\sigma_{\alpha\theta}$ is the interfacial free energy of the precipitate/matrix interface; A is the parameter defined by

$$A=\frac{2}{3}(1-\frac{\sigma_{\alpha\alpha}}{2\sigma_{\alpha\theta}}) \qquad (2.4.2)$$

where $\sigma_{\alpha\alpha}$ is the grain boundary energy;

$$\sigma_{\alpha\alpha}=2\sigma_{\alpha\theta}\cos(\psi) \qquad (2.4.3)$$

B is the parameter defined by

$$B=\frac{1}{2}\ln(\frac{1}{f}) \qquad (2.4.4)$$

where f is the fraction of the grain boundary covered precipitates given by

$$f=\frac{\pi L_c^2}{A_v} \qquad (2.4.5)$$

where A_v is the mean collector plate area at time, t_{cc}.

Chapter Three

Theory (II)

- New Developments of Theories of Grain Boundary Segregation, Nucleation And Precipitation

3.1 *The developments of non-equilibrium segregation model*

As shown in Fig. 2.1.2a the solute concentration profile predicted by Faulkner's non-equilibrium segregation model during segregation process is not well in line with the real situation. Xu & Song's model predicts that the solute concentration of the solute concentrated layer (SCL) changes with time. In Xu & Song's model, the width of the SCL is assumed to be width of three atomic layers. This may not be true as the spatial extent of the segregant solute redistribution may extend to hundreds of atomic layers for non-segregation. Hence it is necessary to construct a new non-equilibrium segregation model. The new model is expected to give a more realistic prediction of the solute concentration profile during the segregation. Two new non-equilibrium segregation models are generated. These models are produced by using both analytical and numerical approaches.

3.1.1 *Numerical model of non-equilibrium segregation*

a. During segregation

The model assumes that the solute concentration distribution of non-equilibrium segregation during the segregation process has a form as shown in Fig. 3.1.1. In Fig. 3.1.1 region 1, whose width is w_{0l}, is the solute concentrated layer (SCL) where the solute concentration is C_b given by Equation (2.1.8) according to Faulkner's formula[70]. Region 2 whose width is w_l is the solute depleted layer (SDL). Depletion of the solute atoms in region 2 is converted to the segregant of the solute in region 1. During heat treatment, both w_{0l} and w_l change with time.

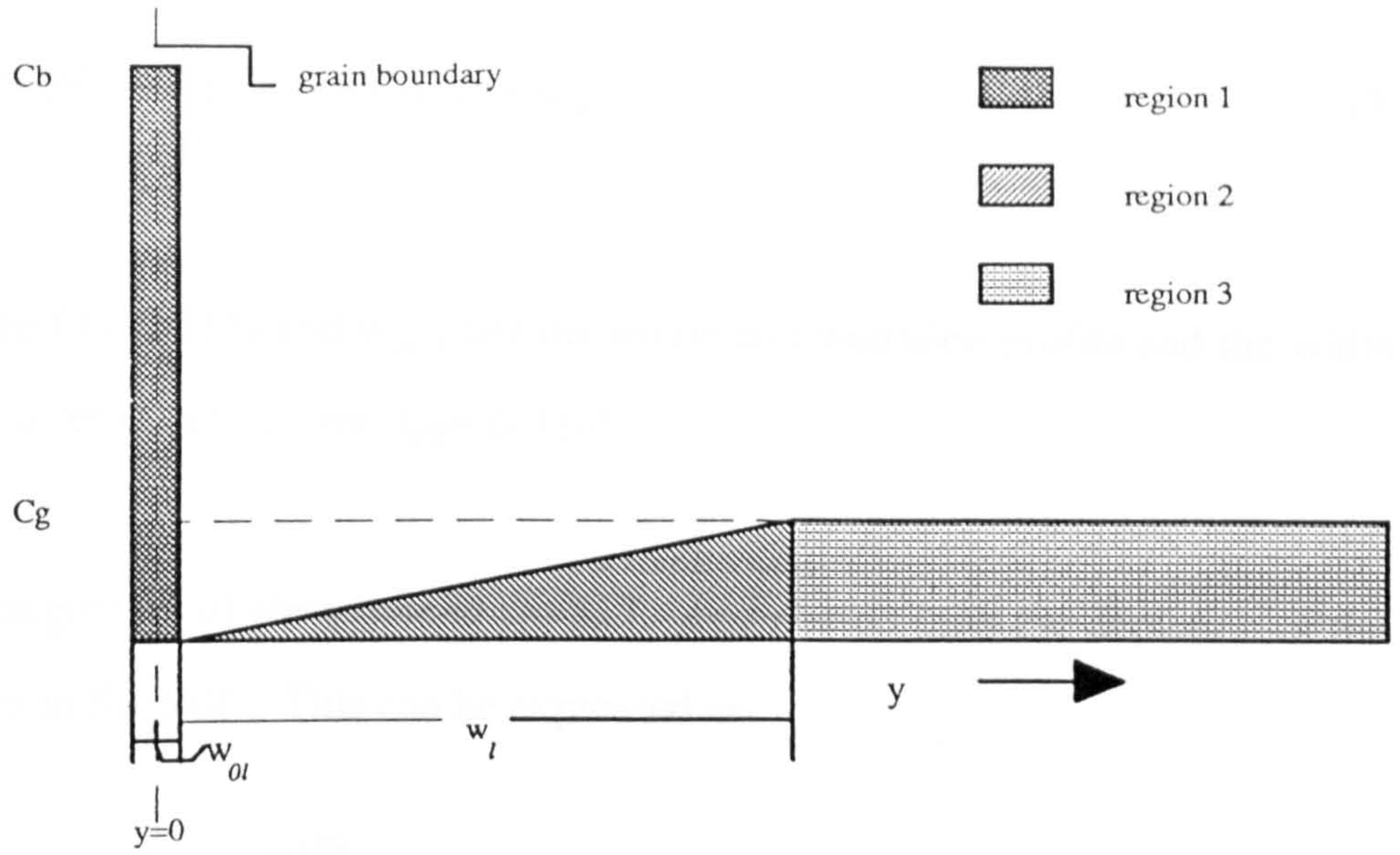

Fig. 3.1.1: Solute concentration profile after effective time t_{eff}.

Modelling starts from dividing the effective time, t_{eff}, into intervals of Δ such that $t_{eff} = l \bullet \Delta$. l is an integer. Δ is chosen to be so small that within it the solute concentration distribution can be considered as constant. Thus the distribution of the solute concentration changes with time in stages of Δ. At the ith stage ($1 \le i \le l$), which is the time, $t_{eff} = i \bullet \Delta$, the solute concentration profile is $C(y, i \bullet \Delta)$, the width of the SCL (region 1 in Fig. 3.1.1) is w_{0i} and the width of the SDL (region 2 in Fig. 3.1.1) is w_i.

During the period of time, $t_{eff} = (i-1) \cdot \Delta \sim t_{eff} = i \cdot \Delta$, all the impurity atoms, which at the time $t_{eff} = (i-1) \cdot \Delta$ are distributed within the distance of $\sqrt{2 D_{ci} \Delta}$ from the SCL/SDL interface to the interior grain formed after effective time $t_{eff} = (i-1) \cdot \Delta$, are drawn to the SCL through the diffusion of vacancy-impurity complexes. $\sqrt{2 D_{ci} \Delta}$ is the mean diffusion distance of the vacancy-impurity complexes during a time interval. These solute atoms are accumulated in the layer in contact with the SCL and a SCL with a new width is formed. The width of the SCL when the effective time reaches the time that $t_{eff} = i \cdot \Delta$ is w_{0i} given by:

$$w_{0i} = \frac{2}{C_b} \int_{\frac{w_{0i-1}}{2}}^{\sqrt{2D_a\Delta}+\frac{w_{0i-1}}{2}} C(y,(i-1)\Delta)dy + w_{0i-1} \qquad (3.1.1)$$

where C(y,(i-1)Δ) and w_{0i-1} are the solute concentration profile and the width of the SCL after effective time, t_{eff}= (i-1)•Δ.

The segregant of the solute in the SCL is converted from the depletion of the solute atoms in the SDL. This can be expressed as

$$\frac{w_{0i}}{2} \cdot C_b = w_i \cdot C_s - \int_{\frac{w_{0i}}{2}}^{w_i+\frac{w_{0i}}{2}} c(y,i\Delta)dy \qquad (3.1.2)$$

where c(y,iΔ) is the concentration profile in the SDL at time t_{eff}= i•Δ and w_i is the width of this layer.

As a simplification, c(y,iΔ) is assumed to have a linear relation with the distance like

$$c(y,i\Delta) = (y - \frac{w_{0i}}{2}) \cdot C_s \Big/ w_i \qquad (3.1.3)$$

Therefore Equation (3.1.2) can have the form

$$\frac{w_{0i}}{2} \cdot C_b = \frac{w_i C_s}{2} \qquad (3.1.4)$$

and

$$w_i = \frac{w_{0i} C_b}{C_s} \qquad (3.1.5)$$

The solute concentration profile, $C(y,t_{eff})$, at the ith stage is:

$$\begin{cases} C(y,t_{eff}) = C_b & (\text{ if } y \le \frac{w_{0i}}{2}) \\ C(y,t_{eff}) = c(y,t_{eff}) = \frac{(2y - w_{0i})C_g}{2w_i} & (\text{if } \frac{w_{oi}}{2} < y \le w_i + \frac{w_{0i}}{2}, w_i = \frac{w_{0i}C_b}{C_g}) \\ C(y,t_{eff}) = C_g & (\text{if } y > w_i + \frac{w_{0i}}{2}, w_i = \frac{w_{0i}C_b}{C_g}) \end{cases} \quad (3.1.6)$$

when i=1, $C(y,(i-1)\Delta)=C_g$, $w_{0i-1}=0$ and $w_{0i} = \frac{2}{C_b}\int_0^{\sqrt{2D_{ai}\Delta}} C_g dy$

The iteration carries on from i=1 till i=l at which point, $C(y,l\Delta)$ is the solute concentration profile of non-equilibrium segregation during the segregation process after effective time, $t_{eff} = l \bullet \Delta$.

b. During de-segregation

When t_{eff} exceeds a critical time, t_c given by Equation (2.2.16), de-segregation becomes dominant and the solute concentration profile is governed by Equation (2.2.17).

3.1.2 *Numerical-analytical model of non-equilibrium segregation*

This segregation model is established by artificially distinguishing the situation during ageing from that during quenching and predicts the solute concentration profile during the quenching and during ageing separately. The reason for this is that the thermodynamic relationship of segregation (see Equation (2.1.8)) may become unsuitable when the material is aged at a temperature lower than t_{mp} after quenched from solution treatment temperature. This is the case for the ageing treatments for 7150 aluminium alloy. During ageing, the width of solute concentrated layer (SCL) will stop increasing with ageing time. The diffusion of impurity-vacancy complexes down the concentration gradients between the grain centre and the SCL/SDL interface created during quench brings the solute atoms towards grain boundaries.

Such arriving solute atoms from grain centre will stay in the vicinity of the solute concentrated layer (SDL) to relieve the depletion situation of the solute in the area adjacent to the SCL.

(1). During segregation

(a). During quench

During quench the solute concentration profile takes the same form as that given by Equation (3.1.6).

$$\begin{cases} C(y,t_{eff}) = C_b & (\text{if } y \le \frac{w_{0i}}{2}) \\ C(y,t_{eff}) = c(y,t_{eff}) = \frac{(2y - w_{0i})C_g}{2w_i} & (\text{if } \frac{w_{oi}}{2} < y \le w_i + \frac{w_{0i}}{2}, w_i = \frac{w_{0i}C_b}{C_g}) \\ C(y,t_{eff}) = C_g . & (\text{if } y > w_i + \frac{w_{0i}}{2}, w_i = \frac{w_{0i}C_b}{C_g}) \end{cases} \quad (3.1.6)$$

where $t_{eff} \le t_q$.

By substituting Equation (3.1.6) into Equation (3.1.1) to calculate w_{0i} and iterating the calculation from i=1 to i=l_q, where l_q is an integer given by $l_q = t_q/\Delta$, we can have w_0, the width of the solute concentrated layer (SCL) after quench.

The width of the solute depleted layer after quench, w, is

$$w = \frac{w_0 C_b}{C_g} \quad (3.1.7)$$

Fig. 3.1.2 is the illustration of the solute concentration profile at a typical grain boundary area in our analysis after quenching and before the beginning of ageing.

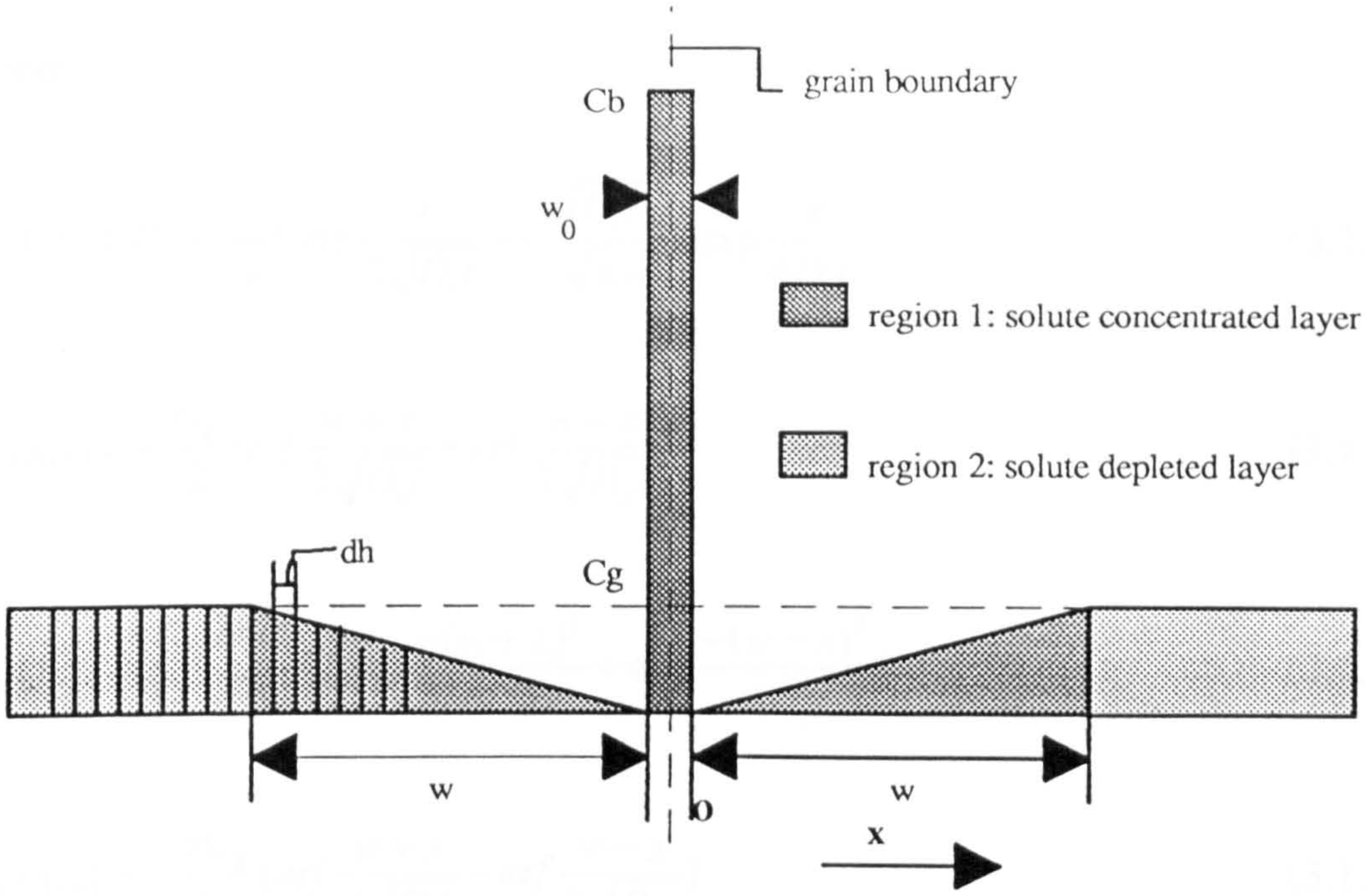

Fig. 3.1.2: Solute concentration profile at a typical grain boundary area in our analysis after quenching and before the beginning of ageing.

(b).During ageing

During ageing, the segregation concentration profile is described by c(x,t), where x is the distance from the SCL/SDL interface into the interior grain as shown in Fig. 3.1.2, $x = y - w_0/2$, t is the ageing time at ageing temperature T.

c(x,t) is the solution of Diffusion Equation and should satisfy the initial condition, which is the concentration profile after quench and before ageing.

$$\frac{\partial c(x,t)}{\partial t} = D_c \frac{\partial^2 c(x,t)}{\partial t^2} \qquad (3.1.8)$$

$$\begin{cases} c(x,0) = \dfrac{x}{w} C_g & (x \le w) \\ c(x,0) = C_g & (x \ge w) \end{cases} \qquad (3.1.9)$$

$$c(x,t) = c_I(x,t) + c_{II}(x,t) + c_{III}(x,t) + c_{IV}(x,t) \qquad (3.1.10)$$

where

$$c_I(x,t) = C_g + \frac{xC_g}{w} erf \frac{x}{2\sqrt{D_c t}} + \frac{2\sqrt{D_c t}C_g}{\sqrt{\pi}w} \exp \frac{-x^2}{4D_c t} \qquad (3.1.11)$$

$$c_{II}(x,t) = -\frac{C_g}{2}(erf \frac{w+x}{2\sqrt{D_c t}} + erf \frac{w-x}{2\sqrt{D_c t}}) \qquad (3.1.12)$$

$$c_{III}(x,t) = -\frac{\sqrt{D_c t}C_g}{\sqrt{\pi}w}[\exp \frac{-(w+x)^2}{4D_c t} + \exp \frac{-(w-x)^2}{4D_c t}] \qquad (3.1.13)$$

$$c_{IV}(x,t) = -\frac{xC_g}{2w}(erf \frac{w+x}{2\sqrt{D_c t}} - erf \frac{w-x}{2\sqrt{D_c t}}) \qquad (3.1.14)$$

Following is the derivation of c(x,t):

The Gauss solution of Diffusion Equation is

$$C = \frac{S}{\sqrt{4\pi D_c t}} \exp \frac{-x^2}{4D_c t} \qquad (3.1.a)$$

where S is the amount of diffusion component, which is held constant from the beginning of the diffusion process to the end. The diffusion process described by the Gauss solution is that at the beginning the diffusion component is all concentrated in a infinitesimal region at the boundary face.

In this case, the diffusion component (the solute-vacancy complexes) is distributed in an infinite region at the beginning of the diffusion process. We can divide the infinite region into intervals of dh (as shown in Fig. 3.1.2). dh is chosen to be so small that each interval can be taken as a infinitesimal part and the Gauss solution can be used in every infinitesimal part. Then, according to the principle of

superposition, the solution for the infinite region is the sum of all the Gauss solutions for the infinitesimal parts.

The amount of diffusion component in each infinitesimal part is

$$S = c(h,t)|_{t=0} \cdot dh \tag{3.1.b}$$

where $c(h,t)|_{t=0}$ which is given by Equation (3.1.9) is the concentration profile after quench and before ageing, dh is the width of an infinitesimal part.

$$c(x,t) = \frac{1}{\sqrt{4\pi D_c t}} \int_{-\infty}^{+\infty} c(h,t)|_{t=0} \cdot \exp \frac{-(x-h)^2}{4D_c t} dh \tag{3.1.c}$$

Consider the solute concentrated layer(region 1 in Fig. 3.1.2) as a channel where complexes can freely pass from one side of the grain to another side, we can ignore the influence of its existence on the solution of the diffusion equation during the solving of the diffusion equation. Therefore, we can have Equation (3.1.c) further written as

$$\begin{aligned} c(x,t) = & \frac{1}{\sqrt{4\pi D_c t}} \left[\int_{-\infty}^{-w} C_g \cdot \exp \frac{-(x-h)^2}{4D_c t} dh + \int_{-w}^{0} \left(\frac{-hC_g}{w} \right) \cdot \exp \frac{-(x-h)^2}{4D_c t} dh \right] \\ & + \frac{1}{\sqrt{4\pi D_c t}} \left[\int_{0}^{w} \left(\frac{hC_g}{w} \right) \cdot \exp \frac{-(x-h)^2}{4D_c t} dh + \int_{w}^{+\infty} C_g \cdot \exp \frac{-(x-h)^2}{4D_c t} dh \right] \end{aligned} \tag{3.1.d}$$

Integrating the right side of Equation (3.1.d) yields Equations (3.1.10) - (3.1.14).

An illustration of the segregation concentration profiles given by the newly generated numerical-analytical non-equilibrium segregation model during the segregation process is given in Fig. 3.1.3.

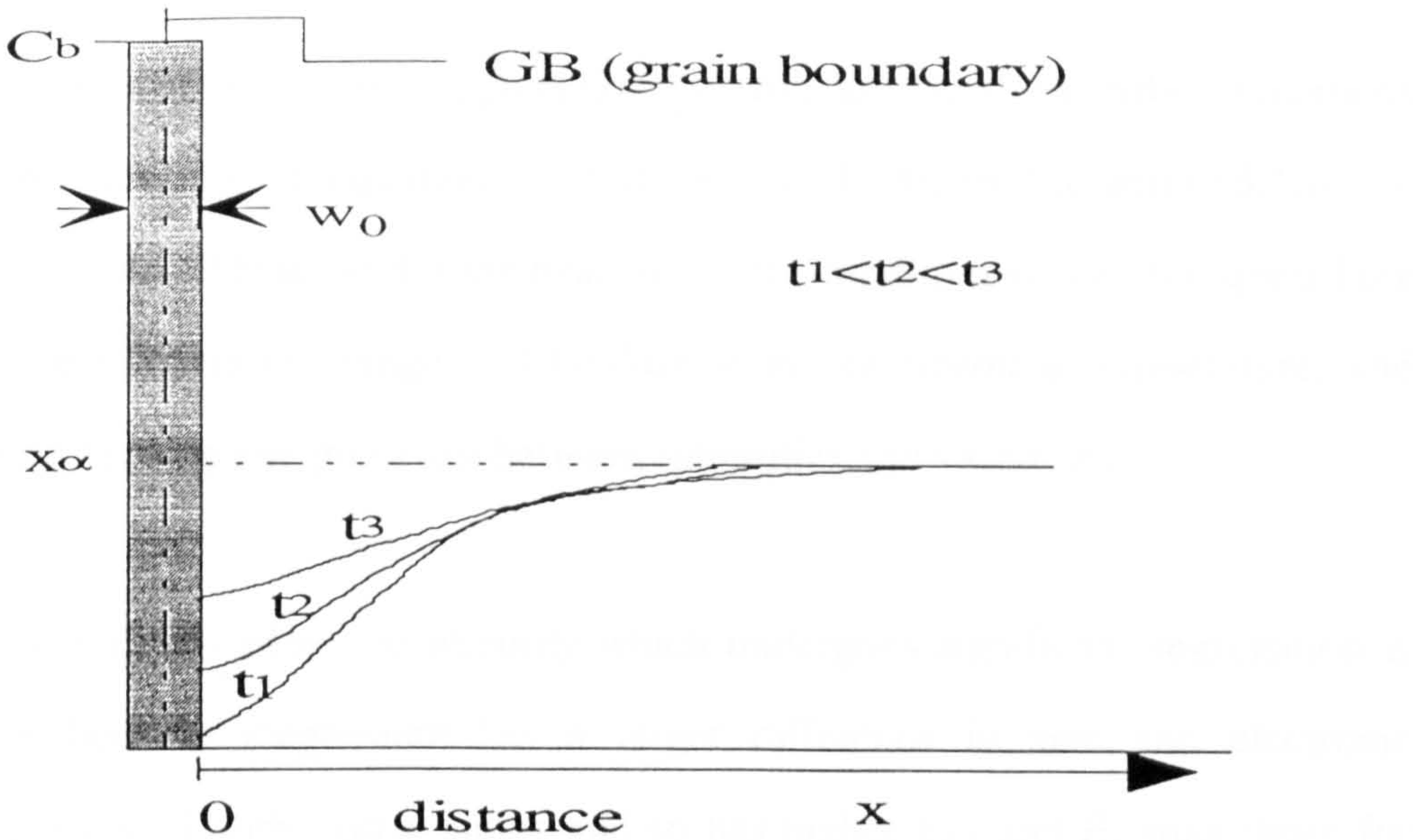

Fig. 3.1.3: Illustration of the segregation concentration profiles predicted by the newly generated numerical-analytical non-equilibrium segregation model during the segregation process.

(2). During de-segregation

When the effective time t_{eff} exceeds a critical time, t_c given by Equation (2.2.16), de-segregation becomes dominant and the solute concentration profile is governed by Equation (2.2.17).

3.1.3 *Combined equilibrium and non-equilibrium segregation*

Segregation either equilibrium, or non-equilibrium, could happen during a heat treatment process with one of them dominant.

For a heat-treatment process that does not encourage non-equilibrium segregation to occur, i.e. very slow cooling to a very low temperature and holding at a low temperature, the result of combined equilibrium and non-equilibrium segregation is equilibrium segregation controlling governed by Equation (2.1.2).

Segregation is non-equilibrium segregation control, governed by either Equations (2.1.15) and (2.1.17), or Equations (2.1.18) and (2.1.24), or Equation (3.1.6), or Equation (3.1.10). These hold if the heat-treatment condition is one that quenching from a large temperature range and holding at an intermediate temperature, and where strong binding energies exist between impurities and vacancies.

For 7150 aluminium alloy, the impurity which undergoes significant segregation is magnesium because magnesium has a larger difference in size and electronic structure compared with matrix atoms and so has higher E_{b1} and E_b than those for zinc and copper.

3.2 *Nucleation kinetics of grain boundary precipitation*

The work of other researchers[90, 91, 92] is used to analyse the nucleation of $MgZn_2$ grain boundary precipitates in 7150 aluminium alloy.

3.2.1 *The number of the critical precipitate nuclei at the grain boundary*

3.2.1.1 *Before combined with segregation*

By adapting Russell's equation for the number of critical nuclei per unit volume[90], we can have the number of the critical precipitate nuclei per unit area of grain boundary, N_0, as follows:

$$N_0 = \frac{N}{x_\theta}\exp(-\frac{\Delta G^*}{kT_{nuc}}) \qquad (3.2.1)$$

where N is the total number of atoms per unit area of grain boundary taken as

$$N = S_0 d_0 \rho_\alpha N_A \tag{3.2.2}$$

where S_0 is the unit area.

ΔG^* is the Gibbs free energy of critical grain boundary precipitate nucleus formation given by[91]

$$\Delta G^* = \frac{16\pi\sigma_{\alpha\theta}^3}{3\Delta G_v^2} s(\psi) \tag{3.2.3}$$

The experimental observation shows that the grain boundary nuclei of $MgZn_2$ phase are cap shaped and $s(\psi)$ is

$$s(\psi) = \frac{2 - 3\cos\psi + \cos^3\psi}{2} \tag{3.2.4}$$

where

$$\cos(\psi) = \frac{\sigma_{\alpha\alpha}}{2\sigma_{\alpha\theta}} \tag{3.2.5}$$

ΔG_v is the driving force for the formation of a nucleus of $MgZn_2$ phase. ΔG_v is given by

$$\Delta G_v = \frac{RT_{nuc}}{2V_\theta} \ln\left(\frac{x_b}{x_{\alpha T_{nuc}}^{\alpha\theta}}\right) \tag{3.2.6}$$

The deduction of $x_{\alpha T_{nuc}}^{\alpha\theta}$ is described in Faulkner and Caisley's paper[97]

$$x_{\alpha T_{nuc}}^{\alpha\theta} = \left[\frac{1}{C_c}\exp\left(-\frac{\Delta H}{kT_{nuc}} + c\right)\right]^{x_E} \cdot \exp\left(\frac{2\sigma_{\alpha\theta}\Omega}{RrT_{nuc}}\right) \tag{3.2.7}$$

where C_c and x_E are the concentration and the number of moles of the other non-rate controlling element (in this case Zn) participating in the precipitation reaction, ΔH and c are the enthalpy term and entropy-connected term of solute in the solubility product equation, Ω is the molar volume of the matrix phase and r_{nuc} is the radius of curvature of the precipitate nucleus at the advancing interface.

3.2.1.2 *Nucleation combined with segregation*

During a heat-treatment segregation will take place. Segregation will affect the grain boundary precipitate nucleation by varying the driving force, ΔG_v, through the modifying of the solute concentration at the grain boundary, x_b to C_b governed by Equation (2.1.8) or to $C_b(t_q)$, which is the segregation concentration at the grain boundary after quenching from the solution treatment temperature governed by Equation (2.1.18).

The modified driving force is

$$\Delta G_v = \frac{RT_{nuc}}{2V_\theta} \ln\left(\frac{C_b}{x_{\alpha T_{nuc}}^{\alpha\theta}}\right) \qquad (3.2.8a)$$

or

$$\Delta G_v = \frac{RT_{nuc}}{2V_\theta} \ln\left[\frac{C_b(t_q)}{x_{\alpha T_{nuc}}^{\alpha\theta}}\right] \qquad (3.2.8b)$$

Bringing Equation (3.2.8a) or (3.2.8b) into Equation (3.2.3) to calculate ΔG^*, and inserting ΔG^* into Equation (3.2.1), gives N_0, the number of critical nuclei per unit grain boundary area for a given heat-treatment condition in the presence of segregation.

3.2.2 *Nucleation time*

3.2.2.1 *Before combined with segregation*

The modified Equation of incubation time given by Vander Velde et al[92] is used to predict nucleation time.

The incubation time, τ, of the nucleation at temperature T_{nuc} is given by

$$\tau = \frac{32kT_{nuc}a^4\sigma_{\alpha\theta}^2 N_A^2}{D_{bnuc}d_0 x_b V_\theta^2 \Delta G_v^3 \sin\psi} \qquad (3.2.9)$$

where ΔG_v is given by Equation (3.2.6), x_b=C_g.

Equation (3.2.9) gives the incubation time of nucleation for the precipitates which are semi-coherent with the matrix. For this kind of precipitate the nucleation kinetics is grain boundary and interface diffusion controlled.

3.2.2.2 *Combined with segregation*

During heat-treatment, segregation will take place, segregation will affect the nucleation time by modifying the solute concentration term, x_b to C_b governed by Equation (2.1.8) or to $C_b(t_q)$ governed by Equation (2.1.18) and varying the driving force, ΔG_v, through the modifying of the solute concentration at the grain boundary. The modified nucleation time is then given by

$$\tau = \frac{32kT_{nuc}a^4\sigma_{\alpha\theta}^2 N_A^2}{D_{bnuc}d_0 C_b V_\theta^2 \Delta G_v^3 \sin\psi} \qquad (3.2.10a)$$

where ΔG_v is given by

$$\Delta G_v = \frac{RT_{nuc}}{2V_\theta} \ln\left(\frac{C_b}{x^{\alpha\theta}_{\alpha T_{nuc}}}\right) \qquad (3.2.8a)$$

or

$$\tau = \frac{32kT_{nuc}a^4\sigma^2_{\alpha\theta}N_A^2}{D_{bnuc}d_0C_b(t_q)V_\theta^2\Delta G_v^3 \sin\psi} \qquad (3.2.10b)$$

where ΔG_v is given by

$$\Delta G_v = \frac{RT_{nuc}}{2V_\theta} \ln\left[\frac{C_b(t_q)}{x^{\alpha\theta}_{\alpha T_{nuc}}}\right] \qquad (3.2.8b)$$

3.2.3 *Distribution density function of grain boundary precipitate nuclei*

Equation (3.1.1) gives the number of the critical nuclei per unit grain boundary area. But how these nuclei are distributed on such an area, or, the dispersion situation of these nuclei on the area, is still unclear until a distribution density function is defined to describe it.

In order to establish the distribution density function, the collector plate concept is introduced. The collector plate is defined as an area of grain boundary that has a precipitate nucleus at its centre, and all such plates together fill up a unit area of grain boundary. The number of plates per unit area of boundary is the same as the number of the critical nuclei per unit area. The plate area shows the dispersion situation of the nuclei on the grain boundary.

The mean area of the collector plate is taken as

$$A_{m0} = \frac{1}{N_0} \qquad (3.2.11)$$

and the distribution density function of the grain boundary precipitate nuclei, n_0, is described by a normal distribution function of collector plate area, A_v.

$$n_0 = \frac{N_0}{2\sqrt{\pi}\sigma}\exp[-\frac{(A_v - A_{m0})^2}{2\sigma^2}] \qquad (3.2.12)$$

where $A_{min} \le A_v \le A_{max}$,

$$A_{min} = 16 D_{bnuc}\tau \qquad (3.2.13)$$

where τ is given by Equation (3.2.9) if the segregation effect is not taken into account or τ is given by Equation (3.2.10a) and Equation (3.2.10b) if it is considered.

$$A_{max} = A_{m0} + (A_{m0} - A_{min}) = 2A_{m0} - 16 D_{bnuc}\tau \qquad (3.2.14)$$

σ is taken as

$$\sigma = (A_{m0} - A_{min})/3 \qquad (3.2.15)$$

Bringing σ given by Equation (3.2.15) into Equation (3.2.12) and then integrating the right side of the equation from A_{min} to A_{max} yields:

$$\int_{A_{min}}^{A_{max}} \{\frac{N_0}{2\sqrt{\pi}\sigma}\exp[\frac{(A_v - A_{m0})^2}{2\sigma^2}]\} dA_v \ge 0.997 N_0 \qquad (3.2.16)$$

So the chosen σ is acceptable and Equation (3.2.12) gives an acceptable description of distribution probability density of the grain boundary precipitate nuclei as a function of the area of collector plate.

3.3 *New developments of the grain boundary precipitation growth model - combined precipitation and segregation*

3.3.1 *General*

In all the previous precipitate growth models of constant square collector plate control, A_v is taken as $A_v = d_v^2$, where d_v is the experimental measured inter-particle spacing which is taken as the inter-particle spacing along the grain boundaries from a TEM micrograph of the samples. Because of the nature of the projective view in the direction parallel to the boundary plane of the micrograph, the measured inter-particle spacing may not represent the real inter-particle spacing. Besides, such measurement is quite difficult and takes a long time.

It becomes more and more necessary to generate a new precipitate growth model to overcome this drawback. The work of the construction of the new model is based on the idea of predicting the collector plate area theoretically by relating it to the number of precipitate nuclei in a unit grain boundary area. This relies on the nucleation condition.

During the heat-treatment that both precipitation and segregation take place, segregation may influence grain boundary precipitation nucleation by altering the driving force. It may also influence the precipitate growth rates by altering the solute flux. Hence a new model should be constructed that will combine the contribution of the solute segregation with precipitation nucleation and growth. The change of the mean collector plate area with time caused by coalescence during the growth and its effect on the precipitate growth is also considered in the new combined model. The combined model is expected to give a more accurate and full prediction of the influence of heat-treatment on the grain boundary precipitation

behaviour. The details of the construction of this combined model is given as follows.

3.3.2 *Details of modelling*

There are assumptions that the precipitates are in cap shape and a constant morphology throughout the early stage of precipitate growth. The mean half volume of a precipitate can then be written as, $V = \pi f(\psi) L^3$, where L is the mean radius of the precipitate along the grain boundary after ageing at a given temperature for a time of t. The combined model is expected to give the prediction of precipitate size, L with time, t during an isothermal process. A numerical approach is used to perform the combined analysis and the combined model is a numerical model.

Modelling starts by dividing the time, t, into intervals of δt such that $t = n\,\delta t$. n is an integer. δt is chosen to be so small that within which the solute concentration, the mean size collector plate area and the mean radius of the precipitate can be considered as constants. Thus the solute concentration at the grain boundary, the mean collector plate area and the mean radius of the precipitate change with time in increments of δt.

At the ith stage ($1 \le i \le n$), the solute concentration in the vicinity of the grain boundary is described by $x_{\alpha i}$; the mean collector plate area is described by A_{mi} which is given by $A_{mi} = 1/N_i$ where N_i is the number of precipitate per unit area of grain boundary at this time; and the mean radius of the precipitate is described by L_i.

L_i is calculated by Carolan and Faulkner's model for a constant square collector plate condition[99]. In Carolan and Faulkner's model, the increase of the precipitate size, dL during the increase of time, dt, at a given temperature, T, is given by a rewritten form of Equation (2.3.33):

$$dL = \frac{(x_\alpha - x_{\alpha T}^{\alpha\theta}) A_v D_I^{\frac{1}{2}} \rho_\alpha t^{-\frac{1}{2}}}{3\pi^{\frac{1}{2}} \rho_\theta (x_\theta - x_{\alpha T}^{\alpha\theta}) L^2 f(\psi)} dt \qquad (3.3.1)$$

Replacing x_α and A_v in equation (3.3.1) with $x_{\alpha i}$ and A_{mi-1}, then integrating from t"=(i-1)δt to t'=iδt yields

$$L_i = \{ \frac{2 A_{mi-1} D_I^{\frac{1}{2}} (x_{\alpha i} - x_{\alpha T}^{\alpha\theta}) [t'^{\frac{1}{2}} - (t'-\delta t)^{\frac{1}{2}}] \rho_\alpha}{\rho_\theta \pi^{\frac{3}{2}} f(\psi)(x_\theta - x_{\alpha T}^{\alpha\theta})} + L_{i-1}^3 \}^{\frac{1}{3}} \qquad (3.3.2)$$

where $x_{\alpha T}^{\alpha\theta}$ is the solute concentration in equilibrium with the precipitate and matrix at ageing temperature, T; x_θ is the solute concentration in the precipitate phase; D_I is the volume diffusion coefficient of the impurity at ageing temperature; A_{mi-1}, which will be discussed later in **Section 3.5**, is the mean collector plate area at the (i-1)th stage; ρ_α is the molar density of the matrix phase; ρ_θ is the molar density of the precipitate phase.

$x_{\alpha i}$ is the solute concentration term which is modified according to the segregation parameter. $x_{\alpha i}$ is taken as the average concentration of the solute in the region from the grain boundary to a distance δl into the grain. δl is the diffusion distance of the solute in the matrix within time t'.

$$\delta l = \sqrt{2 D_I t'} \qquad (3.3.3)$$

Different segregation model gives different $x_{\alpha i}$.

For Faulkner's non-equilibrium segregation model[70],

$$x_{\alpha i} = \frac{A_{mi-1} \int_0^{\sqrt{2 D_I i\delta t}} C(y, t_{eff}^i) dy - \pi f(\psi) L_{i-1}^3 (x_\theta - x_{\alpha T}^{\alpha\theta})}{\sqrt{2 D_I i\delta t} A_{mi-1}} \qquad (3.3.4)$$

where t^i_{eff} is the effective time at solution treatment temperature given by

$$t^i_{eff} = t_q + i\delta t \cdot \exp\frac{-Q_c(T_i - T)}{kT_iT} \tag{3.3.5}$$

$C(y, t^i_{eff})$ the solute concentration distribution at this time. $C(y, t^i_{eff})$ is given by Equation (2.1.15) or (2.1.17) if de-segregation occurs.

For Xu & Song's non-equilibrium segregation model[71],

$$x_{\alpha i} = \frac{A_{mi-1}\int_0^{\sqrt{2D_l i\delta t}-\frac{d_2}{2}} c(x, t^i_{\text{eff}})dx + A_{mi-1}\frac{d_2}{2}C_b(t^i_{\text{eff}}) - \pi f(\psi)L^3_{i-1}(x_\theta - x^{\alpha\theta}_{\alpha T})}{\sqrt{2D_l i\delta t}A_{mi-1}} \tag{3.3.6a}$$

$$(\text{if}\sqrt{2D_l i\delta t} \geq \frac{d_2}{2})$$

or

$$x_{\alpha i} = \frac{A_{mi-1}\sqrt{2D_l i\delta t}C_b(t^i_{\text{eff}}) - f(\psi)\pi L^3_{i-1}(x_\theta - x^{\alpha\delta}_{\alpha T})}{\sqrt{2D_l i\delta t}A_{mi-1}} \quad (\text{if } \sqrt{2D_l i\delta t} \leq \frac{d_2}{2}) \tag{3.3.6b}$$

where t^i_{eff} is the effective time given by Equation (3.3.5), $c(x, t^i_{eff})$ is the solute concentration distribution at this time and is given by Equation (2.1.24), $C_b(t^i_{eff})$ is given by Equation (2.1.18).

For the newly generated numerical-analytical non-equilibrium segregation model,

$$x_{\alpha i} = \frac{A_{mi-1}[\int_0^{\sqrt{2D_l i\delta t}-\frac{w_0}{2}} c(x, i\delta t)dx + \frac{w_0}{2}C_b] - f(\psi)\pi L^3_{i-1}(x_\theta - x^{\alpha\delta}_{\alpha T})}{\sqrt{2D_l i\delta t}A_{mi-1}} \tag{3.3.7a}$$

$$(\text{if}\sqrt{2D_l i\delta t} \geq \frac{w_0}{2})$$

or

$$x_{\alpha i} = \frac{A_{mi-1}\sqrt{2D_l i\delta t}C_b - f(\psi)\pi L_{i-1}^3(x_\theta - x_{\alpha T}^{\alpha\theta})}{\sqrt{2D_l i\delta t}A_{mi-1}} \qquad (\text{if } \sqrt{2D_l i\delta t} \le \frac{w_0}{2}) \qquad (3.3.7b)$$

where c(x,iδt) is the solute concentration distribution at time iδt given by Equation (3.1.10).

For the newly generated numerical non-equilibrium segregation model,

$$x_{\alpha i} = \frac{A_{mi-1}\int_0^{\sqrt{2D_l i\delta t}} C(y,\ l'\cdot\Delta)dy - f(\psi)\pi L_{i-1}^3(x_\theta - x_{\alpha T}^{\alpha\theta})}{\sqrt{2D_l i\delta t}A_{mi-1}} \qquad (3.3.8)$$

where C(y,$l'\cdot\Delta$), which is the solute concentration distribution at time, $l'\Delta$, is given by Equation (3.1.6); $l'\cdot\Delta = t_{eff}^i$, l' is an integer given by

$$l' = \frac{t_{eff}^i}{\Delta} \qquad (3.3.9)$$

Substituting $x_{\alpha i}$ given by Equation (3.3.4), or (3.3.6), or (3.3.7), or (3.3.8) into Equation (3.3.2) yields L_i, the mean radius of the precipitate at this time stage.

when i=1, L_{i-1}=0

$$L_1 = \{\frac{2A_{m_0}D_l^{\frac{1}{2}}(x_{\alpha 1} - x_{\alpha T}^{\alpha\theta})(\delta t)^{\frac{1}{2}}]\rho_\alpha}{\rho_\theta \pi^{\frac{3}{2}} f(\psi)(x_\theta - x_{\alpha T}^{\alpha\theta})}\}^{\frac{1}{3}} \qquad (3.3.10)$$

where A_{m0} is the initial mean collector plate area given by Equation (3.2.11) in **Section 3.2.3.**

The iteration carries on from i=1 till i=n at which point, L the mean radius of the precipitate after ageing for a time of t at ageing temperature T.

$$L=L_n \tag{3.3.11}$$

or

$$L=\{\sum_{i=1}^{i=n} \frac{2A_{mi-1}D_l^{\frac{1}{2}}(x_{\alpha i}-x_{\alpha T}^{\alpha\theta})\{(i\delta t)^{\frac{1}{2}}-[(i-1)\delta t]^{\frac{1}{2}}\}\rho_\alpha}{\rho_\theta \pi^{\frac{3}{2}} f(\psi)(x_\theta - x_{\alpha T}^{\alpha\theta})} + L_0^3 \}^{\frac{1}{3}} \tag{3.3.12}$$

In the case that Faulkner's segregation model is chosen to describe the segregation behaviour for modelling precipitate growth in the presence of segregation, there could be another approach to construct a growth model in which the segregation influence is taken into account. The principle of the approach has been introduced in the paper of Faulkner and the author[101]. Such an approach is based on two equations governing segregation and precipitation. The total flux of the solute atoms to grow precipitates at grain boundaries is $(dm/dt)_{total}$.

$$(dm/dt)_{total} = (dm/dt)_p + (dm/dt)_s \tag{3.3.13}$$

where $(dm/dt)_p$ is the flux coming from the precipitation component and $(dm/dt)_s$ is the flux from the segregation component.

$$(\frac{dm}{dt})_p = A_v D_l \frac{\partial X(y,t)}{\partial y} \tag{3.3.14}$$

$$(\frac{dm}{dt})_s = -\rho_\alpha A_v D_c \frac{\partial C(y,t_{eff})}{\partial y} \tag{3.3.15}$$

where X(y,t) and $C(y,t_{eff})$ are given by Equation (2.3.2) and Equation (2.1.15).

Equating Equations (3.3.13) and (2.3.32) yields

$$3L^2dL=[\frac{A_v D_l^{1/2}(x_\alpha - x_{\alpha T}^{\alpha\theta})t^{-1/2}\rho_\alpha}{\pi^{3/2}f(\psi)(x_\theta - x_{\alpha T}^{\alpha\theta})\rho_\theta}+\frac{A_v D_c(C_b - x_\alpha)(t_q+bt)^{-1/2}\rho_\alpha}{\pi^{3/2}f(\psi)(x_\theta - x_{\alpha T}^{\alpha\theta})\rho_\theta D_{ci}^{1/2}}]dt \qquad (3.3.16)$$

where

$$b=\exp\frac{-Q_c(T_i-T)}{kT_iT} \qquad (3.3.17)$$

Replacing A_v in Equation (3.3.16) with $A_{mi\text{-}1}$, then integrating from $t''=(i-1)\delta t$ to $t'=i\delta t$ yields

$$L_i=\left\{L_{i-1}^3+\frac{2A_{mi-1}D_l^{1/2}(x_\alpha - x_{\alpha T}^{\alpha\theta})[(i\delta t)^{1/2}-(i-1)^{1/2}(\delta t)^{1/2}]\rho_\alpha}{\pi^{3/2}f(\psi)(x_\theta - x_{\alpha T}^{\alpha\theta})\rho_\theta}+\frac{2A_{mi-1}D_c(C_b-x_\alpha)\{(t_q+bi\delta t)^{1/2}-[t_q+b(i-1)(\delta t)]^{1/2}\}\rho_\alpha}{b\pi^{3/2}f(\psi)(x_\theta - x_{\alpha T}^{\alpha\theta})\rho_\theta D_{ci}^{1/2}}\right\}^{1/3} \qquad (3.3.18)$$

and

$$L=\left\{L_0^3+\sum_{i=1}^{i=n}\left[\frac{2A_{mi-1}D_l^{1/2}(x_\alpha - x_{\alpha T}^{\alpha\theta})[(i\delta t)^{1/2}-(i-1)^{1/2}(\delta t)^{1/2}]\rho_\alpha}{\pi^{3/2}f(\psi)(x_\theta - x_{\alpha T}^{\alpha\theta})\rho_\theta}+\frac{2A_{mi-1}D_c(C_b-x_\alpha)\{(t_q+bi\delta t)^{1/2}-[t_q+b(i-1)(\delta t)]^{1/2}\}\rho_\alpha}{b\pi^{3/2}f(\psi)(x_\theta - x_{\alpha T}^{\alpha\theta})\rho_\theta D_{ci}^{1/2}}\right]\right\}^{1/3} \qquad (3.3.19)$$

All the parameters in Equation (3.3.19) have the same definitions as those that appeared earlier and A_{m0} is given by Equation (3.2.11) and L_0=0.

Table 3.3.1 gives a summary of the growth models. The name of the model and the size-time relationship derived is given along with the equation number used in the text.

Table 3.3.1: The summary of growth models.

name of the model	relationship	equation number
Aaron & Aaronson's lengthening model	$L=[\frac{2A_v D_l^{\frac{1}{2}}(x_\alpha - x_{\alpha T}^{\alpha\theta})\rho_\alpha}{\pi^{\frac{1}{2}}(x_\theta - x_{\alpha T}^{\alpha\theta})\rho_\theta r}]^{\frac{1}{2}} t^{\frac{1}{2}}$	(2.3.9)
Aaron & Aaronson's thickening model	$s=\frac{8\delta D_{\alpha\theta}(x_{\alpha T}^{\alpha\theta} - x_{\alpha T}^{\alpha\theta}\|_{r=\infty})\rho_\alpha^2}{\beta(x_\theta - x_{\alpha T}^{\alpha\theta})\rho_\theta^2} \bullet \frac{A_v D_l^{\frac{1}{2}}(x_\alpha - x_{\alpha T}^{\alpha\theta})}{\pi^{\frac{1}{2}}(x_\theta - x_{\alpha T}^{\alpha\theta})r} t^{\frac{1}{2}}$	(2.3.20)
Faulkner & Caisley's collector plate model (thickening)	$s=[\frac{4A_v^2 D_l(x_\alpha - x_{\alpha T}^{\alpha\theta})^2\rho_\alpha^2}{\pi^3 k'^4(x_\theta - x_{\alpha T}^{\alpha\theta})^2\rho_\theta^2}]^{\frac{1}{6}} t^{\frac{1}{6}}$	(2.3.26)
Faulkner & Caisley's collector plate model (lengthening)	$L=[\frac{4A_v^2 D_l k'^2(x_\alpha - x_{\alpha T}^{\alpha\theta})^2\rho_\alpha^2}{\pi^3(x_\theta - x_{\alpha T}^{\alpha\theta})^2\rho_\theta^2}]^{\frac{1}{6}} t^{\frac{1}{6}}$	(2.3.27)
Faulkner & Caisley's interfacial diffusion controlling model (thickening)	$s=[\frac{2\delta D_{\alpha\theta}(x_{\alpha T}^{\alpha\theta} - x_{\alpha T}^{\alpha\theta}\|_{r=\infty})\rho_\alpha}{\beta k'^2(x_\theta - x_{\alpha T}^{\alpha\theta})\rho_\theta}]^{\frac{1}{3}} t^{\frac{1}{3}}$	(2.3.29)
Faulkner & Caisley's interfacial diffusion controlling model (lengthening)	$L=[\frac{2\delta D_{\alpha\theta}k'(x_{\alpha T}^{\alpha\theta} - x_{\alpha T}^{\alpha\theta}\|_{r=\infty})\rho_\alpha}{\beta(x_\theta - x_{\alpha T}^{\alpha\theta})\rho_\theta}]^{\frac{1}{3}} t^{\frac{1}{3}}$	(2.3.30)
Carolan & Faulkner's constant square collector plate controlling model	$L=[\frac{\pi^3\rho_\theta^2(x_\theta - x_{\alpha T}^{\alpha\theta})^2 f^2(\psi)}{4(x_\alpha - x_{\alpha T}^{\alpha\theta})^2 A_v^2 D_l\rho_\alpha^2}]^{\frac{1}{4}} t^{\frac{1}{4}}$	(2.3.36)
Carolan & Faulkner's variable circular collector plate controlling model	$L=[\frac{8(x_\alpha - x_{\alpha T}^{\alpha\theta})D_b D_l^{\frac{1}{2}}\rho_\alpha}{3\pi^{\frac{1}{2}}\rho_\theta(x_\theta - x_{\alpha T}^{\alpha\theta})L^3 f(\psi)}]^{\frac{1}{3}} t^{\frac{1}{2}}$	(2.3.37)
new combined precipitate growth model (segregation component is given by Faulkner's model)	$L=\{\sum_{i=1}^{i=n} [\frac{2A_{mi-1}D_l^{1/2}(x_\alpha - x_{\alpha T}^{\alpha\theta})[(i\delta t)^{1/2} - (i-1)^{1/2}(\delta t)^{1/2}]\rho_\alpha}{\pi^{3/2} f(\psi)(x_\theta - x_{\alpha T}^{\alpha\theta})\rho_\theta} + \frac{2A_{mi-1}D_c(C_b - x_\alpha)[(t_q + b i\delta\alpha)^{3/2} - [t_q + b(i-1)\delta\alpha]^{3/2}]\rho_\alpha}{b\pi^{3/2} f(\psi)(x_\theta - x_{\alpha T}^{\alpha\theta})\rho_\theta}]\}^{\frac{1}{3}}$	(3.3.19)
new combined precipitate growth models	$L=\{\sum_{i=1}^{i=n} \frac{2A_{mi-1}D_l^{\frac{1}{2}}(x_{\alpha i} - x_{\alpha T}^{\alpha\theta})[(i\delta\alpha)^{\frac{1}{2}} - [(i-1)\delta\alpha]^{\frac{1}{2}}]\rho_\alpha}{\rho_\theta\pi^{\frac{3}{2}} f(\psi)(x_\theta - x_{\alpha T}^{\alpha\theta})} + L_0^3\}^{\frac{1}{3}}$	(3.3.12)

3.4 *The coarsening kinetics of grain boundary precipitates*

When the growth of the precipitates from supersaturated solid solution is complete, further ageing leads to precipitate coarsening driven by the interfacial free energy between the precipitate and the matrix - the process known as Ostwald ripening. The physical process by which the microstructure coarsens and releases its excess surface energy is due to the higher solubility of small particles, since these have a larger ratio of surface area to volume. The larger particles thus grow at the expense of the smaller ones.

3.4.1 *Critical time for the onset of coarsening*

The critical time for the onset of coarsening, t_{cc}, is taken as the time when there is no more supersaturation of solute existing in the area adjacent to the grain boundaries and hence no flux of solute to the grain boundary occurs.

$$t_{cc} = g\delta t \qquad (3.4.1)$$

where g is an integer. By bringing g into Equation (3.3.4), or (3.3.6), or(3.3.7), or (3.3.8) to replace i, we will have $x_{\alpha g}$ which satisfies the condition:

$$x_{\alpha g} \equiv x_{\alpha T}^{\alpha\theta} \qquad (3.4.2)$$

A programme is written which leads the computer to carry out an iteration from i=1 till the relation $x_{\alpha g} \leq x_{\alpha T}^{\alpha\theta}$ is satisfied. Such a time is the critical time of the onset of coarsening.

3.4.2 *Coarsening rate*

Kirchner's coarsening theory (1971)[100] has been adapted here to predict the coarsening rate of the grain boundary precipitate of $MgZn_2$ in 7150 aluminium alloy. The relationship of the radius of the grain boundary precipitate with ageing time, L(t), during coarsening is:

$$L(t)=[\frac{9d_0D_b\sigma_{\alpha\theta}x_{\alpha T}^{\alpha\theta}V_\theta(t-t_{cc})}{32ABRT}+L_g^4]^{\frac{1}{4}} \qquad (3.4.3)$$

where,

L_g which is given by Equation (3.3.12) or (3.3.19) is the mean radius of the grain boundary precipitates at the time, t_{cc}; d_0 is the width of the layer of grain boundary within which the diffusion is grain boundary diffusion controlling; T is the ageing temperature; t is the ageing time at T; D_b is the grain boundary diffusion coefficient; $\sigma_{\alpha\theta}$ is the interfacial free energy of the precipitate/matrix interface; A is the parameter defined by

$$A=\frac{2}{3}(1-\frac{\sigma_{\alpha\alpha}}{2\sigma_{\alpha\theta}}) \qquad (3.4.4)$$

where $\sigma_{\alpha\alpha}$ is the grain boundary energy;

$$\sigma_{\alpha\alpha}=2\sigma_{\alpha\theta}\cos(\psi) \qquad (3.4.5)$$

B is the parameter defined by

$$B=\frac{1}{2}\ln(\frac{1}{f}) \qquad (3.4.6)$$

where f is the fraction of the grain boundary covered by precipitates, given by

$$f=\frac{\pi L_g^2}{A_{mg}} \qquad (3.4.7)$$

where A_{mg} is the mean collector plate area at the time, t_{cc}. The derivation of A_{mg} will be given later in other sections.

3.5 *Collector plate area*

The collector plate is defined as an area of the grain boundary that contains a precipitate or precipitate nucleus at its centre. All the collector plates together fill up the whole grain boundary. There is a statistical distribution of such collector plates. The mean collector plate area reflects the situation of how the precipitates disperse on the grain boundaries. The bigger the mean collector plate area is, the more widely spaced the grain boundary precipitates.

The mean collector plate area and the distribution probability density function of collector plates area as a function of the size of the collector plate are established once the nucleation of the grain boundary precipitation is finished. Such distributions and the mean size will not change with time during the growth of the precipitates unless coalescence happens or coarsening begins.

3.5.1 *Before onset of growth*

3.5.1.1 *Before combined with segregation*

The mean size of the collector plates before the onset of growth is

$$A_{m0} = \frac{1}{N_0} \tag{3.5.1}$$

where N_0 is the number of the equilibrium precipitate nuclei in a unit area of a grain boundary. N_0 is given by Equation (3.2.1) with ΔG_v given by Equation (3.2.6).

The distribution of collector plates, n_0, is described by a normal probability density function in terms of collector plate area, A_v.

$$n_0 = \frac{N_0}{2\sqrt{\pi}\sigma}\exp[-\frac{(A_v - A_{m0})^2}{2\sigma^2}] \qquad (3.5.2)$$

where $A_{min} \le A_v \le A_{max}$,

$$A_{min} = 16 D_{bnuc}\tau \qquad (3.5.3)$$

and

$$A_{max} = A_{m0} + (A_{m0} - A_{min}) = 2A_{m0} - 16 D_{bnuc}\tau \qquad (3.5.4)$$

$$\sigma = \frac{A_{m0} - 16 D_{bnuc}\tau}{3} \qquad (3.5.5)$$

τ is the nucleation time given by Equation (3.2.9).

3.5.1.2 *Combined with segregation*

Combined with segregation effect, the mean area of the collector plate is

$$A_{m0} = \frac{1}{N_0} \qquad (3.5.6)$$

where N_0 is the number of the equilibrium precipitate nuclei in a unit area of a grain boundary given by Equation (3.2.1) with ΔG_v given by Equation (3.2.8a) or (3.2.8b).

As for the situation that segregation is not taken into account, in this case the distribution of collector plates as a function of the size of collector plates, n_0, follows a normal probability density function.

$$n_0 = \frac{N_0}{2\sqrt{\pi}\sigma}\exp[-\frac{(A_v - A_{m0})^2}{2\sigma^2}] \qquad (3.5.7)$$

where A_{m0} is given by Equation (3.5.6), σ is given by

$$\sigma = \frac{A_{m0} - 16D_{bnuc}\tau}{3} \qquad (3.5.8)$$

where τ is the nucleation time given by Equation (3.2.10a) or (3.2.10b).

$$A_{min} \le A_v \le A_{max} ,$$

$$A_{min} = 16D_{bnuc}\tau \qquad (3.5.9)$$

and

$$A_{max} = A_{m0} + (A_{m0} - A_{min}) = 2A_{m0} - 16D_{bnuc}\tau \qquad (3.5.10)$$

3.5.2 *During growth*

3.5.2.1 *Before combined with segregation*

During the growth of the precipitates, the mean size of the collector plates may change with time. The change of the mean collector plate area is caused by a

reduction in the number of the precipitates caused by coalescence. The mean collector plate area will not change with time until the coalescence happens.

The mean collector plate area after ageing for a time of t ($t=n\delta t$, n is an integer) at ageing temperature is described by A_{mn}.

$$A_{mn} = \frac{1}{N_n} \tag{3.5.11}$$

and the probability density function of collector plates, n_n, is

$$n_n = \frac{N_n}{2\sqrt{\pi}\sigma} \exp[-\frac{(A_v - A_{mn})^2}{2\sigma^2}] \tag{3.5.12}$$

where N_n is the number of precipitates in a unit area of a grain boundary after ageing for a time of t. N_n is given by

$$N_n = N_{n-1} - \Delta N_n \tag{3.5.13}$$

where ΔN_n is the number of precipitates which vanish because of coalescence; ΔN_n is given by

$$\Delta N_n = N_{A_{min}}^{4L_n^2} \cdot \frac{N_{A_{min}}^{4L_n^2}}{N_{n-1}} \tag{3.5.14}$$

where $N_{A_{min}}^{4L_n^2}$ is the number of all those precipitates which have collector plate areas smaller than $4L_n^2$; $\frac{N_{A_{min}}^{4L_n^2}}{N_{n-1}}$ is the probability of coalescence happening to one of those precipitates. $N_{A_{min}}^{4L_n^2}$ is given by

$$N_{A_{min}}^{4L_n^2} = \int_{A_{min}}^{(2L_n)^2} n_{n-1} dA_v \qquad (3.5.15)$$

where L_n is the mean radius of the precipitate after growing for a time t ($t=n\delta t$); L_n is given by

$$L_n = \{\sum_{i=1}^{i=n} \frac{2A_{mi-1} D_l^{\frac{1}{2}} (C_g - x_{\alpha T}^{\alpha\theta})\{(i\delta t)^{\frac{1}{2}} - [(i-1)\delta t]^{\frac{1}{2}}\}\rho_\alpha}{\rho_\theta \pi^{\frac{3}{2}} f(\psi)(x_\theta - x_{\alpha T}^{\alpha\theta})}\}^{\frac{1}{3}} \qquad (3.5.16)$$

N_{n-1} is the number of precipitates in a unit area of a grain boundary at the time t' where $t' = (n-1)\delta t$; n_{n-1} is the distribution density function of the grain boundary precipitates at time $t' = (n-1)\delta t$. n_{n-1} is given by

$$n_{n-1} = \frac{N_{n-1}}{\sqrt{2\pi}\sigma} \exp[-\frac{(A_v - A_{mn-1})^2}{2\sigma^2}] \qquad (3.5.17)$$

where A_{mn-1} is the mean collector plate area after ageing for a time of $t' = (n-1)\delta t$ at ageing temperature and $A_{mn-1} = 1/N_{n-1}$

Integrating Equation (3.5.15) yields:

$$N_{A_{min}}^{4L_n^2} = 0.5 N_{n-1}[erf(\frac{A_{mn-1} - A_{min}}{\sqrt{2}\sigma}) - erf(\frac{A_{mn-1} - 4L_n^2}{\sqrt{2}\sigma})] \qquad (3.5.19)$$

Substituting Equation (3.5.19) into Equation (3.5.14) and bringing Equation (3.5.14) into Equation (3.5.13) and then bringing Equation (3.5.13) into Equation (3.5.11) gives A_{mn}.

$$A_{mn} = \frac{1}{N_{n-1}\{1 - 0.25[erf(\frac{A_{mn-1} - A_{min}}{\sqrt{2}\sigma}) - erf(\frac{A_{mn-1} - 4L_n^2}{\sqrt{2}\sigma})]^2\}} \qquad (3.5.20)$$

Equation (3.5.20) can be further written as:

$$A_{mn} = \frac{1}{N_0 \prod_{i=1}^{i=n} \{1 - 0.25[erf(\frac{A_{mi-1} - A_{\min}}{\sqrt{2}\sigma}) - erf(\frac{A_{mi-1} - 4L_i^2}{\sqrt{2}\sigma})]^2\}} \qquad (3.5.21)$$

where N_0 is given by Equation (3.2.1) with ΔG_v given by Equation (3.2.6);

$A_{m0} = \frac{1}{N_0}$;

$\sigma = \frac{A_{m0} - 16D_{bnuc}\tau}{3}$ with τ given by Equation (3.2.9).

A computer programme is generated to iterate the calculation of L_i, N_i and A_{mi} from i=1 till i=n. At this time, A_{mn} is the mean collector plate area after ageing for a time t at ageing temperature T.

3.5.2.2 *Combined with segregation*

If segregation influence is taken into account, the mean size of the collector plate is

$$A_{mn} = \frac{1}{N_0 \prod_{i=1}^{i=n} \{1 - 0.25[erf(\frac{A_{mi-1} - A_{\min}}{\sqrt{2}\sigma}) - erf(\frac{A_{mi-1} - 4L_i^2}{\sqrt{2}\sigma})]^2\}} \qquad (3.5.22)$$

and the probability density function of collector plates, n_n, is

$$n_n = \frac{N_n}{2\sqrt{\pi}\sigma} \exp[-\frac{(A_v - A_{mn})^2}{2\sigma^2}] \qquad (3.5.23)$$

where N_0 is given by Equation (3.2.1) with ΔG_v given by Equation (3.2.8a) or (3.2.8b);

$A_{m0} = \frac{1}{N_0}$;

$\sigma = \frac{A_{m0} - 16 D_{bnuc} \tau}{3}$ with τ given by Equation (3.2.10a) or (3.2.10b).

L_n given by Equation (3.3.12) with $x_{\alpha i}$ given by Equation (3.3.6), or (3.3.7), or (3.3.8) for the case of segregation described by Xu & Song's model, or the newly developed numerical-analytical model, or the newly developed numerical model respectively.

For the case that segregation is described by Faulkner's model, there are two expressions of L_n, Equation (3.3.12) with $x_{\alpha i}$ given as Equation (3.3.4), and Equation (3.3.19).

Iteration of the calculation of $x_{\alpha i}$, L_i, and A_{mi} from i=1 till i=n, will give A_{mn}, the mean collector plate area after ageing for a time t at ageing temperature T.

3.5.3 *During coarsening*

Once the coarsening begins, the concentration of the solute atoms at the grain boundaries does not change with time. This can expressed as:

$$N(t)\pi f(\psi) L(t)^3 = N_g \pi f(\psi) L_g^3 \qquad (3.5.24)$$

where L_g and N_g are the mean radius and the number of the precipitates at the time of the onset of coarsening; L(t) and N(t) are the radius and the number of the precipitates at the grain boundary after ageing for a time t ($t \geq t_{cc}, t_{cc} = g\delta t$) at the ageing temperature.

$A_m(t)$, the mean collector plate area after ageing for a time t ($t \geq t_{cc}, t_{cc} = g\delta t$) at ageing temperature is

$$A_m(t) = \frac{1}{N(t)} \tag{3.5.25}$$

which can be written as

$$A_m(t) = A_{mg}[\frac{L(t)}{L_g}]^3 \tag{3.5.26}$$

where A_{mg} and L_g can be obtained from Equation (3.5.22) and Equation (3.3.12) or (3.3.19) by replacing index n with g; L(t) is given by Equation (3.5.5).

The relationship of the mean collector plate area with ageing time after coarsening begins is described by Equation (3.5.26).

3.6 *Precipitate free zones*

Precipitate-free zones adjacent to grain boundaries could have a role in controlling the stress corrosion cracking of the alloy[15-17,23,41-51].

Precipitate-free zones (PFZs) are formed for two reasons. First, there is a narrow (~50nm) region either side of a grain boundary which is depleted of solute (Mg) due to the ready diffusion of the solute atoms into the boundary where relatively large particles of precipitate ($MgZn_2$) are subsequently formed. The remainder of a PFZ arises because of a depletion of vacancies to levels below that needed to assist with nucleation of precipitates at the particular ageing temperature. However, the vacancy depleted part of a PFZ may be absent in some alloys aged at temperatures below the GP zones solvus as GP zones can form homogeneously without the need of vacancies[32-37]. Here the model of the widths of PFZs caused by the segregation resulting in depletion of solute in the area adjacent to the grain boundaries is described.

An illustration of the solute concentration profile adjacent to the grain boundaries after ageing for a time of t at ageing temperature is shown by Fig. 3.6.1.

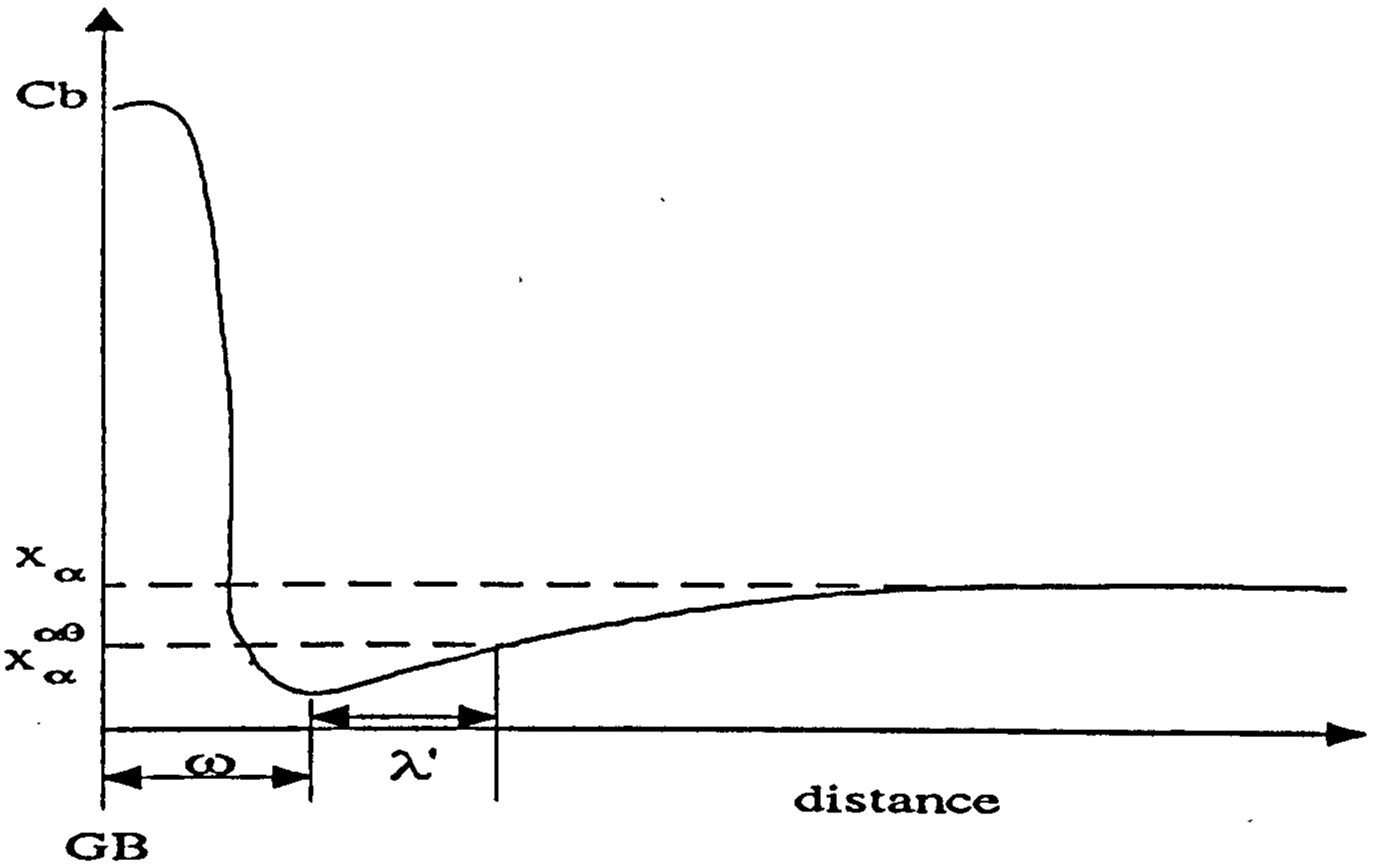

Fig. 3.6.1: The solute concentration profile after ageing for a time of t at ageing temperature T.

The width of the PFZ is defined by w_{pfz}. It is taken as:

$$w_{pfz} = 2y_0 \tag{3.6.1}$$

where

$$y_0 = \varpi + \lambda' \tag{3.6.2}$$

where λ' should satisfy the condition:

$$c(\lambda', t) = x_{\alpha T}^{\alpha\theta} \tag{3.6.3}$$

$c(\lambda', t)$ is the solute concentration distribution function. If the solute concentration distribution is described by Faulkner's non-equilibrium segregation model, $c(\lambda', t) = C(\lambda', t_{eff})$ where $C(\lambda', t_{eff})$ is given by Equation (2.1.15), $\varpi = 0$.

If the solute concentration distribution is described by Xu & Song's non-equilibrium segregation model, $c(\lambda',t)=c(\lambda',t_{eff})$ where $c(\lambda',t_{eff})$ is given by Equation (2.1.24), $\varpi=\frac{d_2}{2}$

If the solute concentration distribution is described by the newly generated numerical-analytical non-equilibrium segregation model, $c(\lambda',t)$ is given by Equation (3.1.10), $\varpi=\frac{w_0}{2}$

If the solute concentration distribution is described by the newly generated numerical non-equilibrium segregation model, $\varpi=0$, and $c(\lambda',t)=C(\lambda',t_{eff})$ where $C(\lambda',t_{eff})$ is given by Equation (3.1.6), in which w_{0l} is given by Equation (3.1.1) with i=l and l is given by

$$l=\frac{t_q+t\cdot\exp\frac{-E_a(T_i-T)}{kT_iT}}{\Delta} \qquad (3.6.4)$$

Normally the ageing treatments of 7150 Aluminium alloy include ageing for different time at different temperatures with the first stage ageing at a temperature below the GP zone solvus. In these cases the vacancy depleted part of a PFZ may be absent as GP zones can form homogeneously without the need for vacancies and the PFZs are mainly caused by the depletion of solute in the area adjacent to the grain boundaries[32-37]. The model may be helpful for our understanding the widths of PFZs during heat-treatments.

3.7 *Combined models*

It is the main aim of the work described in this thesis to construct a combined model in which the segregation of the solute atoms, the nucleation of the grain boundary

precipitates, the precipitate growth and coarsening are taken into account and the model predicts the state of the grain boundary and its environment as a function of heat treatment.

The kinetics of the segregation of the solute atoms, the nucleation kinetics, the precipitate growth and coarsening kinetics and the formation of PFZs have been discussed separately in **section 2.1, section 3.1, section 3.2, section 3.3, section 3.4, section 3.5** and **section 3.6.** There is a strong correlation between the segregation, the nucleation, the formation of PFZs, and the grain boundary precipitate growth and coarsening rates. The nucleation situation decides the initial size of the collector plates. The size of the collector plates strongly affects the growth rate of the grain boundary precipitates. The segregation affects precipitate nucleation and alters the solute supply for the growth. The depletion of the solute arising from segregation and precipitation in the area adjacent to the grain boundaries influences the formation of the PFZs.

Five numerical combined models are generated which can predict the grain boundary precipitation behaviour and the widths of PFZs as a function of heat treatment. These are combined models 1, 2, 3, 4 and 5.

In combined model 1, before the onset of coarsening, the mean radius of the grain boundary precipitates is given by Equation (3.3.12), the mean size of the collector plate by Equation (3.5.22) and the probability density function by Equation (3.5.23). Within these equations $x_{\alpha i}$ is given by Equation (3.3.4), ΔG_v by Equation (3.2.8a) and τ by Equation (3.2.10a). After the onset of coarsening, the mean radius of the grain boundary precipitates is given by Equation (3.4.5) and the mean size of the collector plate by Equation (3.5.26).

In combined model 2, before the onset of coarsening, the mean radius of the grain boundary precipitates is given by Equation (3.3.12), the mean size of the collector plate by Equation (3.5.22) and the probability density function by Equation (3.5.23). Within these equations $x_{\alpha i}$ is given by Equations (3.3.6a) and (3.3.6b), ΔG_v by Equation (3.2.8b) and τ by Equation (3.2.10b). After the onset of coarsening, the mean radius of the grain boundary precipitates is given by Equation (3.4.5) and the mean size of the collector plate by Equation (3.5.26).

In combined model 3, before the onset of coarsening, the mean radius of the grain boundary precipitates is given by Equation (3.3.12), the mean size of the collector plate by Equation (3.5.22) and the probability density function by Equation (3.5.23). Within these equations $x_{\alpha i}$ is given by Equations (3.3.7a) and (3.3.7b), ΔG_v by Equation (3.2.8a) and τ by Equation (3.2.10a). After the onset of coarsening, the mean radius of the grain boundary precipitates is given by Equation (3.4.5) and the mean size of the collector plate by Equation (3.5.26).

In combined model 4, before the onset of coarsening, the mean radius of the grain boundary precipitates is given by Equation (3.3.19), the mean size of the collector plate by Equation (3.5.22) and the probability density function by Equation (3.5.23). Within these equations ΔG_v by Equation (3.2.8a) and τ by Equation (3.2.10a). After the onset of coarsening, the mean radius of the grain boundary precipitates is given by Equation (3.4.5) and the mean size of the collector plate by Equation (3.5.26).

In combined model 5, before the onset of coarsening, the mean radius of the grain boundary precipitates is given by Equation (3.3.12), the mean size of the collector plate by Equation (3.5.22) and the probability density function by Equation (3.5.23). Within these equations $x_{\alpha i}$ is given by Equation (3.3.8), ΔG_v by Equation (3.2.8a) and τ by Equation (3.2.10a). After the onset of coarsening, the mean radius of the

grain boundary precipitates is given by Equation (3.4.5) and the mean size of the collector plate by Equation (3.5.26).

The width of the precipitate free zone is given by Equation (3.6.1) where for combined models 1 and 4, c(λ',t) is given by Equation (2.1.15) and ϖ=0; for combined model 2; $c(\lambda', t)$ is given by Equation (2.1.24) and $\varpi = \frac{d_2}{2}$; for combined model 3, c(λ',t) is given by Equation (3.1.10) and $\varpi = \frac{w_0}{2}$; for combined model 5, $c(\lambda', t)$ is given by Equation (3.1.6) and $\varpi = \frac{w_{0l}}{2}$ and w_{0l} is given by Equation (3.1.1).

The computer programs for the models are written in FORTRAN 77 Language. The following are the flow charts of the modelling process.

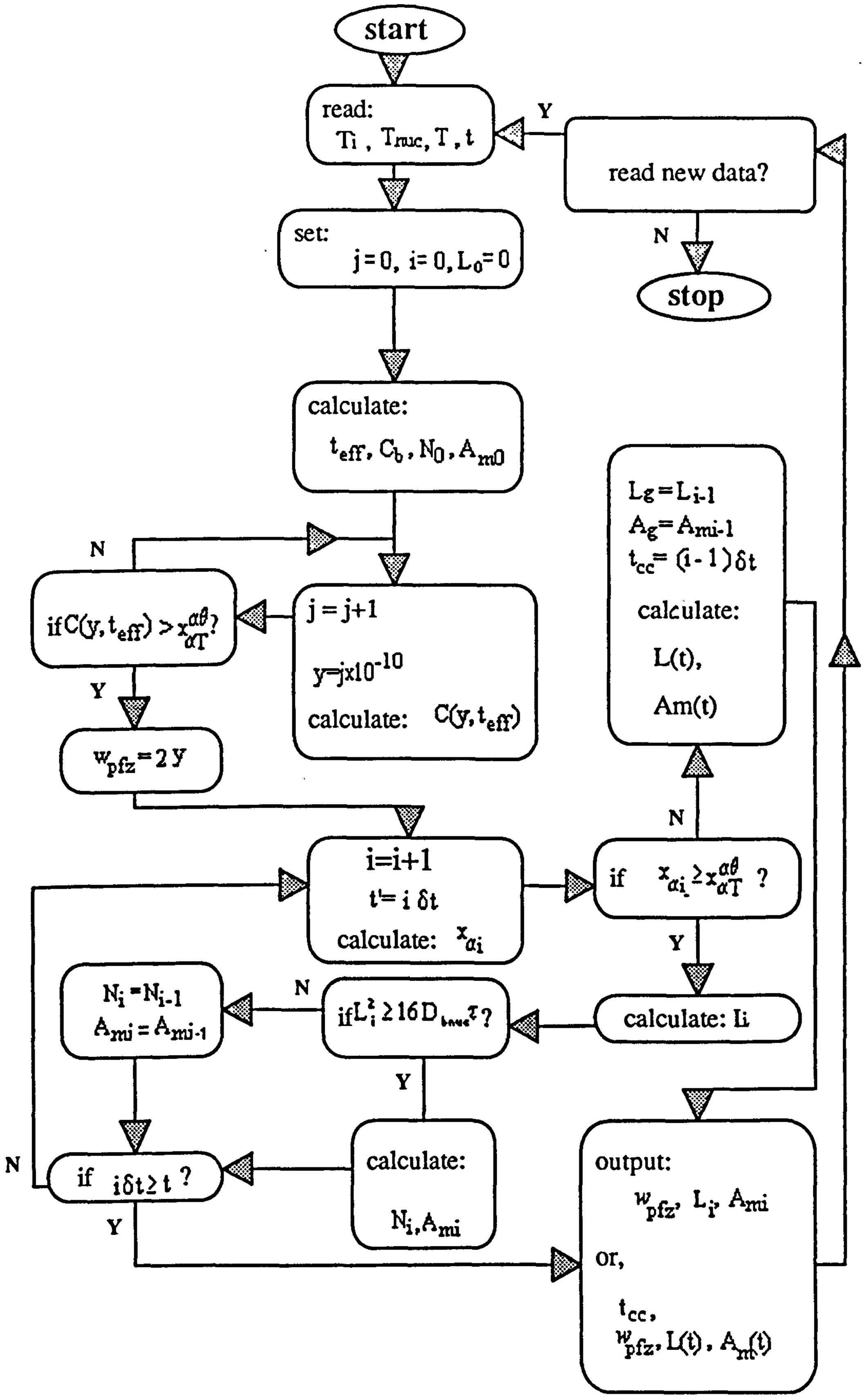

Fig. 3.7.1a: The flow chart of the combined model 1.

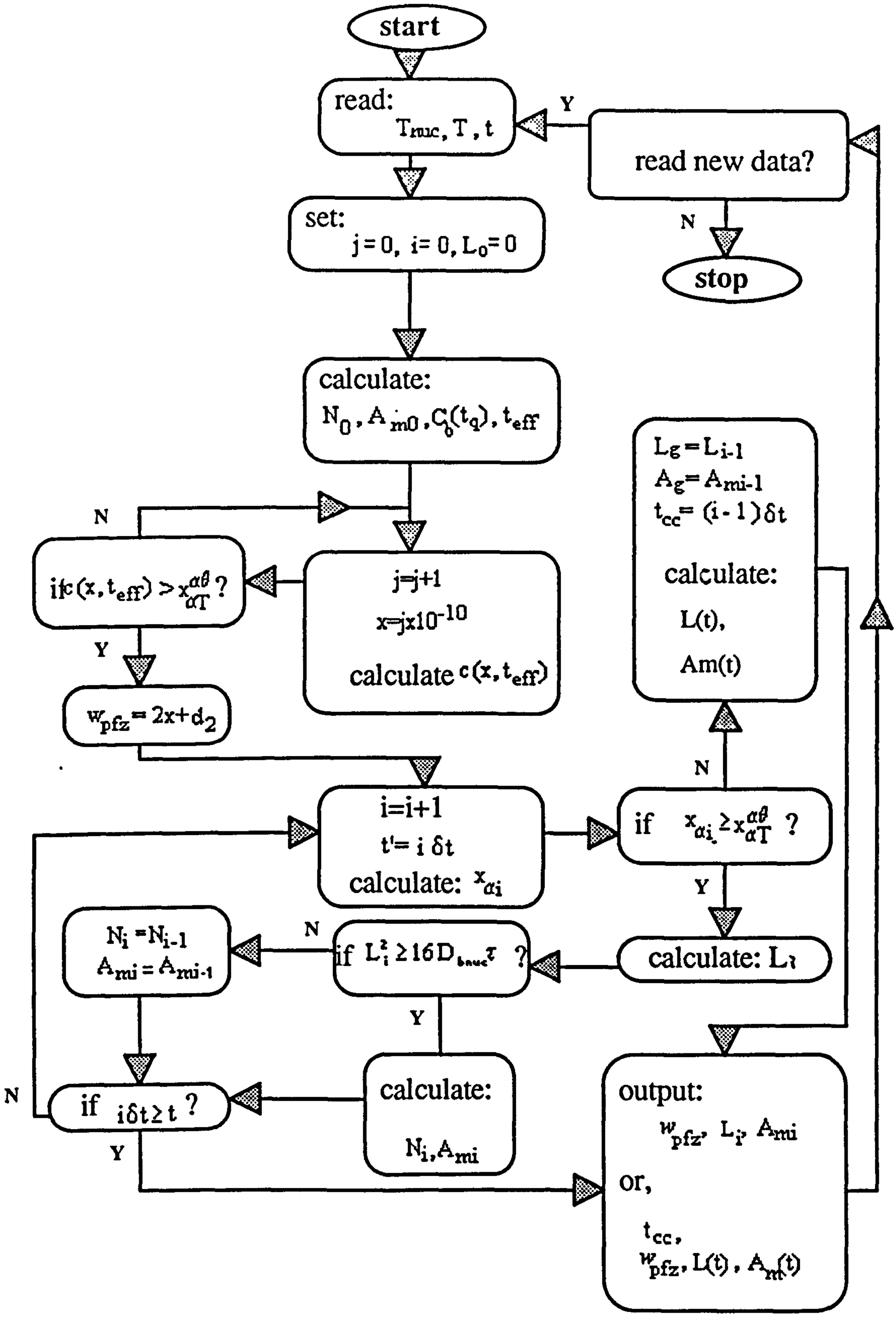

Fig. 3.7.1b: The flow chart of the combined model 2.

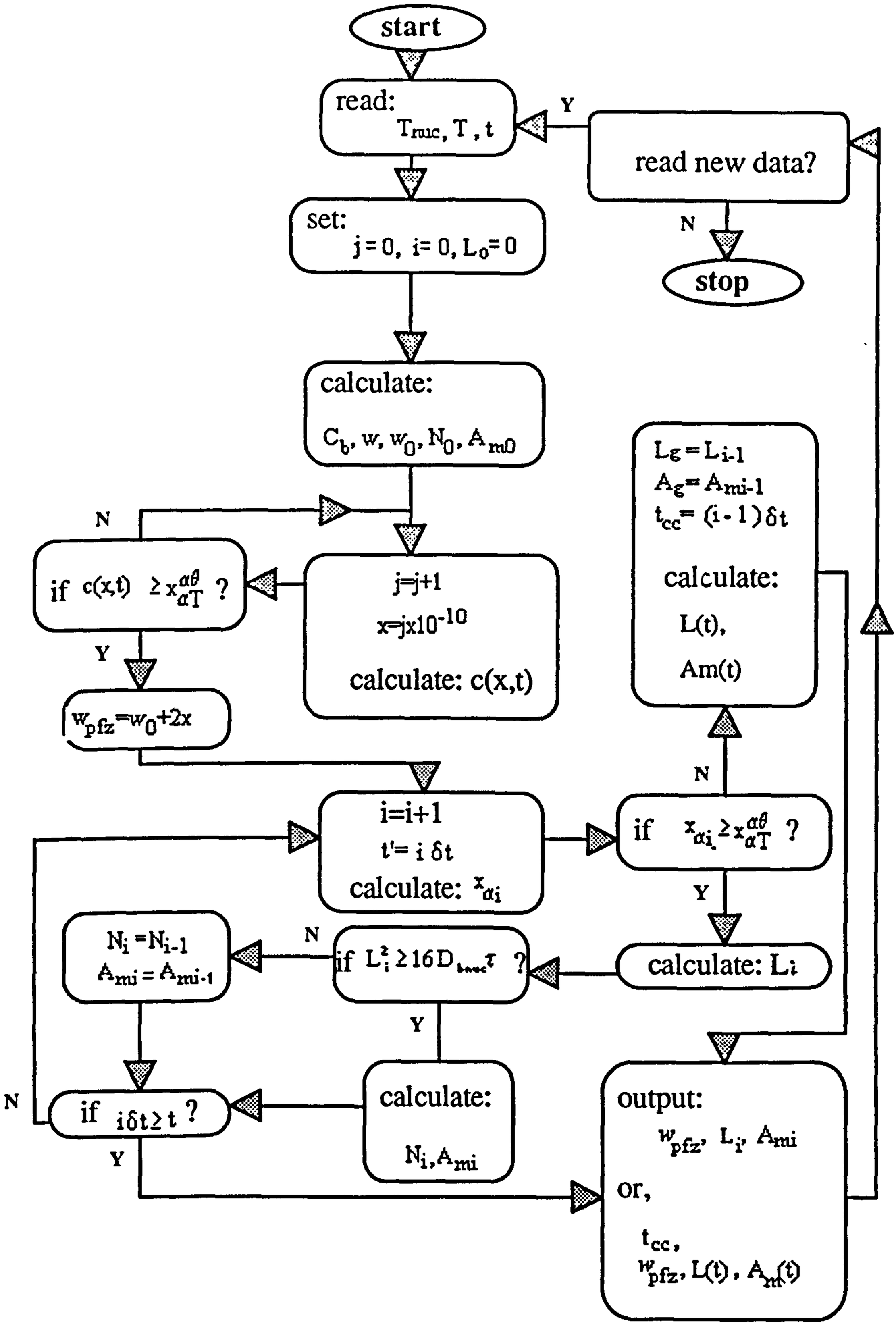

Fig. 3.7.1c: The flow chart of the combined model 3.

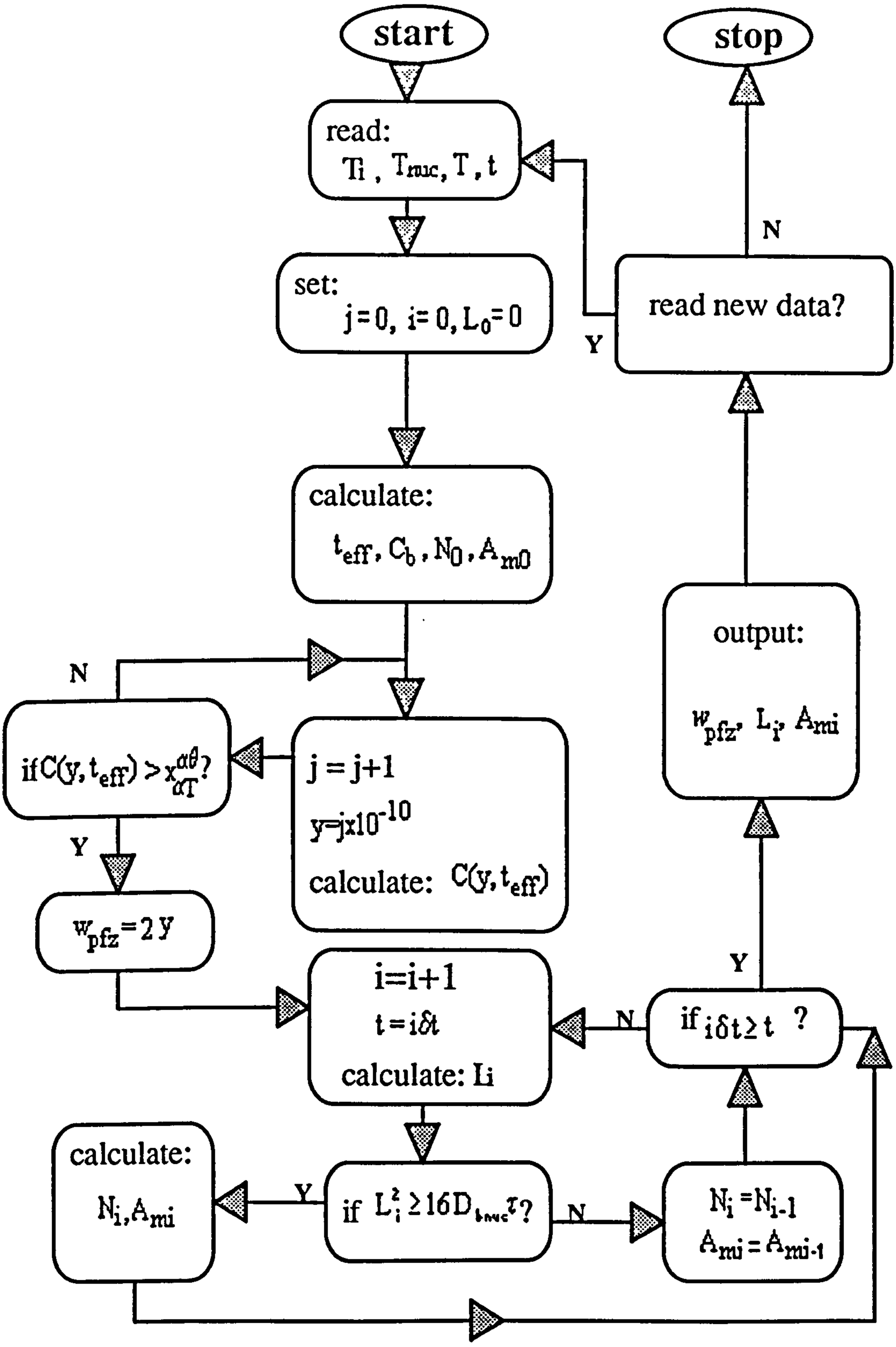

Fig. 3.7.1d: The flow chart of the combined model 4.

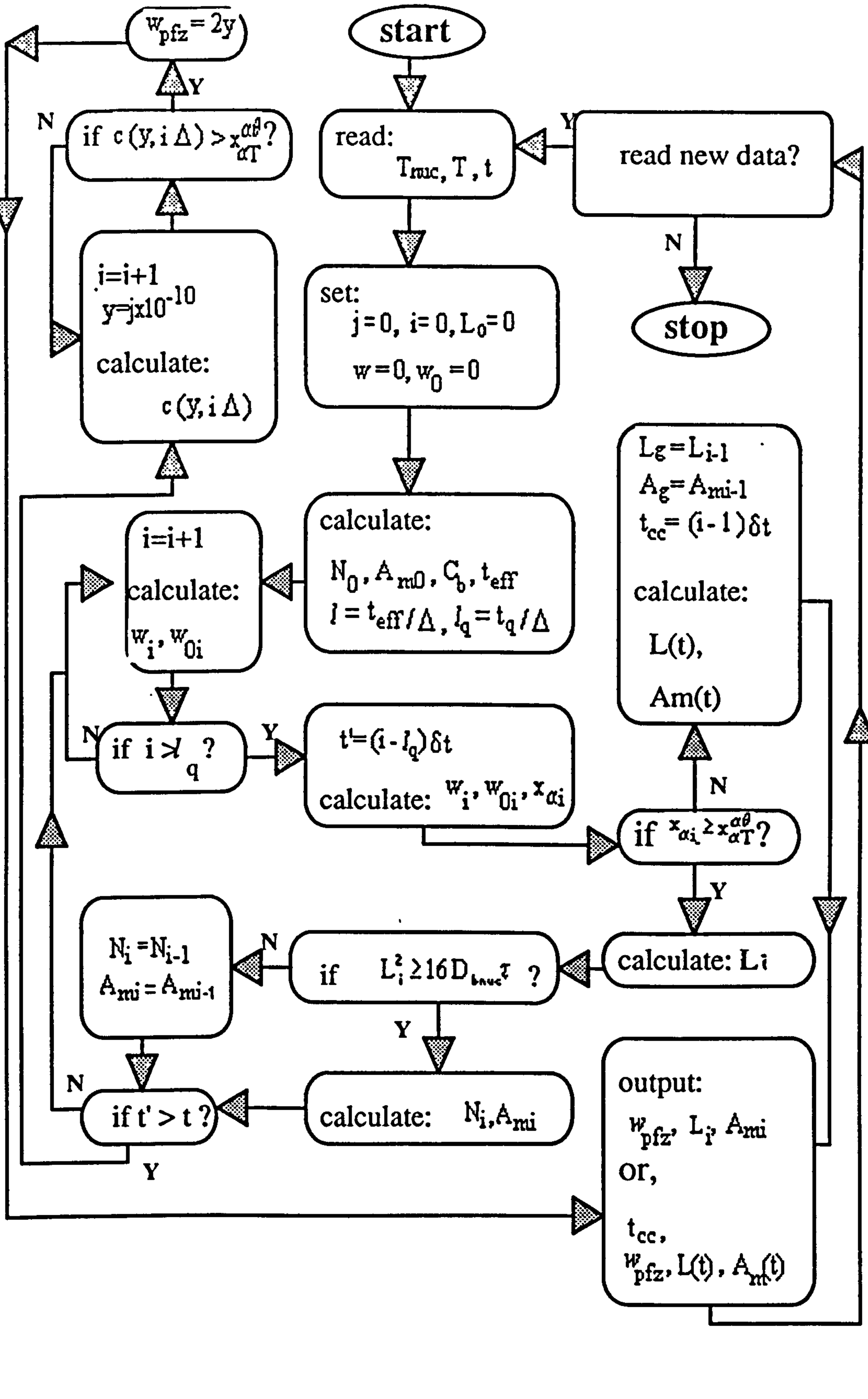

Fig. 3.7.1e: The flow chart of the combined model 5.

The definitions and calculations of the parameters in the flow chart are the same as in previous sections.

3.8 *An attempt at combined modelling for two stage ageing condition*

Combined models 1, 2, 3, and 5 are modified so that they can be used for the situation that samples are subjected to the heat-treatment that two stage ageing is employed after quenching from solution treatment temperature. The samples are aged at the second stage ageing temperature after being aged for time, t, $t=n\delta t$, at the first stage ageing temperature, T.

During the second stage of ageing, the radius of precipitates is

$$L_{n'} = \left\{ \sum_{j=1}^{i=n'} \frac{2A_{mj-1} D_{l2}^{\frac{1}{2}} (x_{\alpha j} - x_{\alpha T}^{\alpha\theta}) \{ (j\delta t)^{\frac{1}{2}} - [(j-1)\delta t]^{\frac{1}{2}} \} \rho_\alpha}{\rho_\theta \pi^{\frac{3}{2}} f(\psi)(x_\theta - x_{\alpha T}^{\alpha\theta})} + L_n^3 \right\}^{\frac{1}{3}} \qquad (3.8.1)$$

where n' is an integer and n' is given by

$$n' = \frac{t_2}{\delta t} \qquad (3.8.2)$$

where t_2 is the ageing time at the second stage ageing temperature, T_2.

For combined model 1, $x_{\alpha j}$ is given by

$$x_{\alpha j} = \frac{A_{mj-1} \int_0^{l_2} C(y, t_{eff}^j) dy - \pi f(\psi) L_{j-1}^3 (x_\theta - x_{\alpha T}^{\alpha\theta})}{l_2 A_{mj-1}} \qquad (3.8.3)$$

where $C(y, t_{eff}^{j})$ is the solute concentration distribution at effective time t_{eff}^{j} given by Equation (2.1.15) or (2.1.17) in which t_{eff}^{j} is

$$t_{eff}^{j} = t_q + t \cdot \exp\frac{-Q_c(T_i - T)}{kT_iT} + j\delta t \cdot \exp\frac{-Q_c(T_i - T_2)}{kT_iT_2} \qquad (3.8.4)$$

l_2 is the mean diffusion distance of the solute atoms for the sample being aged at temperature, T, for time , t, and at temperature, T_2, for time, jδt.

$$l_2 = \sqrt{2D_i t_{eff}^{j}} \qquad (3.8.5)$$

where

$$t_{eff}^{j} = t + j\delta t \cdot \exp\frac{-Q_i(T - T_2)}{kTT_2} \qquad (3.8.6)$$

where Q_i is the activation energy for the calculation of the volume diffusion coefficient of the solute atoms in the matrix.

For combined model 2, $x_{\alpha j}$ is given by

$$x_{\alpha j} = \frac{A_{mj-1}[\int_0^{l_2 - \frac{d_2}{2}} c(x, t_{eff}^{j})dx + \frac{d_2}{2}C_b(t_{eff}^{j})] - \pi f(\psi)L_{j-1}^3(x_\theta - x_{\alpha T}^{\alpha\theta})}{l_2 A_{mj-1}} \quad (\text{if } l_2 > \frac{d_2}{2}) \quad (3.8.7a)$$

or

$$x_{\alpha j} = \frac{A_{mj-1}C_b(t_{eff}^{j})l_2 - \pi f(\psi)L_{j-1}^3(x_\theta - x_{\alpha T}^{\alpha\theta})}{l_2 A_{mj-1}} \quad (\text{if } l_2 \leqslant \frac{d_2}{2}) \quad (3.8.7b)$$

where $c(x, t_{eff}^{j})$ is the solute concentration distribution at effective time t_{eff}^{j} given by Equation (2.1.24) and $C_b(t_{eff}^{j})$ is given by Equation (2.1.18).

For combined model 3, $x_{\alpha j}$ is given by

$$x_{\alpha j} = \frac{A_{mi-1}[\int_0^{l_2-\frac{w_0}{2}} c(x, t^j_{eff''})dx + \frac{w_0}{2}C_b] - f(\psi)\pi L^3_{j-1}(x_\theta - x^{\alpha\delta}_{\alpha T})}{l_2 A_{mj-1}} \quad (\text{if } l_2 > \frac{w_0}{2}) \qquad (3.8.8a)$$

or

$$x_{\alpha j} = \frac{A_{mi-1} l_2 C_b - f(\psi)\pi L^3_{i-1}(x_\theta - x^{\alpha\delta}_{\alpha T})}{l_2 A_{mi-1}} \quad (\text{if } l_2 \leqslant \frac{w_0}{2}) \qquad (3.8.8b)$$

where $c(x, t^j_{eff''})$ is the solute concentration distribution given by Equation (3.1.10), $t^j_{eff''}$ is the effective ageing time at the first ageing temperature given by

$$t^j_{eff''} = t + j\delta t \cdot \exp\frac{-Q_c(T - T_2)}{kTT_2} \qquad (3.8.9)$$

For combined model 5, $x_{\alpha j}$ is given by

$$x_{\alpha j} = \frac{A_{mj-1}\int_0^{l_2} C(y, l' \cdot \Delta)dy - f(\psi)\pi L^3_{j-1}(x_\theta - x^{\alpha\delta}_{\alpha T})}{l_2 A_{mj-1}} \qquad (3.8.10)$$

where $C(y, l'' \cdot \Delta)$ is the solute concentration distribution at time $l''\Delta$; $C(y, l'' \cdot \Delta)$ by Equation (3.1.6); $l'' \cdot \Delta = t^j_{eff}$; l'' is an integer given by

$$l' = \frac{t^j_{eff}}{\Delta} \qquad (3.8.11)$$

D_{l2} is the volume diffusion coefficient of the solute at the second stage ageing temperature. A_{mj-1} is the mean collector plate area after ageing for a time of (j-1)δt at the second stage ageing temperature.

The mean collector plate area after ageing for a time of t_2 at the second stage ageing temperature is given by

$$A_{mn'} = \frac{1}{N_n \prod_{j=1}^{j=n'} \{1-0.25[erf(\frac{A_{mj-1}-A_{\min}}{\sqrt{2}\sigma}) - erf(\frac{A_{mj-1}-4L_j^2}{\sqrt{2}\sigma})]^2\}} \qquad (3.8.12)$$

where

L_j is given by

$$L_j = \{\frac{2A_{mj-1}D_{l2}^{\frac{1}{2}}(x_{\alpha j}-x_{\alpha T}^{\alpha\theta})\{(j\delta t)^{\frac{1}{2}}-[(j-1)\delta t]^{\frac{1}{2}}\}\rho_\alpha}{\rho_\theta \pi^{\frac{3}{2}} f(\psi)(x_\theta - x_{\alpha T}^{\alpha\theta})} + L_{j-1}^3\}^{\frac{1}{3}} \qquad (3.8.13)$$

and the probability density function of collector plates, $n_{n'}$, is

$$n_{n'} = \frac{N_{n'}}{2\sqrt{\pi}\sigma}\exp[-\frac{(A_v - A_{mn})^2}{2\sigma^2}] \qquad (3.8.14)$$

where $N_{n'} = 1/A_{mn'}$, $N_n = 1/A_{mn}$, A_{mn} is given by Equation (3.5.22) in which N_0 is given by Equation (3.2.1) with ΔG_v given by Equation (3.2.8a) for combined models 1, 3 and 5 and by Equation (3.2.8b) for combined model 2. σ is given by Equation (3.2.15) with τ given by Equation (3.2.10a) for combined models 1, 3 and 5 and by Equation (3.2.10b) for combined model 2.

$L_{j-1}=L_n$, when j=1; L_n is the radius of the precipitates after the first stage ageing given by Equation (3.3.12).

The width of the precipitate free zones after ageing for a time of t_2 at the second stage ageing temperature is given by

$$w_{pfz} = 2y_0 \tag{3.8.15}$$

where

$$y_0 = \varpi + \lambda' \tag{3.8.16}$$

and λ' should satisfy the condition that

$$c(\lambda', t) = x_{\alpha T}^{\alpha\theta} \tag{3.8.17}$$

For combined model 1, ϖ=0; $c(\lambda', t)$=$C(\lambda', t_{eff}^{n'})$; $C(\lambda', t_{eff}^{n'})$ is given by Equation (2.1.15) or (3.1.17); $t_{eff}^{n'}$ is the effective time given by

$$c(\lambda', t_{eff}^{n'}) = t_q + t \cdot \exp\frac{-Q_c(T_i - T)}{kT_iT} + n'\,\delta t \cdot \exp\frac{-Q_c(T_i - T_2)}{kT_iT_2} \tag{3.8.18}$$

For combined model 2; $c(\lambda', t) = c(\lambda', t_{eff}^{n'})$; $c(\lambda', t_{eff}^{n'})$ is given by Equation (2.1.24); $t_{eff}^{n'}$ is given by Equation (3.8.18) and $\varpi = \frac{d_2}{2}$.

For combined model 3, $\varpi = \frac{w_0}{2}$; $c(\lambda', t) = c(\lambda', t_{eff''}^{n'})$; $c(\lambda', t_{eff''}^{n'})$ is given by Equation (3.1.10) in which $t_{eff''}^{n'}$ is the effective ageing time at the first ageing temperature given by

$$t_{eff''}^{n'} = t + n'\,\delta t \cdot \exp\frac{-Q_c(T - T_2)}{kTT_2} \tag{3.8.19}$$

For combined model 5, ϖ=0; $c(\lambda', t)$=$C(\lambda', n''\Delta)$; $C(\lambda', n''\Delta)$ is given by Equation (3.1.6) in which $w_{0n''}$ given by Equation (3.1.1) is the width of the solute concentrated layer at this time. In both Equations (3.1.1) and (3.1.6) i=n", n" is an integer given by $n'' = t_{eff}^{n'}/\Delta$

Chapter Four

Experimental Work

4.1 *Sample preparation*

4.1.1. *Material*

The material used for this study is extruded commercial aluminium alloy 7150 in cold rolled condition, supplied by Alcan International Limited, Banbury Laboratory in the form of block. The composition of the material is

element	Cu	Mg	Zn	Fe	Si	Ti	Cr	Ni	Zr	Mn	Al
wt %	1.92	2.33	6.46	0.037	*	.05	.002	0.001	0.12	0.004	bal

4.1.2 *Heat treatment*

Twenty rectangular sections of approximate dimensions 12x12x30mm were cut from the original material of aluminium alloy 7150. All these pieces were prepared for solution treatment. This preparation took the form of heating these pieces in a furnace to a temperature of $475\ ^{\circ}C \pm 5^{\circ}C$ for a period of 20 minutes. This time was sufficient to enable the undissolved precipitates to dissolve in the matrix and also to relieve the distorted structure due to the effects of cold work. The pieces were cooled rapidly to an ambient temperature by dropping directly into a water quench bath from the furnace. The pieces were at this point ready for the ageing process. This took the form of the heat treatment in which these aluminium alloy pieces were re-heated to two different ageing temperatures and for various ageing times. There were in total ten ageing treatment conditions with two of the twenty pieces for each condition. The details of these heat treatment conditions are given in Table 4.1.1.

Table 4.1.1: Heat treatment condition.

sample:	heat treatment condition:
160-0005	solution treated for 20 min. at 475±5°C, water-quenched + aged for 0.5 hr at 160°C
160-0060	solution treated for 20 min. at 475±5°C, water-quenched + aged for 6 hr at 160°C
160-0110	solution treated for 20 min. at 475±5°C, water-quenched + aged for 11 hr at 160°C
160-0200	solution treated for 20 min. at 475±5°C, water-quenched + aged for 20 hr at 160°C
160-0480	solution treated for 20 min. at 475±5°C, water-quenched + aged for 48 hr at 160°C
180-0005	solution treated for 20 min. at 475±5°C, water-quenched + aged for 0.5 hr at 180°C
180-0010	solution treated for 20 min. at 475±5°C, water-quenched + aged for 1 hr at 180°C
180-0020	solution treated for 20 min. at 475±5°C, water-quenched + aged for 2 hr at 180°C
180-0030	solution treated for 20 min. at 475±5°C, water-quenched + aged for 3 hr at 180°C
180-0100	solution treated for 20 min. at 475±5°C, water-quenched + aged for 10 hr at 180°C

4.1.3 *Thin foil specimen preparation*

30 thin foil discs were prepared for the TEM test for each heat treatment. Fig. 4.1.1 gives the flow chart that roughly illustrates the whole process of the preparation of TEM specimens.

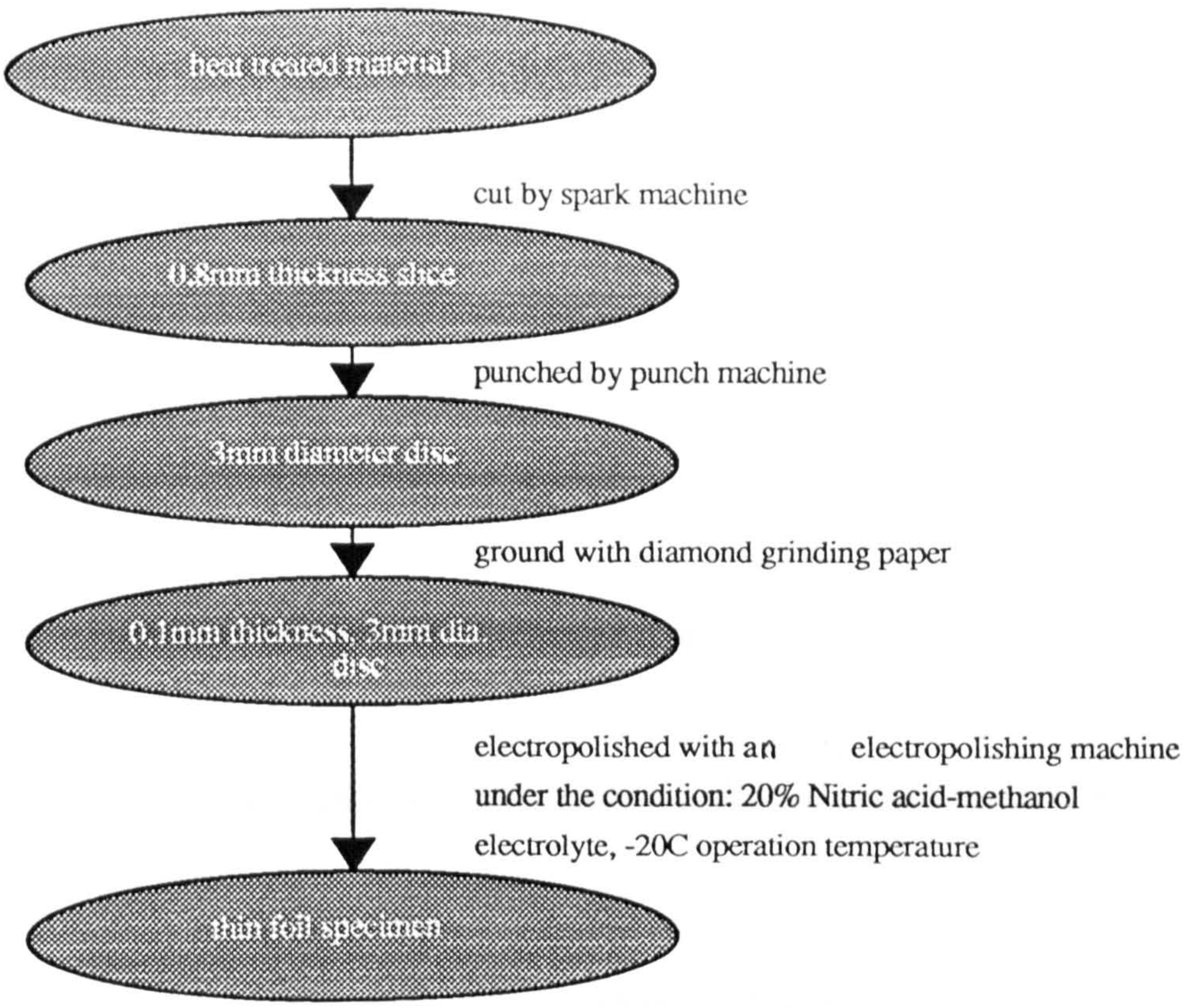

Fig. 4.1.1: Flow chart of the process of thin foil specimen preparation.

Samples in L-ST orientation were cut in the form of thin slices of 0.85 ~ 1 mm thickness using an electric spark discharge cutting machine. Discs of 3 mm diameter were punched from each slice specimen. After having polished them mechanically to reduce their thickness to a thickness within 0.15 ~0.25 mm, further thinning of the discs was performed by using the Struers Tenupol Automatic Polisher in an electrolyte of 20% Nitric acid, 80% methanol at a bath temperature of $-20°C$. To do this, the disc specimen of 0.15 ~ 0.25 mm thickness is held in a screw-in P.T.F.E. holder. This is then inserted into the bath chamber with disc specimen positioned between two small jets through which electrolyte is pumped by an electric motor. A light source is focused on one side of the specimen. On the other side a photo-cell detector is placed to pick up any perforations. On detection a trip switch stops the process, the holder is then removed. Finally the specimen is rinsed in methanol and dried on filter paper. The operation conditions of using the Struers tenupol automatic polisher for this material are:

voltage: 11~13 V

current: 100~120 mA

flow rate: 2~2.6

sensitivity: 6~7

temperature: $-20°C$

4.2 *TEM investigations of the samples*

A schematic illustration of the structure of a transmission electron microscope is shown in Fig. 4.2.1.

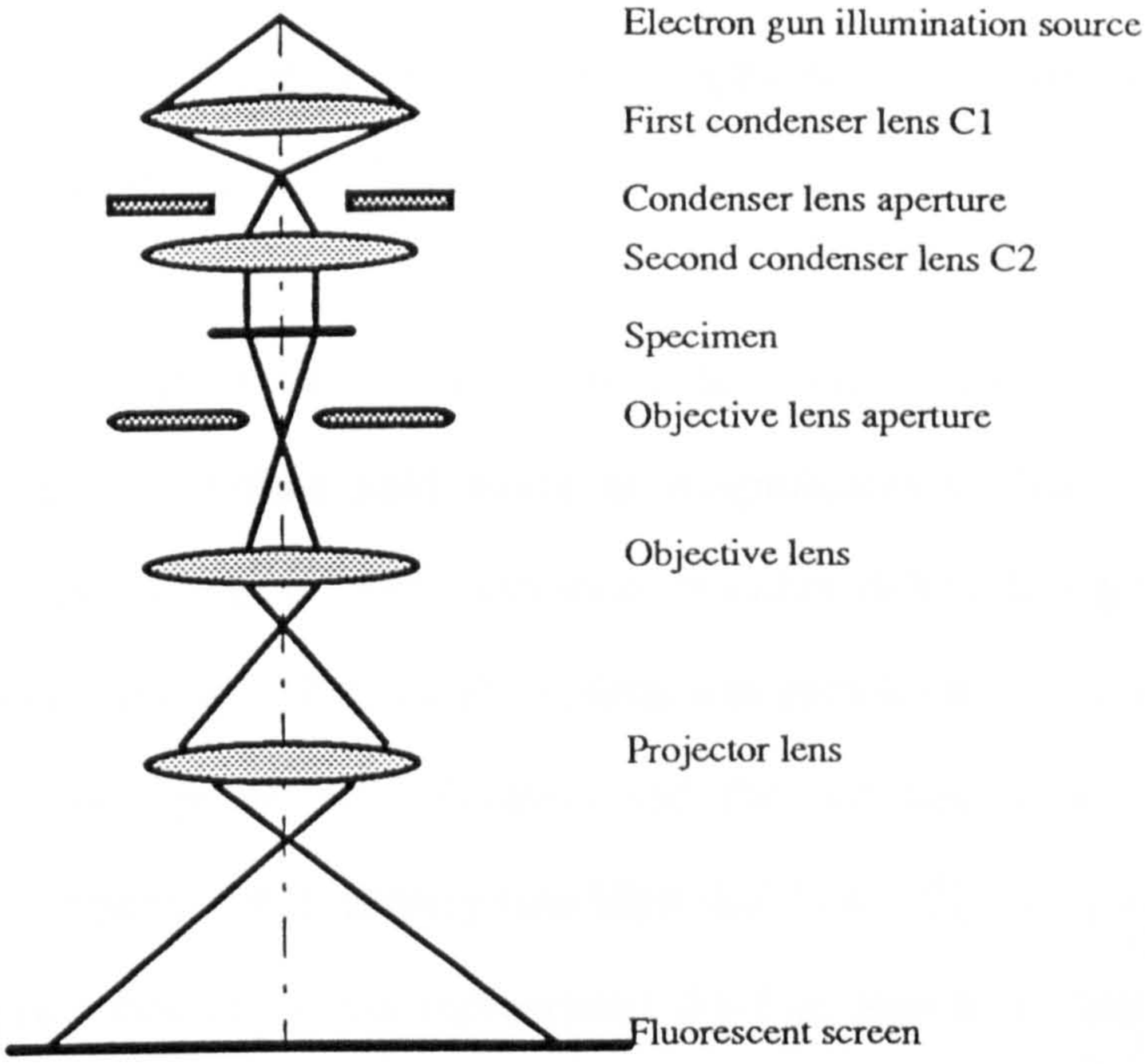

Fig.4.2.1: Illustration of a TEM structure.

In the transmission electron microscope, the strong condenser C1 lens produces a diminished image of the electron source. This is diminished further by the second condenser lens C2. The resolution can be improved by inserting an aperture after the first condenser lens to reduce the angular aperture of the second condenser lens. A

beam of high velocity and well focused electrons is then projected onto a thin foil specimen under examination. The intensity of the beam is modulated by the opacity of the specimen at it passes through and an image is formed on the back focus plane of the objective lens. The image is further magnified by the projector lens and the resulting modulated beam of the electrons hits a fluorescent screen. The operator can then view and photograph the screen.

The sizes, the inter precipitate spacing of grain boundary precipitates and the widths of precipitate-free zones of all the samples were investigated by a transmission electron microscope (TEM). The TEM used in this work was a Jeol 100CX which worked at a voltage of 100kV and its resolution was 0.5 nm.

The procedure for obtaining micrographs of grain boundary precipitates from the TEM was as follows.

The observation of the grain boundary precipitates and their distribution was performed in bright field mode at magnifications x33k ~ x250k. Once a grain boundary was found and confirmed by either diffraction patterns or bend contours, the boundary was tilted until its plane was parallel to the electron beam and a profile of the precipitate was obtained and the sections of each grain boundary were photographed consecutively (see Figs. 4.2.2a-4.2.2j). The length of the profile along the grain boundary line represented the true length of the precipitate, the distance between two particles next to each other along the boundary represented the inter-precipitate spacing, the length of the line crossing from one side of the grain boundary perpendicularly to another side and covering the whole PFZ represented the width of the PFZ. This technique was used for every measurement.

Over 150 TEM photographs were taken for each heat-treatment, these contained about 150 grain boundaries and 2,000 precipitates.

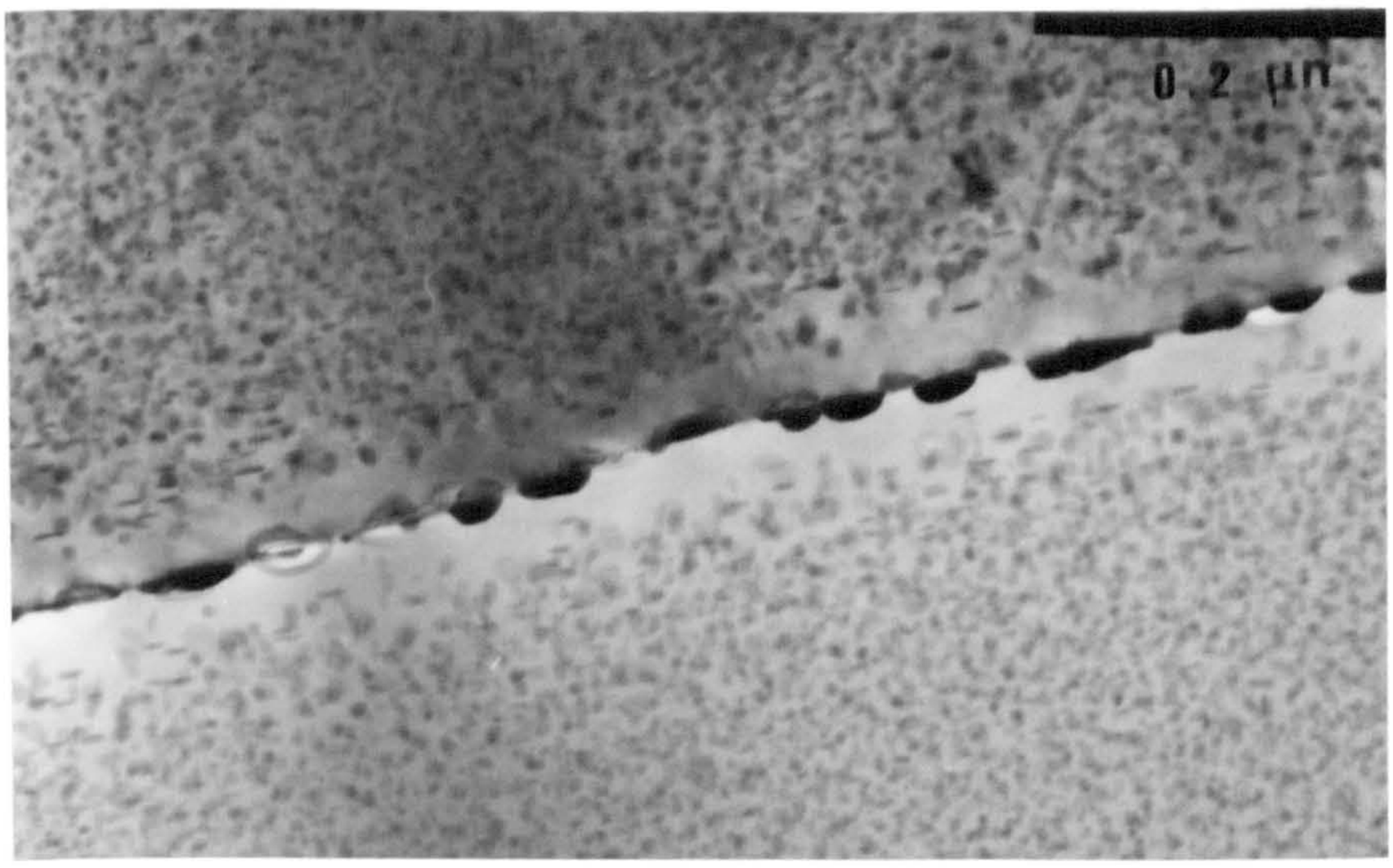

Fig. 4.2.2a: Typical area from which precipitate size, inter-particle spacing and the width of PFZ measurements were made: specimen aged 0.5 h at 180°C (TEM).

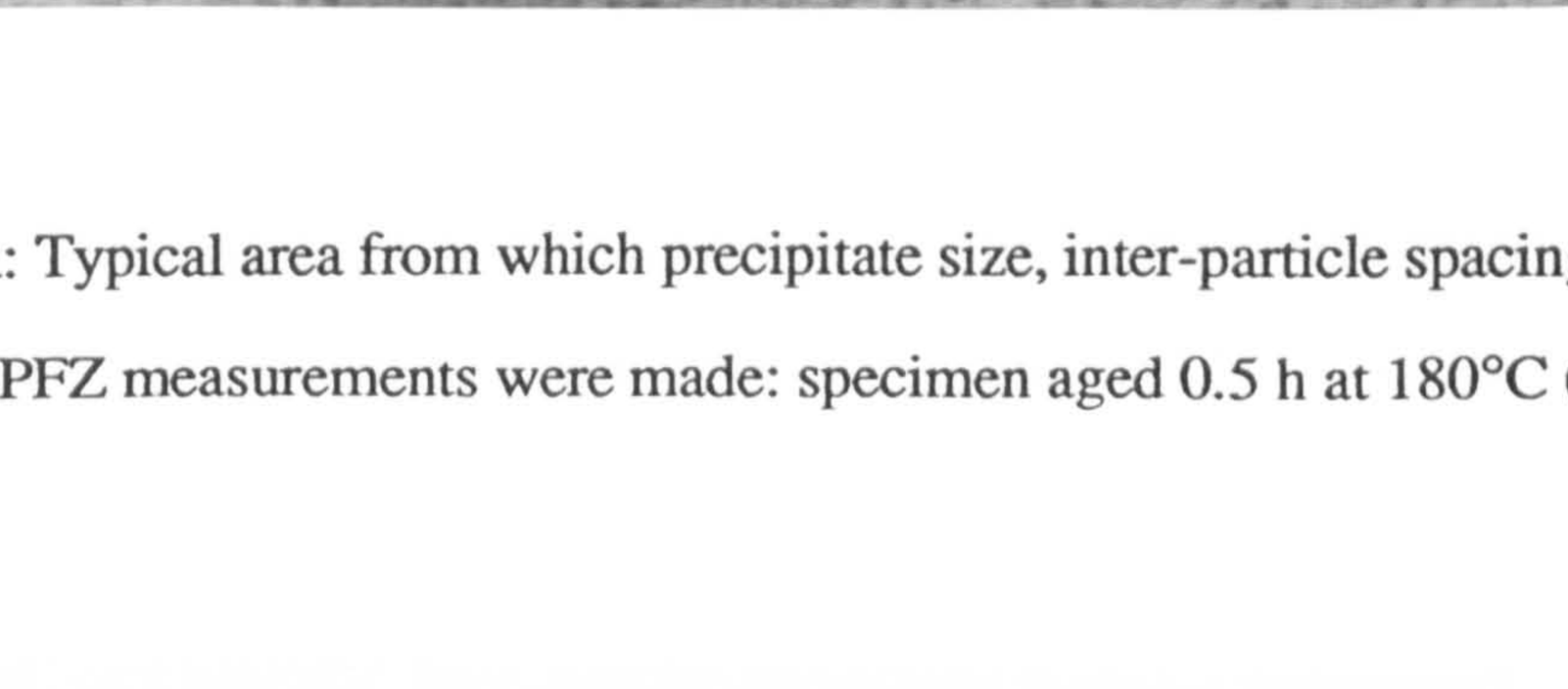

Fig. 4.2.2b: Typical area from which precipitate size, inter-particle spacing and the width of PFZ measurements were made: specimen aged 1 h at 180°C (TEM).

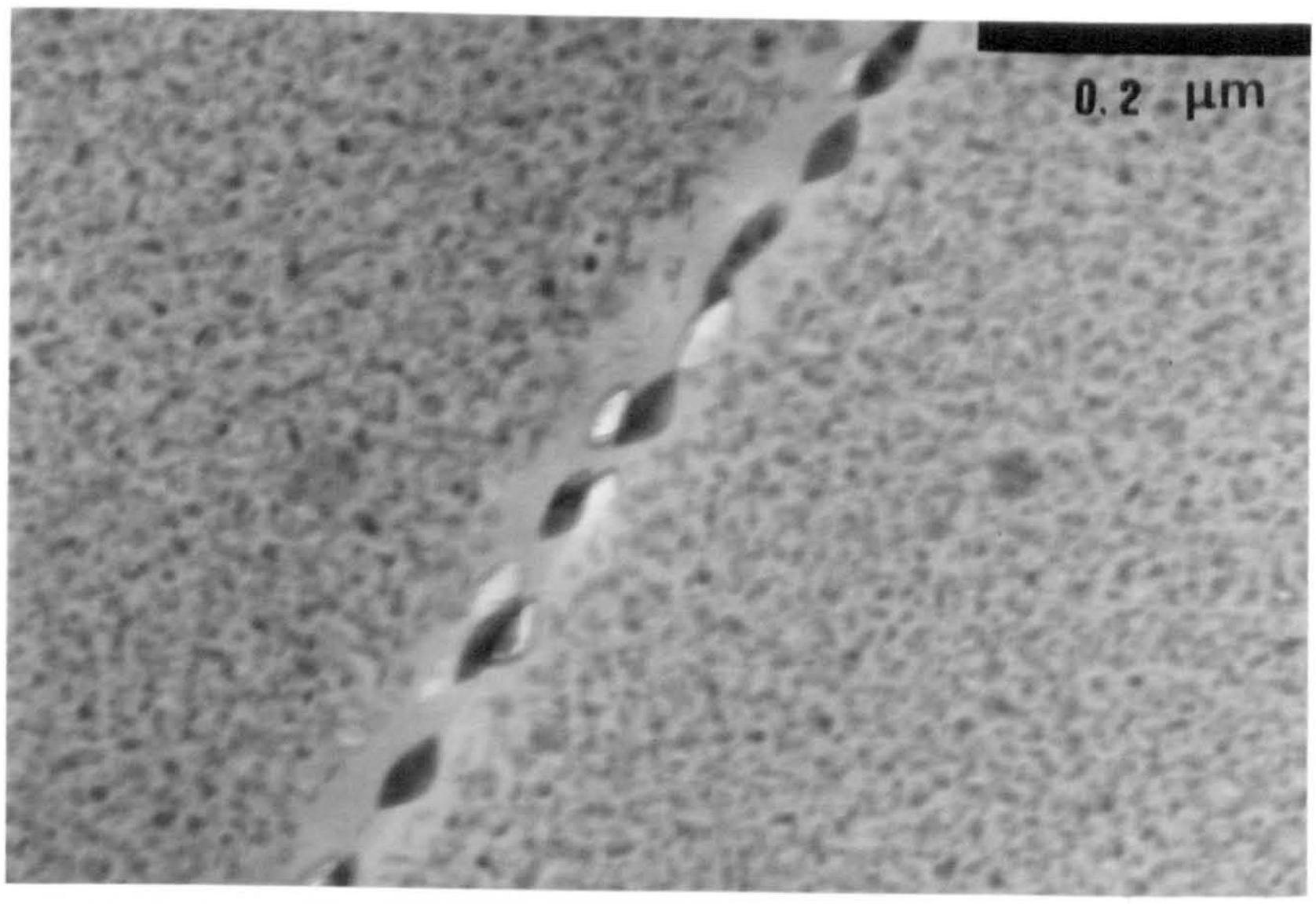

Fig. 4.2.2c: Typical area from which precipitate size, inter-particle spacing and the width of PFZ measurements were made: specimen aged 2 h at 180°C (TEM).

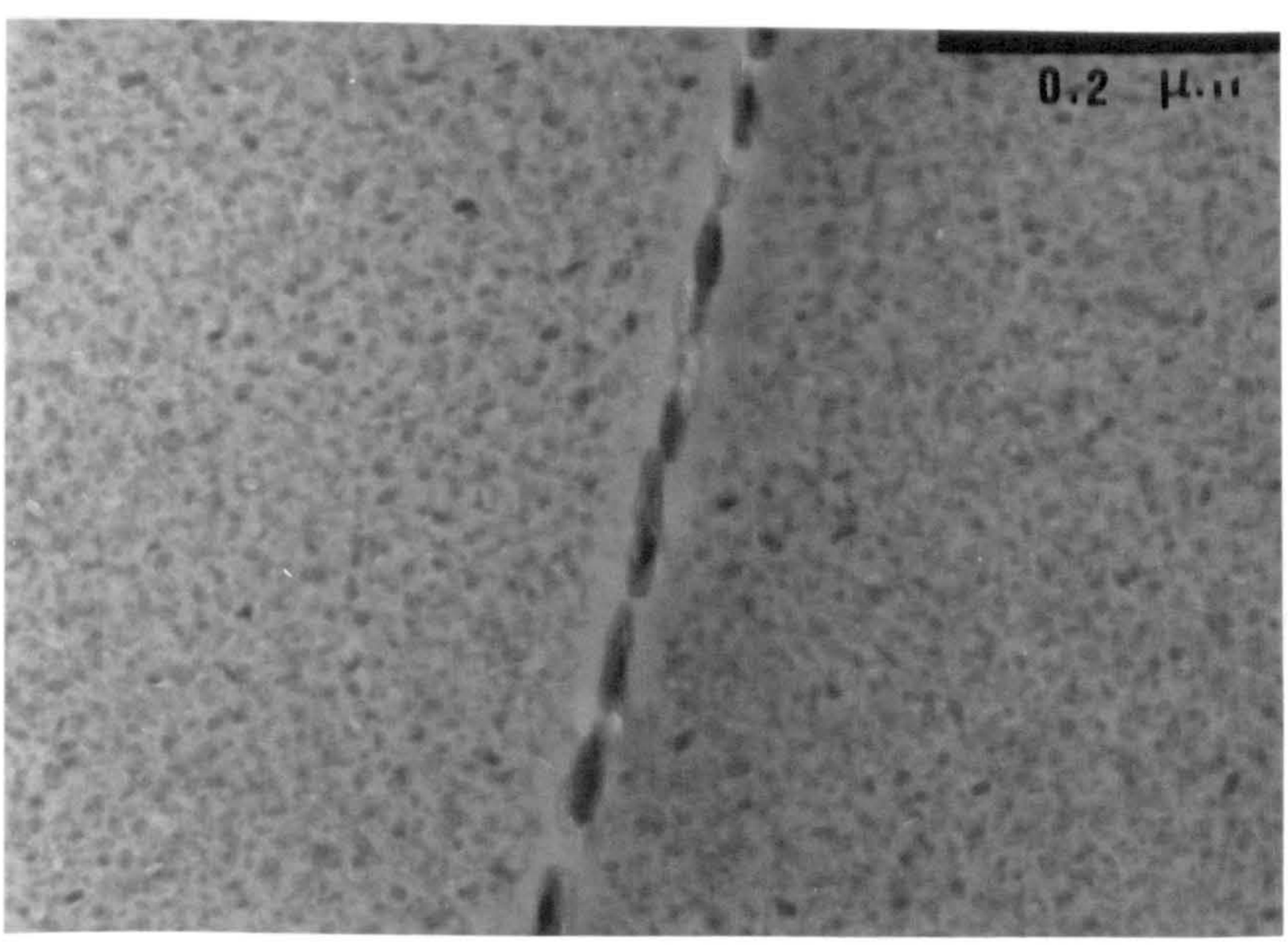

Fig. 4.2.dc: Typical area from which precipitate size, inter-particle spacing and the width of PFZ measurements were made: specimen aged 3 h at 180°C (TEM).

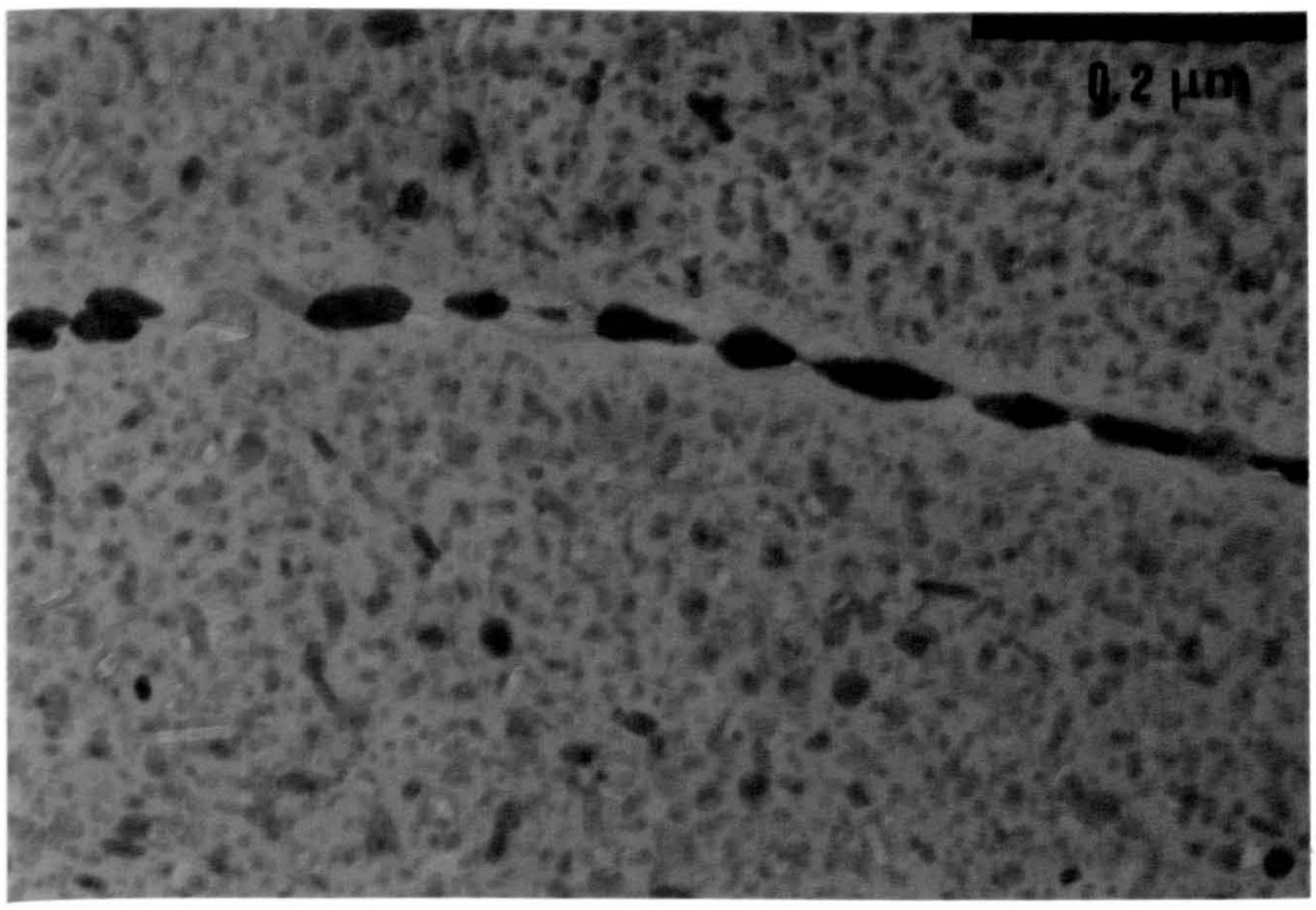

Fig. 4.2.2e: Typical area from which precipitate size, inter-particle spacing and the width of PFZ measurements were made: specimen aged 10 h at 180°C (TEM).

Fig. 4.2.2f: Typical area from which precipitate size, inter-particle spacing and the width of PFZ measurements were made: specimen aged 0.5 h at 160°C (TEM).

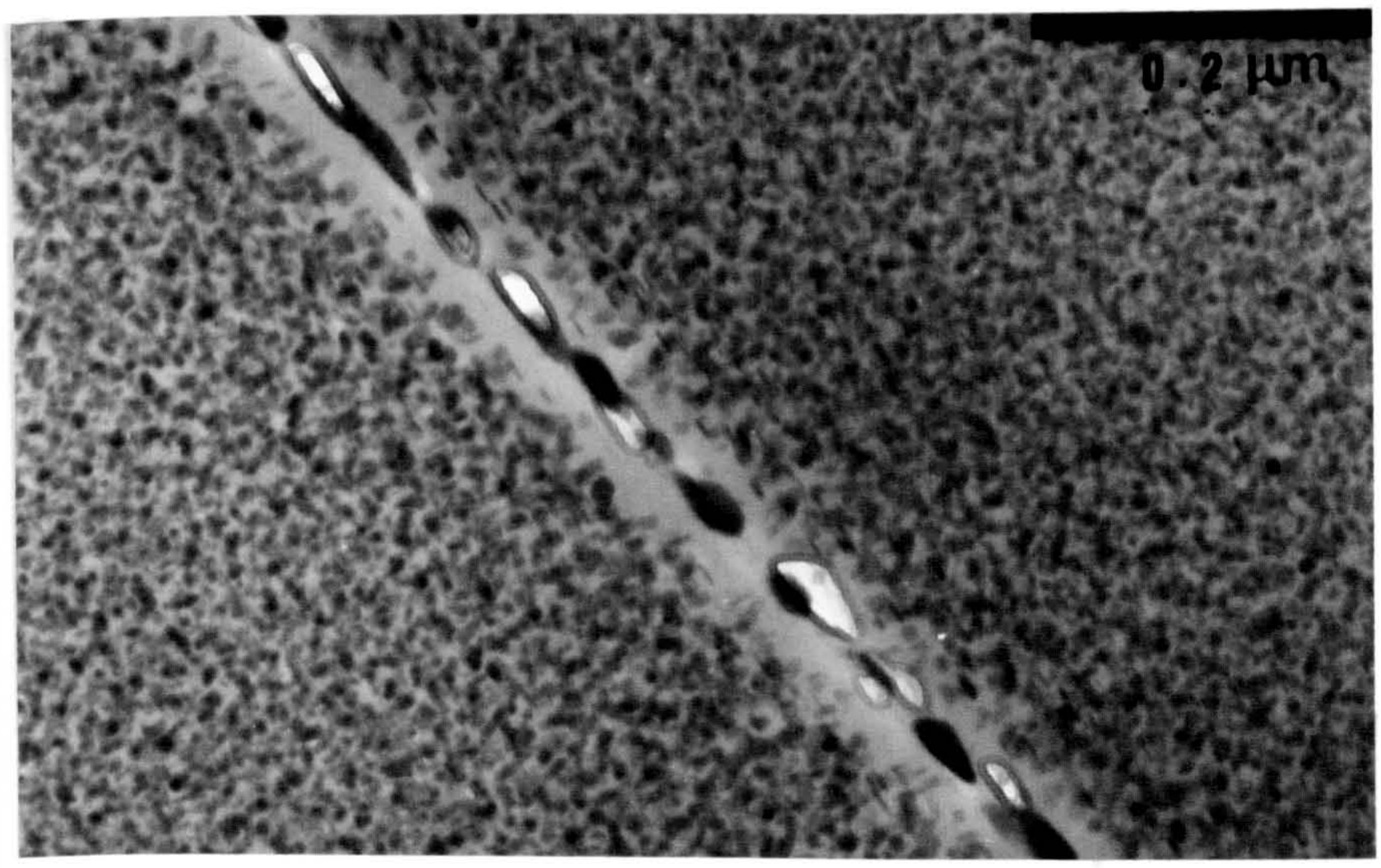

Fig. 4.2.2g: Typical area from which precipitate size, inter-particle spacing and the width of PFZ measurements were made: specimen aged 6 h at 160°C (TEM).

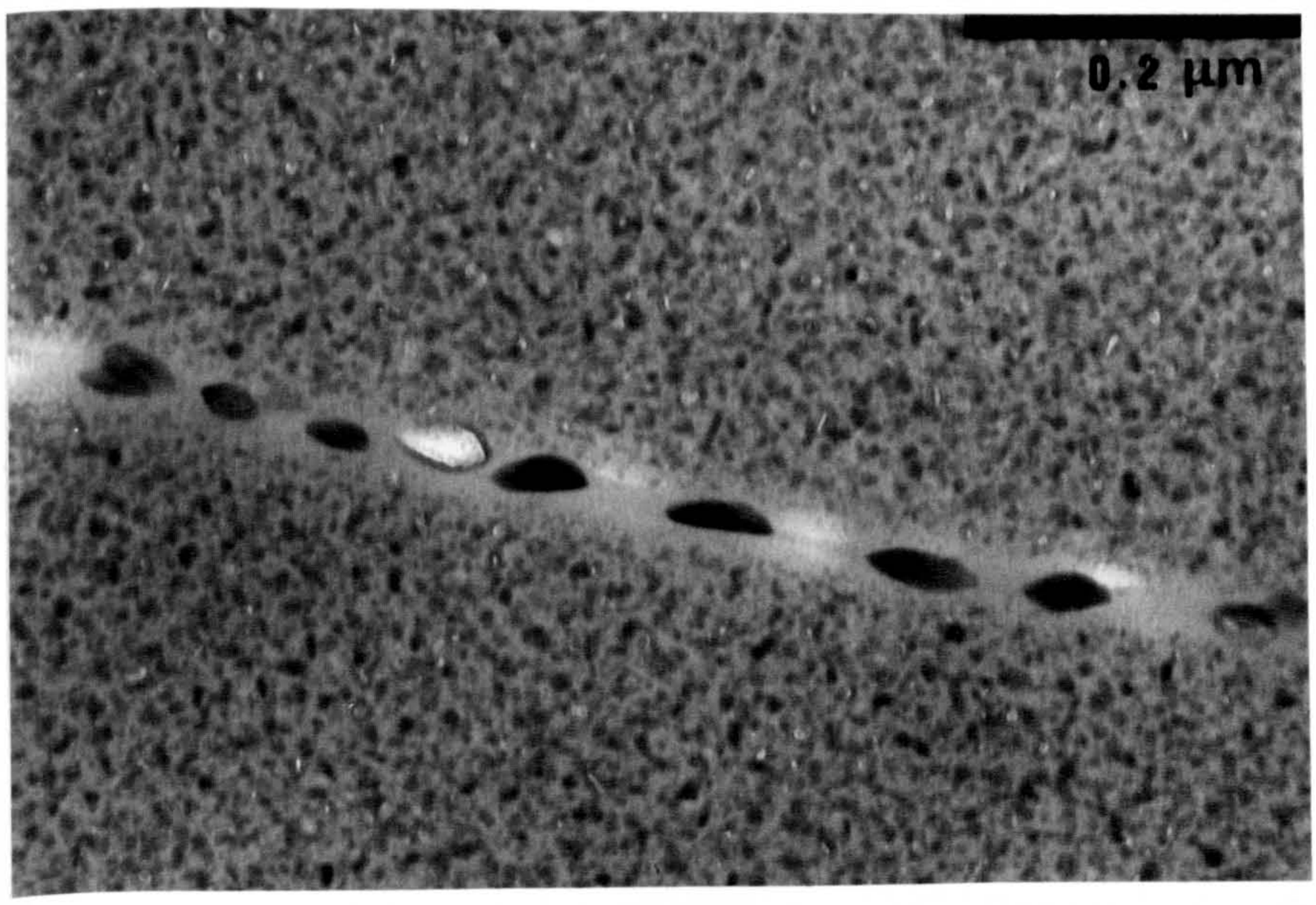

Fig. 4.2.2h: Typical area from which precipitate size, inter-particle spacing and the width of PFZ measurements were made: specimen aged 11 h at 160°C (TEM).

MISSING

PAGE

NOT

AVAILABLE

4.3 *Measurements and statistical analysis*

An image analysis system was then introduced to perform the measurements and the statistical analysis of the measurement results.

4.3.1 *Microcomputer-based image analysis system*

The essential elements of a microcomputer-based image processing and analysing system for the acquisition, processing, storage and display of the data from an electron microscope are shown in Fig. 4.3.1.

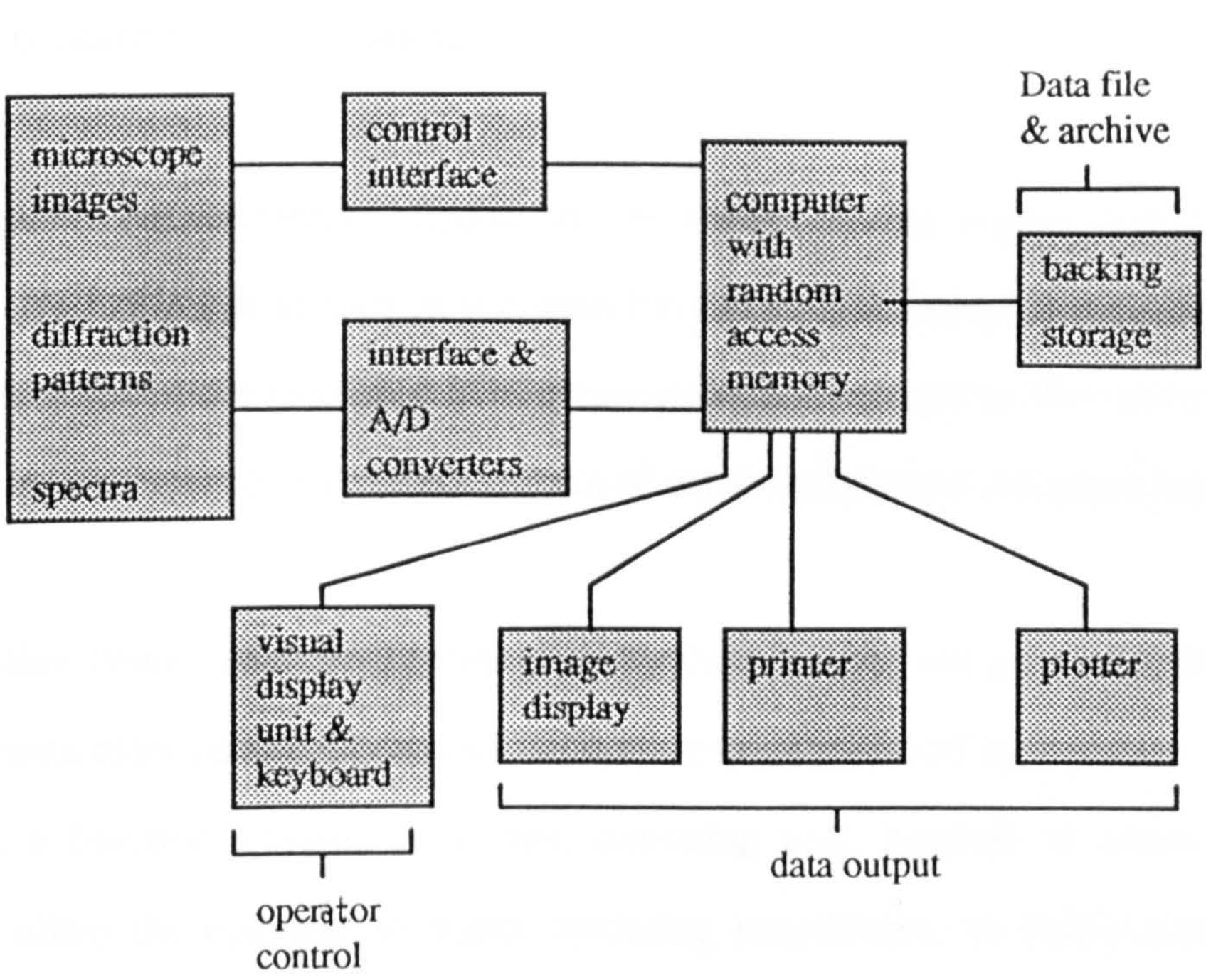

Fig. 4.3.1: Elements of an on-line image analysis system for electron microscopy.

Image, diffraction pattern or spectral information is converted to digital form by means of an analogue/digital converter (ADC) and stored in a digital memory system. Processing of this data is carried out by means of a computer, the output of which can be displayed to the operator. The displayed information may be in the form of an image or it may be presented in the form of graphical or alpha-numerical

data. Many types of processing can be accomplished extremely rapidly so that it is possible for the operator to access the results of any particular operation or procedure and to reprocess the same data or acquire new data as necessary. This mode of operation is referred to as 'interactive' operation. If the conversion, processing and display of data proceeds at, or close to, TV rates, then the system is said to operate in 'real time'.

After acquisition and processing, the data may be filed temporarily or permanently, in some form of digital backing store, usually magnetic disc or tape, from whence the data may be recalled at will. Being in digital form the data are not subjected to any form of distortion or degradation.

In addition to the function of acquisition, processing, display and storage, the on-line system also can serve as part of a closed-loop control system, i.e. information may be extracted from the incoming data, processed and returned to the microscope, via a suitable interface, so as to effect control of some function of the microscope.

The on-line system is normally controlled by the operator using a visual display unit (VDU) with associated keyboard which may be supplemented by a variety of devices such as a function keypad, light pen, digitising pad, joystick or mouse. These devices allow the operator to select operating procedures, to define pixel regions with an image or regions of interest with a spectrum.

Fig. 4.3.2 is an illustration of the automatic measurement system made by linking TEM and an image analysis system. Such an automatic measurement system needs the following hardware:

a. Image capture -Video cameras, or Solid state camera (CCD camera)

(i). Video camera

It is to be appreciated that a number of different video standards have evolved for television transmission. Two common standards for monochrome video are American RS-170 and European CCIR. These differ fundamentally in line and frame rate and in the format of the synchronization pulses. As a result, exactly compatible standards are required between video cameras and digitizers. Apart from technical mis-match, problems can arise when software designed for one standard is applied to hardware of another due to the difference in the number of image lines.

(ii). Solid state cameras

Solid state cameras are commonly known as CCD cameras, referring to the charge coupled device sensor. These devices operate on the principle of the movement of small packets of electrons across photosites in the semiconductor material.

One of the most significant advantages of CCD sensors is the precise positioning of the photosensor locations. In a conventional tube camera, the position of the scanning beam is not as precisely known due to electrical fluctuations in the deflector circuitry. This metric accuracy is clearly advantageous for image analysis applications.

b. Frame Grabber board

The function of the frame grabber board is to capture, store and display live video images from video cameras or VCRs.

c. Video digitizers

The video digitizer converts the analogue video signal into digital data suitable for transfer to computer memory for analysis. There are a multitude of digitizers available for microcomputers and selection of a device appropriate for the intended application requires some knowledge of their design and operation.

d. Computer - control the process of images

A common image format for video digitizers is 512 pixels square. This is in line with the A/D converter characteristics, practical memory buffer limits and the resolution that can be expected from conventional, broadcast standard video cameras. An image of the size occupies 256 kilobytes (KB) of memory. As a consequence, if image analysis is to be by software alone, the success of operation depends on the specifications of the microprocessor on which the computer is based, its cycle speed, and memory access limits imposed by the computer design. Limitations of the processing speed will seriously affect the general utility of the entire system.

Popular microcomputers compatible with the IBM AT, and based on the Intel 80386 and 80486 microprocessors, have prodigious processing speed compared to earlier designs. A wealth of low cost, compatible computers are available and most video digitizers are designed for this standard. They are a clear choice for optimum cost and performance.

e. Monitors - display the image and the information of the procedure function

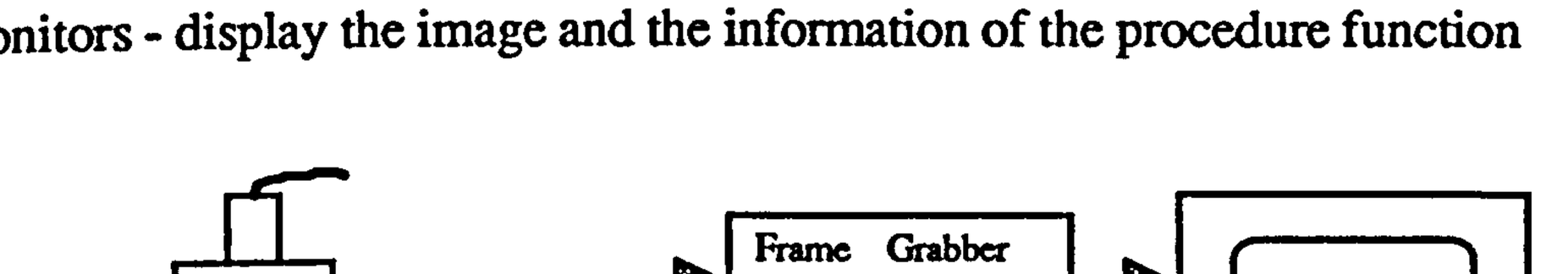

Fig. 4.3.2: Illustration of the automatic measurement system by linking TEM and an image analysis system.

Well designed software is the key to a successful microcomputer image analysis system. The alternatives available are the purchase of a commercial image analysis system, which involves the use of the specific hardware, the purchase of commercial software packages designed for video digitizers and the use of software libraries for the video digitizers to design and develop a unique application program.

4.3.2 *Using the image analysis system in TEM micrographs analysis*

In this work, the measurements of the precipitates size, the inter precipitate spacing, the widths of the PFZs, and the statistical analysis of the measurements were performed by using a PC-Image analysis system produced by FOSTER FINDLEY associates.

The hardware of this image analysis system includes a CCD camera; a computer with an IBM AT 80486 microprocessor, a 4MB RAM and a super VGA monitor; an image display monitor; a Data Translation DT 2855 framestore board which has hardware features such as co-processors and image integration.

The software is called PC-Image for Windows produced by FOSTER FINDLEY associates. It is an application program for image analysis and measurement. It provides tools for problem solving for a variety of imaging applications such as the image processing operations and measurements of the area, the perimeter, the length, the circularity, the orientation, the intercepts, the radius of equivalent circle etc. of the regions of interest in an image. The program is also provided with extensive data analysis facilities such as classifying objects detected, histogram, correlation, and statistics analysis.

Fig. 4.3.3 is an illustration of using the image analysis system to analysis TEM micrographs in this work.

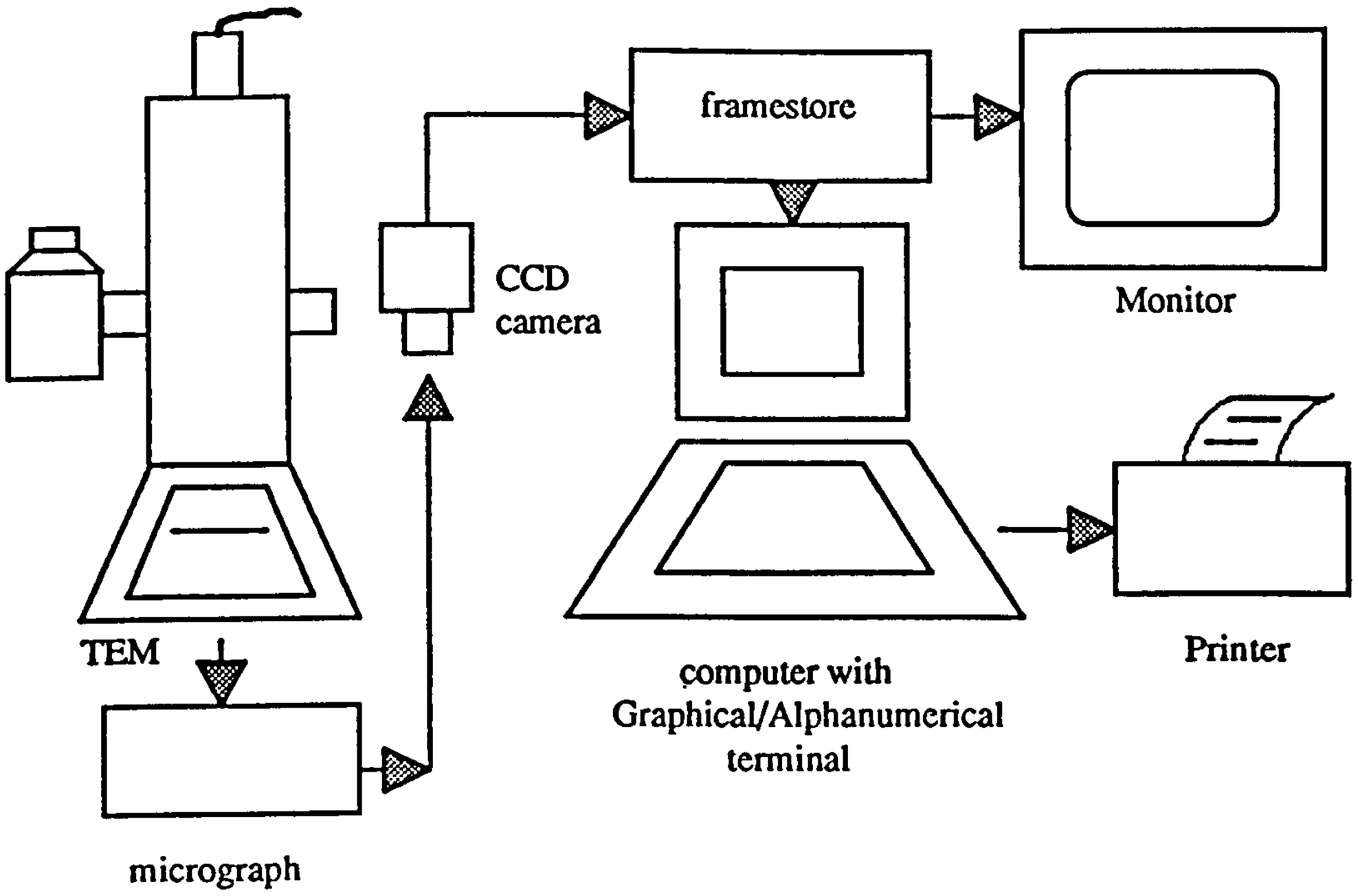

Fig. 4.3.3: Illustration of using image analysis system to analysis TEM micrographs.

Normally the procedure of the image analysis is:

1. The image of an object (i.e. a photograph) is caught by a CCD camera linked to the computer which contains a framestore board and in which PC-Image has been installed. The image captured by a CCD camera is sent to and stored in the computer and displayed on the image monitor as a fullgrey image. The fullgrey image is an image whose contrast is displayed by 256 grey levels.

2. Improving the contrast of the area of interest on the fullgrey image is accomplished by using appreciated linear and non-linear filers provided by the PC-Image.

3. Converting the fullgrey image of the area of interest into a binary image by properly setting grey level threshold limits. By doing this, all the objects we want to measure such as particles have one grey level value while all the others have another grey level value.

4. Selecting the applications to make the required measurements, then giving a file name to the file in which the data of the measurements will be saved. Selecting the function to start the operation of the measurements.

5. Using the data analysis facilities that PC-Image provides to analysis the original measured data saved in the data file. The result of the analysis such as a statistical result, or a histogram, or a list of the measurements etc. is then displayed on the monitor, or printed out, or saved in a file for later use.

This procedure is not suitable for the work here.

Because of the overlapping of the particles and complicated background contrast that is often found in the TEM photographs in this work, it is very difficult, some times even impossible, to create a binary image by setting proper grey level threshold limits on the fullgrey image of the TEM photographs in this work, and the image analysis system hardly works if this procedure is followed. A special procedure has been developed. This procedure is as follows:

1. The image of an object (i.e. a photograph) is caught by a CCD camera linked to the computer which contains a framestore board and in which PC-Image has been installed. The image captured by a CCD camera is sent to and stored in the computer and displayed on the image monitor as a fullgrey image. The fullgrey image is an image whose contrast is displayed by 256 grey levels.

2. At the fullgrey image stage, the contrast of the fullgrey image may be improved by choosing suitable image processing operations the system provided. Arithmetic operation is preferred since it will effectively enhance the contrast. Once the contrast is improved, identifying the overlapped particles, which are found quite often in this work, becomes easier and more accurate.

3. Create the binary image manually by drawing the lines linking the two ends of each precipitate particle, or, the centres of the two neighbouring particles, or, the two PFZ/interior grain edges at each side of the grain boundary. The length of the lines will represent either the particles' size, or the inter-precipitate spacing, or the width of the PFZ. The map of these lines is the binary image and the lines are the objects.

4. The measurement of the lines' length and data analysis such as statistics analysis, or a histogram graph can be processed by selecting appropriate applications and facilities.

This procedure has been adapted to perform the measurements of this work. Although by following this procedure the measurements were not at "automatic" level, it saves a lot of time and makes the measurements much easier and more accurate.

Chapter Five

Results

5.1 *Data used for theoretical prediction*

The data given in Table 5.1.1 were used for theoretical prediction.

Table 5.1.1: Parameters for the theoretical prediction of combined the growth and the distribution of $MgZn_2$ grain boundary precipitates and change of the widths of PFZs with ageing time.

parameter		data	parameter		data
a	nm	0.404	a_b	cm^2s^{-1}	1.7
a_c	cm^2s^{-1}	0.12[a]	a_I	cm^2s^{-1}	0.143
c		-1.365	C_c	mole fraction	0.028
C_e	mole fraction	0.0271	d	nm	5000
d_0	nm	0.1	d_1	nm	0.25
E_b	eV per atom	0.28[c]	E_f	eV per atom	1.25[c]
r	μm	10	Q_b	eV per atom	0.98
Q_c	eV per atom	1.24[a]	Q_I	eV per atom	1.54[c]
T_i	K	748	T_{mp}	K	560
V_θ	cm^3	9.92	x_E		2
x_θ	mole fraction	0.33	δt	s	3
ΔH	mol cm^{-3}	4200[d]	d_2	nm	1
θ	s^{-1}	1	ρ_α	mol cm^{-3}	1.006
ρ_θ	mol cm^{-3}	1.008	$\sigma_{\alpha\theta}$	Jcm^{-2}	0.3[e]
Ω	cm^3	9.94	ψ	°	46.25[f]
ς		0.02[g]	Δ	s	10^{-7}

a: data from ref. 102; b: data from ref. 103; c: data from ref. 72;

d: data from ref. 104; e: data from ref. 105; f: based on experimental observation.

g: data from ref. 70;

The size and the inter-particle spacing of $MgZn_2$ grain boundary precipitate and the widths of precipitate-free zones in 7150 aluminium alloy as the functions of ageing

time for ageing temperature $160°C$ and $180°C$ after water quenched from solution treatment temperature were predicted by using the combined models.

5.2 *Experimental results*

The size and the inter-particle spacing of $MgZn_2$ grain boundary precipitate and the widths of precipitate-free zones in 7150 aluminium alloy as a function of ageing time for ageing temperature $160°C$ and $180°C$ after water quench from solution treatment temperature were investigated by a transmission electron microscope (TEM). The sections of each grain boundary were photographed under the bright field image mode of TEM with the grain boundary tilted until its plane was parallel to the incident electron beam and a profile of the precipitate was obtained. The diameter of the precipitate was taken as the length of the profile along the grain boundary direction, the inter-precipitate spacing was taken as the distance between two particles next to each along the grain boundary, and the width of PFZ was taken as the length of the line crossing from one side of the grain boundary perpendicularly to another side and covering the whole PFZ.

The measurements of the diameter of precipitate, the inter precipitate spacing and the widths of the PFZs were performed by using PC-Image analysis system produced by FOSTER FINDLEY associates. The statistical analysis and the construction of the histogram graphics of the measured data were carried out by using the statistical analysis and histogram facilities provided by PC-Image analysis system. The results for all the samples is presented as Tables 5.2.1-5.2.3 and Figs. 5.2.1-5.2.30.

5.2.1 *Particle size*

5.2.1.1 *Statistical results*

Table 5.2.1: The number of measured precipitates, the mean size (diameter) of precipitates and standard deviation.

sample:	Number of measured prec.	mean size of prec. (nm)	Std Dev (nm)
160-0005	786	21	9
160-0060	2968	37	15
160-0110	1905	37	22
160-0200	2110	46	23
160-0480	2286	53	21
180-0005	2816	34	14
180-0010	1934	37	10
180-0020	1920	41	14
180-0030	2699	45	24
180-0100	3119	58	25

5.2.1.2 *Histograms*

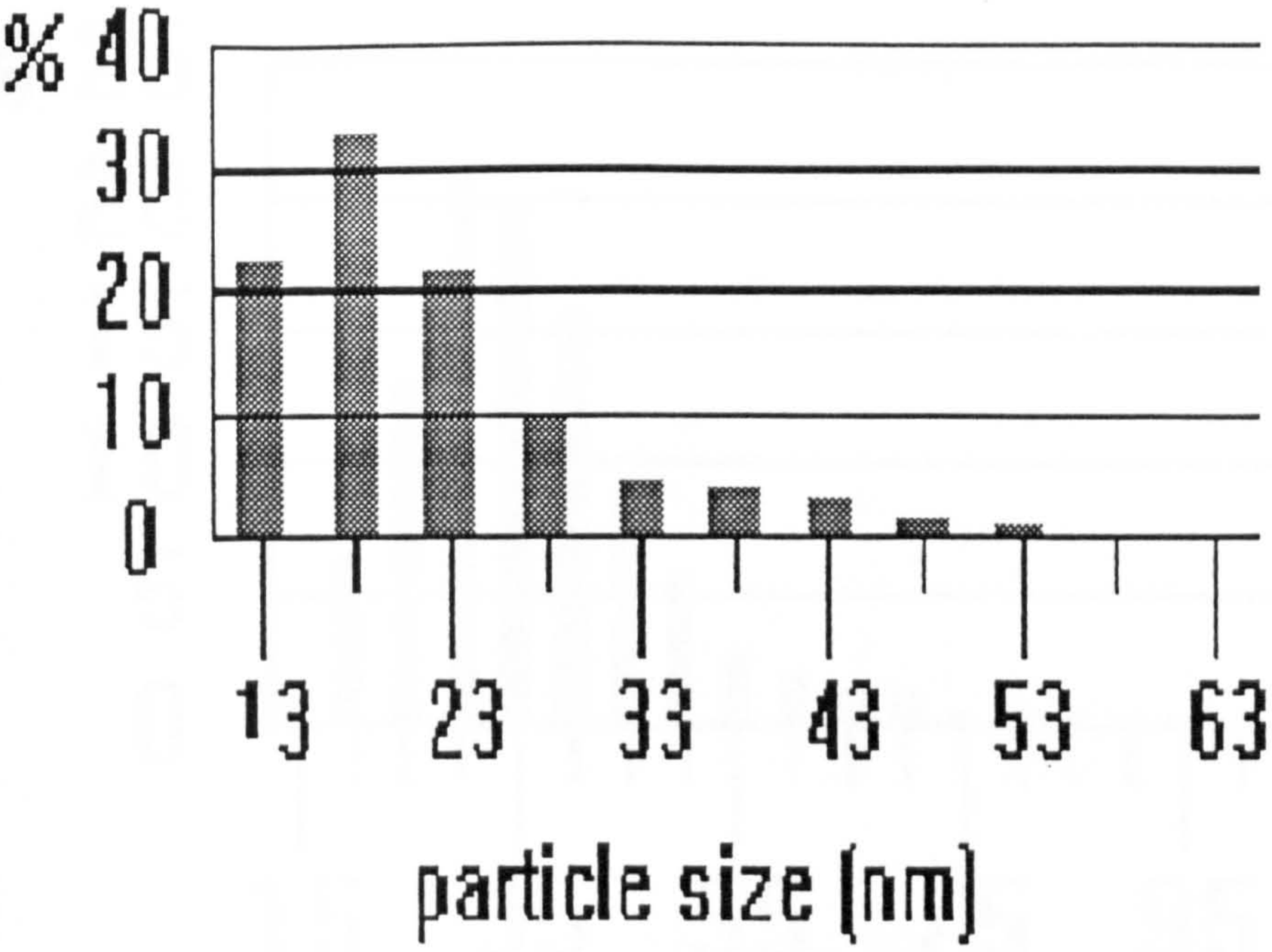

Fig. 5.2.1: The histogram of experimental measured precipitates sizes (diameters) for sample 160-0005 (class size=5nm).

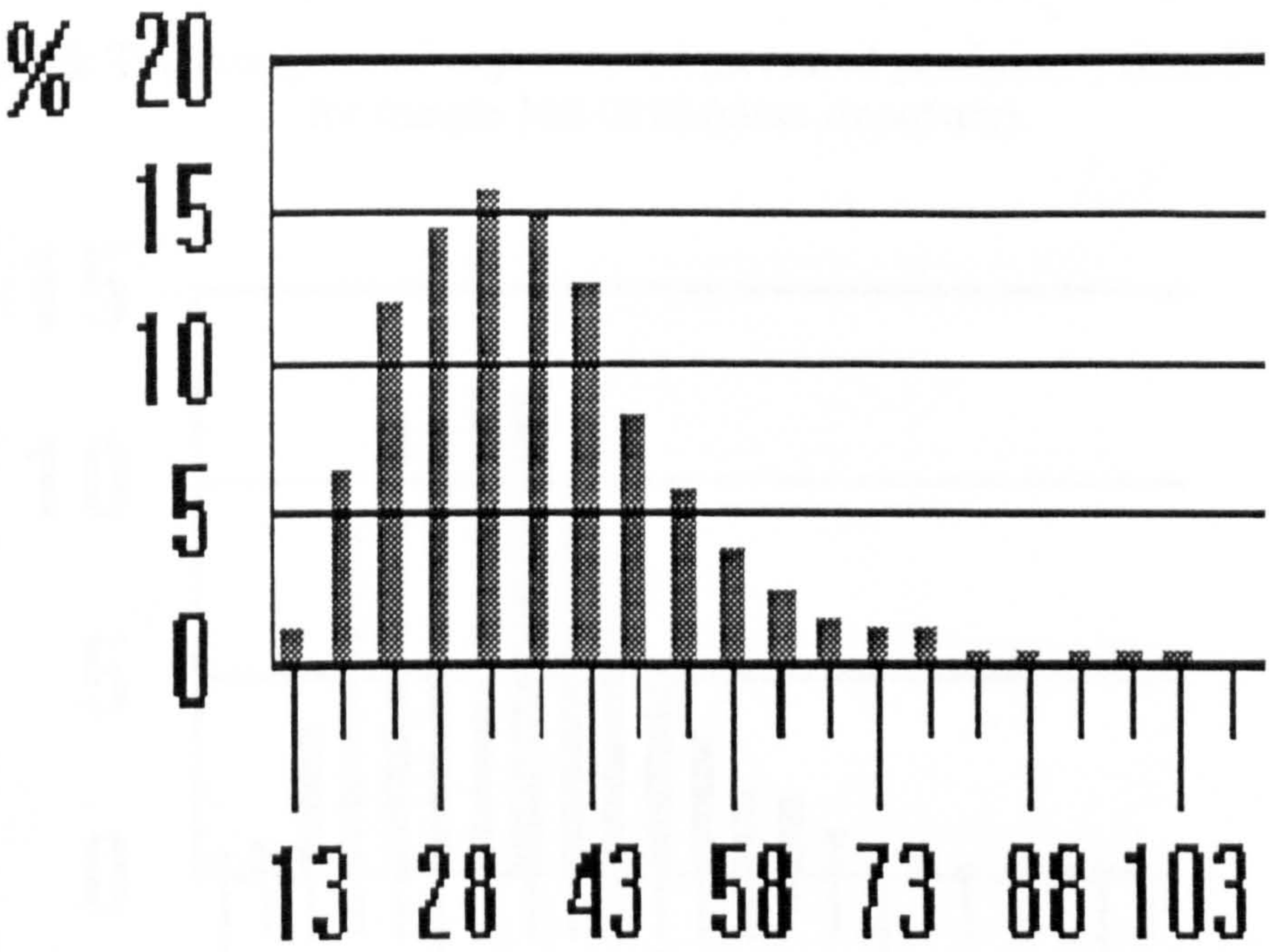

Fig. 5.2.2: The histogram of experimental measured precipitates sizes (diameters) for sample 160-0060 (class size=5nm).

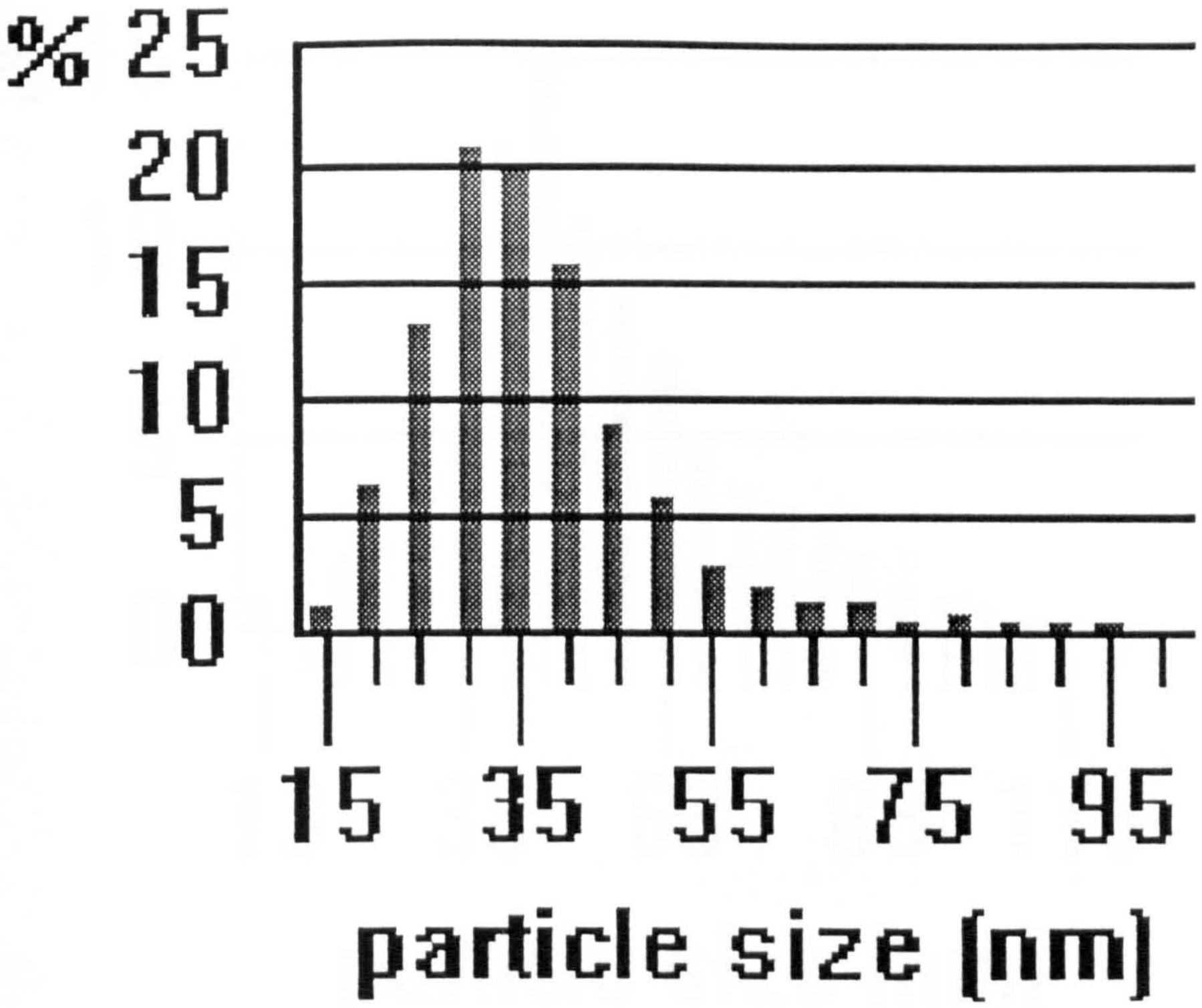

Fig. 5.2.3: The histogram of experimental measured precipitates sizes (diameters) for sample 160-0110 (class size=5nm).

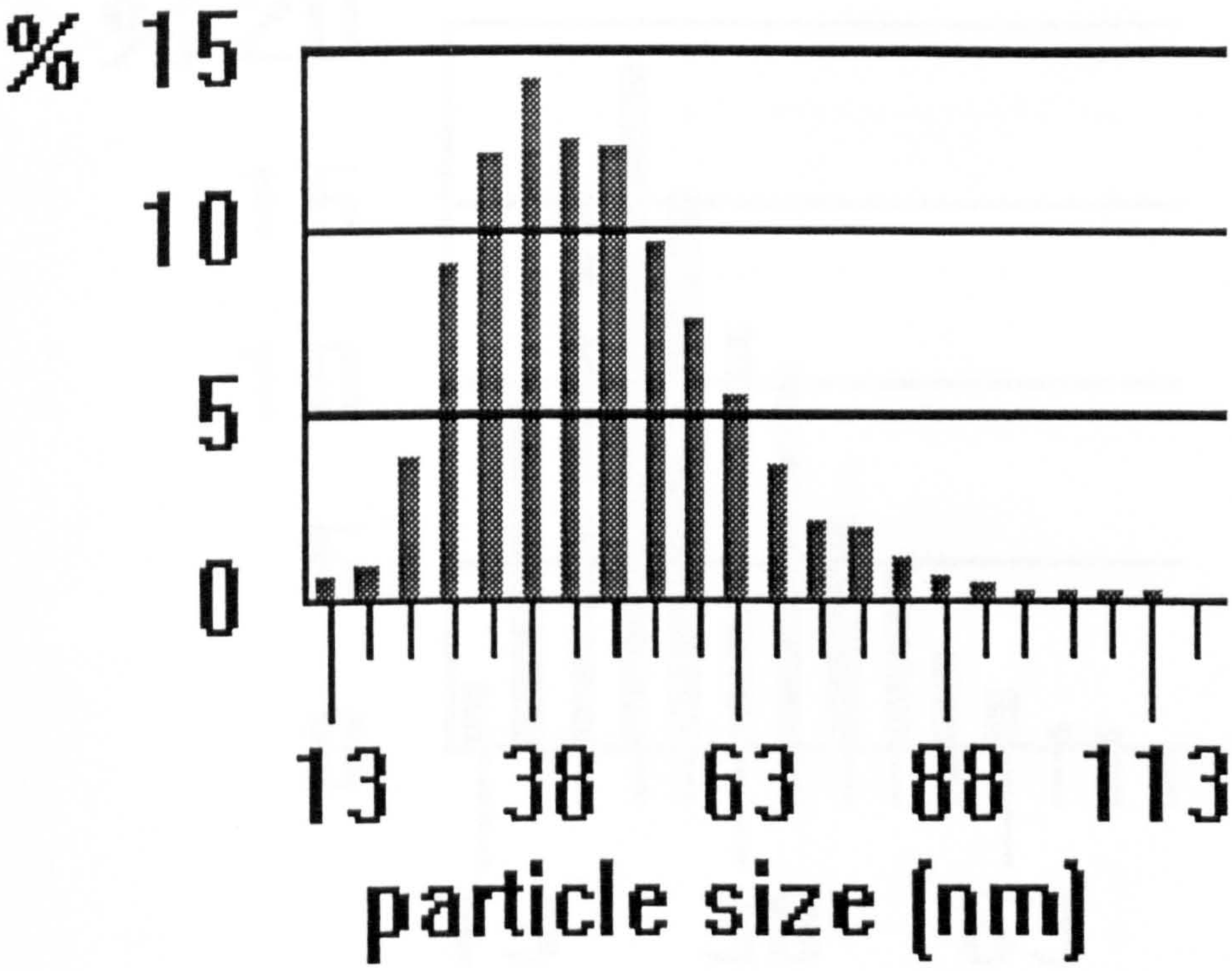

Fig. 5.2.4: The histogram of experimental measured precipitates sizes (diameters) for sample 160-0200 (class size=5nm).

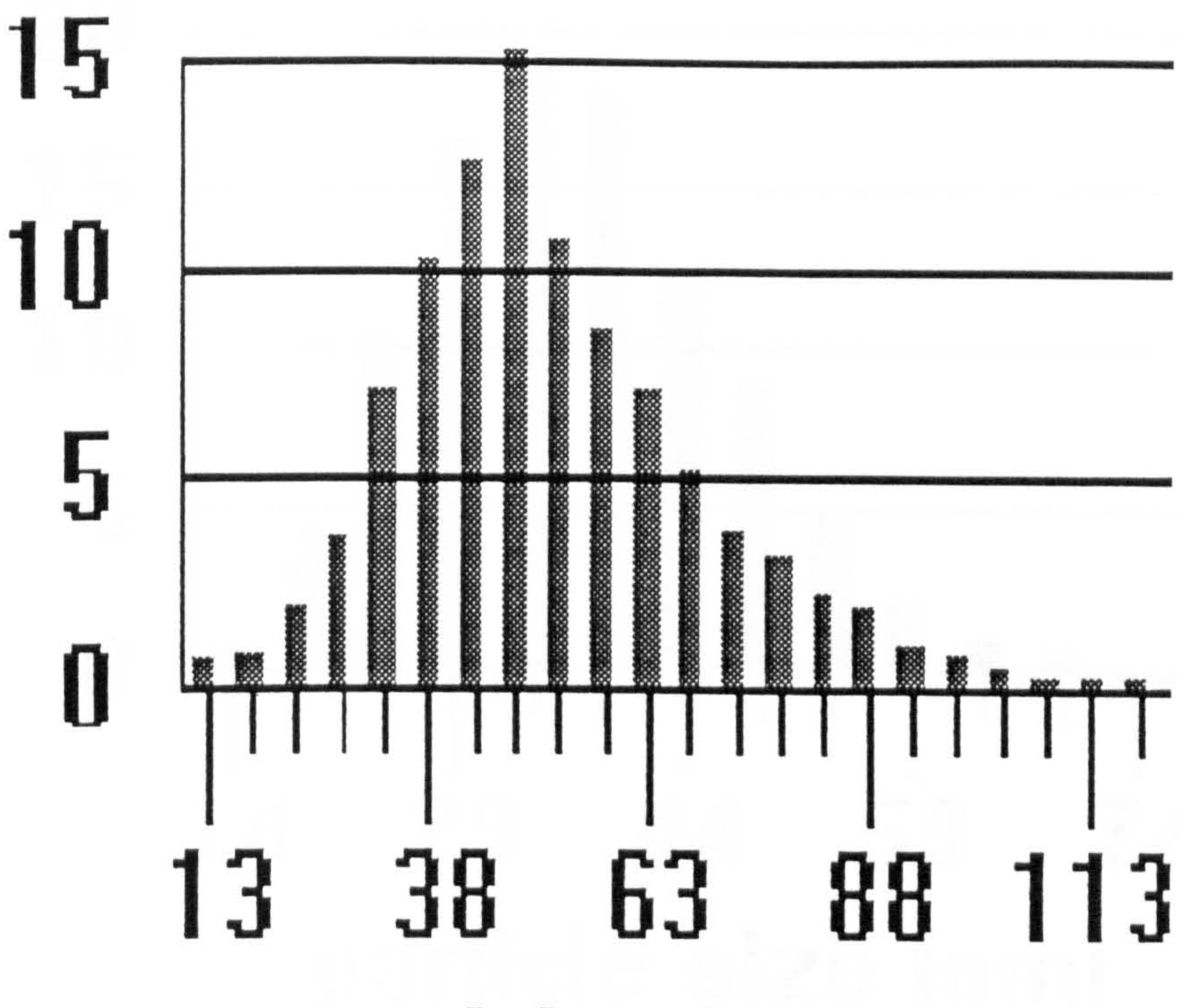

Fig. 5.2.5: The histogram of experimental measured precipitates sizes (diameters) for sample 160-0480 (class size=5nm).

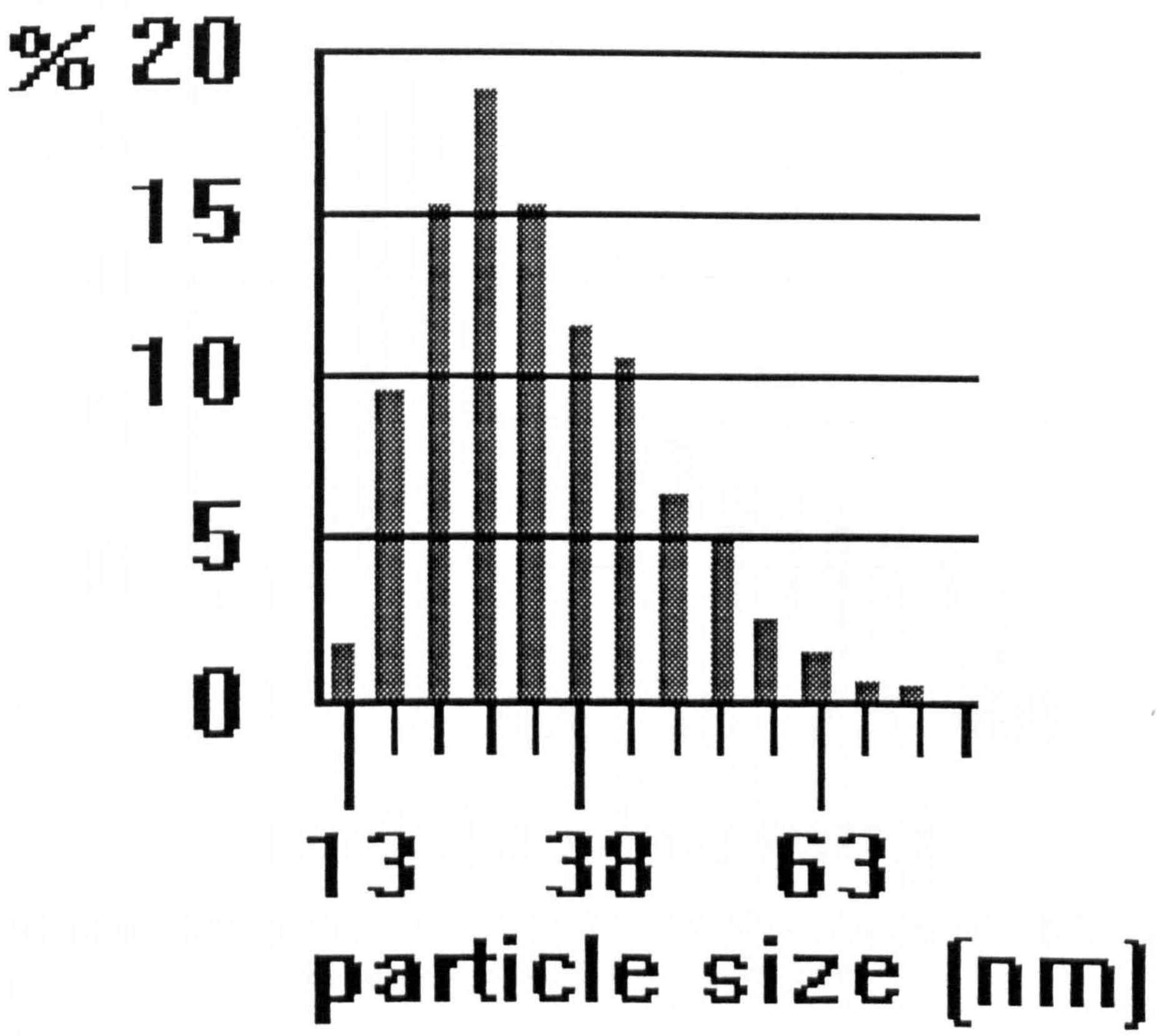

Fig. 5.2.6: The histogram of experimental measured precipitates sizes (diameters) for sample 180-0005 (class size=5nm).

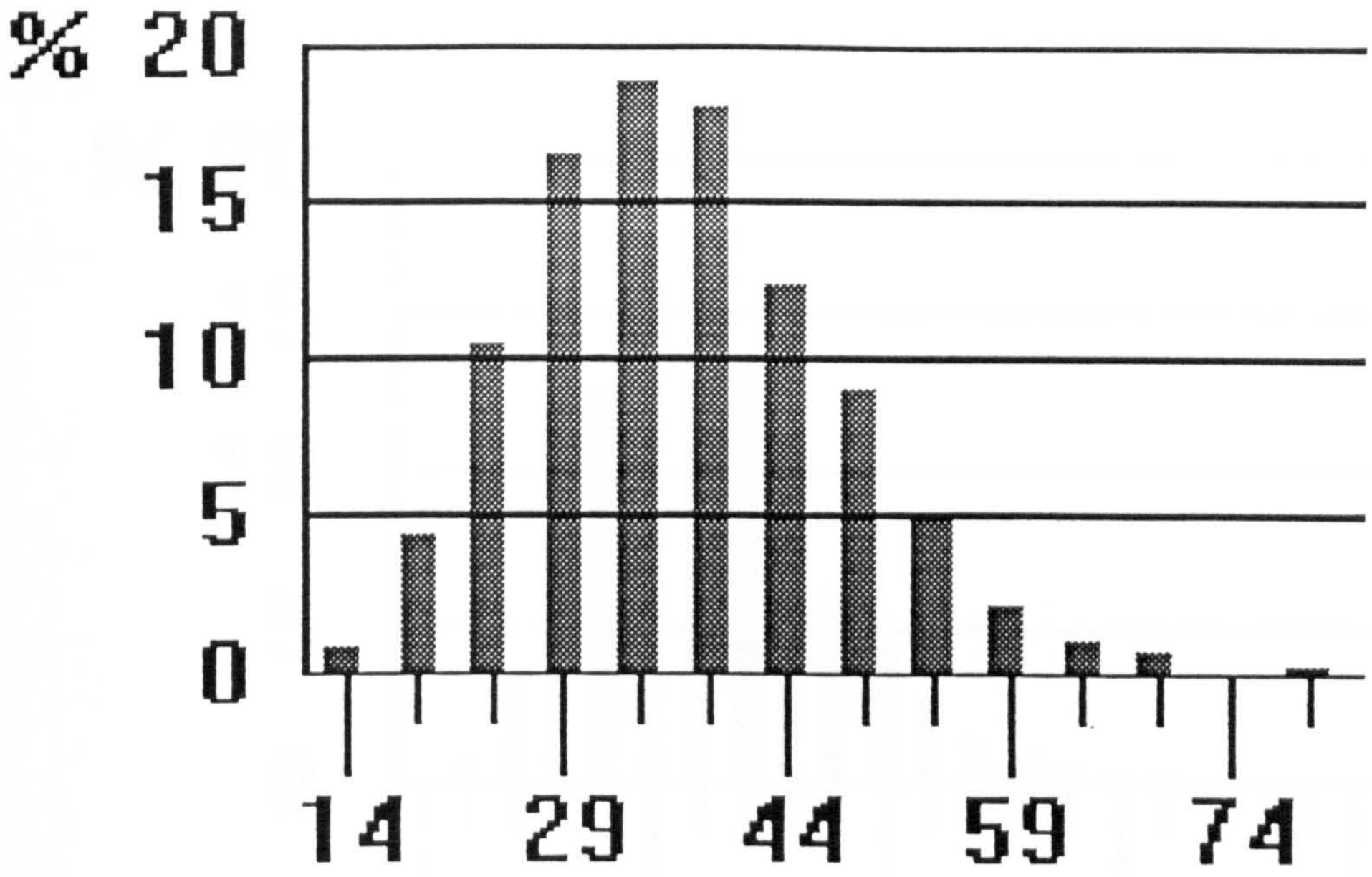

Fig. 5.2.7: The histogram of experimental measured precipitates sizes (diameters) for sample 180-0010 (class size=5nm).

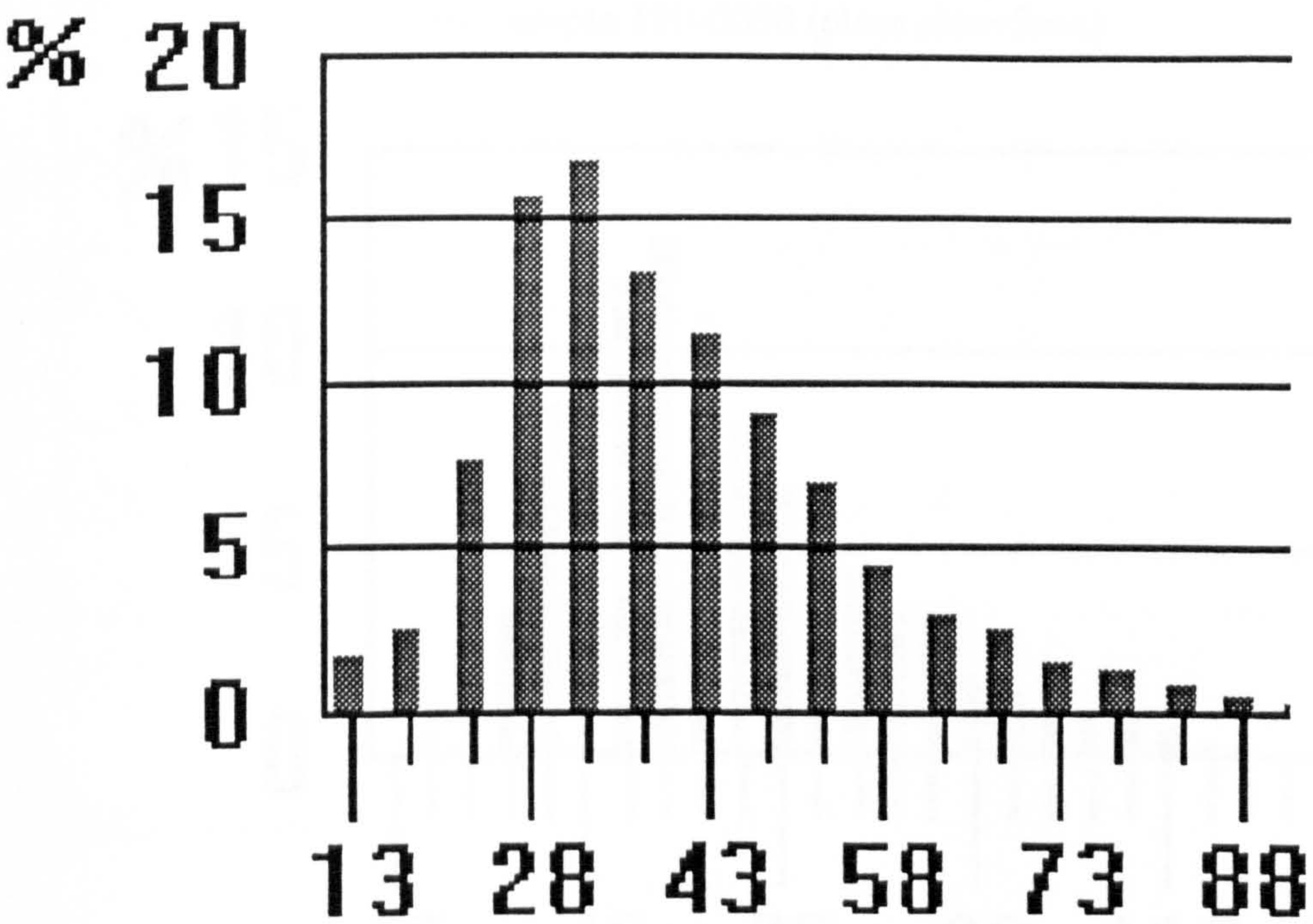

Fig. 5.2.8: The histogram of experimental measured precipitates sizes (diameters) for sample 180-0020 (class size=5nm).

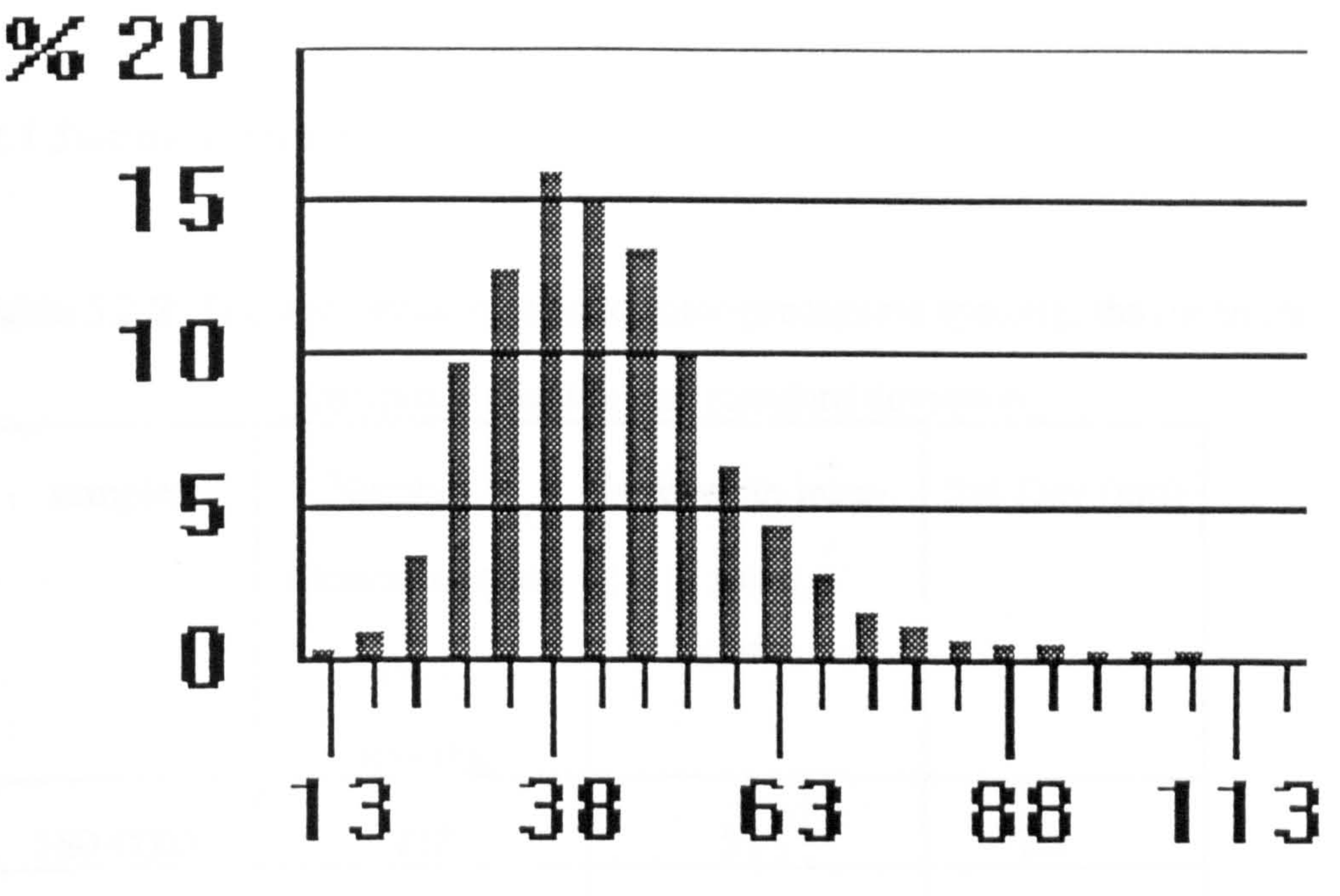

Fig. 5.2.9: The histogram of experimental measured precipitates sizes (diameters) for sample 180-0030 (class size=5nm).

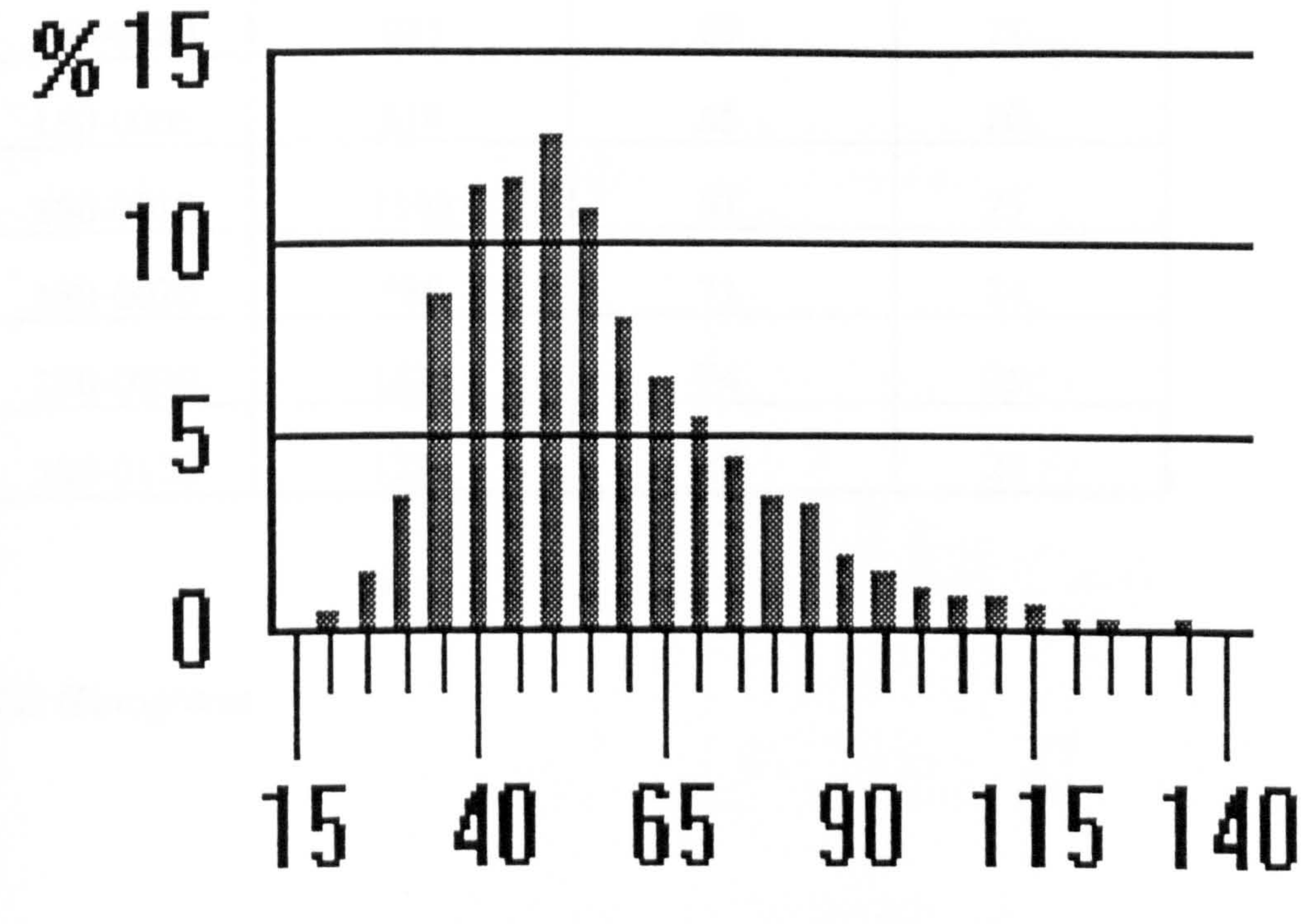

Fig. 5.2.10: The histogram of experimental measured precipitates sizes (diameters) for sample 180-0100 (class size=5nm).

5.2.2 *Inter-precipitate spacing*

5.2.2.1 *Statistical results*

Table 5.2.2: The number of measured inter-precipitate spacing, the mean inter-precipitate spacing and standard deviation.

sample:	Number of measured inter-prec. spacing	the mean inter-prec. (nm)	Std Dev (nm)
160-0005	238	51	20
160-0060	1477	54	19
160-0110	1411	57	18
160-0200	1013	62	22
160-0480	883	69	21
180-0005	818	65	20
180-0010	1168	67	25
180-0020	988	71	24
180-0030	1676	74	25
180-0100	1234	83	25

5.2.2.2 *Histograms*

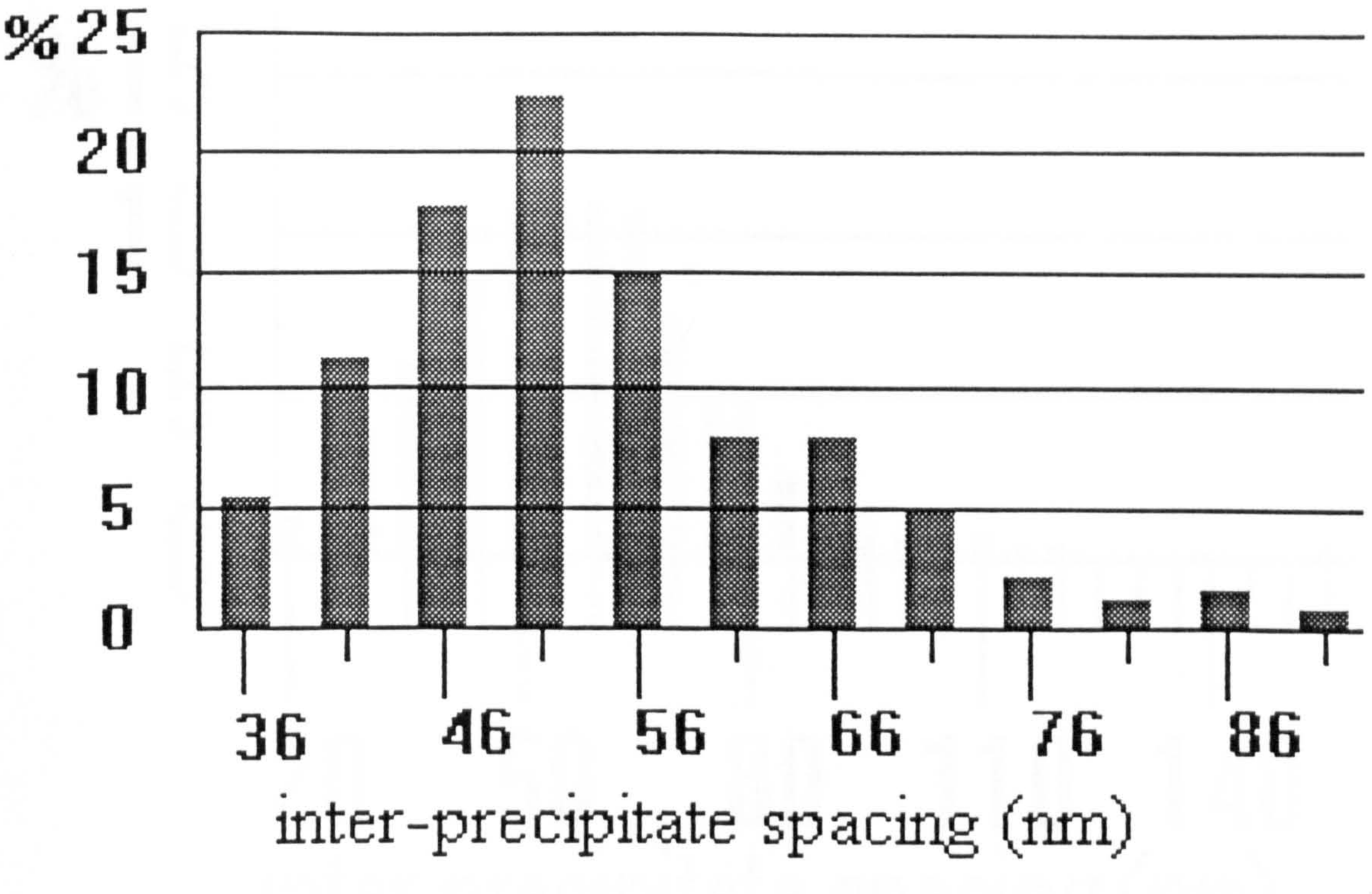

Fig. 5.2.11: The histogram of experimental measured inter-precipitate spacing for sample 160-0005 (class size=5nm).

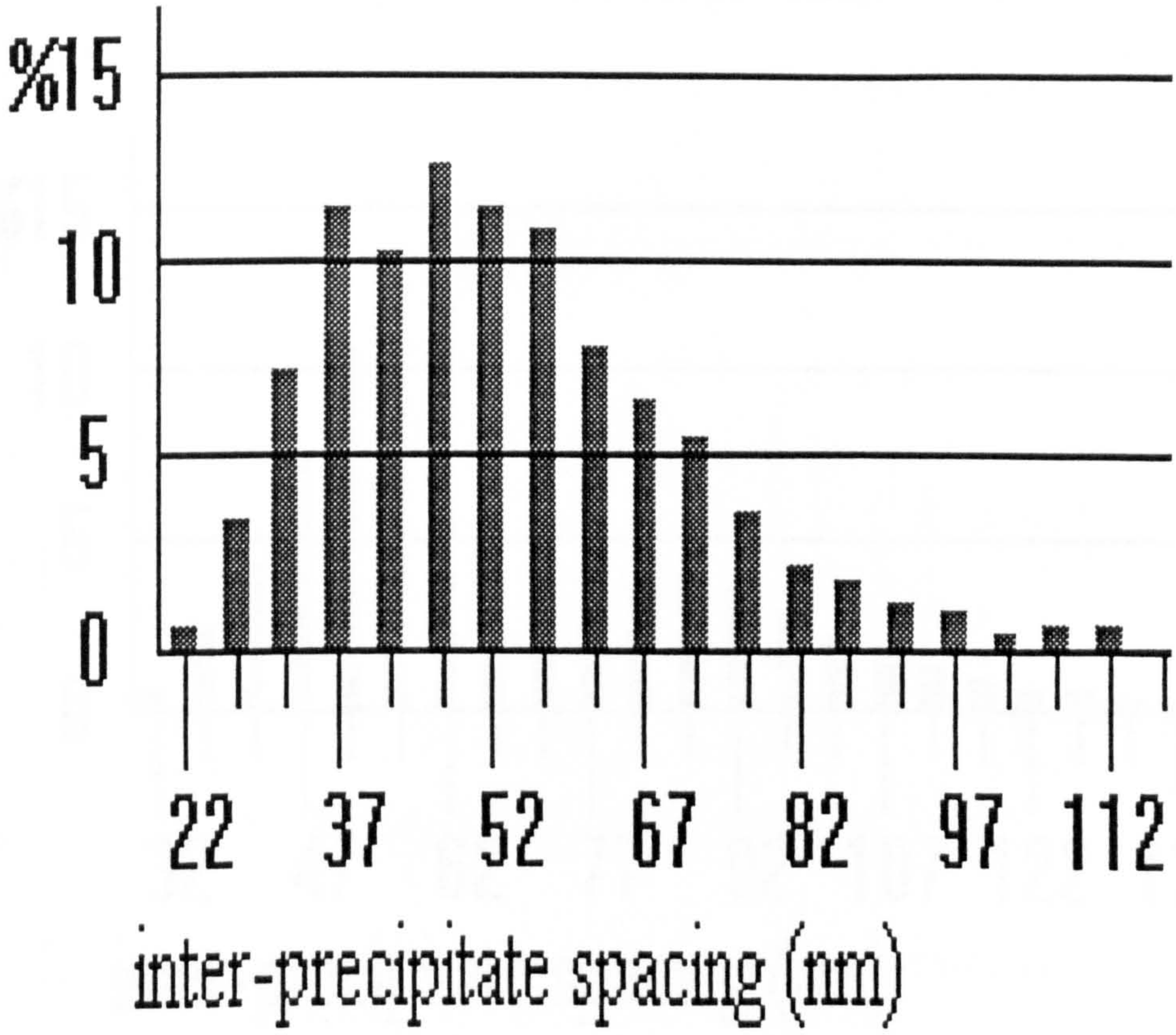

Fig. 5.2.12: The histogram of experimental measured inter-precipitate spacing for sample 160-0060 (class size=5nm).

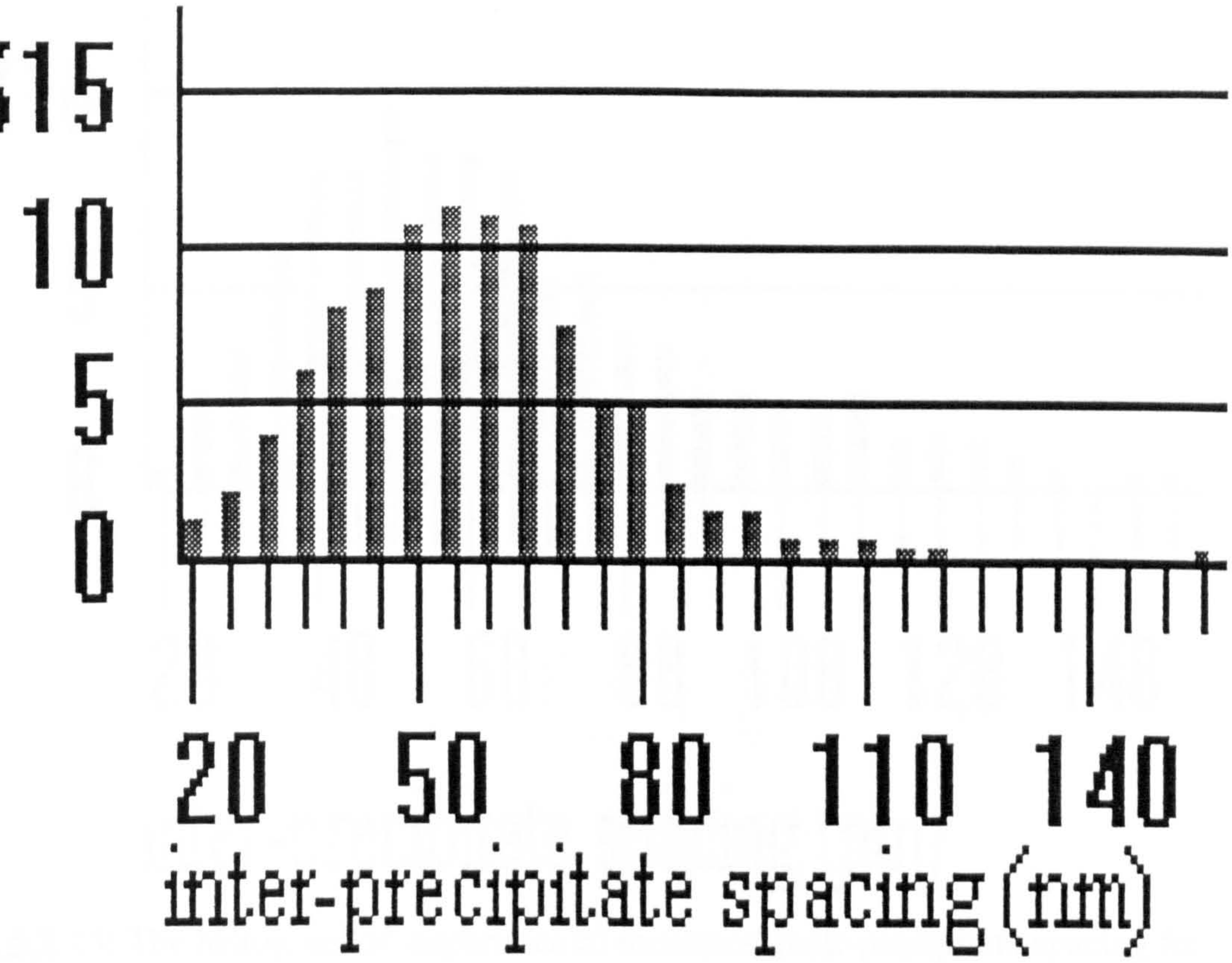

Fig. 5.2.13: The histogram of experimental measured inter-precipitate spacing for sample 160-0110 (class size=5nm).

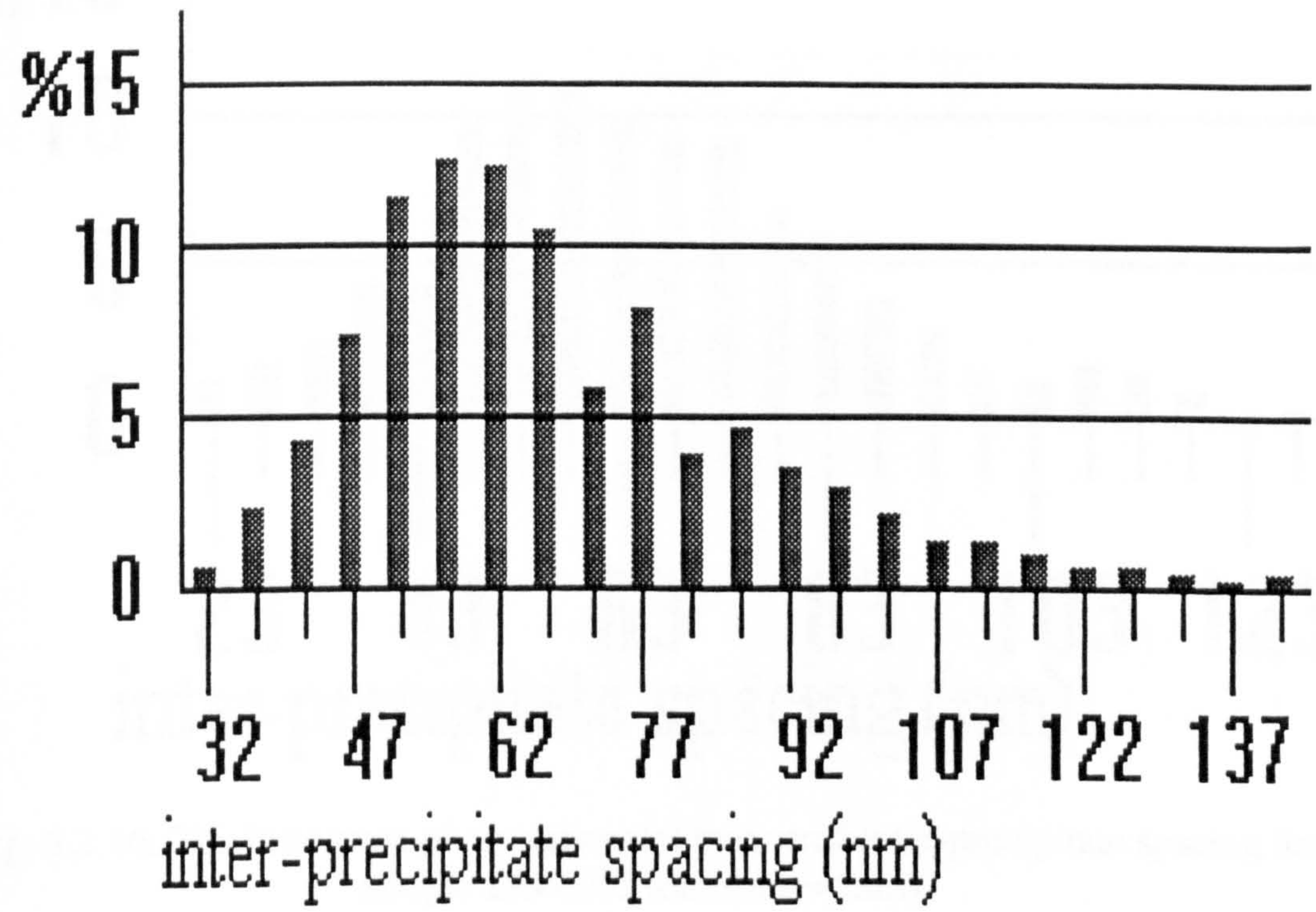

Fig. 5.2.14: The histogram of experimental measured inter-precipitate spacing for sample 160-0200 (class size=5nm).

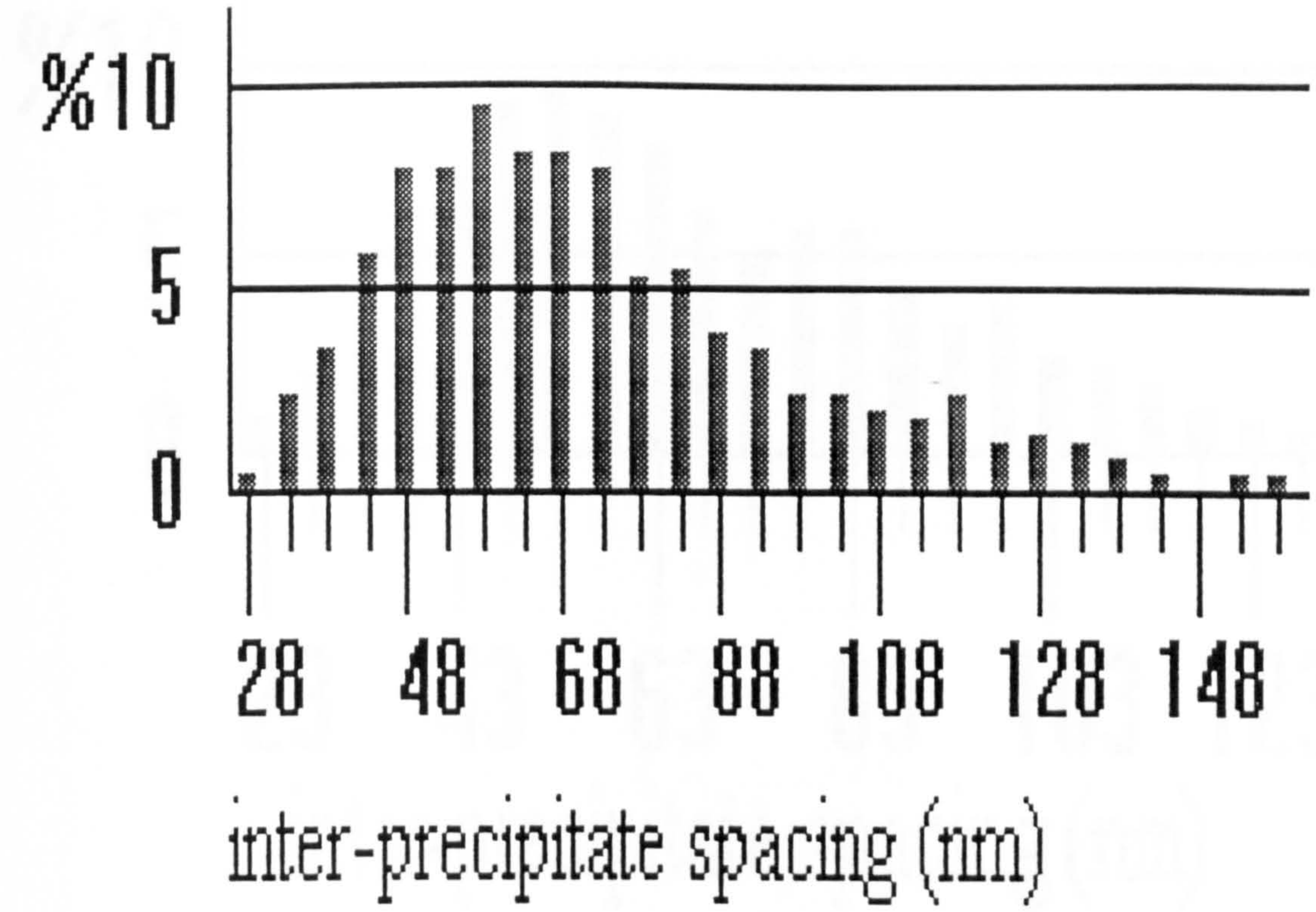

Fig. 5.2.15: The histogram of experimental measured inter-precipitate spacing for sample 160-0480 (class size=5nm).

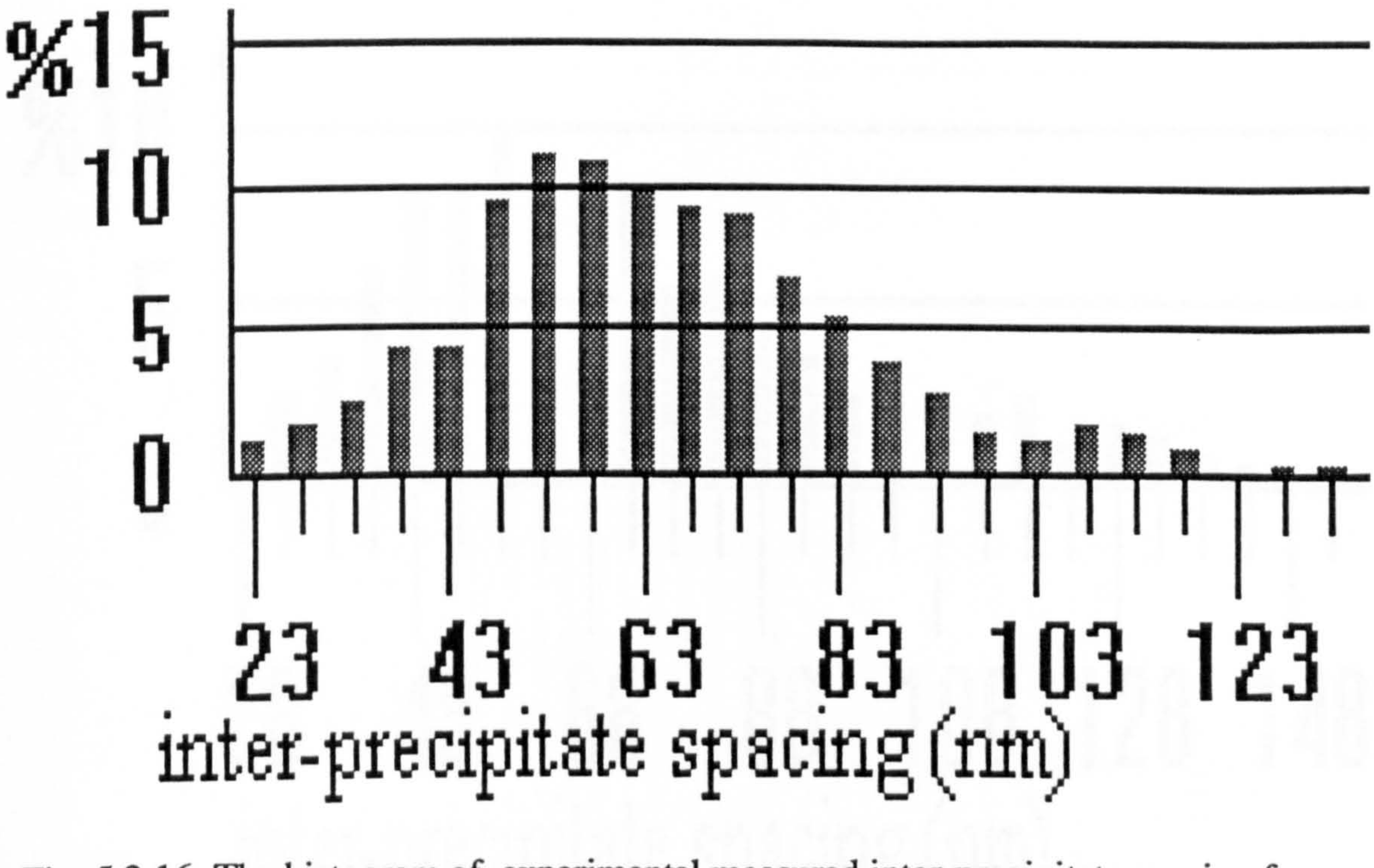

Fig. 5.2.16: The histogram of experimental measured inter-precipitate spacing for sample 180-0005 (class size=5nm).

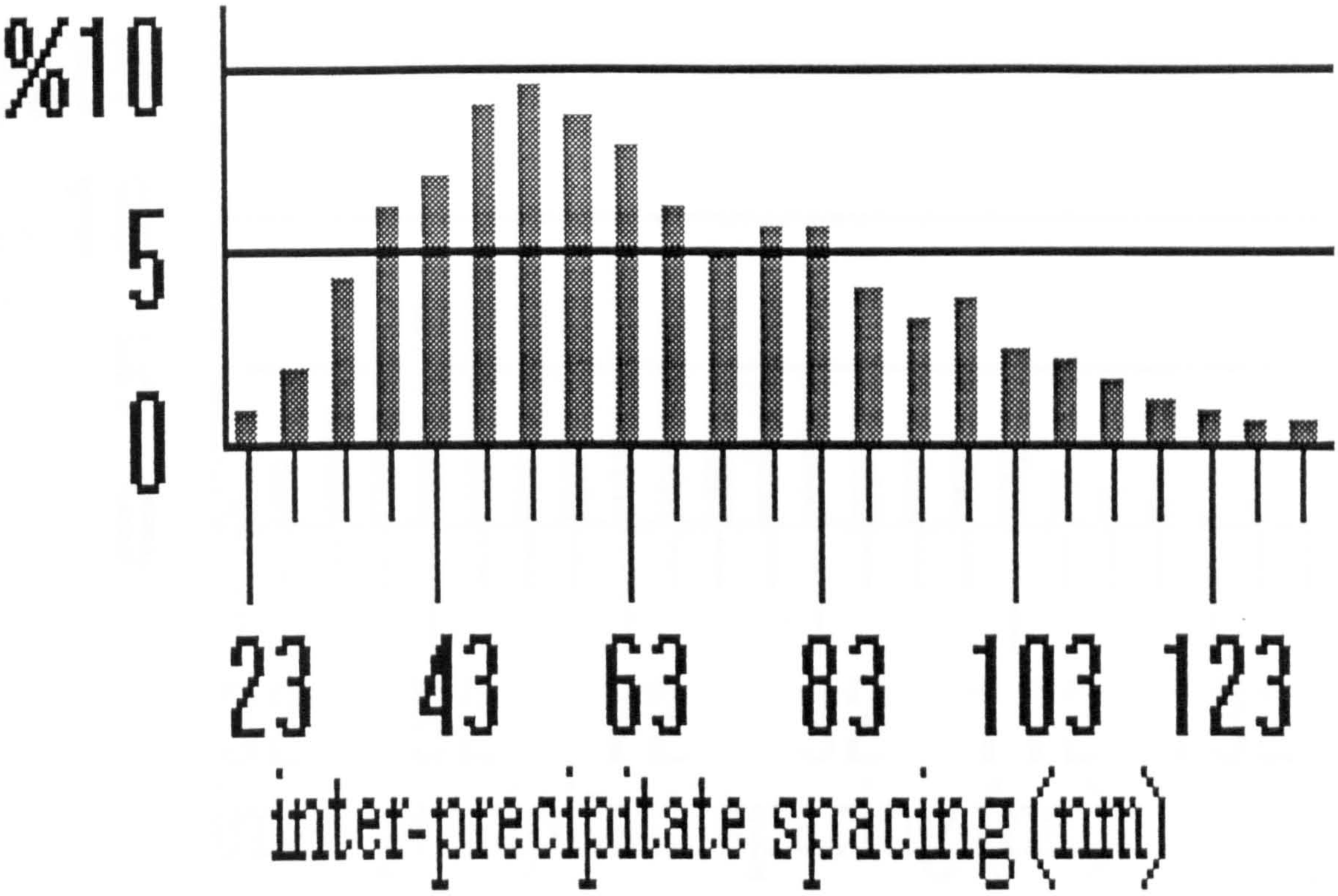

Fig.5.2.17: the histogram of experimental measured inter-precipitate spacing for sample 180-0010. (class size=5nm)

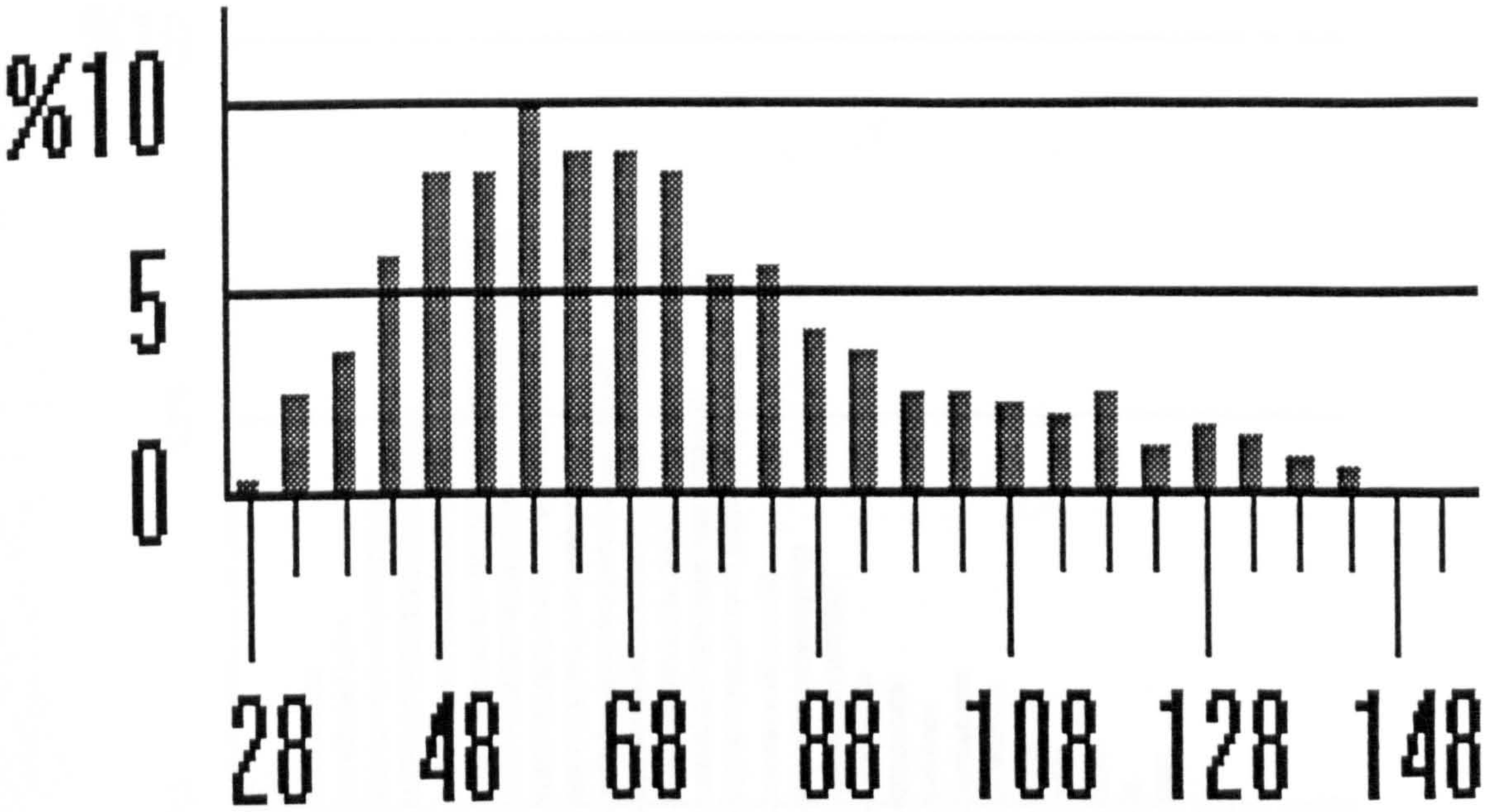

Fig. 5.2.18: The histogram of experimental measured inter-precipitate spacing for sample 180-0020 (class size=5nm).

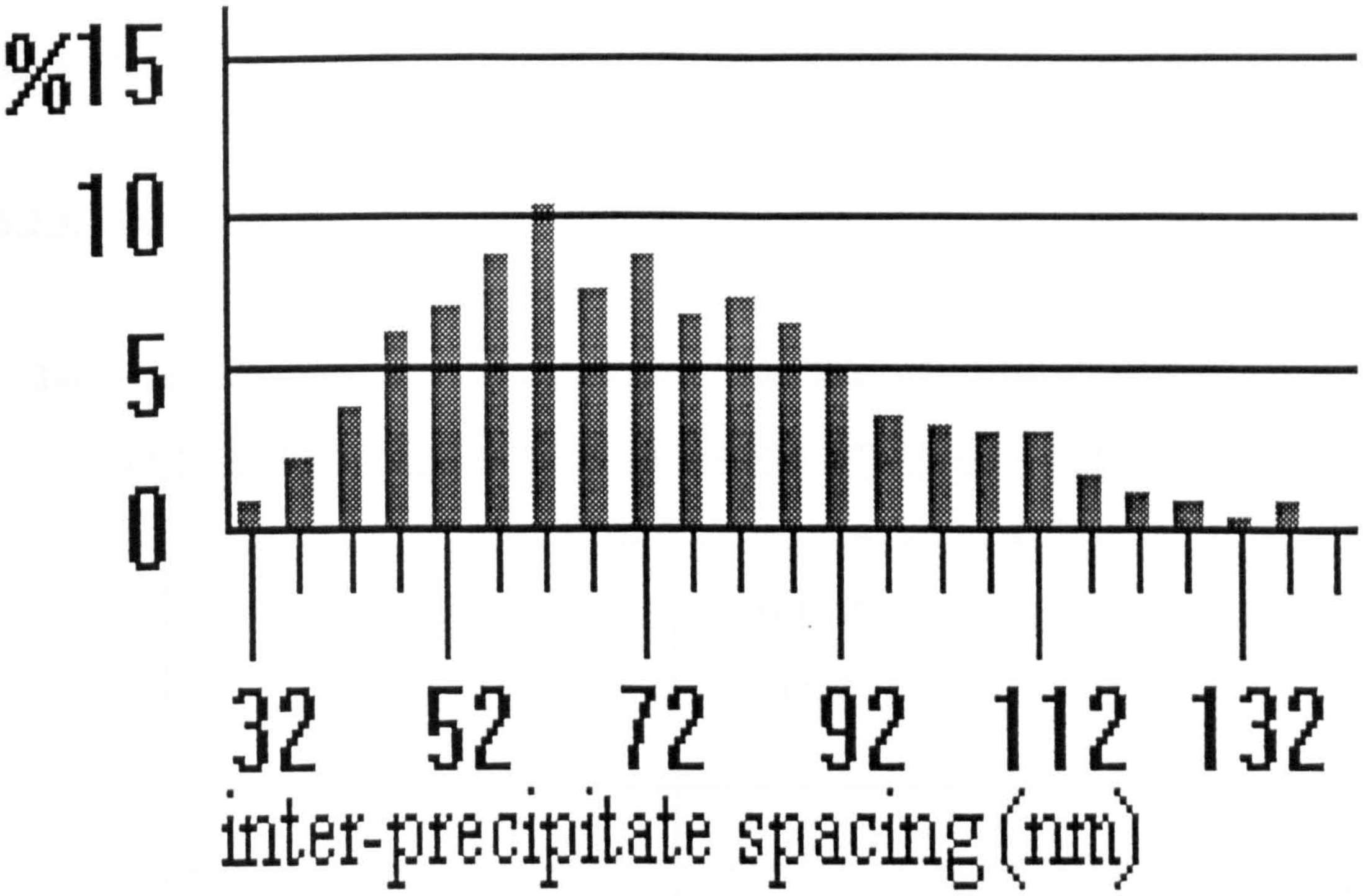

Fig. 5.2.19: The histogram of experimental measured inter-precipitate spacing for sample 180-0030 (class size=5nm).

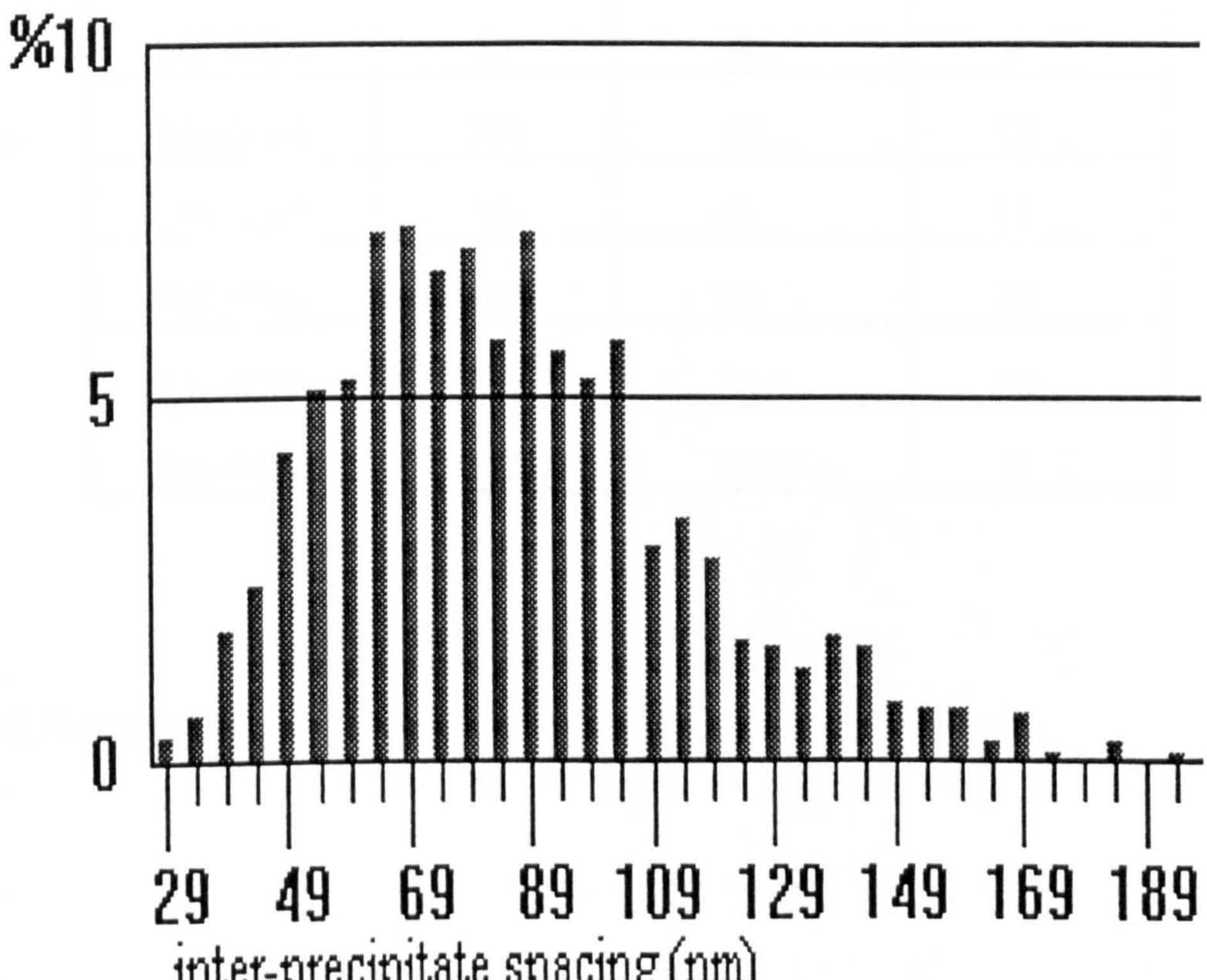

Fig. 5.2.20: The histogram of experimental measured inter-precipitate spacing for sample 180-0100 (class size=5nm).

5.2.3 *Widths of PFZs*

5.2.3.1 *Statistical results*

Table 5.2.3: The number of measured grain boundaries which have PFZs adjacent to them, the mean width of PFZs and standard deviation.

sample:	Number of measure-ments	the mean width of PFZs (nm)	Std Dev (nm)
160-0005	28	60	15
160-0060	135	43	10
160-0110	44	41	10
160-0200	104	36	9
160-0480	87	33	7
180-0005	174	56	12
180-0010	80	42	11
180-0020	99	40	10
180-0030	115	38	12
180-0100	125	35	8

5.2.3.2 *Histograms*

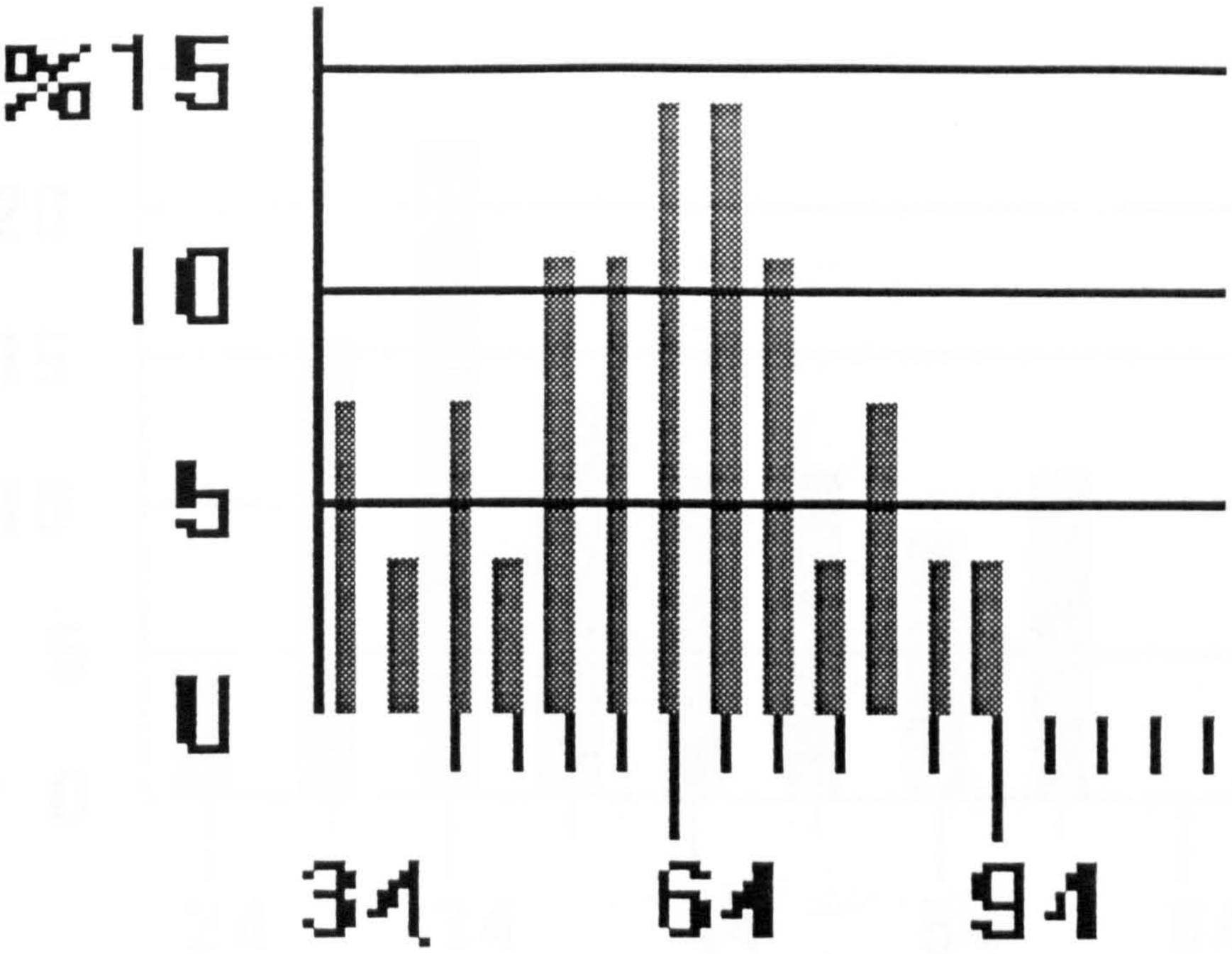

width of precipitate-free zone (nm)

Fig. 5.2.21: The histogram of experimental measured widths of precipitate-free zones for sample 160-0005 (class size=5nm).

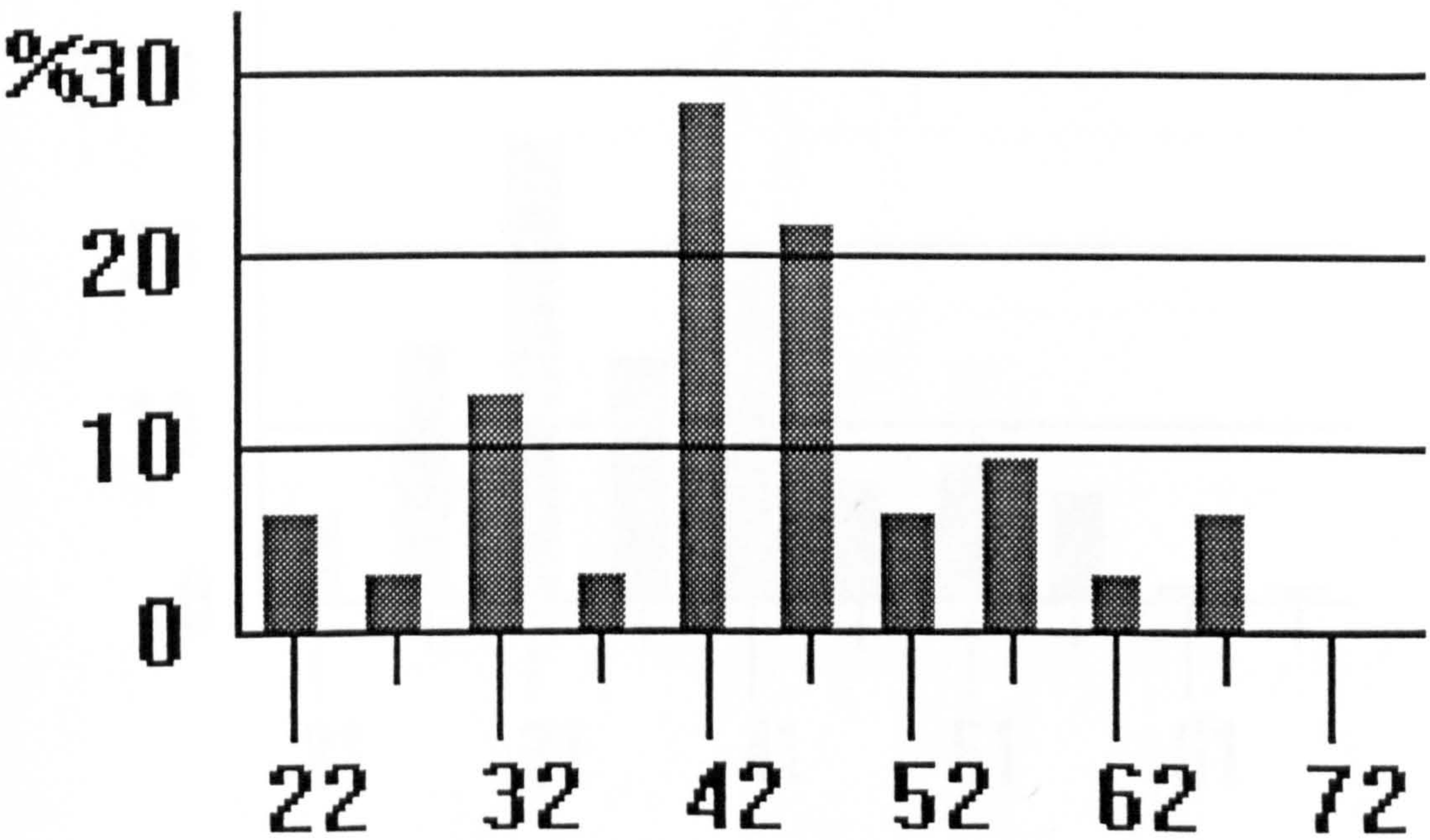

width of precipitate-free zone (nm)

Fig. 5.2.22: The histogram of experimental measured widths of precipitate-free zones for sample 160-0060 (class size=5nm).

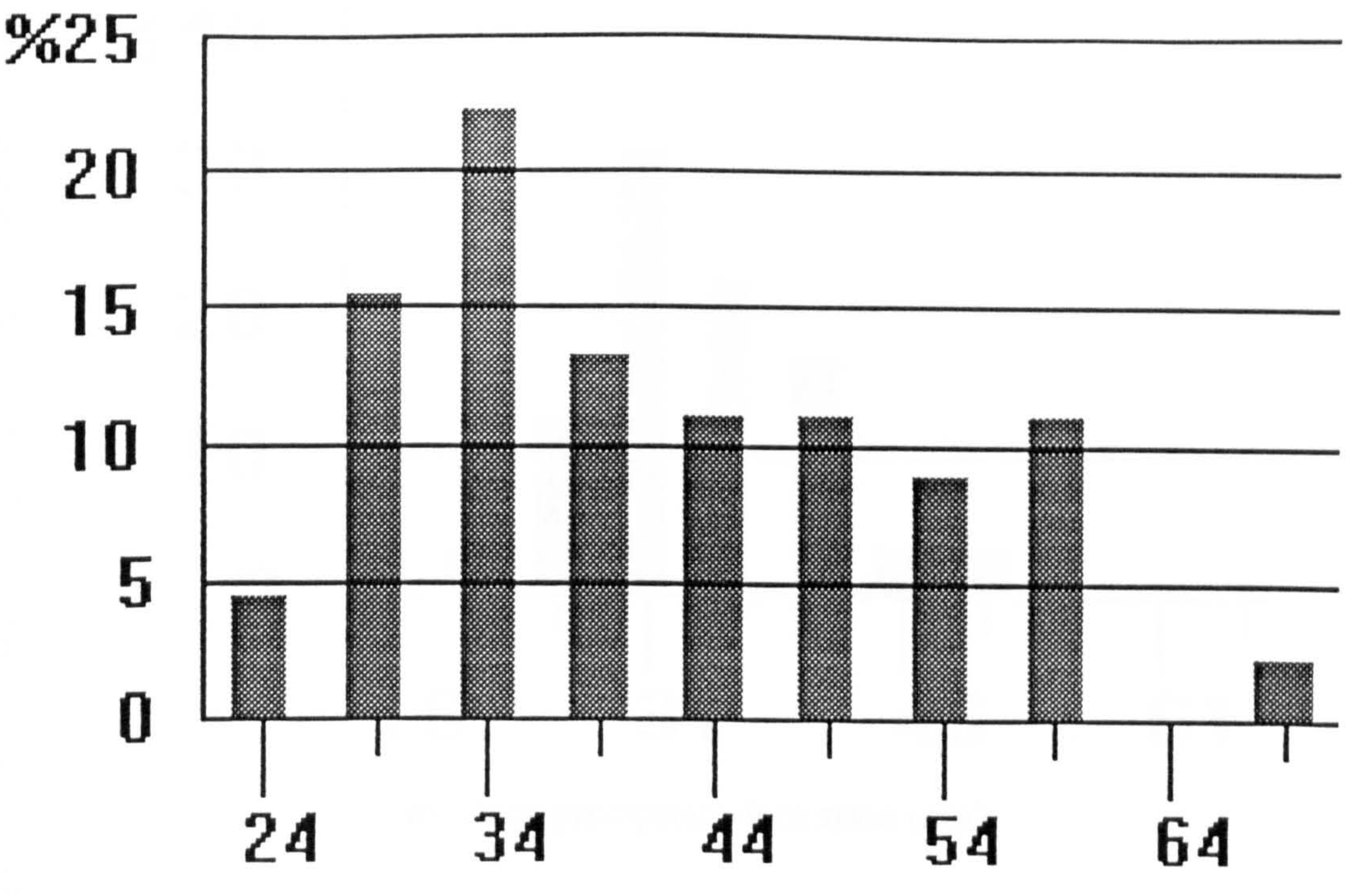

Fig. 5.2.23: The histogram of experimental measured widths of precipitate-free zones for sample 160-0110 (class size=5nm).

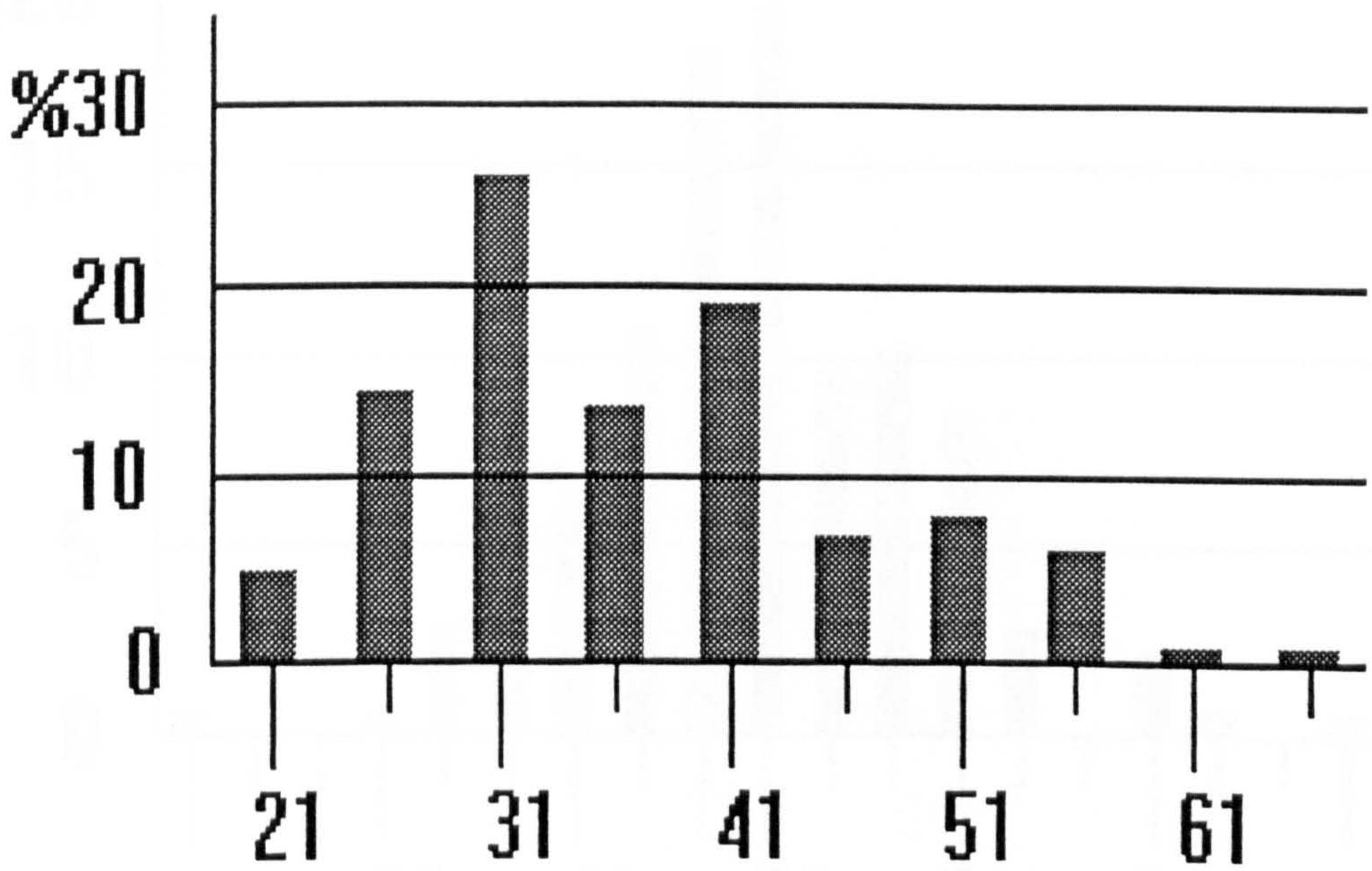

Fig. 5.2.24: The histogram of experimental measured widths of precipitate-free zones for sample 160-0200 (class size=5nm).

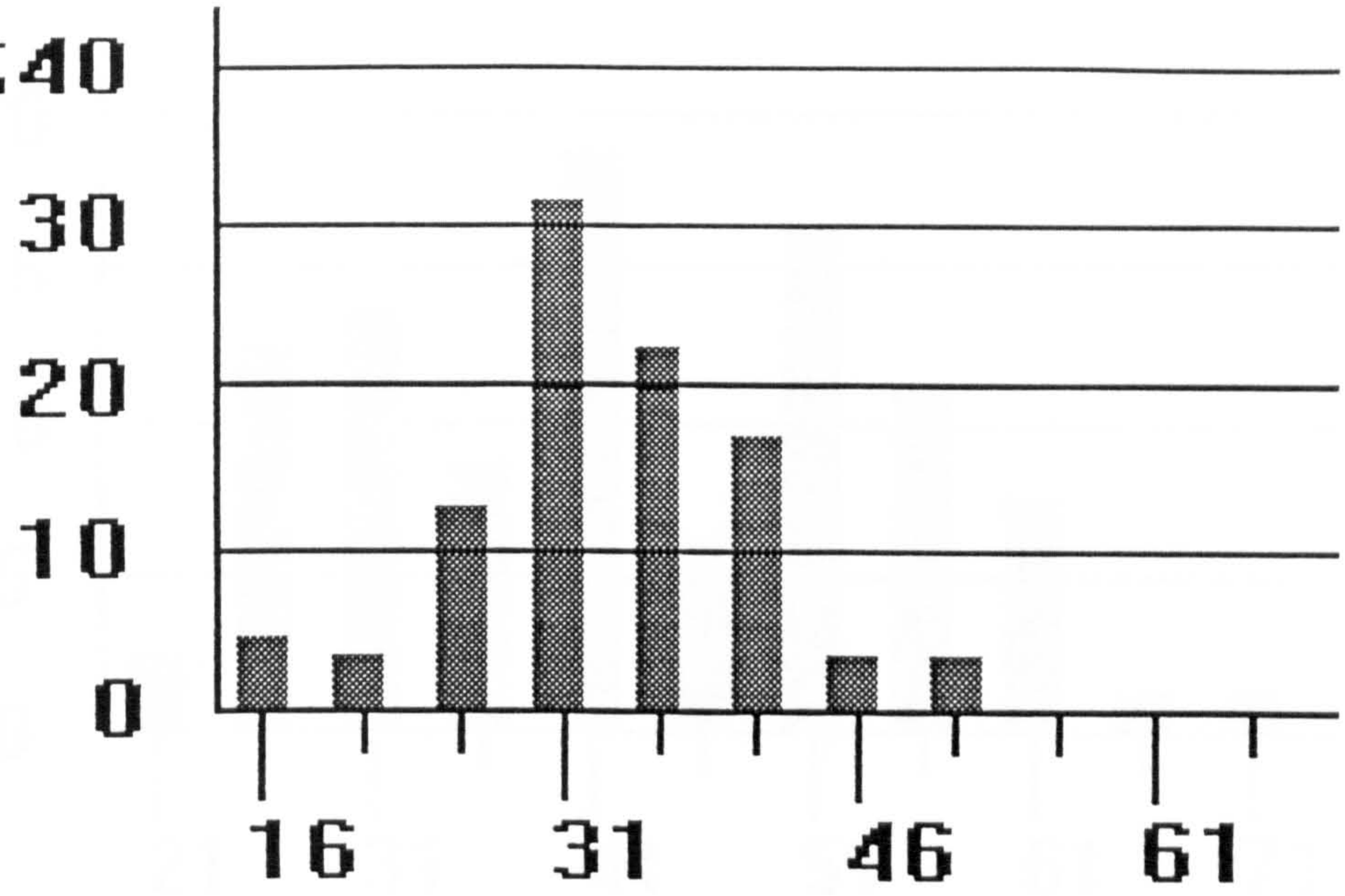

Fig. 5.2.25: The histogram of experimental measured widths of precipitate-free zones for sample 160-0480 (class size=5nm).

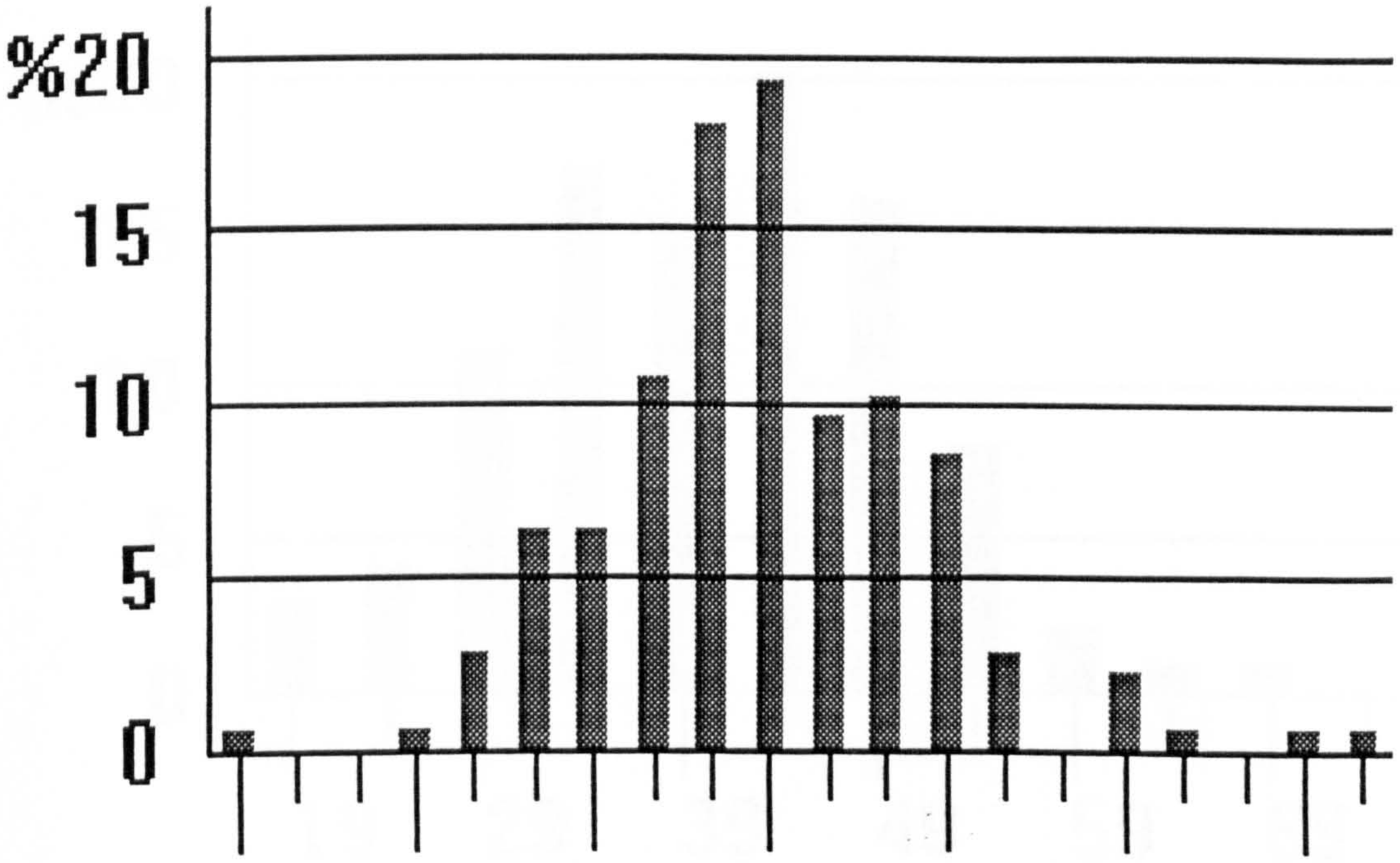

Fig. 5.2.26: The histogram of experimental measured widths of precipitate-free zones for sample 180-0005 (class size=5nm).

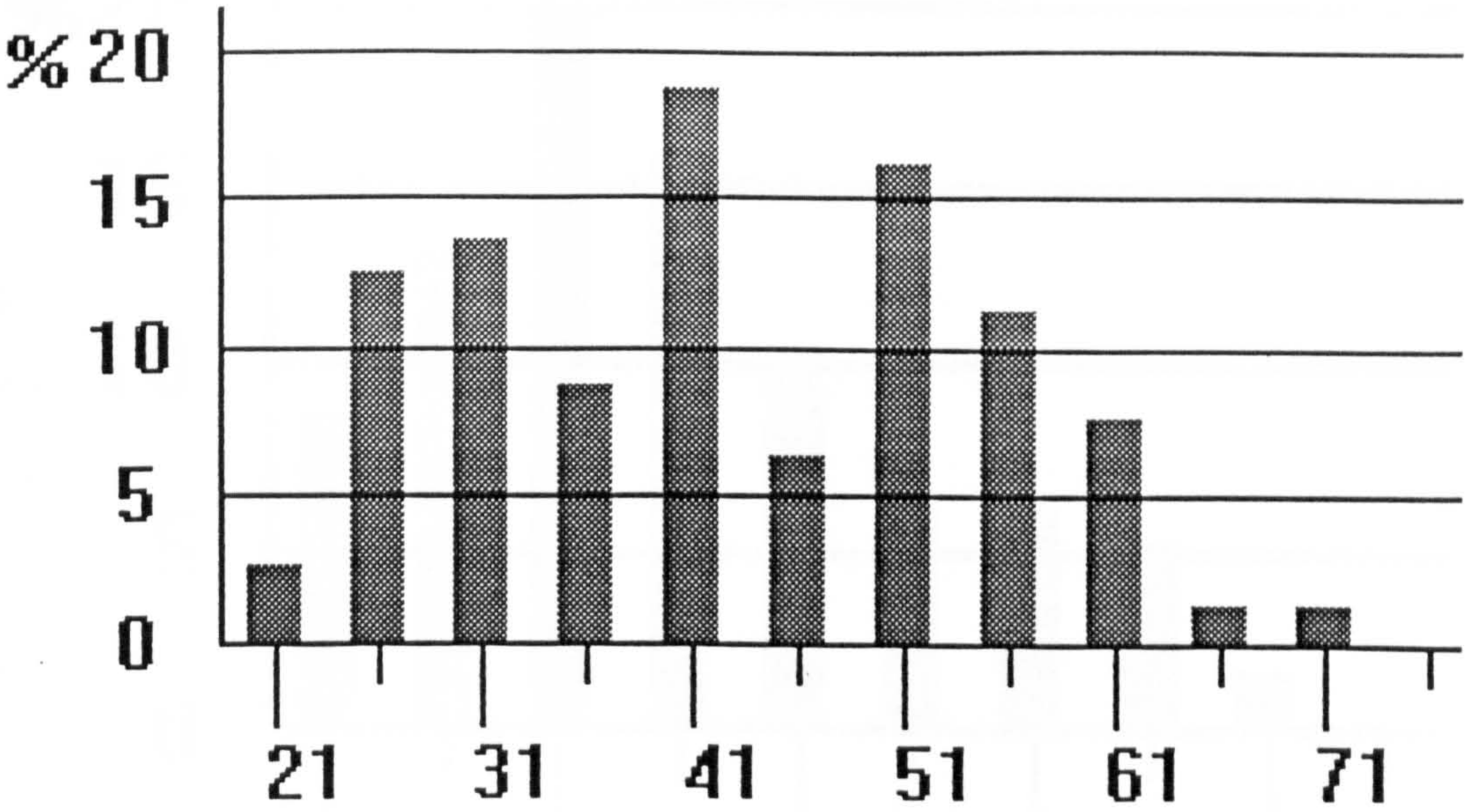

Fig. 5.2.27: The histogram of experimental measured widths of precipitate-free zones for sample 180-0010 (class size=5nm).

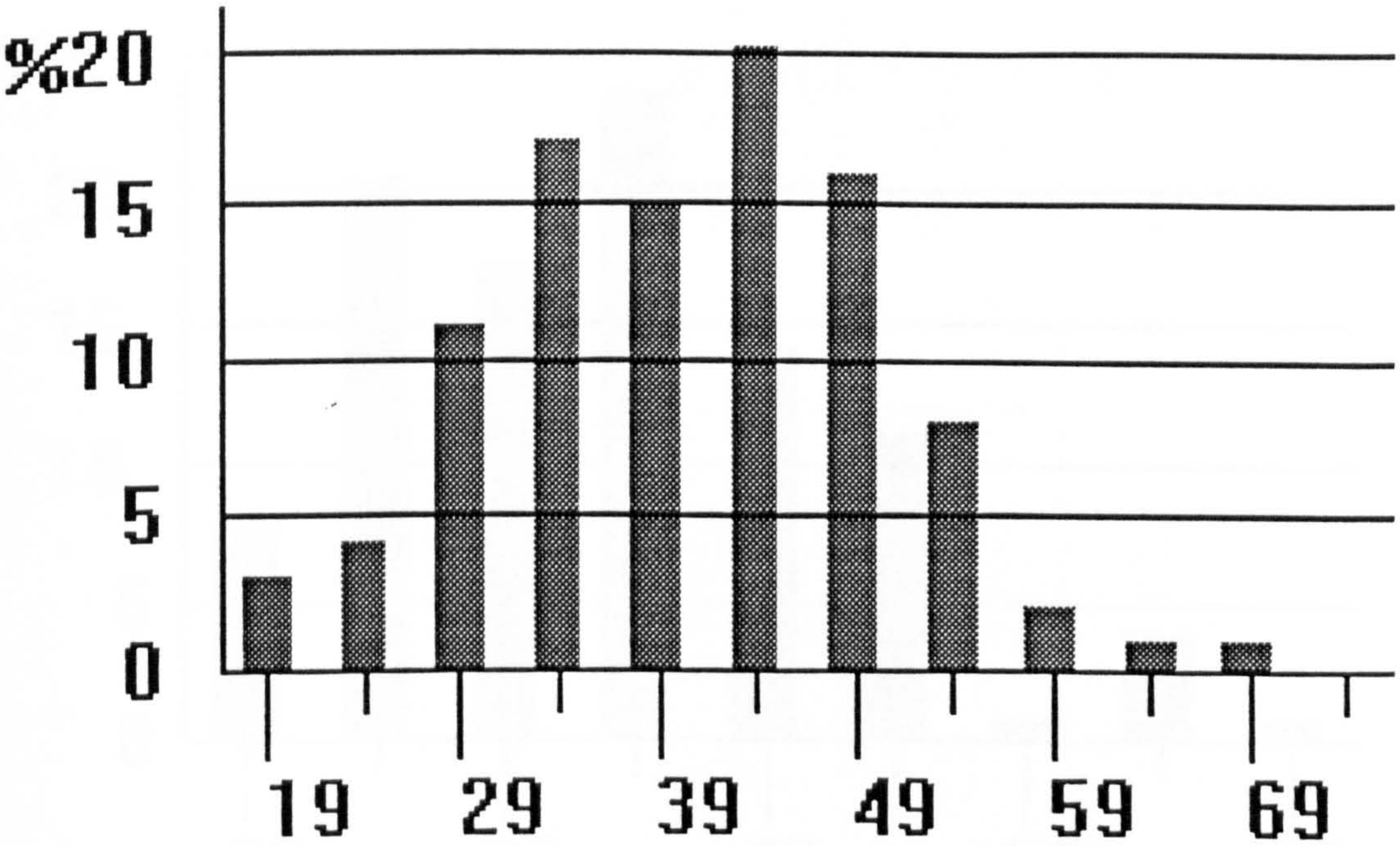

Fig. 5.2.28: The histogram of experimental measured widths of precipitate-free zones for sample 180-0020 (class size=5nm).

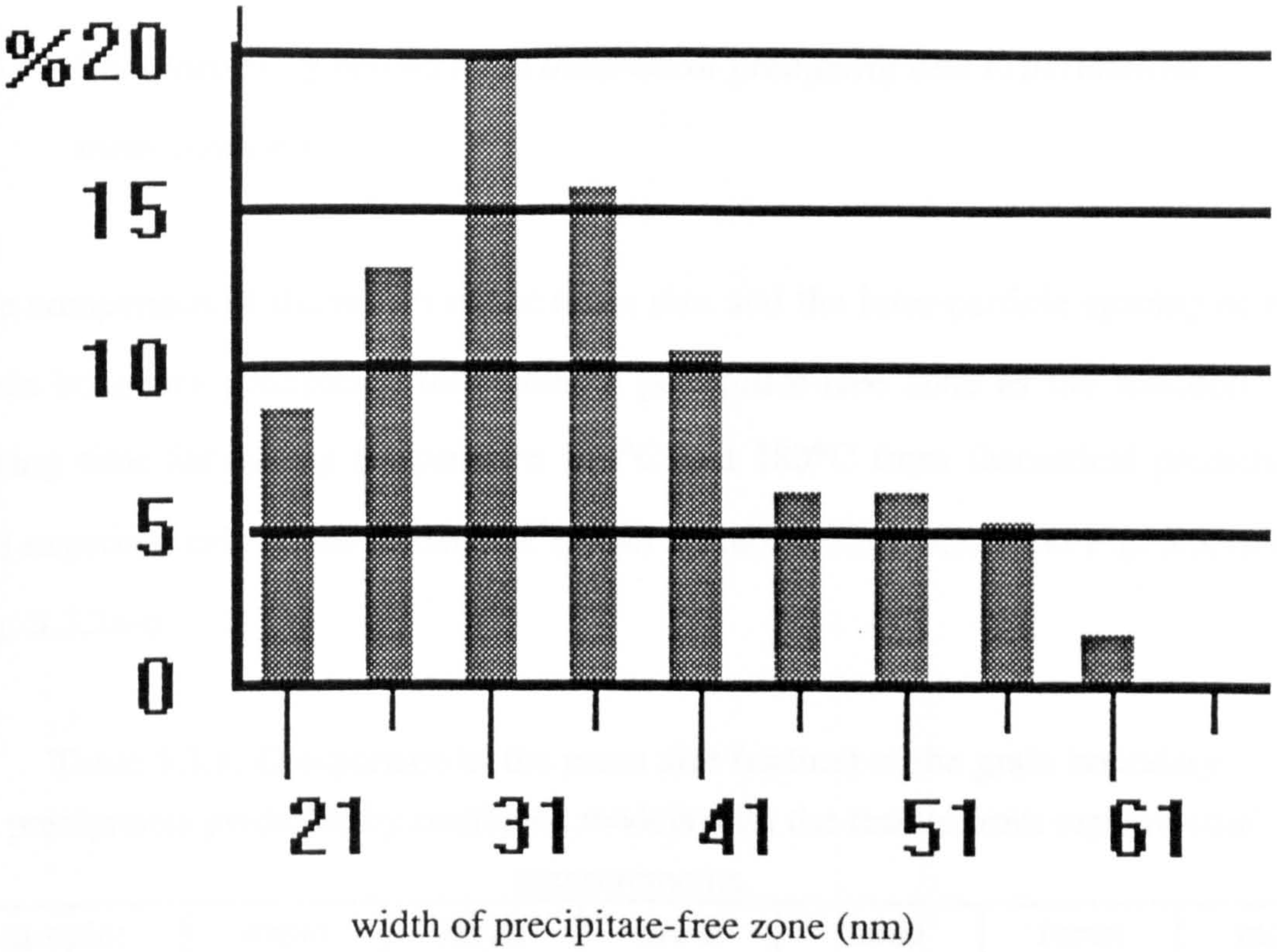

Fig. 5.2.29: The histogram of experimental measured widths of precipitate-free zones for sample 180-0030 (class size=5nm).

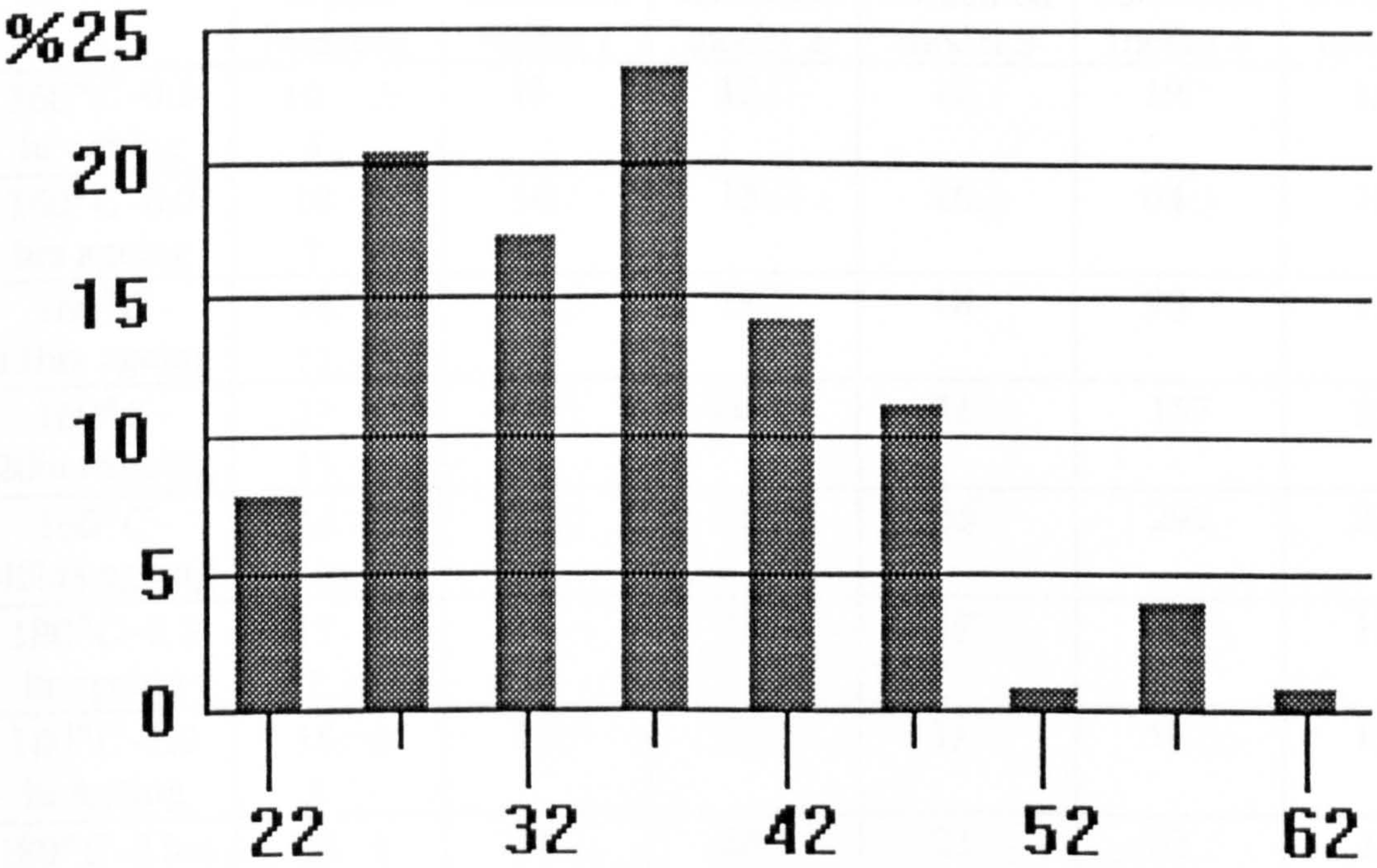

Fig. 5.2.30: The histogram of experimental measured widths of precipitate-free zones for sample 180-0100 (class size=5nm).

5.3 *Comparison of results from theoretical predicting and experimental measurements*

The comparison of the results of the mean size and the inter-particle spacing of the grain boundary precipitate, the width of precipitate-free zone as the functions of ageing time for ageing temperature 160°C and 180°C from theoretical prediction and experimental measurements are shown in Tables 5.3.1-5.3.3 and Fig. 5.3.1a-e - Fig. 5.3.3a-e.

Table 5.3.1: Comparison of the mean size (radius) of the grain boundary precipitates predicted by combined models with the results from experimental measurements.

sample:	mean prec. size and std. dev.(nm) from experi. measure.	mean prec. size (nm) predicted by combined model 1	mean prec. size (nm) predicted by combined model 2	mean prec. size (nm) predicted by combined model 3	mean prec. size (nm) predicted by combined model 4	mean prec. size (nm) predicted by combined model 5
160°C-0.5 hr ageing	10 ± 4	11	12	11	19	11
160°C-6.0 hrs ageing	18 ± 7	16	18	16	64	16
160°C-11hrs ageing	18 ± 11	18	19	18	98	18
160°C-20hrs ageing	23 ± 11	21	20	21	157	21
160°C-48hrs ageing	26 ± 10	25	20	25	291	25
180°C-0.5 hr ageing	17 ± 7	17	19	17	40	17
180°C-1.0 hr ageing	18 ± 5	19	20	19	59	19
180°C-2 hrs ageing	20 ± 7	21	22	21	90	21
180°C-3 hrs ageing	22 ± 12	23	22	23	118	23
180°C-10hrs ageing	29 ± 12	30	24	29	279	30

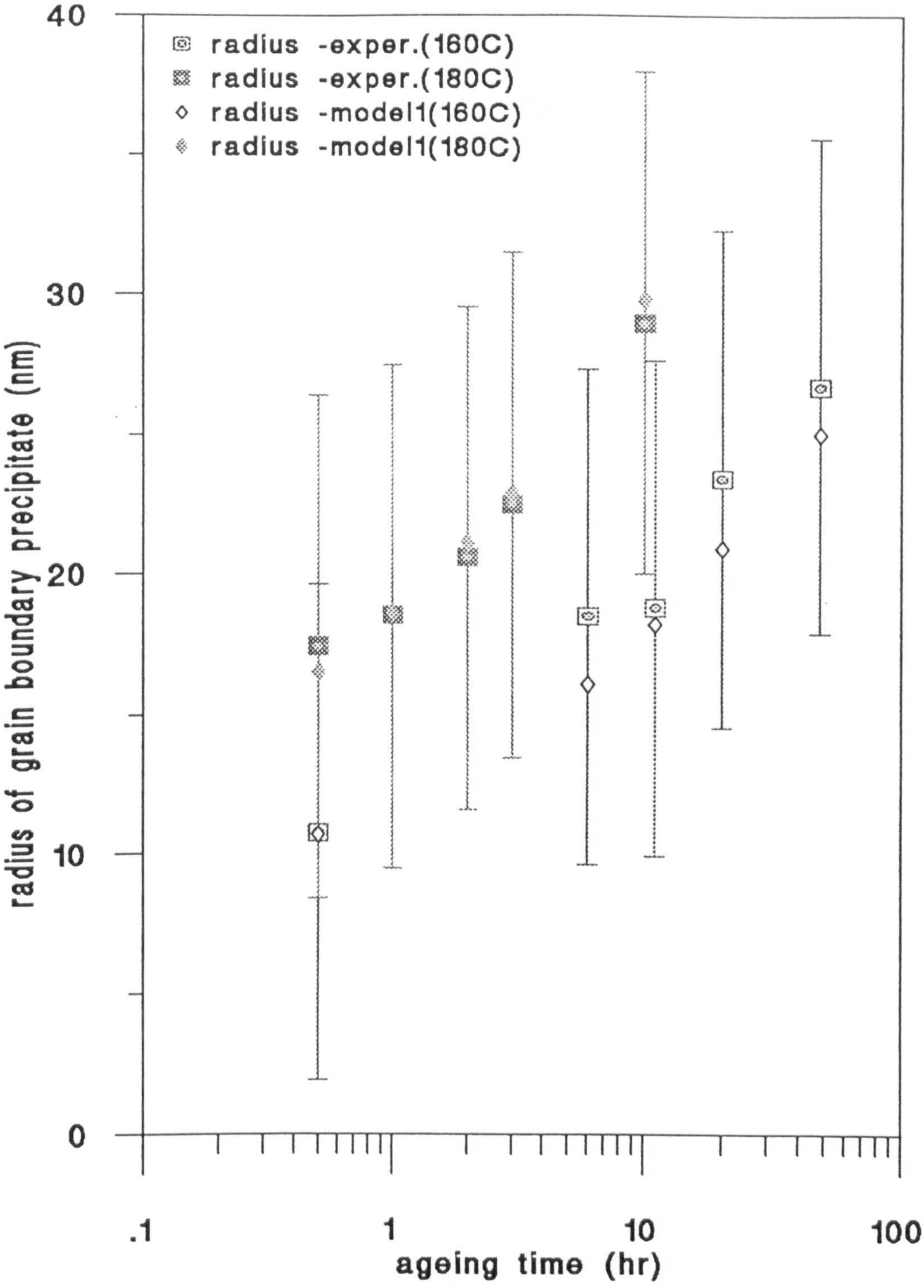

Fig. 5.3.1a: Comparison of the mean size (radius) of the grain boundary precipitates plotted against ageing time predicted by combined model 2 with the results from experimental measurements for ageing temperature 160°C and 180°C.

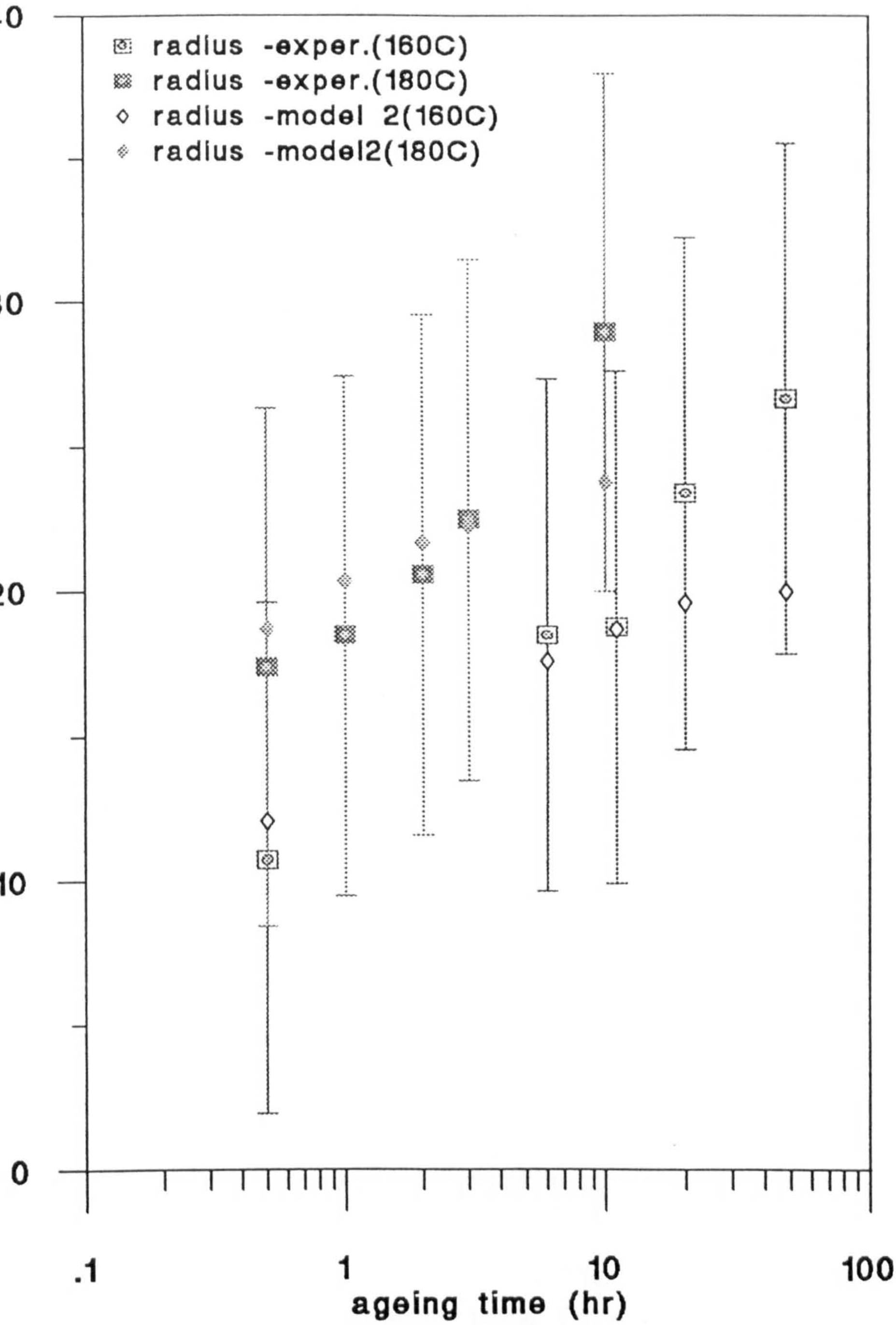

Fig. 5.3.1b: Comparison of the mean size (radius) of the grain boundary precipitates plotted against ageing time predicted by combined model 2 with the results from experimental measurements for ageing temperature 160°C and 180°C.

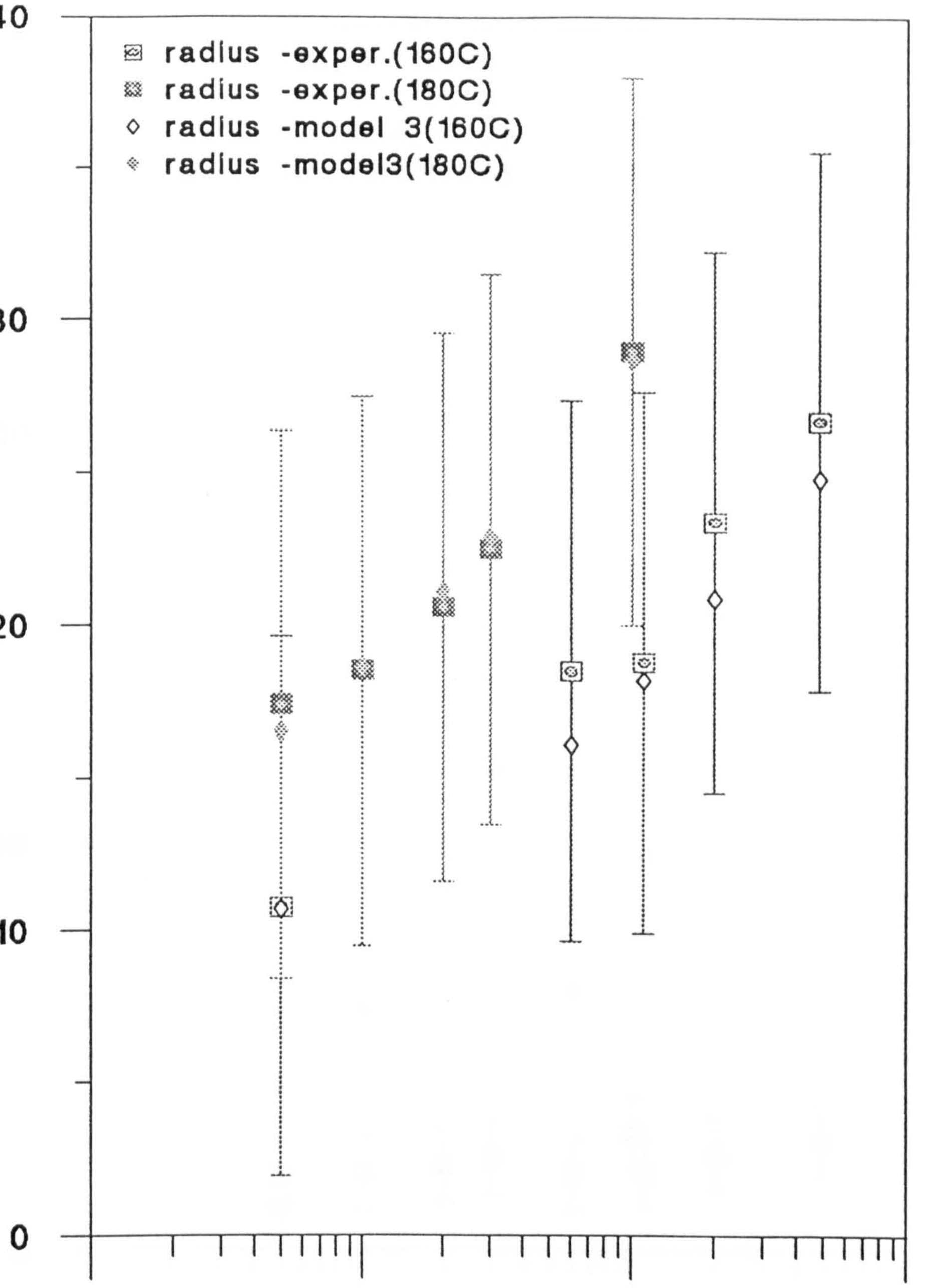

Fig. 5.3.1c: Comparison of the mean size (radius) of the grain boundary precipitates plotted against ageing time predicted by combined model 3 with the results from experimental measurements for ageing temperature 160°C and 180°C.

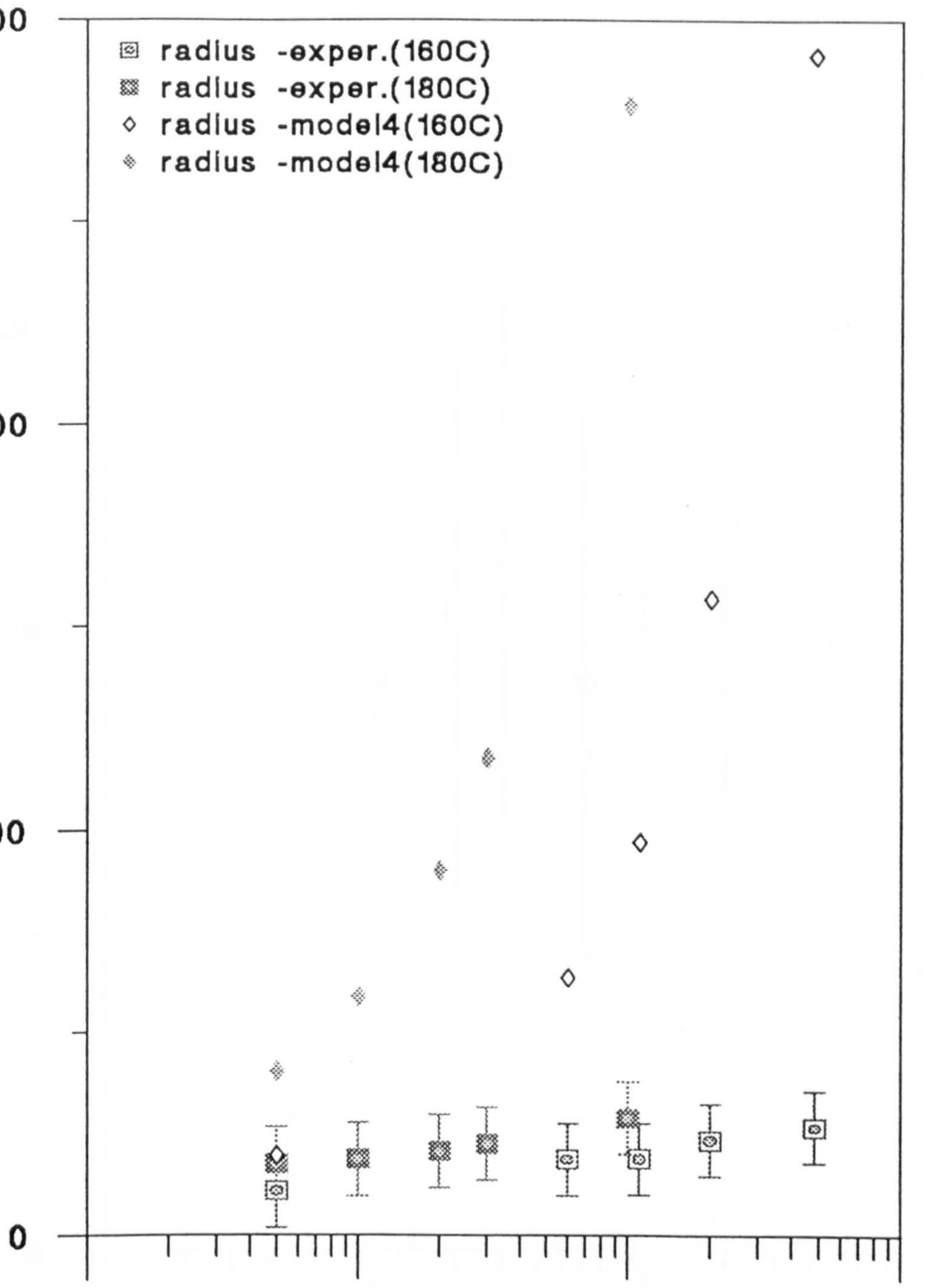

Fig. 5.3.1d:Comparison of the mean size (radius) of the grain boundary precipitates plotted against ageing time predicted by combined model 4 with the results from experimental measurements for ageing temperature 160°C and 180°C.

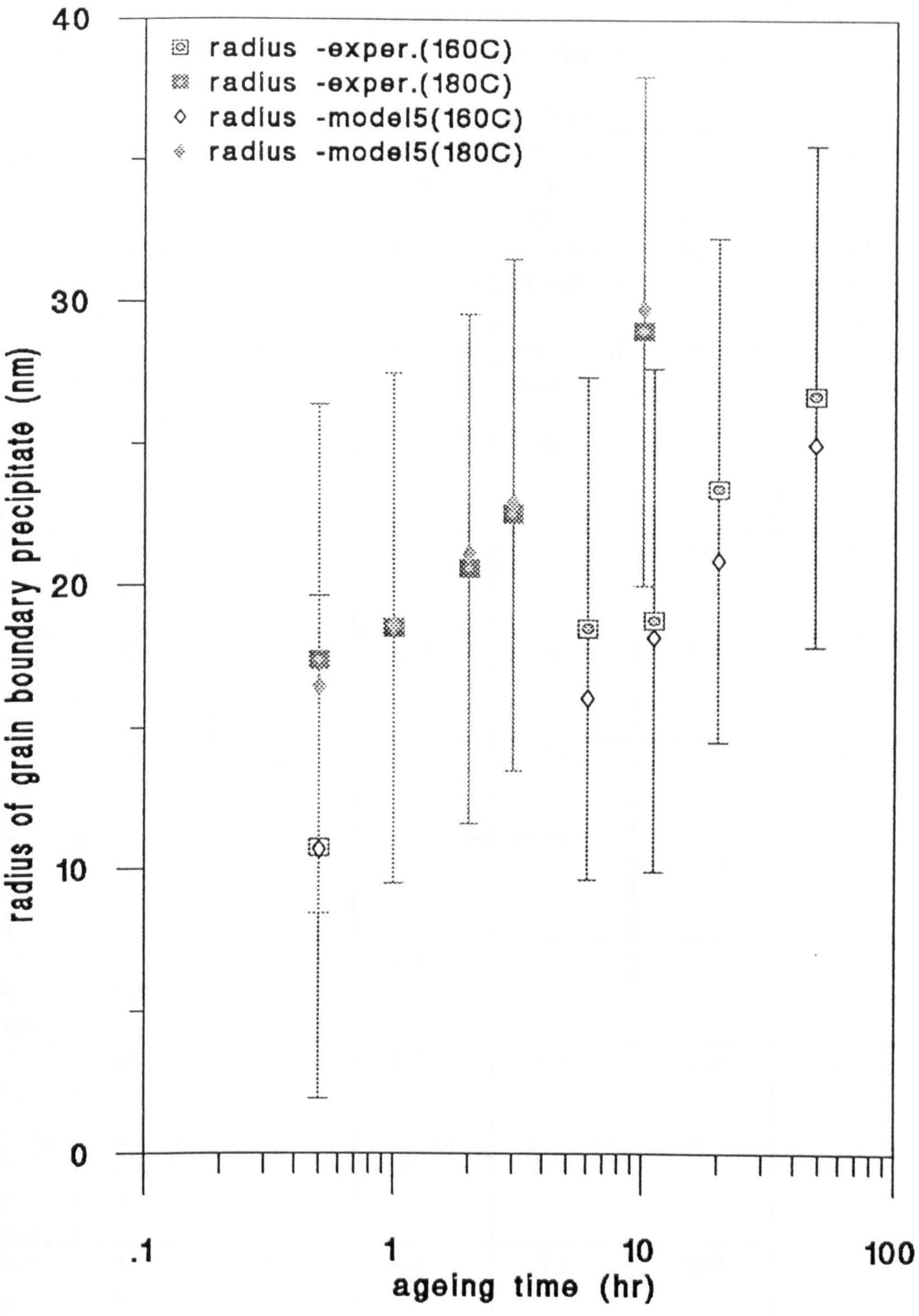

Fig. 5.3.1e: Comparison of the mean size (radius) of the grain boundary precipitates plotted against ageing time predicted by combined model 5 with the results from experimental measurements for ageing temperature 160°C and 180°C.

Table 5.3.2: Comparison of the mean grain boundary inter-particle spacing and standard deviation predicted by combined model with the results from the experimental measurements

sample:	mean inter-part. spacing and std dev.(nm) from experi. measure.	mean int-par. spacing (nm) predicted by combined model 1	mean int-par. spacing (nm) predicted by combined model 2	mean int-par. spacing (nm) predicted by combined model 3	mean int-par. spacing (nm) predicted by combined model 4	mean int-par. spacing (nm) predicted by combined model 5
160°C-0.5hr ageing	51 ± 20	51	66	51	54	51
160°C-6.0hrs ageing	54 ± 19	54	69	54	134	54
160°C-11hrs ageing	57 ± 18	57	71	57	199	57
160°C-20hrs ageing	62 ± 22	61	73	61	317	61
160°C-48hrs ageing	69 ± 21	68	76	68	584	68
180°C-0.5hr ageing	65 ± 20	63	84	63	92	63
180°C-1.0hr ageing	67 ± 25	64	85	64	126	64
180°C-2.0hrs ageing	71 ± 24	67	86	67	187	67
180°C-3.0hrs ageing	74 ± 25	70	87	70	242	70
180°C-10hrs ageing	83 ± 25	80	91	79	561	81

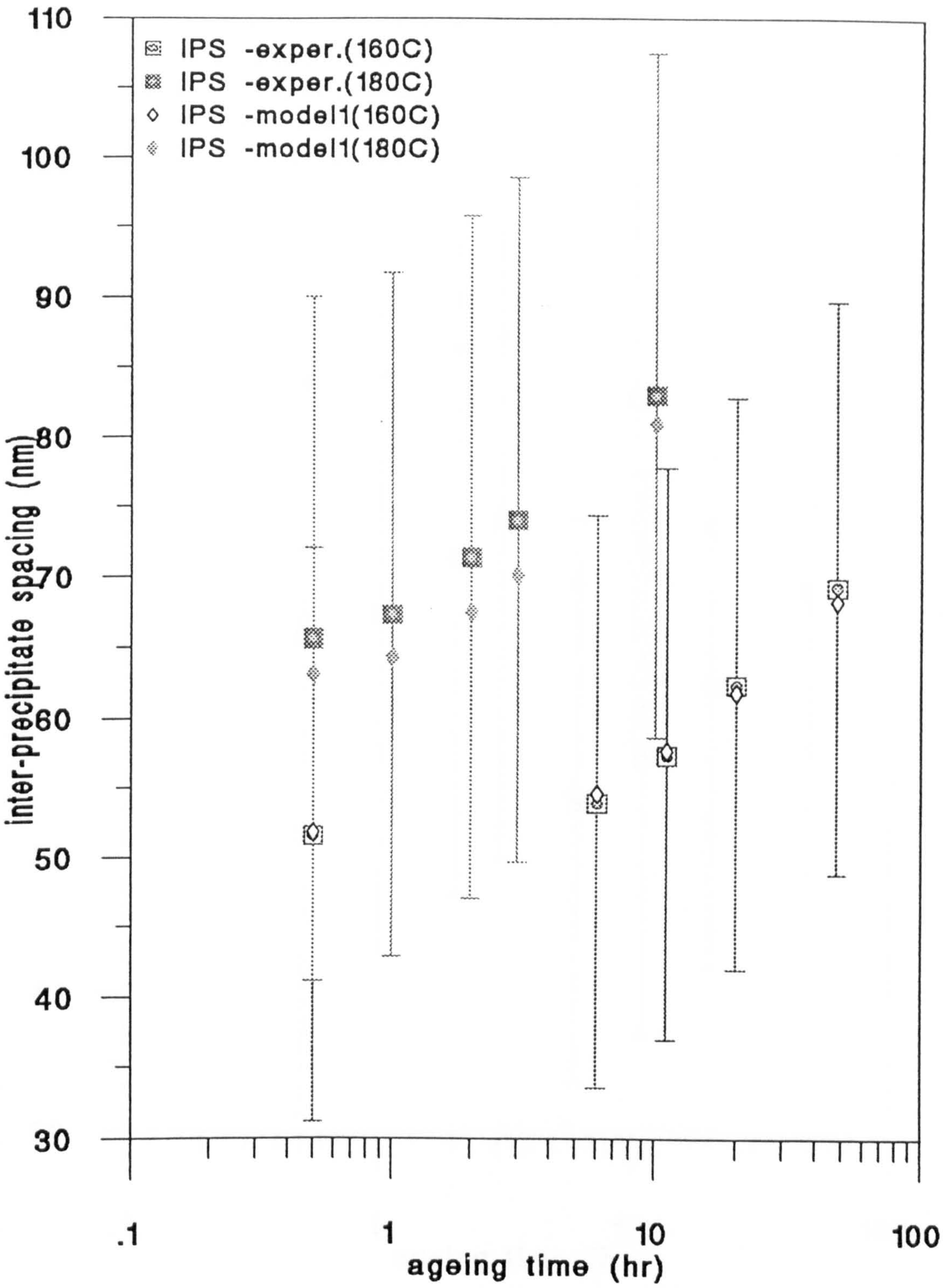

Fig. 5.3.2a: Comparison of the mean grain boundary inter-particle spacing plotted against ageing time predicted by combined model 1 with the results from the experimental measurements for ageing temperature 160°C and 180°C.

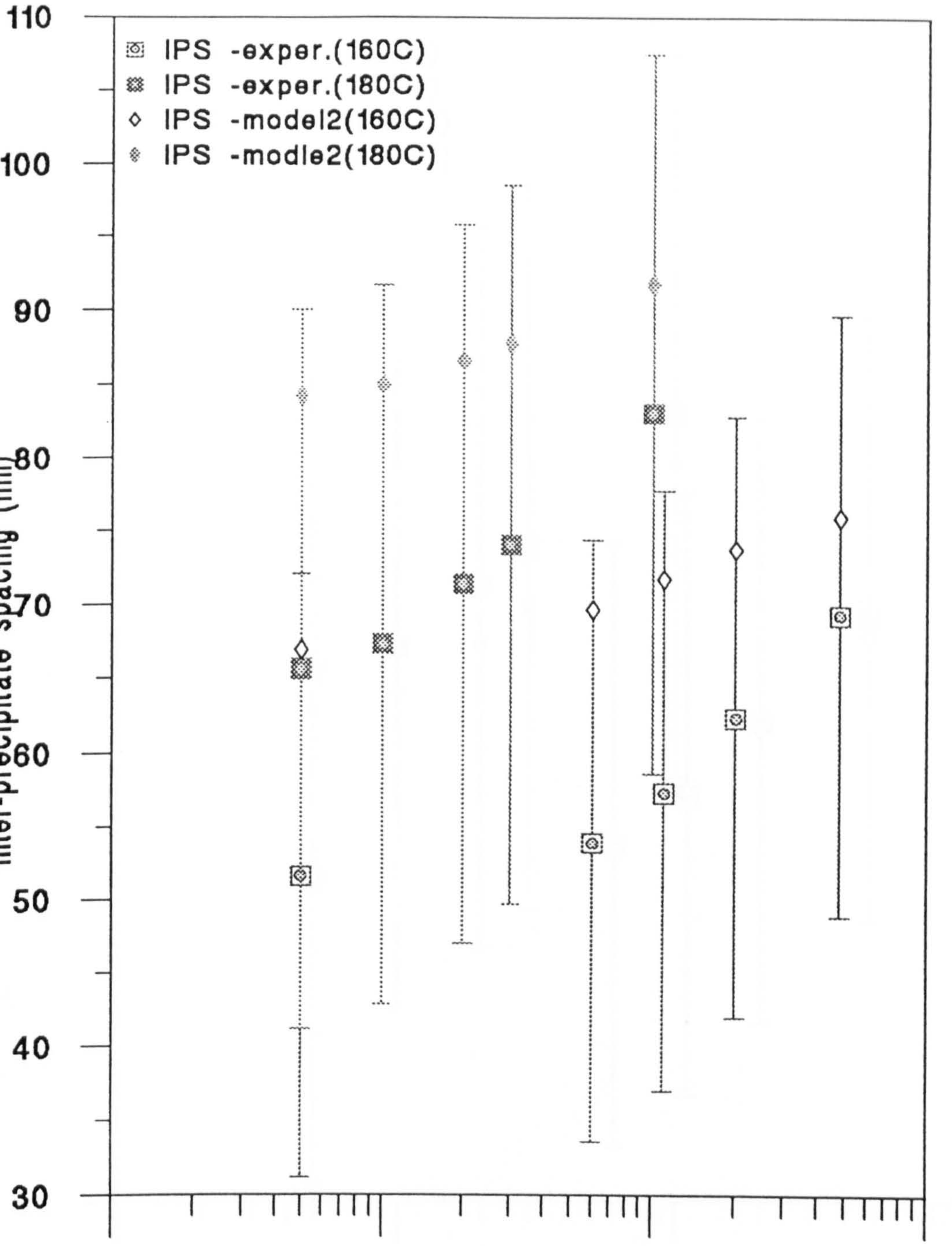

Fig. 5.3.2b: Comparison of the mean grain boundary inter-particle spacing plotted against ageing time predicted by combined model 2 with the results from the experimental measurements for ageing temperature 160°C and 180°C.

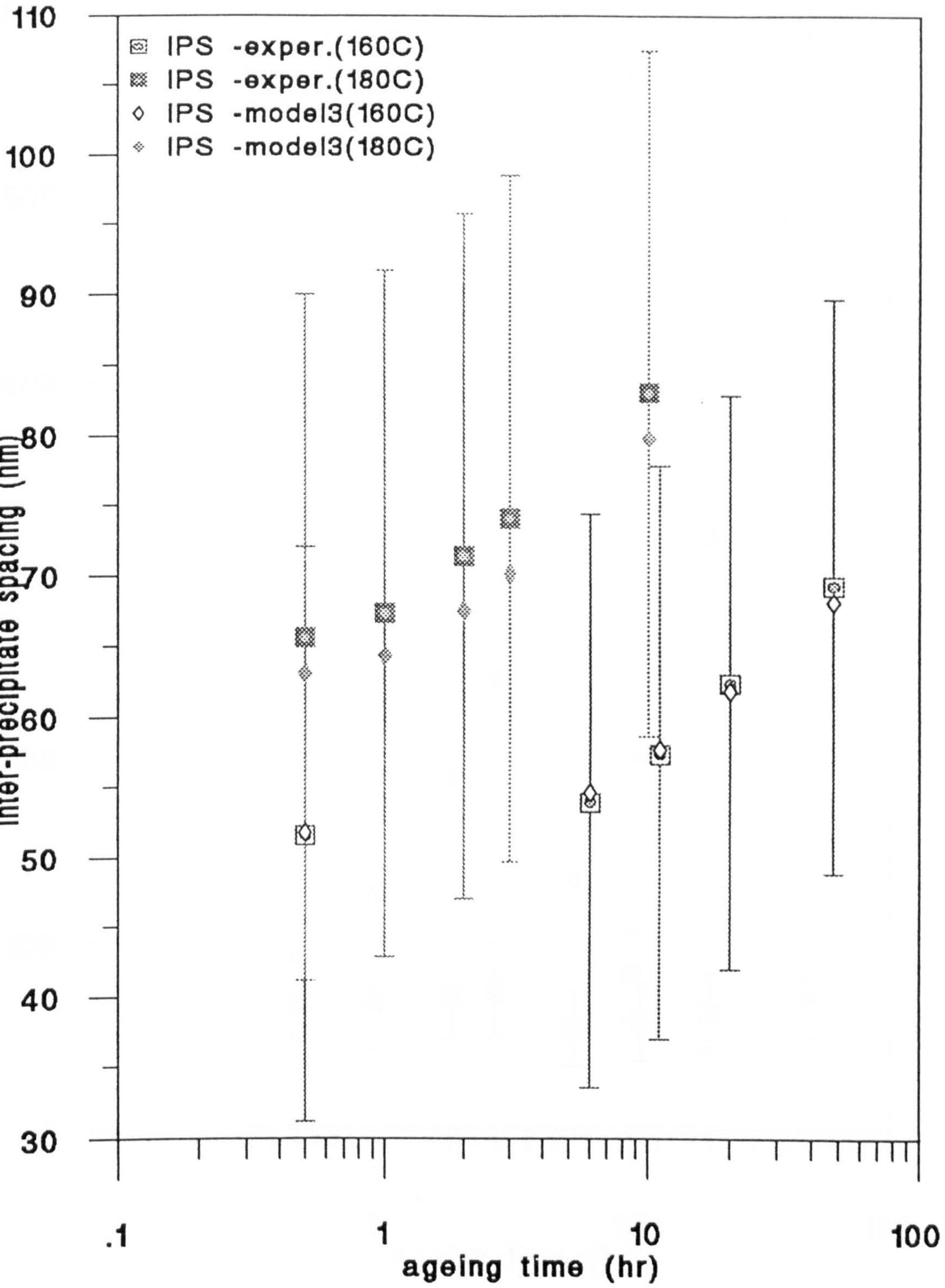

Fig. 5.3.2c: Comparison of the mean grain boundary inter-particle spacing plotted against ageing time predicted by combined model 3 with the results from the experimental measurements for ageing temperature 160°C and 180°C.

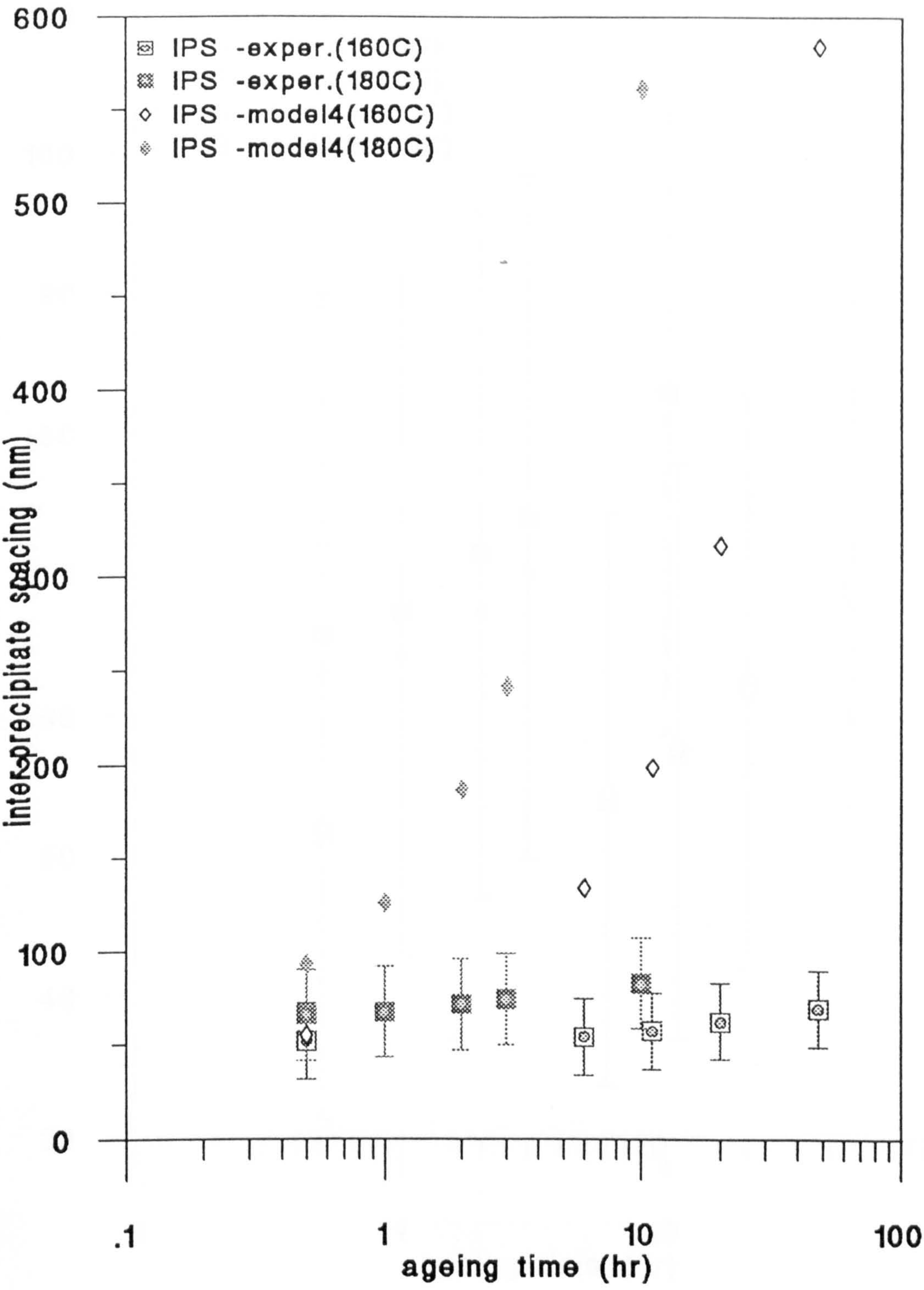

Fig. 5.3.2d: Comparison of the mean grain boundary inter-particle spacing plotted against ageing time predicted by combined model 4 with the results from the experimental measurements for ageing temperature 160°C and 180°C.

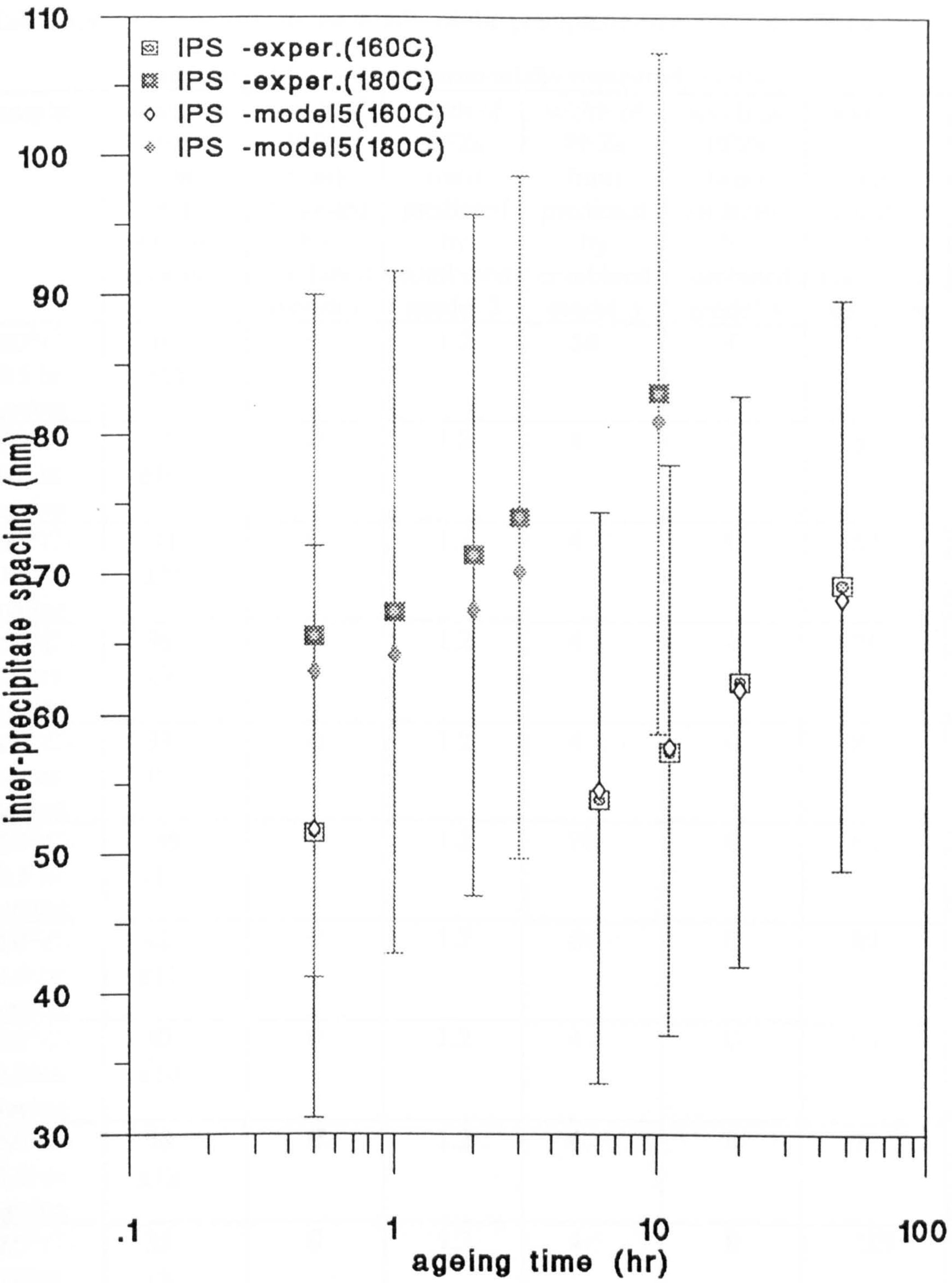

Fig.5.3.2e: Comparison of the mean grain boundary inter-particle spacing plotted against ageing time predicted by combined model 5 with the results from the experimental measurements for ageing temperature 160°C and 180°C.

Table 5.3.3: Comparison of the widths of the precipitate-free zones predicted by combined models with experimentally measured results.

sample:	widths of PFZs (nm) from experi. measure.	width of PFZs (nm) predicted by combined model 1	width of PFZs (nm) predicted by combined model 2	width of PFZs (nm) predicted by combined model 3	width of PFZs (nm) predicted by combined model 4	width of PFZs (nm) predicted by combined model 5
160°C-0.5 hr ageing	60 ±15	0	1.2	54	0	55
160°C-6.0 hr ageing	43 ±10	0	1.2	4	0	59
160°C-11hrs ageing	41 ±10	0	1.2	4	0	63
160°C-20hrs ageing	36 ±9	0	1.2	4	0	71
160°C-48hrs ageing	33 ±7	0	1.2	4	0	88
180°C-0.5 hr ageing	56 ±12	0	1.2	78	0	84
180°C-1.0 hr ageing	42 ±11	0	1.2	64	0	87
180°C-2.0hrs ageing	40 ±10	0	1.2	4	0	93
180°C-3.0hrs ageing	38 ±12	0	1.2	4	0	98
180°C-10hrs ageing	35 ±8	0	1.2	4	0	129

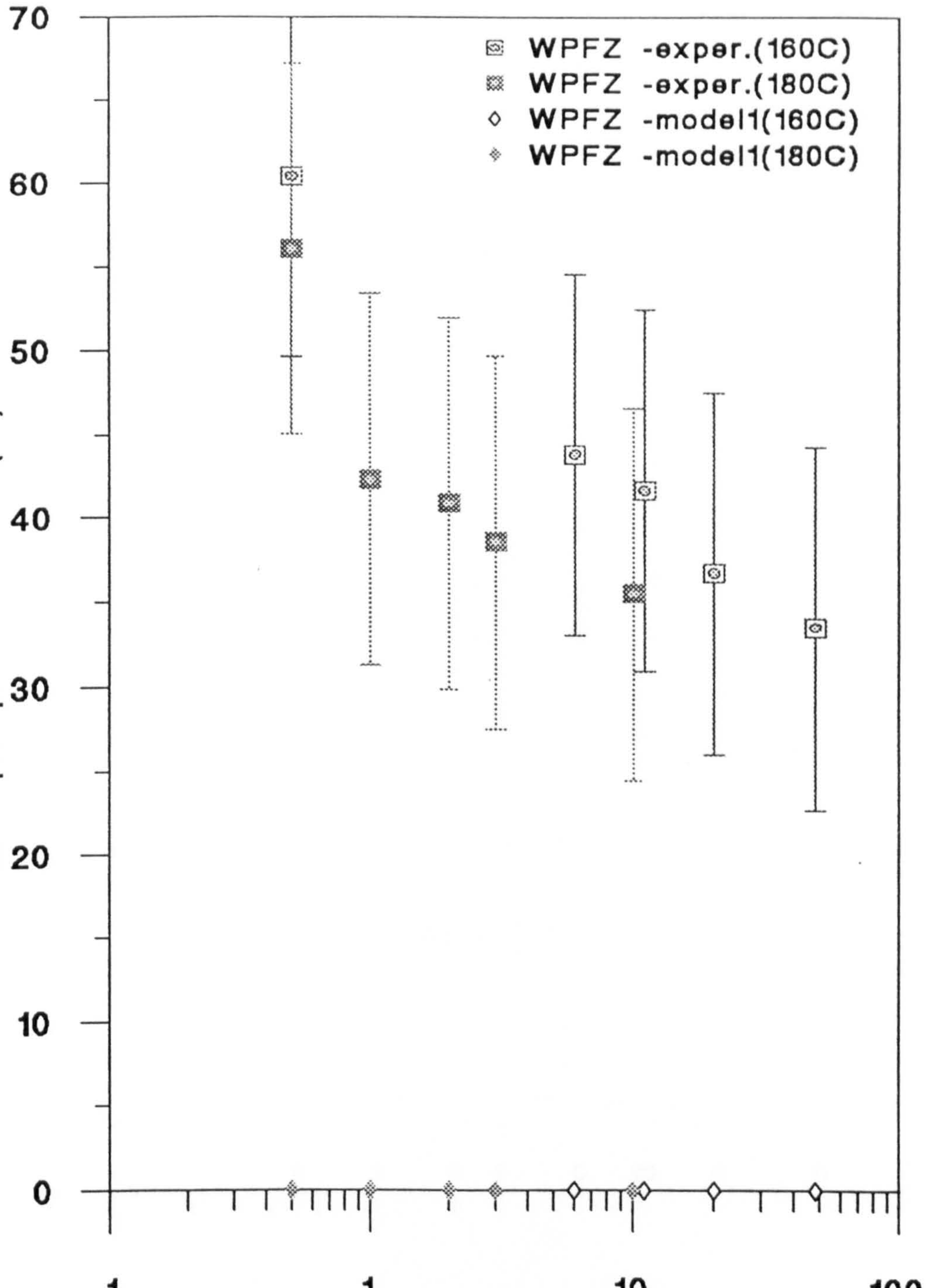

Fig. 5.3.3a: Comparison of the widths of PFZs plotted against ageing time predicted by combined model 1 with the results from the experimental measurements for ageing temperature 160°C and 180°C.

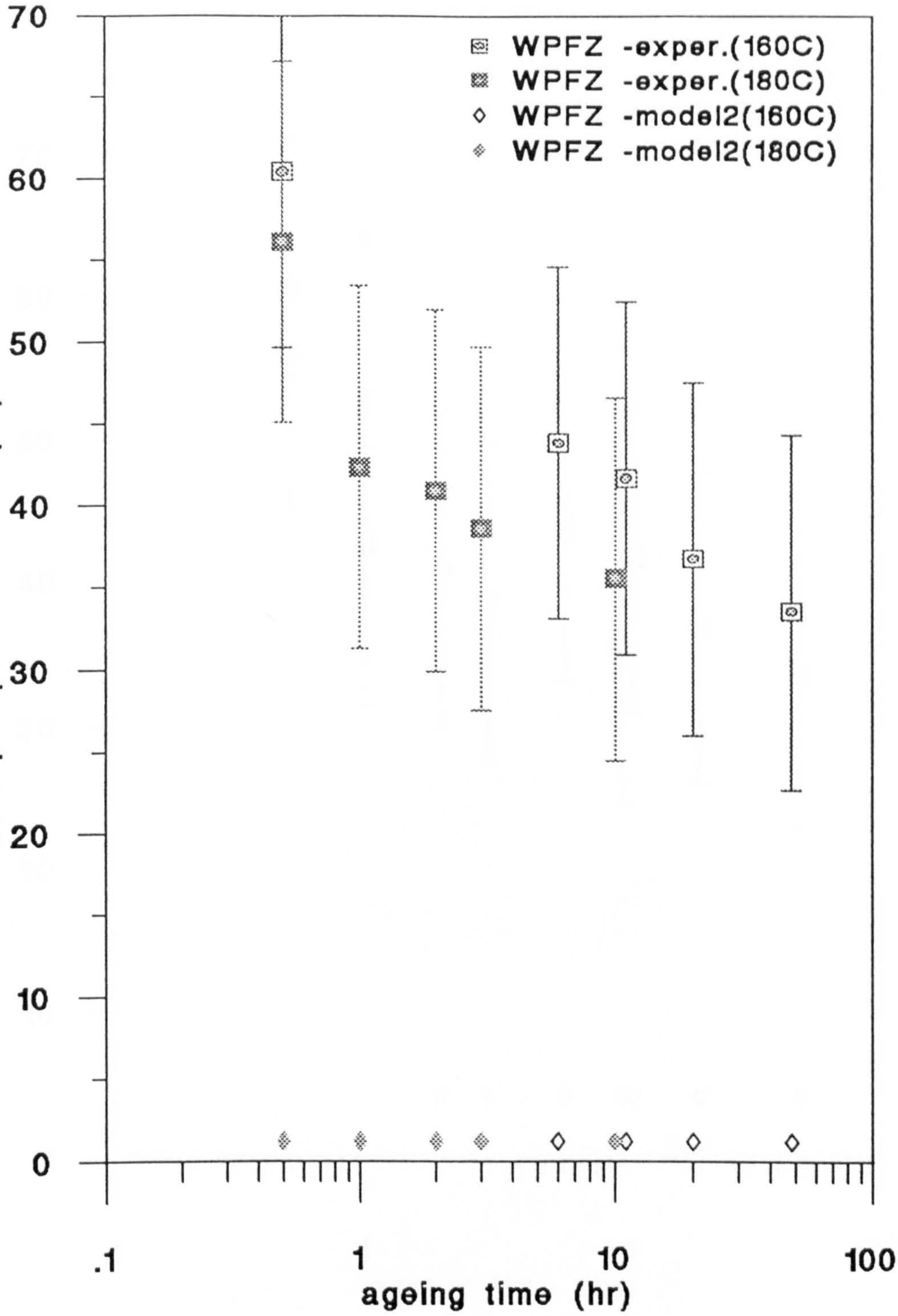

Fig. 5.3.3b: Comparison of the widths of PFZs plotted against ageing time predicted by combined model 2 with the results from the experimental measurements for ageing temperature 160°C and 180°C.

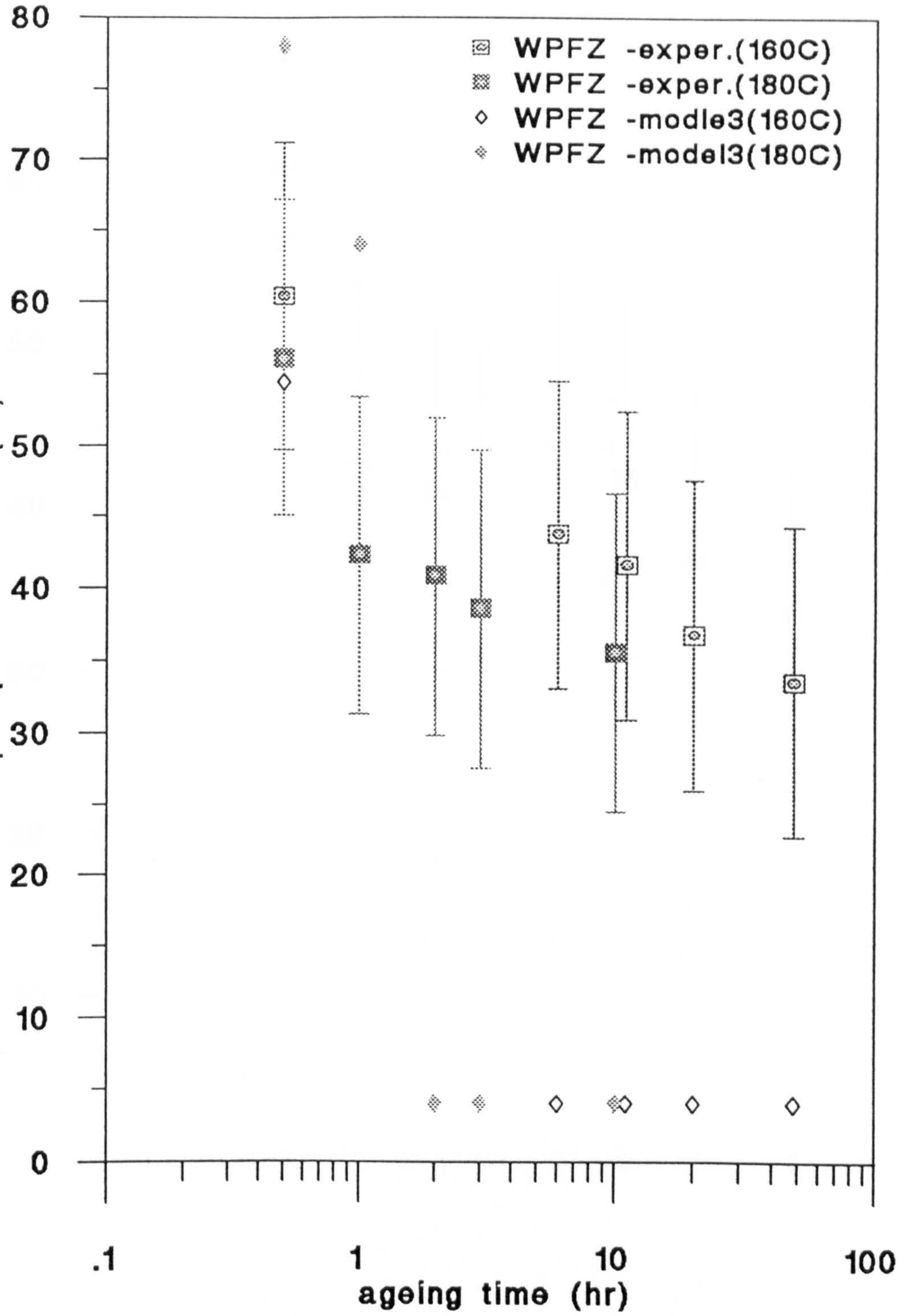

Fig. 5.3.3c: Comparison of the widths of PFZs plotted against ageing time predicted by combined model 3 with the results from the experimental measurements for ageing temperature 160°C and 180°C.

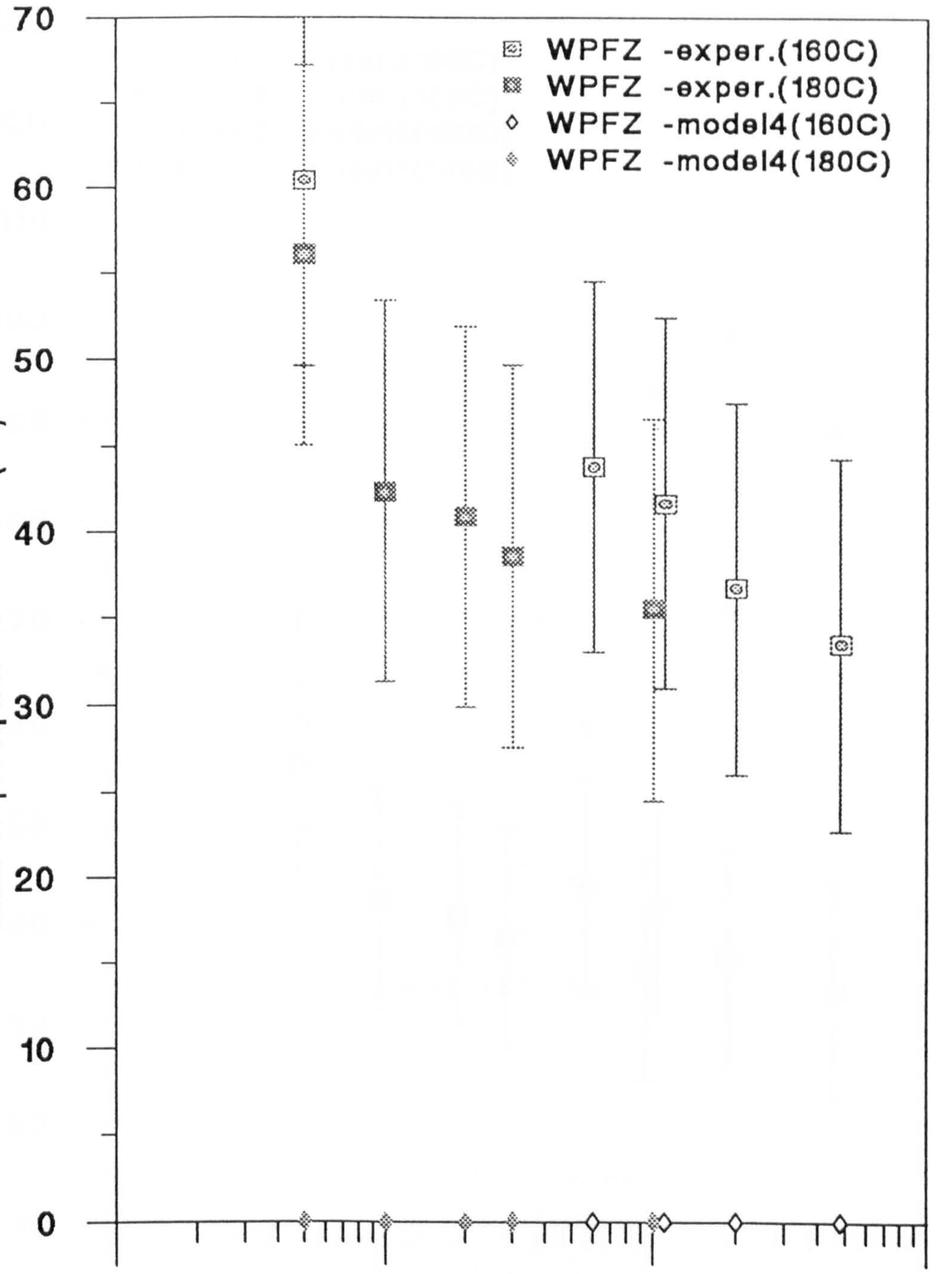

Fig. 5.3.3d: Comparison of the widths of PFZs plotted against ageing time predicted by combined model 4 with the results from the experimental measurements for ageing temperature 160°C and 180°C.

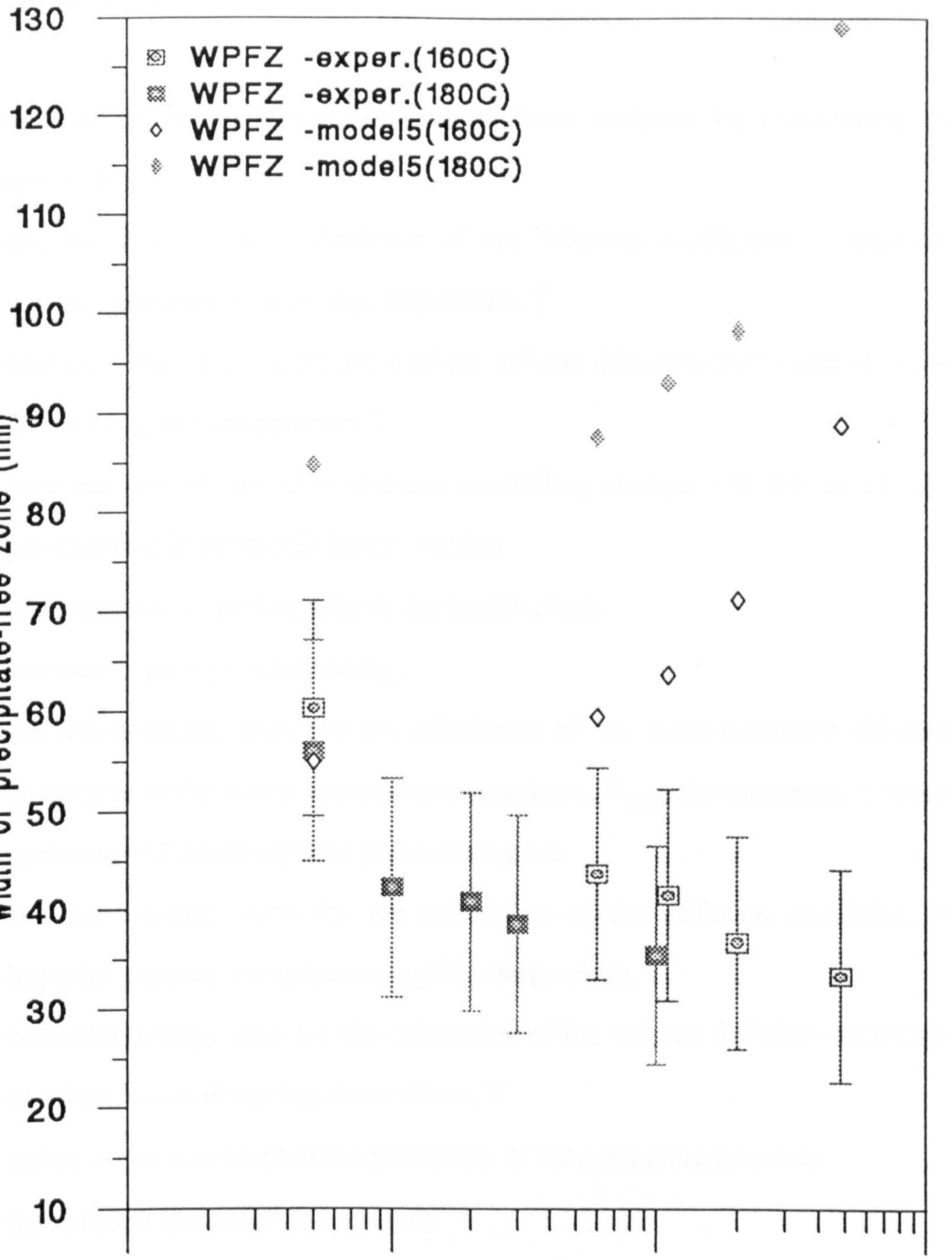

Fig. 5.3.3e: Comparison of the widths of PFZs plotted against ageing time predicted by combined model 5 with the results from the experimental measurements for ageing temperature 160°C and 180°C.

5.4 *Sensitivity analysis*

The sensitivity of the combined models has been analysed by considering the following variables:

a_c: entropy term for the calculation of the diffusion coefficient of impurity-vacancy complexes at ageing temperature, T

a_I: entropy term for the calculation of the volume diffusion coefficient of solute atoms at ageing temperature, T

C_c: concentration of the other non-rate controlling element (in this case is Zn) participating in the precipitation reaction

C_g: concentration of the impurity in the matrix phase

E_b: vacancy-impurity binding energy

Q_{bnuc}: activation energy term for the calculation of the grain-boundary diffusion coefficient of the solute element at temperature, T_{nuc}, the temperature where nucleation of the precipitate phase takes place

Q_c: activation energy term for the calculation of the diffusion coefficient of impurity-vacancy complexes at ageing temperature, T

Q_I: activation energy term for the calculation of the volume diffusion coefficient of solute atoms at ageing temperature, T

r: radius of the curvature of the precipitate at the advancing interface

T_i: the solution treatment temperature

T_{mp}: the temperature at which most of segregation has been completed

δt: time interval

d_2: width of solute concentrated layer

θ: the cooling rate parameter

ψ: the angle where $\cos\psi = {}^{\sigma_{\alpha\alpha}}/_{2\sigma_{\alpha\theta}}$

Table 5.4.1 gives the data of the parameters used for sensitivity analysis. Each time the parameter tested has the value varying from data 1 to data 3 while others have values giving by the data with index * in the table.

Table 5.4.1: Data for the sensitivity analysis of the combined model on predicting the growth and the distribution of $MgZn_2$ grain boundary precipitates and change of the widths of PFZs with ageing time.

	parameter	data 1	data 2	data3
a_C	cm^2s^{-1}	0.012	0.12*	1.2
a_I	cm^2s^{-1}	0.0143	0.143*	1.43
C_C	mole frac.	0.0373	0.0280*	0.0187
C_g	mole frac.	0.0371	0.0272*	0.0181
E_b	eV	0.373	0.28*	0.25
r	nm	10	10000*	500
Q_{bnuc}	eV	0.74	0.98*	1.10
Q_C	eV	1.12	1.24*	1.36
Q_I	eV	1.38	1.54*	1.69
T_j	K	733	748*	763
T_{mp}	K	600	560*	520
δt	s	5	3*	10
d_2	nm	5	1*	10
θ	s^{-1}	0.1	1*	0.01
ψ	o	45.0	46.25*	47.5

*: the data of the parameters not subjected for sensitivity analysis.

Table 5.4.1 -Table 5.4.15 show the effects of varying a_c, a_I, C_c, C_g, E_b, Q_{bnuc}, Q_c, Q_I, r, T_{mp}, δt, d_2, θ, ψ on the predicted curves of the precipitate size, inter-precipitate spacing and width of precipitate-free zones against ageing time for ageing temperature 160 °C and 180°C.

Table 5.4.1a: The effect of varying a_c on the prediction of the radius, the inter-precipitate spacing and width of PFZs given by combined model 1.

ageing treatment:	variable: a_c (cm^2s^{-1})	radius of precipitate: (nm)	inter-precipitate spacing: (nm)	width of PFZs: (nm)
160°C -0.5 hr	$a_c=1.2x10^{-6}$	10.7	51.8	0
	$a_c=1.2x10^{-5}$	10.7	51.8	0
	$a_c=1.2x10^{-4}$	10.7	51.8	0
160°C -5.5 hrs	$a_c=1.2x10^{-6}$	16.1	54.7	0
	$a_c=1.2x10^{-5}$	16.1	54.7	0
	$a_c=1.2x10^{-4}$	16.1	54.7	0
160°C -10.5 hrs	$a_c=1.2x10^{-6}$	18.2	57.7	0
	$a_c=1.2x10^{-5}$	18.2	57.8	0
	$a_c=1.2x10^{-4}$	18.2	57.8	0
160°C -20.5 hrs	$a_c=1.2x10^{-6}$	20.8	61.8	0
	$a_c=1.2x10^{-5}$	20.9	61.8	0
	$a_c=1.2x10^{-4}$	20.9	61.8	0
160°C -48 hrs	$a_c=1.2x10^{-6}$	24.9	68.1	0
	$a_c=1.2x10^{-5}$	25.0	68.2	0
	$a_c=1.2x10^{-4}$	25.0	68.3	0
180°C -0.5 hr	$a_c=1.2x10^{-6}$	16.5	63.1	0
	$a_c=1.2x10^{-5}$	16.5	63.1	0
	$a_c=1.2x10^{-4}$	16.5	63.1	0
180°C -1 hr	$a_c=1.2x10^{-6}$	18.5	64.3	0
	$a_c=1.2x10^{-5}$	18.6	64.3	0
	$a_c=1.2x10^{-4}$	18.6	64.3	0
180°C -2 hrs	$a_c=1.2x10^{-6}$	21.0	67.4	0
	$a_c=1.2x10^{-5}$	21.1	67.5	0
	$a_c=1.2x10^{-4}$	21.1	67.5	0
180°C -3 hrs	$a_c=1.2x10^{-6}$	22.8	70.1	0
	$a_c=1.2x10^{-5}$	22.9	70.1	0
	$a_c=1.2x10^{-4}$	22.9	70.2	0
180°C -10 hrs	$a_c=1.2x10^{-6}$	29.6	80.7	0
	$a_c=1.2x10^{-5}$	29.8	80.9	0
	$a_c=1.2x10^{-4}$	29.8	81.0	0

Table 5.5.1b: The effect of varying a_c on the prediction of the radius, the inter-precipitate spacing and width of PFZs given by combined model 2.

ageing treatment:	variable: a_c (cm^2s^{-1})	radius of precipitate: (nm)	inter-precipitate spacing: (nm)	width of PFZs: (nm)
160°C -0.5 hr	$a_c=1.2x10^{-6}$	18.9	153	1.2
	$a_c=1.2x10^{-5}$	12.1	66.9	1.2
	$a_c=1.2x10^{-4}$	10.7	51.8	1.2
160°C -5.5 hrs	$a_c=1.2x10^{-6}$	26.9	156	1.2
	$a_c=1.2x10^{-5}$	17.6	69.7	1.2
	$a_c=1.2x10^{-4}$	15.2	54.2	1.2
160°C -10.5 hrs	$a_c=1.2x10^{-6}$	28.3	159	1.2
	$a_c=1.2x10^{-5}$	18.7	71.8	1.2
	$a_c=1.2x10^{-4}$	16.0	55.9	1.2
160°C -20.5 hrs	$a_c=1.2x10^{-6}$	29.3	162	1.2
	$a_c=1.2x10^{-5}$	19.6	73.8	1.2
	$a_c=1.2x10^{-4}$	16.6	57.4	1.2
160°C -48 hrs	$a_c=1.2x10^{-6}$	29.7	166	1.2
	$a_c=1.2x10^{-5}$	20.0	76.0	1.2
	$a_c=1.2x10^{-4}$	16.7	58.9	1.2
180°C -0.5 hr	$a_c=1.2x10^{-6}$	32.0	217	1.2
	$a_c=1.2x10^{-5}$	18.7	84.2	1.2
	$a_c=1.2x10^{-4}$	16.3	63.1	1.2
180°C -1 hr	$a_c=1.2x10^{-6}$	34.2	217	1.2
	$a_c=1.2x10^{-5}$	20.4	85.0	1.2
	$a_c=1.2x10^{-4}$	17.4	63.9	1.2
180°C -2 hrs	$a_c=1.2x10^{-6}$	35.8	219	1.2
	$a_c=1.2x10^{-5}$	21.7	86.6	1.2
	$a_c=1.2x10^{-4}$	18.2	65.4	1.2
180°C -3 hrs	$a_c=1.2x10^{-6}$	36.6	220	1.2
	$a_c=1.2x10^{-5}$	22.3	87.8	1.2
	$a_c=1.2x10^{-4}$	18.6	66.4	1.2
180°C -10 hrs	$a_c=1.2x10^{-6}$	38.5	225	1.2
	$a_c=1.2x10^{-5}$	23.8	91.8	1.2
	$a_c=1.2x10^{-4}$	19.5	69.2	1.2

Table 5.4.1c: The effect of varying a_c on the prediction of the radius, the inter-precipitate spacing and width of PFZs given by combined model 3.

ageing treatment:	variable: a_c (cm^2s^{-1})	radius of precipitate: (nm)	inter-precipitate spacing: (nm)	width of PFZs: (nm)
160°C -0.5 hr	$a_c=1.2x10^{-6}$	10.7	51.8	17.2
	$a_c=1.2x10^{-5}$	10.7	51.8	54.4
	$a_c=1.2x10^{-4}$	10.7	51.8	172
160°C -5.5 hrs	$a_c=1.2x10^{-6}$	15.7	54.5	1.41
	$a_c=1.2x10^{-5}$	16.1	54.7	4.02
	$a_c=1.2x10^{-4}$	16.1	54.7	12.3
160°C -10.5 hrs	$a_c=1.2x10^{-6}$	16.7	56.6	1.41
	$a_c=1.2x10^{-5}$	18.2	57.8	4.02
	$a_c=1.2x10^{-4}$	18.2	57.8	12.3
160°C -20.5 hrs	$a_c=1.2x10^{-6}$	17.6	58.4	1.41
	$a_c=1.2x10^{-5}$	20.9	61.9	4.02
	$a_c=1.2x10^{-4}$	20.9	61.9	12.3
160°C -48 hrs	$a_c=1.2x10^{-6}$	18.0	60.2	1.41
	$a_c=1.2x10^{-5}$	24.8	68.1	4.02
	$a_c=1.2x10^{-4}$	25.0	68.3	12.3
180°C -0.5 hr	$a_c=1.2x10^{-6}$	16.5	63.1	24.8
	$a_c=1.2x10^{-5}$	16.5	63.1	78.0
	$a_c=1.2x10^{-4}$	16.5	63.1	247
180°C -1 hr	$a_c=1.2x10^{-6}$	18.0	64.1	20.4
	$a_c=1.2x10^{-5}$	18.6	64.3	64.0
	$a_c=1.2x10^{-4}$	18.6	64.3	202
180°C -2 hrs	$a_c=1.2x10^{-6}$	19.1	66.0	1.41
	$a_c=1.2x10^{-5}$	21.1	67.5	4.02
	$a_c=1.2x10^{-4}$	21.1	67.5	12.3
180°C -3 hrs	$a_c=1.2x10^{-6}$	19.6	67.3	1.41
	$a_c=1.2x10^{-5}$	22.9	70.2	4.02
	$a_c=1.2x10^{-4}$	22.9	70.2	12.3
180°C -10 hrs	$a_c=1.2x10^{-6}$	20.9	72.4	1.41
	$a_c=1.2x10^{-5}$	28.7	79.9	4.02
	$a_c=1.2x10^{-4}$	29.7	81.0	12.3

Table 5.4.1d: The effect of varying a_c on the prediction of the radius, the inter-precipitate spacing and width of PFZs given by combined model 4.

ageing treatment:	variable: a_c (cm^2s^{-1})	radius of precipitate: (nm)	inter-precipitate spacing: (nm)	width of PFZs: (nm)
160°C -0.5 hr	$a_c=1.2x10^{-6}$	13.3	51.8	0
	$a_c=1.2x10^{-5}$	19.5	54.9	0
	$a_c=1.2x10^{-4}$	31.3	72.7	0
160°C -5.5 hrs	$a_c=1.2x10^{-6}$	33.4	78.9	0
	$a_c=1.2x10^{-5}$	63.6	134	0
	$a_c=1.2x10^{-4}$	148	298	0
160°C -10.5 hrs	$a_c=1.2x10^{-6}$	46.3	102	0
	$a_c=1.2x10^{-5}$	97.5	199	0
	$a_c=1.2x10^{-4}$	250	501	0
160°C -20.5 hrs	$a_c=1.2x10^{-6}$	67.1	141	0
	$a_c=1.2x10^{-5}$	157	317	0
	$a_c=1.2x10^{-4}$	434	868	0
160°C -48 hrs	$a_c=1.2x10^{-6}$	111	226	0
	$a_c=1.2x10^{-5}$	291	584	0
	$a_c=1.2x10^{-4}$	855	1710	0
180°C -0.5 hr	$a_c=1.2x10^{-6}$	24.8	68.6	0
	$a_c=1.2x10^{-5}$	40.4	92.8	0
	$a_c=1.2x10^{-4}$	78.0	162	0
180°C -1 hr	$a_c=1.2x10^{-6}$	32.8	81.4	0
	$a_c=1.2x10^{-5}$	58.7	126	0
	$a_c=1.2x10^{-4}$	128	260	0
180°C -2 hrs	$a_c=1.2x10^{-6}$	45.4	103	0
	$a_c=1.2x10^{-5}$	90.1	187	0
	$a_c=1.2x10^{-4}$	219	442	0
180°C -3 hrs	$a_c=1.2x10^{-6}$	56.0	123	0
	$a_c=1.2x10^{-5}$	118	242	0
	$a_c=1.2x10^{-4}$	305	612	0
180°C -10 hrs	$a_c=1.2x10^{-6}$	111	228	0
	$a_c=1.2x10^{-5}$	279	561	0
	$a_c=1.2x10^{-4}$	806	1610	0

Table 5.4.1e: The effect of varying a_c on the prediction of the radius, the inter-precipitate spacing and width of PFZs given by combined model 5.

ageing treatment:	variable: a_c (cm^2s^{-1})	radius of precipitate: (nm)	inter-precipitate spacing: (nm)	width of PFZs: (nm)
160°C -0.5 hr	$a_c=1.2x10^{-6}$	10.7	51.8	17.4
	$a_c=1.2x10^{-5}$	10.7	51.8	55.1
	$a_c=1.2x10^{-4}$	10.7	51.8	174
160°C -5.5 hrs	$a_c=1.2x10^{-6}$	15.8	54.6	18.8
	$a_c=1.2x10^{-5}$	16.1	54.7	59.6
	$a_c=1.2x10^{-4}$	16.1	54.7	188
160°C -10.5 hrs	$a_c=1.2x10^{-6}$	17.1	56.9	20.2
	$a_c=1.2x10^{-5}$	18.2	57.8	63.7
	$a_c=1.2x10^{-4}$	18.2	57.8	202
160°C -20.5 hrs	$a_c=1.2x10^{-6}$	18.2	59.0	22.6
	$a_c=1.2x10^{-5}$	20.9	61.9	71.3
	$a_c=1.2x10^{-4}$	20.9	61.9	226
160°C -48 hrs	$a_c=1.2x10^{-6}$	19.8	61.8	28.1
	$a_c=1.2x10^{-5}$	25.0	68.3	88.9
	$a_c=1.2x10^{-4}$	25.0	68.3	281
180°C -0.5 hr	$a_c=1.2x10^{-6}$	16.5	63.1	26.8
	$a_c=1.2x10^{-5}$	16.5	63.1	84.8
	$a_c=1.2x10^{-4}$	16.5	63.1	268
180°C -1 hr	$a_c=1.2x10^{-6}$	18.1	64.2	27.7
	$a_c=1.2x10^{-5}$	18.6	64.3	87.7
	$a_c=1.2x10^{-4}$	18.6	64.3	277
180°C -2 hrs	$a_c=1.2x10^{-6}$	19.4	66.3	29.5
	$a_c=1.2x10^{-5}$	21.1	67.5	93.2
	$a_c=1.2x10^{-4}$	21.1	67.5	295
180°C -3 hrs	$a_c=1.2x10^{-6}$	20.1	67.6	31.1
	$a_c=1.2x10^{-5}$	22.9	70.2	98.4
	$a_c=1.2x10^{-4}$	22.9	70.2	311
180°C -10 hrs	$a_c=1.2x10^{-6}$	22.4	72.0	40.8
	$a_c=1.2x10^{-5}$	29.8	81.0	129
	$a_c=1.2x10^{-4}$	29.7	81.0	408

Table 5.4.2a: The effect of varying a_i on the prediction of the radius, the inter-precipitate spacing and width of PFZs given by combined model 1.

ageing treatment:	variable: a_i (cm^2s^{-1})	radius of precipitate: (nm)	inter-precipitate spacing: (nm)	width of PFZs: (nm)
160°C -0.5 hr	$a_i=1.43x10^{-6}$	7.28	51.8	0
	$a_i=1.43x10^{-5}$	10.7	51.8	0
	$a_i=1.43x10^{-4}$	15.7	52.4	0
160°C -5.5 hrs	$a_i=1.43x10^{-6}$	10.8	51.8	0
	$a_i=1.43x10^{-5}$	16.1	54.7	0
	$a_i=1.43x10^{-4}$	25.6	67.1	0
160°C -10.5 hrs	$a_i=1.43x10^{-6}$	12.0	52.3	0
	$a_i=1.43x10^{-5}$	18.2	57.8	0
	$a_i=1.43x10^{-4}$	30.1	74.5	0
160°C -20.5 hrs	$a_i=1.43x10^{-6}$	13.5	53.7	0
	$a_i=1.43x10^{-5}$	20.9	61.8	0
	$a_i=1.43x10^{-4}$	35.8	84.5	0
160°C -48 hrs	$a_i=1.43x10^{-6}$	15.7	56.6	0
	$a_i=1.43x10^{-5}$	25.0	68.2	0
	$a_i=1.43x10^{-4}$	45.4	102	0
180°C -0.5 hr	$a_i=1.43x10^{-6}$	11.2	62.8	0
	$a_i=1.43x10^{-5}$	16.5	63.1	0
	$a_i=1.43x10^{-4}$	24.8	69.5	0
180°C -1 hr	$a_i=1.43x10^{-6}$	12.6	62.8	0
	$a_i=1.43x10^{-5}$	18.6	64.3	0
	$a_i=1.43x10^{-4}$	28.8	76.5	0
180°C -2 hrs	$a_i=1.43x10^{-6}$	14.1	63.1	0
	$a_i=1.43x10^{-5}$	21.1	67.5	0
	$a_i=1.43x10^{-4}$	34.1	85.4	0
180°C -3 hrs	$a_i=1.43x10^{-6}$	15.1	63.5	0
	$a_i=1.43x10^{-5}$	22.9	70.1	0
	$a_i=1.43x10^{-4}$	37.9	92.0	0
180°C -10 hrs	$a_i=1.43x10^{-6}$	18.7	67.3	0
	$a_i=1.43x10^{-5}$	29.8	80.9	0
	$a_i=1.43x10^{-4}$	53.3	119	0

Table 5.4.2b: The effect of varying a_i on the prediction of the radius, the inter-precipitate spacing and width of PFZs given by combined model 2.

ageing treatment:	variable: a_i (cm^2s^{-1})	radius of precipitate: (nm)	inter-precipitate spacing: (nm)	width of PFZs: (nm)
160°C -0.5 hr	$a_i=1.43x10^{-6}$	8.25	66.9	1.2
	$a_i=1.43x10^{-5}$	12.1	66.9	1.2
	$a_i=1.43x10^{-4}$	17.0	67.3	1.2
160°C -5.5 hrs	$a_i=1.43x10^{-6}$	12.5	67.2	1.2
	$a_i=1.43x10^{-5}$	17.6	69.7	1.2
	$a_i=1.43x10^{-4}$	19.8	72.3	1.2
160°C -10.5 hrs	$a_i=1.43x10^{-6}$	14.1	68.1	1.2
	$a_i=1.43x10^{-5}$	18.7	71.8	1.2
	$a_i=1.43x10^{-4}$	20.6	74.1	1.2
160°C -20.5 hrs	$a_i=1.43x10^{-6}$	15.9	70.0	1.2
	$a_i=1.43x10^{-5}$	19.6	73.8	1.2
	$a_i=1.43x10^{-4}$	21.3	75.9	1.2
160°C -48 hrs	$a_i=1.43x10^{-6}$	17.8	73.0	1.2
	$a_i=1.43x10^{-5}$	20.0	76.0	1.2
	$a_i=1.43x10^{-4}$	21.6	77.8	1.2
180°C -0.5 hr	$a_i=1.43x10^{-6}$	12.9	83.9	1.2
	$a_i=1.43x10^{-5}$	18.7	84.2	1.2
	$a_i=1.43x10^{-4}$	21.8	85.2	1.2
180°C -1 hr	$a_i=1.43x10^{-6}$	14.9	84.0	1.2
	$a_i=1.43x10^{-5}$	20.4	85.0	1.2
	$a_i=1.43x10^{-4}$	22.8	86.6	1.2
180°C -2 hrs	$a_i=1.43x10^{-6}$	16.9	84.4	1.2
	$a_i=1.43x10^{-5}$	21.7	86.6	1.2
	$a_i=1.43x10^{-4}$	23.6	88.5	1.2
180°C -3 hrs	$a_i=1.43x10^{-6}$	18.2	85.0	1.2
	$a_i=1.43x10^{-5}$	22.3	87.8	1.2
	$a_i=1.43x10^{-4}$	24.1	87.8	1.2
180°C -10 hrs	$a_i=1.43x10^{-6}$	21.2	89.8	1.2
	$a_i=1.43x10^{-5}$	23.8	91.8	1.2
	$a_i=1.43x10^{-4}$	25.6	93.7	1.2

Table 5.4.2c: The effect of varying a_i on the prediction of the radius, the inter-precipitate spacing and width of PFZs given by combined model 3.

ageing treatment:	variable: a_i (cm^2s^{-1})	radius of precipitate: (nm)	inter-precipitate spacing: (nm)	width of PFZs: (nm)
160°C -0.5 hr	$a_i=1.43x10^{-6}$	7.28	51.8	54.4
	$a_i=1.43x10^{-5}$	10.7	51.8	54.4
	$a_i=1.43x10^{-4}$	15.7	52.4	54.4
160°C -5.5 hrs	$a_i=1.43x10^{-6}$	10.8	51.8	4.02
	$a_i=1.43x10^{-5}$	16.1	54.7	4.02
	$a_i=1.43x10^{-4}$	25.0	66.4	4.02
160°C -10.5 hrs	$a_i=1.43x10^{-6}$	12.0	52.3	4.02
	$a_i=1.43x10^{-5}$	18.2	57.8	4.02
	$a_i=1.43x10^{-4}$	27.3	70.7	4.02
160°C -20.5 hrs	$a_i=1.43x10^{-6}$	13.5	53.7	4.02
	$a_i=1.43x10^{-5}$	20.9	61.9	4.02
	$a_i=1.43x10^{-4}$	29.1	74.3	4.02
160°C -48 hrs	$a_i=1.43x10^{-6}$	15.7	56.6	4.02
	$a_i=1.43x10^{-5}$	24.8	68.1	4.02
	$a_i=1.43x10^{-4}$	30.6	77.9	4.02
180°C -0.5 hr	$a_i=1.43x10^{-6}$	11.2	62.8	78.0
	$a_i=1.43x10^{-5}$	16.5	63.1	78.0
	$a_i=1.43x10^{-4}$	24.8	69.5	78.0
180°C -1 hr	$a_i=1.43x10^{-6}$	12.6	62.8	64.0
	$a_i=1.43x10^{-5}$	18.6	64.3	64.0
	$a_i=1.43x10^{-4}$	27.9	75.5	64.0
180°C -2 hrs	$a_i=1.43x10^{-6}$	14.1	63.1	69.3
	$a_i=1.43x10^{-5}$	21.1	67.5	69.3
	$a_i=1.43x10^{-4}$	32.2	83.0	69.3
180°C -3 hrs	$a_i=1.43x10^{-6}$	15.1	63.5	4.02
	$a_i=1.43x10^{-5}$	22.9	70.2	4.02
	$a_i=1.43x10^{-4}$	30.3	80.5	4.02
180°C -10 hrs	$a_i=1.43x10^{-6}$	18.8	67.3	4.02
	$a_i=1.43x10^{-5}$	28.7	79.9	4.02
	$a_i=1.43x10^{-4}$	34.7	89.4	4.02

Table 5.4.2d: The effect of varying a_i on the prediction of the radius, the inter-precipitate spacing and width of PFZs given by combined model 4.

ageing treatment:	variable: a_i (cm^2s^{-1})	radius of precipitate: (nm)	inter-precipitate spacing: (nm)	width of PFZs: (nm)
160°C -0.5 hr	$a_i=1.43x10^{-6}$	19.5	54.9	0
	$a_i=1.43x10^{-5}$	19.5	54.9	0
	$a_i=1.43x10^{-4}$	19.6	55.1	0
160°C -5.5 hrs	$a_i=1.43x10^{-6}$	63.5	134	0
	$a_i=1.43x10^{-5}$	63.6	134	0
	$a_i=1.43x10^{-4}$	63.8	134	0
160°C -10.5 hrs	$a_i=1.43x10^{-6}$	97.4	199	0
	$a_i=1.43x10^{-5}$	97.5	199	0
	$a_i=1.43x10^{-4}$	97.7	200	0
160°C -20.5 hrs	$a_i=1.43x10^{-6}$	157	317	0
	$a_i=1.43x10^{-5}$	157	317	0
	$a_i=1.43x10^{-4}$	157	318	0
160°C -48 hrs	$a_i=1.43x10^{-6}$	291	584	0
	$a_i=1.43x10^{-5}$	291	584	0
	$a_i=1.43x10^{-4}$	292	585	0
180°C -0.5 hr	$a_i=1.43x10^{-6}$	40.4	92.7	0
	$a_i=1.43x10^{-5}$	40.4	92.8	0
	$a_i=1.43x10^{-4}$	40.6	93.0	0
180°C -1 hr	$a_i=1.43x10^{-6}$	58.6	126	0
	$a_i=1.43x10^{-5}$	58.7	126	0
	$a_i=1.43x10^{-4}$	58.9	127	0
180°C -2 hrs	$a_i=1.43x10^{-6}$	90.1	186	0
	$a_i=1.43x10^{-5}$	90.1	187	0
	$a_i=1.43x10^{-4}$	90.4	187	0
180°C -3 hrs	$a_i=1.43x10^{-6}$	118	242	0
	$a_i=1.43x10^{-5}$	118	242	0
	$a_i=1.43x10^{-4}$	119	243	0
180°C -10 hrs	$a_i=1.43x10^{-6}$	279	561	0
	$a_i=1.43x10^{-5}$	279	561	0
	$a_i=1.43x10^{-4}$	280	562	0

Table 5.4.2e: The effect of varying a_i on the prediction of the radius, the inter-precipitate spacing and width of PFZs given by combined model 5.

ageing treatment:	variable: a_i (cm^2s^{-1})	radius of precipitate: (nm)	inter-precipitate spacing: (nm)	width of PFZs: (nm)
160°C -0.5 hr	$a_i=1.43x10^{-6}$	7.28	51.8	55.1
	$a_i=1.43x10^{-5}$	10.7	51.8	55.1
	$a_i=1.43x10^{-4}$	15.7	52.4	55.1
160°C -5.5 hrs	$a_i=1.43x10^{-6}$	10.8	51.8	59.6
	$a_i=1.43x10^{-5}$	16.1	54.7	59.6
	$a_i=1.43x10^{-4}$	25.2	66.7	59.6
160°C -10.5 hrs	$a_i=1.43x10^{-6}$	12.0	52.3	63.7
	$a_i=1.43x10^{-5}$	18.2	57.8	63.7
	$a_i=1.43x10^{-4}$	27.9	71.6	63.7
160°C -20.5 hrs	$a_i=1.43x10^{-6}$	13.5	53.7	71.3
	$a_i=1.43x10^{-5}$	20.9	61.9	71.3
	$a_i=1.43x10^{-4}$	30.6	76.3	71.3
160°C -48 hrs	$a_i=1.43x10^{-6}$	15.7	56.6	88.9
	$a_i=1.43x10^{-5}$	25.0	68.3	88.9
	$a_i=1.43x10^{-4}$	34.0	82.6	88.9
180°C -0.5 hr	$a_i=1.43x10^{-6}$	11.2	62.8	84.8
	$a_i=1.43x10^{-5}$	16.5	63.1	84.8
	$a_i=1.43x10^{-4}$	24.8	69.5	84.8
180°C -1 hr	$a_i=1.43x10^{-6}$	12.6	62.8	87.7
	$a_i=1.43x10^{-5}$	18.6	64.3	87.7
	$a_i=1.43x10^{-4}$	28.1	75.8	87.7
180°C -2 hrs	$a_i=1.43x10^{-6}$	14.1	63.1	93.2
	$a_i=1.43x10^{-5}$	21.1	67.5	93.2
	$a_i=1.43x10^{-4}$	31.0	81.2	93.2
180°C -3 hrs	$a_i=1.43x10^{-6}$	15.1	63.5	98.4
	$a_i=1.43x10^{-5}$	22.9	70.2	98.4
	$a_i=1.43x10^{-4}$	32.6	84.2	98.4
180°C -10 hrs	$a_i=1.43x10^{-6}$	18.8	67.3	129
	$a_i=1.43x10^{-5}$	29.8	81.0	129
	$a_i=1.43x10^{-4}$	37.6	93.5	129

Table 5.4.3a: The effect of varying C_c on the prediction of the radius, the inter-precipitate spacing and width of PFZs given by combined model 1.

ageing treatment:	variable: C_c (mole frac.)	radius of precipitate: (nm)	inter-precipitate spacing: (nm)	width of PFZs: (nm)
160°C -0.5 hr	C_c=0.0373	5.43	18.8	0
	C_c=0.028	10.7	51.8	0
	C_c=0.0187	44.9	443	0
160°C -5.5 hrs	C_c=0.0373	8.07	18.8	0
	C_c=0.028	16.1	54.7	0
	C_c=0.0187	67.0	451	0
160°C -10.5 hrs	C_c=0.0373	8.96	18.8	0
	C_c=0.028	18.2	57.8	0
	C_c=0.0187	74.9	459	0
160°C -20.5 hrs	C_c=0.0373	10.1	20.6	0
	C_c=0.028	20.9	61.8	0
	C_c=0.0187	84.1	470	0
160°C -48 hrs	C_c=0.0373	12.3	25.1	0
	C_c=0.028	25.0	68.2	0
	C_c=0.0187	97.6	487	0
180°C -0.5 hr	C_c=0.0373	7.76	20.3	0
	C_c=0.028	16.5	63.1	0
	C_c=0.0187	86.9	754	0
180°C -1 hr	C_c=0.0373	8.69	20.3	0
	C_c=0.028	18.6	64.3	0
	C_c=0.0187	97.5	755	0
180°C -2 hrs	C_c=0.0373	9.75	20.3	0
	C_c=0.028	21.1	67.5	0
	C_c=0.0187	109	758	0
180°C -3 hrs	C_c=0.0373	10.5	21.5	0
	C_c=0.028	22.9	70.1	0
	C_c=0.0187	117	762	0
180°C -10 hrs	C_c=0.0373	14.5	28.7	0
	C_c=0.028	29.8	80.9	0
	C_c=0.0187	144	787	0

Table 5.4.3b: The effect of varying C_c on the prediction of the radius, the inter-precipitate spacing and width of PFZs given by combined model 2.

ageing treatment:	variable: C_c (mole frac.)	radius of precipitate: (nm)	inter-precipitate spacing: (nm)	width of PFZs: (nm)
160°C -0.5 hr	C_c=0.0373	5.88	22.7	1.2
	C_c=0.028	12.1	66.9	1.2
	C_c=0.0187	56.9	678	1.2
160°C -5.5 hrs	C_c=0.0373	8.46	22.7	1.2
	C_c=0.028	17.6	69.7	1.2
	C_c=0.0187	82.2	687	1.2
160°C -10.5 hrs	C_c=0.0373	8.90	22.7	1.2
	C_c=0.028	18.7	71.8	1.2
	C_c=0.0187	86.7	695	1.2
160°C -20.5 hrs	C_c=0.0373	9.21	22.7	1.2
	C_c=0.028	19.6	73.8	1.2
	C_c=0.0187	90.0	704	1.2
160°C -48 hrs	C_c=0.0373	9.26	22.7	1.2
	C_c=0.028	20.0	76.0	1.2
	C_c=0.0187	90.9	718	1.2
180°C -0.5 hr	C_c=0.0373	8.32	25.0	1.2
	C_c=0.028	18.7	84.2	1.2
	C_c=0.0187	114	1250	1.2
180°C -1 hr	C_c=0.0373	9.07	25.0	1.2
	C_c=0.028	20.4	85.0	1.2
	C_c=0.0187	124	1250	1.2
180°C -2 hrs	C_c=0.0373	9.59	25.0	1.2
	C_c=0.028	21.7	86.6	1.2
	C_c=0.0187	131	1250	1.2
180°C -3 hrs	C_c=0.0373	9.81	25.0	1.2
	C_c=0.028	22.3	87.8	1.2
	C_c=0.0187	134	1260	1.2
180°C -10 hrs	C_c=0.0373	10.3	25.2	1.2
	C_c=0.028	23.8	91.8	1.2
	C_c=0.0187	141	1280	1.2

Table 5.4.3c: The effect of varying C_c on the prediction of the radius, the inter-precipitate spacing and width of PFZs given by combined model 3.

ageing treatment:	variable: C_c (mole frac.)	radius of precipitate: (nm)	inter-precipitate spacing: (nm)	width of PFZs: (nm)
160°C -0.5 hr	C_c=0.0373	5.43	18.8	27.8
	C_c=0.028	10.7	51.8	54.4
	C_c=0.0187	44.9	443	118
160°C -5.5 hrs	C_c=0.0373	8.07	18.8	4.02
	C_c=0.028	16.1	54.7	4.02
	C_c=0.0187	67.0	451	109
160°C -10.5 hrs	C_c=0.0373	8.97	18.8	4.02
	C_c=0.028	18.2	57.8	4.02
	C_c=0.0187	75.0	459	83.8
160°C -20.5 hrs	C_c=0.0373	10.1	20.7	4.02
	C_c=0.028	20.9	61.9	4.02
	C_c=0.0187	84.2	470	4.02
160°C -48 hrs	C_c=0.0373	12.1	24.6	4.02
	C_c=0.028	24.8	68.1	4.02
	C_c=0.0187	96.2	487	4.02
180°C -0.5 hr	C_c=0.0373	7.76	20.3	19.0
	C_c=0.028	16.5	63.1	78.0
	C_c=0.0187	86.9	753	179
180°C -1 hr	C_c=0.0373	8.70	20.3	4.02
	C_c=0.028	18.6	64.3	64.0
	C_c=0.0187	97.5	755	179
180°C -2 hrs	C_c=0.0373	9.76	20.3	4.02
	C_c=0.028	21.1	67.5	4.02
	C_c=0.0187	110	758	174
180°C -3 hrs	C_c=0.0373	10.5	21.5	4.02
	C_c=0.028	22.9	70.2	4.02
	C_c=0.0187	117	762	166
180°C -10 hrs	C_c=0.0373	13.5	27.5	4.02
	C_c=0.028	28.7	79.9	4.02
	C_c=0.0187	140	786	4.02

Table 5.4.3d: The effect of varying C_c on the prediction of the radius, the inter-precipitate spacing and width of PFZs given by combined model 4.

ageing treatment:	variable: C_c (mole frac.)	radius of precipitate: (nm)	inter-precipitate spacing: (nm)	width of PFZs: (nm)
160°C -0.5 hr	C_c=0.0373	9.88	20.1	0
	C_c=0.028	19.5	54.9	0
	C_c=0.0187	81.5	444	0
160°C -5.5 hrs	C_c=0.0373	44.2	88.5	0
	C_c=0.028	63.6	134	0
	C_c=0.0187	192	555	0
160°C -10.5 hrs	C_c=0.0373	75.8	152	0
	C_c=0.028	97.5	199	0
	C_c=0.0187	251	646	0
160°C -20.5 hrs	C_c=0.0373	133	266	0
	C_c=0.028	157	317	0
	C_c=0.0187	339	793	0
160°C -48 hrs	C_c=0.0373	265	531	0
	C_c=0.028	291	584	0
	C_c=0.0187	506	1100	0
180°C -0.5 hr	C_c=0.0373	22.4	45.0	0
	C_c=0.028	40.4	92.8	0
	C_c=0.0187	190	764	0
180°C -1 hr	C_c=0.0373	37.3	74.8	0
	C_c=0.028	58.7	126	0
	C_c=0.0187	241	810	0
180°C -2 hrs	C_c=0.0373	65.6	131	0
	C_c=0.028	90.1	187	0
	C_c=0.0187	311	906	0
180°C -3 hrs	C_c=0.0373	92.3	186	0
	C_c=0.028	118	242	0
	C_c=0.0187	366	988	0
180°C -10 hrs	C_c=0.0373	262	547	0
	C_c=0.028	279	561	0
	C_c=0.0187	609	1400	0

Table 5.4.3e: The effect of varying C_c on the prediction of the radius, the inter-precipitate spacing and width of PFZs given by combined model 5.

ageing treatment:	variable: C_c (mole frac.)	radius of precipitate: (nm)	inter-precipitate spacing: (nm)	width of PFZs: (nm)
160°C -0.5 hr	C_c=0.0373	5.43	18.8	32.7
	C_c=0.028	10.7	51.8	55.1
	C_c=0.0187	44.9	443	119
160°C -5.5 hrs	C_c=0.0373	8.07	18.8	35.4
	C_c=0.028	16.1	54.7	59.6
	C_c=0.0187	67.0	451	128
160°C -10.5 hrs	C_c=0.0373	8.96	18.8	37.9
	C_c=0.028	18.2	57.8	63.7
	C_c=0.0187	74.9	459	137
160°C -20.5 hrs	C_c=0.0373	10.1	20.6	42.4
	C_c=0.028	20.9	61.8	71.3
	C_c=0.0187	84.1	470	154
160°C -48 hrs	C_c=0.0373	12.4	25.1	52.8
	C_c=0.028	25.0	68.3	88.9
	C_c=0.0187	97.8	487	192
180°C -0.5 hr	C_c=0.0373	7.76	20.3	49.5
	C_c=0.028	16.5	63.1	84.8
	C_c=0.0187	86.9	754	185
180°C -1 hr	C_c=0.0373	8.69	20.3	51.2
	C_c=0.028	18.6	64.3	87.7
	C_c=0.0187	97.5	755	192
180°C -2 hrs	C_c=0.0373	9.75	20.3	54.4
	C_c=0.028	21.1	67.5	93.2
	C_c=0.0187	109	758	204
180°C -3 hrs	C_c=0.0373	10.5	21.5	57.5
	C_c=0.028	22.9	70.1	98.4
	C_c=0.0187	117	762	215
180°C -10 hrs	C_c=0.0373	14.2	28.7	75.4
	C_c=0.028	29.8	81.0	129
	C_c=0.0187	145	787	282

Table 5.4.4a: The effect of varying C_g on the prediction of the radius, the inter-precipitate spacing and width of PFZs given by combined model 1.

ageing treatment:	variable: C_g (mole frac.)	radius of precipitate: (nm)	inter-precipitate spacing: (nm)	width of PFZs: (nm)
160°C -0.5 hr	C_g=0.0371	7.99	28.6	0
	C_g=0.0272	10.7	51.8	0
	C_g=0.0181	17.3	132	0
160°C -5.5 hrs	C_g=0.0371	12.3	32.6	0
	C_g=0.0272	16.1	54.7	0
	C_g=0.0181	26.1	135	0
160°C -10.5 hrs	C_g=0.0371	14.2	35.8	0
	C_g=0.0272	18.2	57.8	0
	C_g=0.0181	29.2	138	0
160°C -20.5 hrs	C_g=0.0371	16.8	40.1	0
	C_g=0.0272	20.9	61.8	0
	C_g=0.0181	32.8	143	0
160°C -48 hrs	C_g=0.0371	21.0	47.7	0
	C_g=0.0272	25.0	68.2	0
	C_g=0.0181	38.3	150	0
180°C -0.5 hr	C_g=0.0371	11.8	33.1	0
	C_g=0.0272	16.5	63.1	0
	C_g=0.0181	29.4	184	0
180°C -1 hr	C_g=0.0371	13.5	35.6	0
	C_g=0.0272	18.6	64.3	0
	C_g=0.0181	33.0	184	0
180°C -2 hrs	C_g=0.0371	15.7	39.3	0
	C_g=0.0272	21.1	67.5	0
	C_g=0.0181	37.1	186	0
180°C -3 hrs	C_g=0.0371	17.3	42.1	0
	C_g=0.0272	22.9	70.1	0
	C_g=0.0181	39.8	188	0
180°C -10 hrs	C_g=0.0371	24.1	54.1	0
	C_g=0.0272	29.8	80.9	0
	C_g=0.0181	49.4	200	0

Table 5.4.4b: The effect of varying C_g on the prediction of the radius, the inter-precipitate spacing and width of PFZs given by combined model 2.

ageing treatment:	variable: C_g (mole frac.)	radius of precipitate: (nm)	inter-precipitate spacing: (nm)	width of PFZs: (nm)
160°C -0.5 hr	C_g=0.0371	8.81	35.5	1.2
	C_g=0.0272	12.1	66.9	1.2
	C_g=0.0181	20.7	184	1.2
160°C -5.5 hrs	C_g=0.0371	13.0	38.9	1.2
	C_g=0.0272	17.6	69.7	1.2
	C_g=0.0181	29.9	187	1.2
160°C -10.5 hrs	C_g=0.0371	13.9	40.8	1.2
	C_g=0.0272	18.7	71.8	1.2
	C_g=0.0181	31.6	189	1.2
160°C -20.5 hrs	C_g=0.0371	14.7	42.4	1.2
	C_g=0.0272	19.6	73.8	1.2
	C_g=0.0181	32.9	193	1.2
160°C -48 hrs	C_g=0.0371	15.3	44.0	1.2
	C_g=0.0272	20.0	76.0	1.2
	C_g=0.0181	33.3	197	1.2
180°C -0.5 hr	C_g=0.0371	12.9	41.5	1.2
	C_g=0.0272	18.7	84.2	1.2
	C_g=0.0181	35.3	268	1.2
180°C -1 hr	C_g=0.0371	14.2	43.1	1.2
	C_g=0.0272	20.4	85.0	1.2
	C_g=0.0181	38.6	268	1.2
180°C -2 hrs	C_g=0.0371	15.2	45.2	1.2
	C_g=0.0272	21.7	86.6	1.2
	C_g=0.0181	40.8	270	1.2
180°C -3 hrs	C_g=0.0371	15.8	46.3	1.2
	C_g=0.0272	22.3	87.8	1.2
	C_g=0.0181	41.8	271	1.2
180°C -10 hrs	C_g=0.0371	17.1	49.3	1.2
	C_g=0.0272	23.8	91.8	1.2
	C_g=0.0181	44.0	277	1.2

Table 5.4.4c: The effect of varying C_g on the prediction of the radius, the inter-precipitate spacing and width of PFZs given by combined model 3.

ageing treatment:	variable: C_g (mole frac.)	radius of precipitate: (nm)	inter-precipitate spacing: (nm)	width of PFZs: (nm)
160°C -0.5 hr	C_g=0.0371	7.99	28.6	39.2
	C_g=0.0272	10.7	51.8	54.4
	C_g=0.0181	17.4	132	80.0
160°C -5.5 hrs	C_g=0.0371	12.3	32.6	4.02
	C_g=0.0272	16.1	54.7	4.02
	C_g=0.0181	26.1	135	47.6
160°C -10.5 hrs	C_g=0.0371	14.2	35.8	4.02
	C_g=0.0272	18.2	57.8	4.02
	C_g=0.0181	29.2	138	4.02
160°C -20.5 hrs	C_g=0.0371	16.8	40.2	4.02
	C_g=0.0272	20.9	61.9	4.02
	C_g=0.0181	32.9	143	4.02
160°C -48 hrs	C_g=0.0371	20.5	46.9	4.02
	C_g=0.0272	24.8	68.1	4.02
	C_g=0.0181	37.9	150	4.02
180°C -0.5 hr	C_g=0.0371	11.8	33.1	49.4
	C_g=0.0272	16.5	63.1	78.0
	C_g=0.0181	29.4	184	121
180°C -1 hr	C_g=0.0371	13.5	35.6	4.02
	C_g=0.0272	18.6	64.3	64.0
	C_g=0.0181	33.0	184	116
180°C -2 hrs	C_g=0.0371	15.7	39.4	4.02
	C_g=0.0272	21.1	67.5	4.02
	C_g=0.0181	37.1	186	99.6
180°C -3 hrs	C_g=0.0371	17.4	42.2	4.02
	C_g=0.0272	22.9	70.2	4.02
	C_g=0.0181	39.8	188	70.4
180°C -10 hrs	C_g=0.0371	23.1	52.5	4.02
	C_g=0.0272	28.7	79.9	4.02
	C_g=0.0181	47.9	199	4.02

Table 5.4.4d: The effect of varying C_g on the prediction of the radius, the inter-precipitate spacing and width of PFZs given by combined model 4.

ageing treatment:	variable: C_g (mole frac.)	radius of precipitate: (nm)	inter-precipitate spacing: (nm)	width of PFZs: (nm)
160°C -0.5 hr	C_g=0.0371	15.2	35.4	0
	C_g=0.0272	19.5	54.9	0
	C_g=0.0181	31.7	133	0
160°C -5.5 hrs	C_g=0.0371	66.1	134	0
	C_g=0.0272	63.6	134	0
	C_g=0.0181	79.8	197	0
160°C -10.5 hrs	C_g=0.0371	110	221	0
	C_g=0.0272	97.5	199	0
	C_g=0.0181	109	247	0
160°C -20.5 hrs	C_g=0.0371	190	380	0
	C_g=0.0272	157	317	0
	C_g=0.0181	155	333	0
160°C -48 hrs	C_g=0.0371	372	748	0
	C_g=0.0272	291	584	0
	C_g=0.0181	252	518	0
180°C -0.5 hr	C_g=0.0371	35.1	73.2	0
	C_g=0.0272	40.4	92.8	0
	C_g=0.0181	64.8	197	0
180°C -1 hr	C_g=0.0371	56.7	115	0
	C_g=0.0272	58.7	126	0
	C_g=0.0181	84.8	226	0
180°C -2 hrs	C_g=0.0371	96.5	194	0
	C_g=0.0272	90.1	187	0
	C_g=0.0181	115	277	0
180°C -3 hrs	C_g=0.0371	134	268	0
	C_g=0.0272	118	242	0
	C_g=0.0181	140	320	0
180°C -10 hrs	C_g=0.0371	351	702	0
	C_g=0.0272	279	561	0
	C_g=0.0181	263	550	0

Table 5.4.4e: The effect of varying C_g on the prediction of the radius, the inter-precipitate spacing and width of PFZs given by combined model 5.

ageing treatment:	variable: C_g (mole frac.)	radius of precipitate: (nm)	inter-precipitate spacing: (nm)	width of PFZs: (nm)
160°C -0.5 hr	C_g=0.0371	7.99	28.6	41.3
	C_g=0.0272	10.7	51.8	55.1
	C_g=0.0181	17.4	132	80.6
160°C -5.5 hrs	C_g=0.0371	12.3	32.6	44.6
	C_g=0.0272	16.1	54.7	59.6
	C_g=0.0181	26.1	135	87.1
160°C -10.5 hrs	C_g=0.0371	14.2	35.8	47.8
	C_g=0.0272	18.2	57.8	63.7
	C_g=0.0181	29.2	138	93.2
160°C -20.5 hrs	C_g=0.0371	16.8	40.2	53.4
	C_g=0.0272	20.9	61.9	71.3
	C_g=0.0181	32.9	143	104
160°C -48 hrs	C_g=0.0371	21.0	47.8	66.6
	C_g=0.0272	25.0	68.3	88.9
	C_g=0.0181	38.4	150	130
180°C -0.5 hr	C_g=0.0371	11.8	33.1	63.0
	C_g=0.0272	16.5	63.1	84.8
	C_g=0.0181	29.4	184	125
180°C -1 hr	C_g=0.0371	13.5	35.6	65.2
	C_g=0.0272	18.6	64.3	87.7
	C_g=0.0181	33.0	184	129
180°C -2 hrs	C_g=0.0371	15.7	39.4	69.3
	C_g=0.0272	21.1	67.5	93.2
	C_g=0.0181	37.1	186	137
180°C -3 hrs	C_g=0.0371	17.4	42.2	73.1
	C_g=0.0272	22.9	70.2	98.4
	C_g=0.0181	39.8	188	145
180°C -10 hrs	C_g=0.0371	24.1	54.2	96.0
	C_g=0.0272	29.8	81.0	129
	C_g=0.0181	49.5	200	190

Table 5.4.5a: The effect of varying E_b on the prediction of the radius, the inter-precipitate spacing and width of PFZs given by combined model 1.

ageing treatment:	variable: E_b (eV per atom)	radius of precipitate: (nm)	inter-precipitate spacing: (nm)	width of PFZs: (nm)
160°C -0.5 hr	E_b=0.373	13.3	79.9	0
	E_b=0.28	10.7	51.8	0
	E_b=0.25	10.2	47.4	0
160°C -5.5 hrs	E_b=0.373	20.0	82.6	0
	E_b=0.28	16.1	54.7	0
	E_b=0.25	15.4	50.5	0
160°C -10.5 hrs	E_b=0.373	22.5	85.7	0
	E_b=0.28	18.2	57.8	0
	E_b=0.25	17.5	53.5	0
160°C -20.5 hrs	E_b=0.373	25.5	89.9	0
	E_b=0.28	20.9	61.8	0
	E_b=0.25	20.2	57.6	0
160°C -48 hrs	E_b=0.373	30.0	96.4	0
	E_b=0.28	25.0	68.2	0
	E_b=0.25	24.2	64.0	0
180°C -0.5 hr	E_b=0.373	21.4	103	0
	E_b=0.28	16.5	63.1	0
	E_b=0.25	15.7	57.2	0
180°C -1 hr	E_b=0.373	24.0	104	0
	E_b=0.28	18.6	64.3	0
	E_b=0.25	17.6	58.6	0
180°C -2 hrs	E_b=0.373	27.1	106	0
	E_b=0.28	21.1	67.5	0
	E_b=0.25	20.1	61.9	0
180°C -3 hrs	E_b=0.373	29.2	109	0
	E_b=0.28	22.9	70.1	0
	E_b=0.25	21.8	64.5	0
180°C -10 hrs	E_b=0.373	37.0	120	0
	E_b=0.28	29.8	80.9	0
	E_b=0.25	28.6	75.3	0

Table 5.4.5b: The effect of varying E_b on the prediction of the radius, the inter-precipitate spacing and width of PFZs given by combined model 2.

ageing treatment:	variable: E_b (eV per atom)	radius of precipitate: (nm)	inter-precipitate spacing: (nm)	width of PFZs: (nm)
160°C -0.5 hr	E_b=0.373	13.3	79.9	1.2
	E_b=0.28	12.1	66.9	1.2
	E_b=0.25	11.9	64.5	1.2
160°C -5.5 hrs	E_b=0.373	19.0	82.3	1.2
	E_b=0.28	17.6	69.7	1.2
	E_b=0.25	17.0	67.3	1.2
160°C -10.5 hrs	E_b=0.373	19.9	84.2	1.2
	E_b=0.28	18.7	71.8	1.2
	E_b=0.25	18.2	69.3	1.2
160°C -20.5 hrs	E_b=0.373	20.7	86.2	1.2
	E_b=0.28	19.6	73.8	1.2
	E_b=0.25	19.2	71.4	1.2
160°C -48 hrs	E_b=0.373	21.0	88.4	1.2
	E_b=0.28	20.0	76.0	1.2
	E_b=0.25	19.7	73.6	1.2
180°C -0.5 hr	E_b=0.373	21.2	103	1.2
	E_b=0.28	18.7	84.2	1.2
	E_b=0.25	18.5	80.8	1.2
180°C -1 hr	E_b=0.373	22.6	104	1.2
	E_b=0.28	20.4	85.0	1.2
	E_b=0.25	19.7	81.6	1.2
180°C -2 hrs	E_b=0.373	23.7	105	1.2
	E_b=0.28	21.7	86.6	1.2
	E_b=0.25	21.1	83.2	1.2
180°C -3 hrs	E_b=0.373	24.2	106	1.2
	E_b=0.28	22.3	87.8	1.2
	E_b=0.25	21.7	84.5	1.2
180°C -10 hrs	E_b=0.373	25.5	110	1.2
	E_b=0.28	23.8	91.8	1.2
	E_b=0.25	23.3	88.5	1.2

Table 5.4.5c: The effect of varying E_b on the prediction of the radius, the inter-precipitate spacing and width of PFZs given by combined model 3.

ageing treatment:	variable: E_b (eV per atom)	radius of precipitate: (nm)	inter-precipitate spacing: (nm)	width of PFZs: (nm)
160°C -0.5 hr	E_b=0.373	13.3	79.9	55.3
	E_b=0.28	10.7	51.8	54.4
	E_b=0.25	10.2	47.4	54.3
160°C -5.5 hrs	E_b=0.373	20.0	82.6	4.86
	E_b=0.28	16.1	54.7	4.02
	E_b=0.25	15.4	50.5	38.6
160°C -10.5 hrs	E_b=0.373	22.5	85.7	4.86
	E_b=0.28	18.2	57.8	4.02
	E_b=0.25	17.5	53.6	3.86
160°C -20.5 hrs	E_b=0.373	25.5	89.9	4.86
	E_b=0.28	20.9	61.9	4.02
	E_b=0.25	20.2	57.6	3.86
160°C -48 hrs	E_b=0.373	30.1	96.4	4.86
	E_b=0.28	24.8	68.1	4.02
	E_b=0.25	23.8	63.6	3.86
180°C -0.5 hr	E_b=0.373	21.4	103	78.9
	E_b=0.28	16.5	63.1	78.0
	E_b=0.25	15.7	57.2	77.9
180°C -1 hr	E_b=0.373	24.1	104	64.9
	E_b=0.28	18.6	64.3	64.0
	E_b=0.25	17.7	58.6	63.9
180°C -2 hrs	E_b=0.373	27.1	106	4.86
	E_b=0.28	21.1	67.5	4.02
	E_b=0.25	20.1	61.9	3.86
180°C -3 hrs	E_b=0.373	29.2	109	4.86
	E_b=0.28	22.9	70.2	4.02
	E_b=0.25	21.9	64.6	3.86
180°C -10 hrs	E_b=0.373	36.8	120	4.86
	E_b=0.28	28.7	79.9	4.02
	E_b=0.25	27.4	73.9	3.86

Table 5.4.5c: The effect of varying E_b on the prediction of the radius, the inter-precipitate spacing and width of PFZs given by combined model 3.

ageing treatment:	variable: E_b (eV per atom)	radius of precipitate: (nm)	inter-precipitate spacing: (nm)	width of PFZs: (nm)
160°C -0.5 hr	E_b=0.373	13.3	79.9	55.3
	E_b=0.28	10.7	51.8	54.4
	E_b=0.25	10.2	47.4	54.3
160°C -5.5 hrs	E_b=0.373	20.0	82.6	4.86
	E_b=0.28	16.1	54.7	4.02
	E_b=0.25	15.4	50.5	38.6
160°C -10.5 hrs	E_b=0.373	22.5	85.7	4.86
	E_b=0.28	18.2	57.8	4.02
	E_b=0.25	17.5	53.6	3.86
160°C -20.5 hrs	E_b=0.373	25.5	89.9	4.86
	E_b=0.28	20.9	61.9	4.02
	E_b=0.25	20.2	57.6	3.86
160°C -48 hrs	E_b=0.373	30.1	96.4	4.86
	E_b=0.28	24.8	68.1	4.02
	E_b=0.25	23.8	63.6	3.86
180°C -0.5 hr	E_b=0.373	21.4	103	78.9
	E_b=0.28	16.5	63.1	78.0
	E_b=0.25	15.7	57.2	77.9
180°C -1 hr	E_b=0.373	24.1	104	64.9
	E_b=0.28	18.6	64.3	64.0
	E_b=0.25	17.7	58.6	63.9
180°C -2 hrs	E_b=0.373	27.1	106	4.86
	E_b=0.28	21.1	67.5	4.02
	E_b=0.25	20.1	61.9	3.86
180°C -3 hrs	E_b=0.373	29.2	109	4.86
	E_b=0.28	22.9	70.2	4.02
	E_b=0.25	21.9	64.6	3.86
180°C -10 hrs	E_b=0.373	36.8	120	4.86
	E_b=0.28	28.7	79.9	4.02
	E_b=0.25	27.4	73.9	3.86

Table 5.4.5e: The effect of varying E_b on the prediction of the radius, the inter-precipitate spacing and width of PFZs given by combined model 5.

ageing treatment:	variable: E_b (eV per atom)	radius of precipitate: (nm)	inter-precipitate spacing: (nm)	width of PFZs: (nm)
160°C -0.5 hr	E_b=0.373	13.3	79.9	56.0
	E_b=0.28	10.7	51.8	55.1
	E_b=0.25	10.2	47.4	55.0
160°C -5.5 hrs	E_b=0.373	20.0	82.6	60.5
	E_b=0.28	16.1	54.7	59.6
	E_b=0.25	15.4	50.5	59.4
160°C -10.5 hrs	E_b=0.373	22.5	85.7	64.7
	E_b=0.28	18.2	57.8	63.7
	E_b=0.25	17.5	53.6	63.5
160°C -20.5 hrs	E_b=0.373	25.5	89.9	72.4
	E_b=0.28	20.9	61.9	71.3
	E_b=0.25	20.2	57.6	71.1
160°C -48 hrs	E_b=0.373	30.1	96.4	90.2
	E_b=0.28	25.0	68.3	88.9
	E_b=0.25	24.2	64.1	88.6
180°C -0.5 hr	E_b=0.373	21.4	103	85.7
	E_b=0.28	16.5	63.1	84.8
	E_b=0.25	15.7	57.2	84.7
180°C -1 hr	E_b=0.373	24.1	104	88.6
	E_b=0.28	18.6	64.3	87.7
	E_b=0.25	17.7	58.6	87.6
180°C -2 hrs	E_b=0.373	27.1	106	94.2
	E_b=0.28	21.1	67.5	93.2
	E_b=0.25	20.1	61.9	93.1
180°C -3 hrs	E_b=0.373	29.2	109	99.5
	E_b=0.28	22.9	70.2	98.4
	E_b=0.25	21.9	64.6	98.3
180°C -10 hrs	E_b=0.373	37.1	120	130
	E_b=0.28	29.8	81.0	129
	E_b=0.25	28.7	75.4	129

Table 5.4.6a: The effect of varying r on the prediction of the radius, the inter-precipitate spacing and width of PFZs given by combined model 1.

ageing treatment:	variable: r (°A)	radius of precipitate: (nm)	inter-precipitate spacing: (nm)	width of PFZs: (nm)
160°C -0.5 hr	r=100	13.6	74.1	0
	r=10000	10.7	51.8	0
	r=5000	10.7	52.1	0
160°C -5.5 hrs	r=100	20.4	78.2	0
	r=10000	16.1	54.7	0
	r=5000	16.1	55.1	0
160°C -10.5 hrs	r=100	23.1	81.8	0
	r=10000	18.2	57.8	0
	r=5000	18.3	58.2	0
160°C -20.5 hrs	r=100	26.4	86.5	0
	r=10000	20.9	61.8	0
	r=5000	21.0	62.2	0
160°C -48 hrs	r=100	31.3	93.8	0
	r=10000	25.0	68.2	0
	r=5000	25.1	68.6	0
180°C -0.5 hr	r=100	21.4	93.0	0
	r=10000	16.5	63.1	0
	r=5000	16.6	63.6	0
180°C -1 hr	r=100	24.0	94.3	0
	r=10000	18.6	64.3	0
	r=5000	18.7	64.8	0
180°C -2 hrs	r=100	27.2	97.8	0
	r=10000	21.1	67.5	0
	r=5000	21.2	68.0	0
180°C -3 hrs	r=100	29.4	101	0
	r=10000	22.9	70.1	0
	r=5000	23.0	70.6	0
180°C -10 hrs	r=100	37.8	113	0
	r=10000	29.8	80.9	0
	r=5000	29.9	81.4	0

Table 5.4.6b: The effect of varying r on the prediction of the radius, the inter-precipitate spacing and width of PFZs given by combined model 2.

ageing treatment:	variable: r (°A)	radius of precipitate: (nm)	inter-precipitate spacing: (nm)	width of PFZs: (nm)
160°C -0.5 hr	r=100	15.7	98.3	1.2
	r=10000	12.1	66.9	1.2
	r=5000	12.2	67.4	1.2
160°C -5.5 hrs	r=100	22.7	102	1.2
	r=10000	17.6	69.7	1.2
	r=5000	17.7	70.2	1.2
160°C -10.5 hrs	r=100	24.1	105	1.2
	r=10000	18.7	71.8	1.2
	r=5000	18.8	72.3	1.2
160°C -20.5 hrs	r=100	25.3	107	1.2
	r=10000	19.6	73.8	1.2
	r=5000	19.7	74.4	1.2
160°C -48 hrs	r=100	25.7	110	1.2
	r=10000	20.0	76.0	1.2
	r=5000	20.1	76.5	1.2
180°C -0.5 hr	r=100	24.7	128	1.2
	r=10000	18.7	84.2	1.2
	r=5000	18.8	84.8	1.2
180°C -1 hr	r=100	27.0	129	1.2
	r=10000	20.4	85.0	1.2
	r=5000	20.5	85.6	1.2
180°C -2 hrs	r=100	28.6	131	1.2
	r=10000	21.7	86.6	1.2
	r=5000	21.8	87.2	1.2
180°C -3 hrs	r=100	29.4	132	1.2
	r=10000	22.3	87.8	1.2
	r=5000	22.4	88.4	1.2
180°C -10 hrs	r=100	31.2	137	1.2
	r=10000	23.8	91.8	1.2
	r=5000	23.9	92.5	1.2

Table 5.4.6c: The effect of varying r on the prediction of the radius, the inter-precipitate spacing and width of PFZs given by combined model 3.

ageing treatment:	variable: r (°A)	radius of precipitate: (nm)	inter-precipitate spacing: (nm)	width of PFZs: (nm)
160°C -0.5 hr	r=100	13.6	74.1	63.8
	r=10000	10.7	51.8	54.4
	r=5000	10.7	52.1	54.4
160°C -5.5 hrs	r=100	20.5	78.2	4.02
	r=10000	16.1	54.7	4.02
	r=5000	16.2	55.1	4.02
160°C -10.5 hrs	r=100	23.1	81.9	4.02
	r=10000	18.2	57.8	4.02
	r=5000	18.3	58.2	4.02
160°C -20.5 hrs	r=100	26.4	86.6	4.02
	r=10000	20.9	61.9	4.02
	r=5000	21.0	62.3	4.02
160°C -48 hrs	r=100	31.0	93.7	4.02
	r=10000	24.8	68.1	4.02
	r=5000	24.9	68.5	4.02
180°C -0.5 hr	r=100	21.4	93.0	93.4
	r=10000	16.5	63.1	78.0
	r=5000	16.6	63.6	78.4
180°C -1 hr	r=100	24.1	94.3	84.6
	r=10000	18.6	64.3	64.0
	r=5000	18.7	64.8	64.4
180°C -2 hrs	r=100	27.3	97.8	47.0
	r=10000	21.1	67.5	4.02
	r=5000	21.2	68.0	4.02
180°C -3 hrs	r=100	29.5	101	4.02
	r=10000	22.9	70.2	4.02
	r=5000	23.0	64.6	4.02
180°C -10 hrs	r=100	36.5	112	4.02
	r=10000	28.7	79.9	4.02
	r=5000	28.8	80.3	4.02

Table 5.4.6d: The effect of varying r on the prediction of the radius, the inter-precipitate spacing and width of PFZs given by combined model 4.

ageing treatment:	variable: r (°A)	radius of precipitate: (nm)	inter-precipitate spacing: (nm)	width of PFZs: (nm)
160°C -0.5 hr	r=100	24.8	77.4	0
	r=10000	19.5	54.9	0
	r=5000	19.6	55.3	0
160°C -5.5 hrs	r=100	74.1	161	0
	r=10000	63.6	134	0
	r=5000	63.8	134	0
160°C -10.5 hrs	r=100	110	228	0
	r=10000	97.5	199	0
	r=5000	97.7	200	0
160°C -20.5 hrs	r=100	171	348	0
	r=10000	157	317	0
	r=5000	157	317	0
160°C -48 hrs	r=100	306	616	0
	r=10000	291	584	0
	r=5000	292	585	0
180°C -0.5 hr	r=100	50.3	123	0
	r=10000	40.4	92.8	0
	r=5000	40.6	93.2	0
180°C -1 hr	r=100	70.6	158	0
	r=10000	58.7	126	0
	r=5000	58.9	127	0
180°C -2 hrs	r=100	104	221	0
	r=10000	90.1	187	0
	r=5000	90.4	187	0
180°C -3 hrs	r=100	134	278	0
	r=10000	118	242	0
	r=5000	119	243	0
180°C -10 hrs	r=100	298	602	0
	r=10000	279	561	0
	r=5000	280	562	0

Table 5.4.6e: The effect of varying r on the prediction of the radius, the inter-precipitate spacing and width of PFZs given by combined model 5.

ageing treatment:	variable: r (°A)	radius of precipitate: (nm)	inter-precipitate spacing: (nm)	width of PFZs: (nm)
160°C -0.5 hr	r=100	13.6	74.1	64.4
	r=10000	10.7	51.8	55.1
	r=5000	10.7	52.1	55.3
160°C -5.5 hrs	r=100	20.5	78.2	69.6
	r=10000	16.1	54.7	59.6
	r=5000	16.2	55.1	59.8
160°C -10.5 hrs	r=100	23.1	81.9	74.4
	r=10000	18.2	57.8	63.7
	r=5000	18.3	58.2	63.9
160°C -20.5 hrs	r=100	26.4	86.6	83.3
	r=10000	20.9	61.9	71.3
	r=5000	21.0	62.3	71.5
160°C -48 hrs	r=100	31.3	93.9	104
	r=10000	25.0	68.3	88.9
	r=5000	25.1	68.7	89.1
180°C -0.5 hr	r=100	21.4	93.0	98.7
	r=10000	16.5	63.1	84.8
	r=5000	16.6	63.6	85.1
180°C -1 hr	r=100	24.1	94.3	102
	r=10000	18.6	64.3	87.7
	r=5000	18.7	64.8	88.0
180°C -2 hrs	r=100	27.3	97.8	108
	r=10000	21.1	67.5	93.2
	r=5000	21.2	68.0	93.5
180°C -3 hrs	r=100	29.5	101	115
	r=10000	22.9	70.2	98.4
	r=5000	23.0	64.6	98.7
180°C -10 hrs	r=100	37.9	113	150
	r=10000	29.8	81.0	129
	r=5000	30.0	81.5	130

Table 7.4.7a: The effect of varying Q_{bnuc} on the prediction of the radius, the inter-precipitate spacing and width of PFZs given by combined model 1.

ageing treatment:	variable: Q_{bnuc} (cal/ mole)	radius of precipitate: (nm)	inter-precipitate spacing: (nm)	width of PFZs: (nm)
160°C -0.5 hr	Q_{bnuc}=17168	10.7	51.8	0
	Q_{bnuc}=22736	10.7	51.8	0
	Q_{bnuc}=25520	10.7	51.8	0
160°C -5.5 hrs	Q_{bnuc}=17168	16.1	54.7	0
	Q_{bnuc}=22736	16.1	54.7	0
	Q_{bnuc}=25520	16.1	54.7	0
160°C -10.5 hrs	Q_{bnuc}=17168	18.2	57.8	0
	Q_{bnuc}=22736	18.2	57.8	0
	Q_{bnuc}=25520	18.2	57.8	0
160°C -20.5 hrs	Q_{bnuc}=17168	20.9	61.8	0
	Q_{bnuc}=22736	20.9	61.8	0
	Q_{bnuc}=25520	20.9	61.8	0
160°C -48 hrs	Q_{bnuc}=17168	25.0	68.2	0
	Q_{bnuc}=22736	25.0	68.2	0
	Q_{bnuc}=25520	25.0	68.2	0
180°C -0.5 hr	Q_{bnuc}=17168	16.5	63.1	0
	Q_{bnuc}=22736	16.5	63.1	0
	Q_{bnuc}=25520	16.5	63.1	0
180°C -1 hr	Q_{bnuc}=17168	18.6	64.3	0
	Q_{bnuc}=22736	18.6	64.3	0
	Q_{bnuc}=25520	18.6	64.3	0
180°C -2 hrs	Q_{bnuc}=17168	21.1	67.5	0
	Q_{bnuc}=22736	21.1	67.5	0
	Q_{bnuc}=25520	21.1	67.5	0
180°C -3 hrs	Q_{bnuc}=17168	22.9	70.2	0
	Q_{bnuc}=22736	22.9	70.2	0
	Q_{bnuc}=25520	22.9	70.2	0
180°C -10 hrs	Q_{bnuc}=17168	29.8	80.9	0
	Q_{bnuc}=22736	29.8	80.9	0
	Q_{bnuc}=25520	29.8	80.9	0

Table 5.4.7b: The effect of varying Q_{bnuc} on the prediction of the radius, the inter-precipitate spacing and width of PFZs given by combined model 2.

ageing treatment:	variable: Q_{bnuc} (cal/ mole)	radius of precipitate: (nm)	inter-precipitate spacing: (nm)	width of PFZs: (nm)
160°C -0.5 hr	Q_{bnuc}=17168	12.1	66.9	1.2
	Q_{bnuc}=22736	12.1	66.9	1.2
	Q_{bnuc}=25520	12.1	66.9	1.2
160°C -5.5 hrs	Q_{bnuc}=17168	17.6	69.7	1.2
	Q_{bnuc}=22736	17.6	69.7	1.2
	Q_{bnuc}=25520	17.6	69.7	1.2
160°C -10.5 hrs	Q_{bnuc}=17168	18.7	71.8	1.2
	Q_{bnuc}=22736	18.7	71.8	1.2
	Q_{bnuc}=25520	18.7	71.8	1.2
160°C -20.5 hrs	Q_{bnuc}=17168	19.6	73.8	1.2
	Q_{bnuc}=22736	19.6	73.8	1.2
	Q_{bnuc}=25520	19.6	73.8	1.2
160°C -48 hrs	Q_{bnuc}=17168	20.0	76.0	1.2
	Q_{bnuc}=22736	20.0	76.0	1.2
	Q_{bnuc}=25520	20.0	76.0	1.2
180°C -0.5 hr	Q_{bnuc}=17168	18.7	84.2	1.2
	Q_{bnuc}=22736	18.7	84.2	1.2
	Q_{bnuc}=25520	18.7	84.2	1.2
180°C -1 hr	Q_{bnuc}=17168	20.4	85.0	1.2
	Q_{bnuc}=22736	20.4	85.0	1.2
	Q_{bnuc}=25520	20.4	85.0	1.2
180°C -2 hrs	Q_{bnuc}=17168	21.7	86.6	1.2
	Q_{bnuc}=22736	21.7	86.6	1.2
	Q_{bnuc}=25520	21.7	86.6	1.2
180°C -3 hrs	Q_{bnuc}=17168	22.3	87.8	1.2
	Q_{bnuc}=22736	22.3	87.8	1.2
	Q_{bnuc}=25520	22.3	87.8	1.2
180°C -10 hrs	Q_{bnuc}=17168	23.8	91.8	1.2
	Q_{bnuc}=22736	23.8	91.8	1.2
	Q_{bnuc}=25520	23.8	91.8	1.2

Table 5.4.7c: The effect of varying Q_{bnuc} on the prediction of the radius, the inter-precipitate spacing and width of PFZs given by combined model 3.

ageing treatment:	variable: Q_{bnuc} (cal/ mole)	radius of precipitate: (nm)	inter-precipitate spacing: (nm)	width of PFZs: (nm)
160°C -0.5 hr	Q_{bnuc}=17168	10.7	71.8	54.4
	Q_{bnuc}=22736	10.7	51.8	54.4
	Q_{bnuc}=25520	10.7	51.8	54.4
160°C -5.5 hrs	Q_{bnuc}=17168	16.1	54.7	4.02
	Q_{bnuc}=22736	16.1	54.7	4.02
	Q_{bnuc}=25520	16.1	54.7	4.02
160°C -10.5 hrs	Q_{bnuc}=17168	18.2	57.8	4.02
	Q_{bnuc}=22736	18.2	57.8	4.02
	Q_{bnuc}=25520	18.2	57.8	4.02
160°C -20.5 hrs	Q_{bnuc}=17168	20.9	61.9	4.02
	Q_{bnuc}=22736	20.9	61.9	4.02
	Q_{bnuc}=25520	20.9	61.9	4.02
160°C -48 hrs	Q_{bnuc}=17168	24.8	68.1	4.02
	Q_{bnuc}=22736	24.8	68.1	4.02
	Q_{bnuc}=25520	24.8	68.1	4.02
180°C -0.5 hr	Q_{bnuc}=17168	16.5	63.1	78.0
	Q_{bnuc}=22736	16.5	63.1	78.0
	Q_{bnuc}=25520	16.5	63.1	78.0
180°C -1 hr	Q_{bnuc}=17168	18.6	64.3	64.0
	Q_{bnuc}=22736	18.6	64.3	64.0
	Q_{bnuc}=25520	18.6	64.3	64.0
180°C -2 hrs	Q_{bnuc}=17168	21.1	67.5	40.2
	Q_{bnuc}=22736	21.1	67.5	4.02
	Q_{bnuc}=25520	21.1	67.5	4.02
180°C -3 hrs	Q_{bnuc}=17168	22.9	70.2	4.02
	Q_{bnuc}=22736	22.9	70.2	4.02
	Q_{bnuc}=25520	22.9	70.2	4.02
180°C -10 hrs	Q_{bnuc}=17168	28.7	79.9	4.02
	Q_{bnuc}=22736	28.7	79.9	4.02
	Q_{bnuc}=25520	28.7	79.9	4.02

Table 5.4.7d: The effect of varying Q_{bnuc} on the prediction of the radius, the inter-precipitate spacing and width of PFZs given by combined model 4.

ageing treatment:	variable: Q_{bnuc} (cal/ mole)	radius of precipitate: (nm)	inter-precipitate spacing: (nm)	width of PFZs: (nm)
160°C -0.5 hr	Q_{bnuc}=17168	19.5	54.9	0
	Q_{bnuc}=22736	19.5	54.9	0
	Q_{bnuc}=25520	19.5	54.9	0
160°C -5.5 hrs	Q_{bnuc}=17168	63.6	134	0
	Q_{bnuc}=22736	63.6	134	0
	Q_{bnuc}=25520	63.6	134	0
160°C -10.5 hrs	Q_{bnuc}=17168	97.5	199	0
	Q_{bnuc}=22736	97.5	199	0
	Q_{bnuc}=25520	97.5	199	0
160°C -20.5 hrs	Q_{bnuc}=17168	157	317	0
	Q_{bnuc}=22736	157	317	0
	Q_{bnuc}=25520	157	317	0
160°C -48 hrs	Q_{bnuc}=17168	291	584	0
	Q_{bnuc}=22736	291	584	0
	Q_{bnuc}=25520	291	584	0
180°C -0.5 hr	Q_{bnuc}=17168	40.4	92.8	0
	Q_{bnuc}=22736	40.4	92.8	0
	Q_{bnuc}=25520	40.4	92.8	0
180°C -1 hr	Q_{bnuc}=17168	58.7	126	0
	Q_{bnuc}=22736	58.7	126	0
	Q_{bnuc}=25520	58.7	126	0
180°C -2 hrs	Q_{bnuc}=17168	90.1	187	0
	Q_{bnuc}=22736	90.1	187	0
	Q_{bnuc}=25520	90.1	187	0
180°C -3 hrs	Q_{bnuc}=17168	118	242	0
	Q_{bnuc}=22736	118	242	0
	Q_{bnuc}=25520	118	242	0
180°C -10 hrs	Q_{bnuc}=17168	279	561	0
	Q_{bnuc}=22736	279	561	0
	Q_{bnuc}=25520	279	561	0

Table 5.4.7e: The effect of varying Q_{bnuc} on the prediction of the radius, the inter-precipitate spacing and width of PFZs given by combined model 5.

ageing treatment:	variable: Q_{bnuc} (cal/ mole)	radius of precipitate: (nm)	inter-precipitate spacing: (nm)	width of PFZs: (nm)
160°C -0.5 hr	Q_{bnuc}=17168	10.7	71.8	55.1
	Q_{bnuc}=22736	10.7	51.8	55.1
	Q_{bnuc}=25520	10.7	51.8	55.1
160°C -5.5 hrs	Q_{bnuc}=17168	16.1	54.7	59.6
	Q_{bnuc}=22736	16.1	54.7	59.6
	Q_{bnuc}=25520	16.1	54.7	59.6
160°C -10.5 hrs	Q_{bnuc}=17168	18.2	57.8	63.7
	Q_{bnuc}=22736	18.2	57.8	63.7
	Q_{bnuc}=25520	18.2	57.8	63.7
160°C -20.5 hrs	Q_{bnuc}=17168	20.9	61.9	71.3
	Q_{bnuc}=22736	20.9	61.9	71.3
	Q_{bnuc}=25520	20.9	61.9	71.3
160°C -48 hrs	Q_{bnuc}=17168	25.0	68.3	88.9
	Q_{bnuc}=22736	24.8	68.3	88.9
	Q_{bnuc}=25520	25.0	68.3	88.9
180°C -0.5 hr	Q_{bnuc}=17168	16.5	63.1	84.8
	Q_{bnuc}=22736	16.5	63.1	84.8
	Q_{bnuc}=25520	16.5	63.1	84.8
180°C -1 hr	Q_{bnuc}=17168	18.6	64.3	87.7
	Q_{bnuc}=22736	18.6	64.3	87.7
	Q_{bnuc}=25520	18.6	64.3	87.7
180°C -2 hrs	Q_{bnuc}=17168	21.1	67.5	93.2
	Q_{bnuc}=22736	21.1	67.5	93.2
	Q_{bnuc}=25520	21.1	67.5	93.2
180°C -3 hrs	Q_{bnuc}=17168	22.9	70.2	98.4
	Q_{bnuc}=22736	22.9	70.2	98.4
	Q_{bnuc}=25520	22.9	70.2	98.4
180°C -10 hrs	Q_{bnuc}=17168	29.8	81.0	129
	Q_{bnuc}=22736	29.8	81.0	129
	Q_{bnuc}=25520	29.8	81.0	129

Table 5.4.8a: The effect of varying Q_c on the prediction of the radius, the inter-precipitate spacing and width of PFZs given by combined model 1.

ageing treatment:	variable: Q_{hmuc} (cal/ mole)	radius of precipitate: (nm)	inter-precipitate spacing: (nm)	width of PFZs: (nm)
160°C -0.5 hr	Q_c=25984	10.7	51.8	0
	Q_c=28768	10.7	51.8	0
	Q_c=31552	10.7	51.8	0
160°C -5.5 hrs	Q_c=25984	16.1	54.7	0
	Q_c=28768	16.1	54.7	0
	Q_c=31552	16.1	54.7	0
160°C -10.5 hrs	Q_c=25984	18.2	57.8	0
	Q_c=28768	18.2	57.8	0
	Q_c=31552	18.2	57.8	0
160°C -20.5 hrs	Q_c=25984	20.9	61.9	0
	Q_c=28768	20.9	61.8	0
	Q_c=31552	20.9	61.8	0
160°C -48 hrs	Q_c=25984	25.0	68.3	0
	Q_c=28768	25.0	68.2	0
	Q_c=31552	24.9	68.1	0
180°C -0.5 hr	Q_c=25984	16.5	63.1	0
	Q_c=28768	16.5	63.1	0
	Q_c=31552	16.5	63.1	0
180°C -1 hr	Q_c=25984	18.6	64.3	0
	Q_c=28768	18.6	64.3	0
	Q_c=31552	18.5	64.3	0
180°C -2 hrs	Q_c=25984	21.1	67.5	0
	Q_c=28768	21.1	67.5	0
	Q_c=31552	21.0	67.5	0
180°C -3 hrs	Q_c=25984	22.9	70.2	0
	Q_c=28768	22.9	70.2	0
	Q_c=31552	22.8	70.1	0
180°C -10 hrs	Q_c=25984	29.8	81.0	0
	Q_c=28768	29.8	80.9	0
	Q_c=31552	29.6	80.7	0

Table 5.4.8b: The effect of varying Q_c on the prediction of the radius, the inter-precipitate spacing and width of PFZs given by combined model 2.

ageing treatment:	variable: Q_{bnuc} (cal/ mole)	radius of precipitate: (nm)	inter-precipitate spacing: (nm)	width of PFZs: (nm)
160°C -0.5 hr	Q_c=25984	10.7	51.8	1.0
	Q_c=28768	12.1	66.9	1.2
	Q_c=31552	17.3	130	1.2
160°C -5.5 hrs	Q_c=25984	15.2	54.2	1.0
	Q_c=28768	17.6	69.7	1.2
	Q_c=31552	24.6	134	1.2
160°C -10.5 hrs	Q_c=25984	16.0	55.9	1.0
	Q_c=28768	18.7	71.8	1.2
	Q_c=31552	25.7	136	1.2
160°C -20.5 hrs	Q_c=25984	16.6	57.4	1.0
	Q_c=28768	19.6	73.8	1.2
	Q_c=31552	26.6	139	1.2
160°C -48 hrs	Q_c=25984	16.7	58.9	1.0
	Q_c=28768	20.0	76.0	1.2
	Q_c=31552	26.8	142	1.2
180°C -0.5 hr	Q_c=25984	16.3	63.1	1.0
	Q_c=28768	18.7	84.2	1.2
	Q_c=31552	28.8	180	1.2
180°C -1 hr	Q_c=25984	17.4	63.9	1.0
	Q_c=28768	20.4	85.0	1.2
	Q_c=31552	30.7	181	1.2
180°C -2 hrs	Q_c=25984	18.2	66.4	1.0
	Q_c=28768	21.7	86.6	1.2
	Q_c=31552	32.1	182	1.2
180°C -3 hrs	Q_c=25984	18.6	66.4	1.0
	Q_c=28768	22.3	87.8	1.2
	Q_c=31552	32.7	183	1.2
180°C -10 hrs	Q_c=25984	19.5	74.9	1.0
	Q_c=28768	23.8	91.8	1.2
	Q_c=31552	34.2	188	1.2

Table 5.4.8c: The effect of varying Q_c on the prediction of the radius, the inter-precipitate spacing and width of PFZs given by combined model 3.

ageing treatment:	variable: Q_{hnuc} (cal/ mole)	radius of precipitate: (nm)	inter-precipitate spacing: (nm)	width of PFZs: (nm)
160°C -0.5 hr	Q_c=25984	10.7	51.8	118
	Q_c=28768	10.7	51.8	54.4
	Q_c=31552	10.7	51.8	20.6
160°C -5.5 hrs	Q_c=25984	16.1	54.7	10.4
	Q_c=28768	16.1	54.7	4.02
	Q_c=31552	16.0	54.7	17.6
160°C -10.5 hrs	Q_c=25984	18.2	57.8	10.4
	Q_c=28768	18.2	57.8	4.02
	Q_c=31552	17.3	57.1	7.02
160°C -20.5 hrs	Q_c=25984	20.9	61.9	10.4
	Q_c=28768	20.9	61.9	4.02
	Q_c=31552	18.4	59.3	1.64
160°C -48 hrs	Q_c=25984	25.0	68.3	10.4
	Q_c=28768	24.8	68.1	4.02
	Q_c=31552	19.0	61.4	1.64
180°C -0.5 hr	Q_c=25984	16.5	63.1	95.2
	Q_c=28768	16.5	63.1	78.0
	Q_c=31552	16.5	63.1	31.0
180°C -1 hr	Q_c=25984	18.6	64.3	10.4
	Q_c=28768	18.6	64.3	64.0
	Q_c=31552	18.4	64.3	30.4
180°C -2 hrs	Q_c=25984	21.1	67.5	10.4
	Q_c=28768	21.1	67.5	4.02
	Q_c=31552	19.8	66.6	28.2
180°C -3 hrs	Q_c=25984	22.9	70.2	10.4
	Q_c=28768	22.9	70.2	4.02
	Q_c=31552	20.5	68.1	24.4
180°C -10 hrs	Q_c=25984	29.8	81.0	10.4
	Q_c=28768	28.7	79.9	4.02
	Q_c=31552	22.0	71.9	1.64

Table 5.4.8d: The effect of varying Q_c on the prediction of the radius, the inter-precipitate spacing and width of PFZs given by combined model 4.

ageing treatment:	variable: Q_{hnuc} (cal/ mole)	radius of precipitate: (nm)	inter-precipitate spacing: (nm)	width of PFZs: (nm)
160°C -0.5 hr	Q_c=25984	55.3	116	0
	Q_c=28768	19.5	54.9	0
	Q_c=31552	9.26	51.8	0
160°C -5.5 hrs	Q_c=25984	342	685	0
	Q_c=28768	63.6	134	0
	Q_c=31552	20.9	59.8	0
160°C -10.5 hrs	Q_c=25984	575	1150	0
	Q_c=28768	97.5	199	0
	Q_c=31552	27.3	69.7	0
160°C -20.5 hrs	Q_c=25984	959	1920	0
	Q_c=28768	157	317	0
	Q_c=31552	37.2	86.4	0
160°C -48 hrs	Q_c=25984	1750	3490	0
	Q_c=28768	291	584	0
	Q_c=31552	57.9	124	0
180°C -0.5 hr	Q_c=25984	149	301	0
	Q_c=28768	40.4	92.8	0
	Q_c=31552	17.8	63.2	0
180°C -1 hr	Q_c=25984	257	517	0
	Q_c=28768	58.7	126	0
	Q_c=31552	22.6	67.5	0
180°C -2 hrs	Q_c=25984	450	902	0
	Q_c=28768	90.1	187	0
	Q_c=31552	29.7	78.0	0
180°C -3 hrs	Q_c=25984	620	1240	0
	Q_c=28768	118	242	0
	Q_c=31552	35.4	87.3	0
180°C -10 hrs	Q_c=25984	1510	3020	0
	Q_c=28768	279	561	0
	Q_c=31552	64.7	140	0

Table 5.4.8e: The effect of varying Q_c on the prediction of the radius, the inter-precipitate spacing and width of PFZs given by combined model 5.

ageing treatment:	variable: Q_{hnuc} (cal/ mole)	radius of precipitate: (nm)	inter-precipitate spacing: (nm)	width of PFZs: (nm)
160°C -0.5 hr	Q_c=25984	10.7	51.8	150
	Q_c=28768	10.7	51.8	55.1
	Q_c=31552	10.7	51.8	20.6
160°C -5.5 hrs	Q_c=25984	16.1	54.7	188
	Q_c=28768.	16.1	54.7	59.6
	Q_c=31552	16.0	54.7	21.1
160°C -10.5 hrs	Q_c=25984	18.2	57.8	219
	Q_c=28768	18.2	57.8	63.7
	Q_c=31552	17.4	57.2	21.6
160°C -20.5 hrs	Q_c=25984	20.9	61.9	271
	Q_c=28768	20.9	61.9	71.3
	Q_c=31552	18.6	59.5	22.5
160°C -48 hrs	Q_c=25984	25.0	68.3	379
	Q_c=28768	25.0	68.3	88.9
	Q_c=31552	19.6	62.0	24.9
180°C -0.5 hr	Q_c=25984	16.5	63.1	242
	Q_c=28768	16.5	63.1	84.8
	Q_c=31552	16.5	63.1	31.2
180°C -1 hr	Q_c=25984	18.6	64.3	263
	Q_c=28768	18.6	64.3	87.7
	Q_c=31552	18.4	64.3	31.6
180°C -2 hrs	Q_c=25984	21.1	67.5	301
	Q_c=28768	21.1	67.5	93.2
	Q_c=31552	19.9	66.7	32.3
180°C -3 hrs	Q_c=25984	22.9	70.2	335
	Q_c=28768	22.9	70.2	98.4
	Q_c=31552	20.7	68.2	33.0
180°C -10 hrs	Q_c=25984	29.8	81.0	514
	Q_c=28768	29.8	81.0	129
	Q_c=31552	22.7	72.5	37.6

Table 5.4.9a: The effect of varying Q_i on the prediction of the radius, the inter-precipitate spacing and width of PFZs given by combined model 1.

ageing treatment:	variable: Q_i (cal/ mole)	radius of precipitate: (nm)	inter-precipitate spacing: (nm)	width of PFZs: (nm)
160°C -0.5 hr	Q_i=32016	22.7	59.7	0
	Q_i=35728	10.7	51.8	0
	Q_i=39208	5.47	51.8	0
160°C -5.5 hrs	Q_i=32016	42.6	95.2	0
	Q_i=35728	16.1	54.7	0
	Q_i=39208	8.12	54.7	0
160°C -10.5 hrs	Q_i=32016	52.1	113	0
	Q_i=35728	18.2	57.8	0
	Q_i=39208	9.03	51.8	0
160°C -20.5 hrs	Q_i=32016	64.9	137	0
	Q_i=35728	20.9	61.8	0
	Q_i=39208	10.1	51.8	0
160°C -48 hrs	Q_i=32016	87.5	181	0
	Q_i=35728	25.0	68.2	0
	Q_i=39208	11.5	52.8	0
180°C -0.5 hr	Q_i=32016	36.8	87.4	0
	Q_i=35728	16.5	63.1	0
	Q_i=39208	8.69	62.8	0
180°C -1 hr	Q_i=32016	44.5	102	0
	Q_i=35728	18.6	64.3	0
	Q_i=39208	9.75	62.8	0
180°C -2 hrs	Q_i=32016	54.9	121	0
	Q_i=35728	21.1	67.5	0
	Q_i=39208	10.9	62.8	0
180°C -3 hrs	Q_i=32016	62.5	135	0
	Q_i=35728	22.9	70.2	0
	Q_i=39208	11.7	62.8	0
180°C -10 hrs	Q_i=32016	94.8	197	0
	Q_i=35728	29.8	80.9	0
	Q_i=39208	14.3	63.9	0

Table 4.4.9b: The effect of varying Q_i on the prediction of the radius, the inter-precipitate spacing and width of PFZs given by combined model 2.

ageing treatment:	variable: Q_i (cal/ mole)	radius of precipitate: (nm)	inter-precipitate spacing: (nm)	width of PFZs: (nm)
160°C -0.5 hr	Q_i=32016	19.1	68.5	1.2
	Q_i=35728	12.1	66.9	1.2
	Q_i=39208	6.20	66.9	1.2
160°C -5.5 hrs	Q_i=32016	21.3	73.9	1.2
	Q_i=35728	17.6	69.7	1.2
	Q_i=39208	9.42	66.9	1.2
160°C -10.5 hrs	Q_i=32016	22.2	75.8	1.2
	Q_i=35728	18.7	71.8	1.2
	Q_i=39208	10.6	66.9	1.2
160°C -20.5 hrs	Q_i=32016	23.2	77.8	1.2
	Q_i=35728	19.6	73.8	1.2
	Q_i=39208	11.9	67.5	1.2
160°C -48 hrs	Q_i=32016	24.2	80.5	1.2
	Q_i=35728	20.0	76.0	1.2
	Q_i=39208	13.7	69.5	1.2
180°C -0.5 hr	Q_i=32016	23.1	86.1	1.2
	Q_i=35728	18.7	84.2	1.2
	Q_i=39208	9.98	83.9	1.2
180°C -1 hr	Q_i=32016	24.1	87.7	1.2
	Q_i=35728	20.4	85.0	1.2
	Q_i=39208	11.5	83.9	1.2
180°C -2 hrs	Q_i=32016	25.0	89.9	1.2
	Q_i=35728	21.7	86.6	1.2
	Q_i=39208	13.1	84.0	1.2
180°C -3 hrs	Q_i=32016	25.7	91.3	1.2
	Q_i=35728	22.3	87.8	1.2
	Q_i=39208	14.0	84.2	1.2
180°C -10 hrs	Q_i=32016	27.9	95.9	1.2
	Q_i=35728	23.8	91.8	1.2
	Q_i=39208	17.3	86.0	1.2

Table 5.4.9c: The effect of varying Q_i on the prediction of the radius, the inter-precipitate spacing and width of PFZs given by combined model 3.

ageing treatment:	variable: Q_i (cal/ mole)	radius of precipitate: (nm)	inter-precpitate spacing: (nm)	width of PFZs: (nm)
160°C -0.5 hr	Q_i=32016	22.6	59.8	54.4
	Q_i=35728	10.7	51.8	54.4
	Q_i=39208	5.47	51.8	54.4
160°C -5.5 hrs	Q_i=32016	30.1	74.9	4.02
	Q_i=35728	16.1	54.7	4.02
	Q_i=39208	8.13	51.8	4.02
160°C -10.5 hrs	Q_i=32016	31.5	77.8	4.02
	Q_i=35728	18.2	57.8	4.02
	Q_i=39208	9.03	51.8	4.02
160°C -20.5 hrs	Q_i=32016	32.8	80.5	4.02
	Q_i=35728	20.9	61.9	4.02
	Q_i=39208	10.1	51.8	4.02
160°C -48 hrs	Q_i=32016	33.4	82.7	4.02
	Q_i=35728	24.8	68.1	4.02
	Q_i=39208	11.5	52.8	4.02
180°C -0.5 hr	Q_i=32016	30.7	79.1	78.0
	Q_i=35728	16.5	63.1	78.0
	Q_i=39208	8.69	62.8	78.0
180°C -1 hr	Q_i=32016	32.5	83.2	64.0
	Q_i=35728	18.6	64.3	64.0
	Q_i=39208	9.75	62.8	64.0
180°C -2 hrs	Q_i=32016	34.1	86.7	40.2
	Q_i=35728	21.1	67.5	4.02
	Q_i=39208	10.9	62.8	4.02
180°C -3 hrs	Q_i=32016	35.0	88.6	4.02
	Q_i=35728	22.9	70.2	4.02
	Q_i=39208	11.7	62.8	4.02
180°C -10 hrs	Q_i=32016	37.4	93.8	4.02
	Q_i=35728	28.7	79.9	4.02
	Q_i=39208	14.3	63.9	4.02

Table 4.4.9d: The effect of varying Q_i on the prediction of the radius, the inter-precipitate spacing and width of PFZs given by combined model 4.

ageing treatment:	variable: Q_i (cal/ mole)	radius of precipitate: (nm)	inter-precipitate spacing: (nm)	width of PFZs: (nm)
160°C -0.5 hr	Q_i=32016	19.7	55.1	0
	Q_i=35728	19.5	54.9	0
	Q_i=39208	19.3	54.6	0
160°C -5.5 hrs	Q_i=32016	62.9	132	0
	Q_i=35728	63.6	134	0
	Q_i=39208	62.9	131	0
160°C -10.5 hrs	Q_i=32016	96.0	197	0
	Q_i=35728	97.5	199	0
	Q_i=39208	95.0	195	0
160°C -20.5 hrs	Q_i=32016	154	311	0
	Q_i=35728	157	317	0
	Q_i=39208	153	308	0
160°C -48 hrs	Q_i=32016	284	571	0
	Q_i=35728	291	584	0
	Q_i=39208	282	567	0
180°C -0.5 hr	Q_i=32016	40.3	92.6	0
	Q_i=35728	40.4	92.8	0
	Q_i=39208	39.8	91.7	0
180°C -1 hr	Q_i=32016	58.3	126	0
	Q_i=35728	58.7	126	0
	Q_i=39208	57.6	124	0
180°C -2 hrs	Q_i=32016	89.1	185	0
	Q_i=35728	90.1	187	0
	Q_i=39208	8.2	183	0
180°C -3 hrs	Q_i=32016	117	239	0
	Q_i=35728	118	242	0
	Q_i=39208	116	237	0
180°C -10 hrs	Q_i=32016	274	550	0
	Q_i=35728	279	561	0
	Q_i=39208	272	547	0

Table 5.4.9e: The effect of varying Q_i on the prediction of the radius, the inter-precipitate spacing and width of PFZs given by combined model 5.

ageing treatment:	variable: Q_i (cal/ mole)	radius of precipitate: (nm)	inter-precpitate spacing: (nm)	width of PFZs: (nm)
160°C -0.5 hr	Q_i=32016	22.6	59.8	55.1
	Q_i=35728	10.7	51.8	55.1
	Q_i=39208	5.47	51.8	55.1
160°C -5.5 hrs	Q_i=32016	30.5	75.5	59.6
	Q_i=35728	16.1	54.7	59.6
	Q_i=39208	8.13	51.8	59.6
160°C -10.5 hrs	Q_i=32016	32.2	78.8	63.7
	Q_i=35728	18.2	57.8	63.7
	Q_i=39208	9.03	51.8	63.7
160°C -20.5 hrs	Q_i=32016	33.9	82.1	71.3
	Q_i=35728	20.9	61.9	71.3
	Q_i=39208	10.1	51.8	71.3
160°C -48 hrs	Q_i=32016	36.6	86.9	88.9
	Q_i=35728	25.0	68.3	88.9
	Q_i=39208	11.5	52.8	88.9
180°C -0.5 hr	Q_i=32016	30.8	79.3	84.8
	Q_i=35728	16.5	63.1	84.8
	Q_i=39208	8.69	62.8	84.8
180°C -1 hr	Q_i=32016	32.8	83.6	87.7
	Q_i=35728	18.6	64.3	87.7
	Q_i=39208	9.75	62.8	87.7
180°C -2 hrs	Q_i=32016	34.7	87.5	93.2
	Q_i=35728	21.1	67.5	93.2
	Q_i=39208	10.9	62.8	93.2
180°C -3 hrs	Q_i=32016	35.8	89.7	98.4
	Q_i=35728	22.9	70.2	98.4
	Q_i=39208	11.7	62.8	98.4
180°C -10 hrs	Q_i=32016	39.6	97.0	129
	Q_i=35728	29.8	81.0	129
	Q_i=39208	14.3	63.9	129

Table 5.4.10a: The effect of varying T_{mp} on the prediction of the radius, the inter-precipitate spacing and width of PFZs given by combined model 1.

ageing treatment:	variable: T_{mp} (K)	radius of precipitate: (nm)	inter-precipitate spacing: (nm)	width of PFZs: (nm)
160°C -0.5 hr	T_{mp}=600	124	4060	0
	T_{mp}=560	10.7	51.8	0
	T_{mp}=520	4.19	5.84	0
160°C -5.5 hrs	T_{mp}=600	185	4090	0
	T_{mp}=560	16.1	54.7	0
	T_{mp}=520	-	-	0
160°C -10.5 hrs	T_{mp}=600	207	4110	0
	T_{mp}=560	18.2	57.8	0
	T_{mp}=520	-	-	0
160°C -20.5 hrs	T_{mp}=600	231	4150	0
	T_{mp}=560	20.9	61.8	0
	T_{mp}=520	-	-	0
160°C -48 hrs	T_{mp}=600	268	4210	0
	T_{mp}=560	25.0	68.2	0
	T_{mp}=520	-	-	0
180°C -0.5 hr	T_{mp}=600	328	11000	0
	T_{mp}=560	16.5	63.1	0
	T_{mp}=520	-	-	0
180°C -1 hr	T_{mp}=600	368	11000	0
	T_{mp}=560	18.6	64.3	0
	T_{mp}=520	-	-	0
180°C -2 hrs	T_{mp}=600	413	11100	0
	T_{mp}=560	21.1	67.5	0
	T_{mp}=520	-	-	0
180°C -3 hrs	T_{mp}=600	441	11100	0
	T_{mp}=560	22.9	70.2	0
	T_{mp}=520	-	-	0
180°C -10 hrs	T_{mp}=600	540	11200	0
	T_{mp}=560	29.8	80.9	0
	T_{mp}=520	-	-	0

Table 4.4.10b: The effect of varying T_{mp} on the prediction of the radius, the inter-precipitate spacing and width of PFZs given by combined model 2.

ageing treatment:	variable: T_{mp} (K)	radius of precipitate: (nm)	inter-precipitate spacing: (nm)	width of PFZs: (nm)
160°C -0.5 hr	T_{mp}=600	124	4060	1.0
	T_{mp}=560	12.1	66.9	1.2
	T_{mp}=520	5.59	13.5	1.2
160°C -5.5 hrs	T_{mp}=600	176	4090	1.0
	T_{mp}=560	17.6	69.7	1.2
	T_{mp}=520	10.1	21.9	1.2
160°C -10.5 hrs	T_{mp}=600	183	4110	1.0
	T_{mp}=560	18.7	71.8	1.2
	T_{mp}=520	11.2	24.1	1.2
160°C -20.5 hrs	T_{mp}=600	188	4150	1.0
	T_{mp}=560	19.6	73.8	1.2
	T_{mp}=520	12.4	26.3	1.2
160°C -48 hrs	T_{mp}=600	189	4200	1.0
	T_{mp}=560	20.0	76.0	1.2
	T_{mp}=520	13.7	28.9	1.2
180°C -0.5 hr	T_{mp}=600	324	11000	1.0
	T_{mp}=560	18.7	84.2	1.2
	T_{mp}=520	8.86	19.3	1.2
180°C -1 hr	T_{mp}=600	345	11000	1.0
	T_{mp}=560	20.4	85.0	1.2
	T_{mp}=520	10.2	22.0	1.2
180°C -2 hrs	T_{mp}=600	358	11100	1.0
	T_{mp}=560	21.7	86.6	1.2
	T_{mp}=520	11.4	24.4	1.2
180°C -3 hrs	T_{mp}=600	364	11100	1.0
	T_{mp}=560	22.3	87.8	1.2
	T_{mp}=520	12.1	25.7	1.2
180°C -10 hrs	T_{mp}=600	372	11200	1.0
	T_{mp}=560	23.8	91.8	1.2
	T_{mp}=520	14.2	29.7	1.2

Table 5.4.10c: The effect of varying T_{mp} on the prediction of the radius, the inter-precipitate spacing and width of PFZs given by combined model 3.

ageing treatment:	variable: T_{mp} (K)	radius of precipitate: (nm)	inter-precpitate spacing: (nm)	width of PFZs: (nm)
160°C -0.5 hr	T_{mp}=600	124	4060	65.0
	T_{mp}=560	10.7	51.8	54.4
	T_{mp}=520	4.19	5.84	51.4
160°C -5.5 hrs	T_{mp}=600	186	4090	14.8
	T_{mp}=560	16.1	54.7	4.02
	T_{mp}=520	-	-	1.01
160°C -10.5 hrs	T_{mp}=600	207	4110	14.8
	T_{mp}=560	18.2	57.8	4.02
	T_{mp}=520	-	-	1.01
160°C -20.5 hrs	T_{mp}=600	232	4150	14.8
	T_{mp}=560	20.9	61.9	4.02
	T_{mp}=520	-	-	1.01
160°C -48 hrs	T_{mp}=600	268	4210	14.8
	T_{mp}=560	24.8	68.1	4.02
	T_{mp}=520	-	-	1.01
180°C -0.5 hr	T_{mp}=600	328	11000	88.6
	T_{mp}=560	16.5	63.1	78.0
	T_{mp}=520	-	-	75.0
180°C -1 hr	T_{mp}=600	368	11000	74.4
	T_{mp}=560	18.6	64.3	64.0
	T_{mp}=520	-	-	61.0
180°C -2 hrs	T_{mp}=600	413	11100	14.8
	T_{mp}=560	21.1	67.5	4.02
	T_{mp}=520	-	-	1.01
180°C -3 hrs	T_{mp}=600	442	11100	14.8
	T_{mp}=560	22.9	70.2	4.02
	T_{mp}=520	-	-	1.01
180°C -10 hrs	T_{mp}=600	541	11200	14.8
	T_{mp}=560	28.7	79.9	4.02
	T_{mp}=520	-	-	1.01

Table 5.4.10d: The effect of varying T_{mp} on the prediction of the radius, the inter-precipitate spacing and width of PFZs given by combined model 4.

ageing treatment:	variable: T_{mn} (K)	radius of precipitate: (nm)	inter-precipitate spacing: (nm)	width of PFZs: (nm)
160°C -0.5 hr	T_{mn}=600	222	4060	0
	T_{mn}=560	19.5	54.9	0
	T_{mn}=520	-	-	0
160°C -5.5 hrs	T_{mn}=600	486	4110	0
	T_{mn}=560	63.6	134	0
	T_{mn}=520	-	-	0
160°C -10.5 hrs	T_{mn}=600	597	4170	0
	T_{mn}=560	97.5	199	0
	T_{mn}=520	-	-	0
160°C -20.5 hrs	T_{mn}=600	735	4270	0
	T_{mn}=560	157	317	0
	T_{mn}=520	-	-	0
160°C -48 hrs	T_{mn}=600	946	4480	0
	T_{mn}=560	291	584	0
	T_{mn}=520	-	-	0
180°C -0.5 hr	T_{mn}=600	701	11000	0
	T_{mn}=560	40.4	92.8	0
	T_{mn}=520	-	-	0
180°C -1 hr	T_{mn}=600	877	11100	0
	T_{mn}=560	58.7	126	0
	T_{mn}=520	-	-	0
180°C -2 hrs	T_{mn}=600	1090	11100	0
	T_{mn}=560	90.1	187	0
	T_{mn}=520	-	-	0
180°C -3 hrs	T_{mn}=600	1240	11100	0
	T_{mn}=560	118	242	0
	T_{mn}=520	-	-	0
180°C -10 hrs	T_{mn}=600	1760	11400	0
	T_{mn}=560	279	561	0
	T_{mn}=520	-	-	0

Table 5.4.10e: The effect of varying T_{mp} on the prediction of the radius, the inter-precipitate spacing and width of PFZs given by combined model 5.

ageing treatment:	variable: T_{mp} (K)	radius of precipitate: (nm)	inter-precpitate spacing: (nm)	width of PFZs: (nm)
160°C -0.5 hr	T_{mp}=600 T_{mp}=560 T_{mp}=520	124 10.7 4.19	4060 51.8 5.84	65.8 55.1 52.1
160°C -5.5 hrs	T_{mp}=600 T_{mp}=560 T_{mp}=520	186 16.1 -	4090 54.7 -	71.2 59.6 56.3
160°C -10.5 hrs	T_{mp}=600 T_{mp}=560 T_{mp}=520	207 18.2 -	4110 57.8 -	76.1 63.7 60.3
160°C -20.5 hrs	T_{mp}=600 T_{mp}=560 T_{mp}=520	232 20.9 -	4150 61.9 -	85.1 71.3 67.4
160°C -48 hrs	T_{mp}=600 T_{mp}=560 T_{mp}=520	268 25.0 -	4210 68.3 -	106 88.9 84.0
180°C -0.5 hr	T_{mp}=600 T_{mp}=560 T_{mp}=520	328 16.5 -	11000 63.1 -	95.7 84.8 81.8
180°C -1 hr	T_{mp}=600 T_{mp}=560 T_{mp}=520	368 18.6 -	11000 64.3 -	99.0 87.7 84.5
180°C -2 hrs	T_{mp}=600 T_{mp}=560 T_{mp}=520	413 21.1 -	11100 67.5 -	105 93.2 89.9
180°C -3 hrs	T_{mp}=600 T_{mp}=560 T_{mp}=520	442 22.9 -	11100 70.2 -	111 98.4 94.9
180°C -10 hrs	T_{mp}=600 T_{mp}=560 T_{mp}=520	541 29.8 -	11200 81.0 -	146 129 124

Table 5.4.11a: The effect of varying δt on the prediction of the radius, the inter-precipitate spacing and width of PFZs given by combined model 1.

ageing treatment:	variable: δt (s)	radius of precipitate: (nm)	inter-precipitate spacing: (nm)	width of PFZs: (nm)
160°C -0.5 hr	δt=5	10.7	51.8	0
	δt=3	10.7	51.8	0
	δt=10	10.7	51.8	0
160°C -5.5 hrs	δt=5	16.0	54.2	0
	δt=3	16.1	54.7	0
	δt=10	16.0	53.5	0
160°C -10.5 hrs	δt=5	18.2	57.2	0
	δt=3	18.2	57.8	0
	δt=10	18.1	56.3	0
160°C -20.5 hrs	δt=5	20.9	61.2	0
	δt=3	20.9	61.8	0
	δt=10	20.7	60.4	0
160°C -48 hrs	δt=5	25.2	68.0	0
	δt=3	25.0	68.2	0
	δt=10	25.1	67.2	0
180°C -0.5 hr	δt=5	16.5	63.0	0
	δt=3	16.5	63.1	0
	δt=10	16.5	62.9	0
180°C -1 hr	δt=5	18.5	63.9	0
	δt=3	18.6	64.3	0
	δt=10	18.5	63.4	0
180°C -2 hrs	δt=5	21.0	66.7	0
	δt=3	21.1	67.5	0
	δt=10	20.9	65.7	0
180°C -3 hrs	δt=5	22.8	69.3	0
	δt=3	22.9	70.2	0
	δt=10	22.6	68.1	0
180°C -10 hrs	δt=5	29.6	80.0	0
	δt=3	29.8	80.9	0
	δt=10	29.4	78.8	0

Table 5.4.11b: The effect of varying δt on the prediction of the radius, the inter-precipitate spacing and width of PFZs given by combined model 2.

ageing treatment:	variable: δt (s)	radius of precipitate: (nm)	inter-precipitate spacing: (nm)	width of PFZs: (nm)
160°C -0.5 hr	δt=5	12.1	66.9	1.2
	δt=3	12.1	66.9	1.2
	δt=10	12.1	66.9	1.2
160°C -5.5 hrs	δt=5	17.6	69.0	1.2
	δt=3	17.6	69.7	1.2
	δt=10	17.5	68.3	1.2
160°C -10.5 hrs	δt=5	18.6	71.0	1.2
	δt=3	18.7	71.8	1.2
	δt=10	18.6	70.0	1.2
160°C -20.5 hrs	δt=5	19.5	73.1	1.2
	δt=3	19.6	73.8	1.2
	δt=10	19.5	72.0	1.2
160°C -48 hrs	δt=5	20.4	75.4	1.2
	δt=3	20.0	76.0	1.2
	δt=10	20.4	74.4	1.2
180°C -0.5 hr	δt=5	18.7	84.1	1.2
	δt=3	18.7	84.2	1.2
	δt=10	18.8	84.0	1.2
180°C -1 hr	δt=5	20.4	84.6	1.2
	δt=3	20.4	85.0	1.2
	δt=10	20.4	84.3	1.2
180°C -2 hrs	δt=5	21.6	85.9	1.2
	δt=3	21.7	86.6	1.2
	δt=10	21.6	85.1	1.2
180°C -3 hrs	δt=5	22.2	86.9	1.2
	δt=3	22.3	87.8	1.2
	δt=10	22.3	85.9	1.2
180°C -10 hrs	δt=5	23.7	90.7	1.2
	δt=3	23.8	91.8	1.2
	δt=10	23.6	89.3	1.2

Table 5.4.11c: The effect of varying δt on the prediction of the radius, the inter-precipitate spacing and width of PFZs given by combined model 3.

ageing treatment:	variable: δt (s)	radius of precipitate: (nm)	inter-precpitate spacing: (nm)	width of PFZs: (nm)
160°C -0.5 hr	δt=5	10.7	51.8	54.4
	δt=3	10.7	51.8	54.4
	δt=10	10.7	51.8	54.4
160°C -5.5 hrs	δt=5	16.0	54.2	4.02
	δt=3	16.1	54.7	4.02
	δt=10	16.0	53.5	4.02
160°C -10.5 hrs	δt=5	18.2	57.2	4.02
	δt=3	18.2	57.8	4.02
	δt=10	18.1	56.3	4.02
160°C -20.5 hrs	δt=5	20.9	61.3	4.02
	δt=3	20.9	61.9	4.02
	δt=10	20.8	60.4	4.02
160°C -48 hrs	δt=5	24.7	67.6	4.02
	δt=3	24.8	68.1	4.02
	δt=10	24.7	66.9	4.02
180°C -0.5 hr	δt=5	16.5	63.0	78.0
	δt=3	16.5	63.1	78.0
	δt=10	16.6	62.9	78.0
180°C -1 hr	δt=5	18.6	63.9	64.0
	δt=3	18.6	64.3	64.0
	δt=10	18.6	63.4	64.0
180°C -2 hrs	δt=5	21.0	66.7	40.2
	δt=3	21.1	67.5	4.02
	δt=10	21.0	65.7	4.02
180°C -3 hrs	δt=5	22.8	69.3	4.02
	δt=3	22.9	70.2	4.02
	δt=10	22.7	68.1	4.02
180°C -10 hrs	δt=5	28.6	79.0	4.02
	δt=3	28.7	79.9	4.02
	δt=10	28.3	77.8	4.02

Table 5.4.11d: The effect of varying δt on the prediction of the radius, the inter-precipitate spacing and width of PFZs given by combined model 4.

ageing treatment:	variable: δt (s)	radius of precipitate: (nm)	inter-precipitate spacing: (nm)	width of PFZs: (nm)
160°C -0.5 hr	δt=5	19.5	54.2	0
	δt=3	19.5	54.9	0
	δt=10	19.4	53.4	0
160°C -5.5 hrs	δt=5	63.2	133	0
	δt=3	63.6	134	0
	δt=10	62.6	131	0
160°C -10.5 hrs	δt=5	97.1	199	0
	δt=3	97.5	199	0
	δt=10	96.5	197	0
160°C -20.5 hrs	δt=5	157	316	0
	δt=3	157	317	0
	δt=10	156	315	0
160°C -48 hrs	δt=5	292	585	0
	δt=3	291	584	0
	δt=10	292	585	0
180°C -0.5 hr	δt=5	40.1	91.5	0
	δt=3	40.4	92.8	0
	δt=10	39.6	89.7	0
180°C -1 hr	δt=5	58.2	125	0
	δt=3	58.7	126	0
	δt=10	57.5	123	0
180°C -2 hrs	δt=5	89.6	185	0
	δt=3	90.1	187	0
	δt=10	88.7	183	0
180°C -3 hrs	δt=5	118	241	0
	δt=3	118	242	0
	δt=10	118	242	0
180°C -10 hrs	δt=5	279	560	0
	δt=3	279	561	0
	δt=10	279	561	0

Table 5.4.11e: The effect of varying δt on the prediction of the radius, the inter-precipitate spacing and width of PFZs given by combined model 5.

ageing treatment:	variable: δt (s)	radius of precipitate: (nm)	inter-precpitate spacing: (nm)	width of PFZs: (nm)
160°C -0.5 hr	δt=5	10.7	51.8	55.1
	δt=3	10.7	51.8	55.1
	δt=10	10.7	51.8	55.1
160°C -5.5 hrs	δt=5	16.0	54.2	59.6
	δt=3	16.1	54.7	59.6
	δt=10	16.0	53.5	59.6
160°C -10.5 hrs	δt=5	18.2	57.2	63.7
	δt=3	18.2	57.8	63.7
	δt=10	18.1	56.3	63.7
160°C -20.5 hrs	δt=5	20.9	61.3	71.3
	δt=3	20.9	61.9	71.3
	δt=10	20.8	60.4	71.3
160°C -48 hrs	δt=5	25.3	68.1	88.9
	δt=3	25.0	68.3	88.9
	δt=10	25.2	67.3	88.9
180°C -0.5 hr	δt=5	16.5	63.0	84.8
	δt=3	16.5	63.1	84.8
	δt=10	16.6	62.9	84.8
180°C -1 hr	δt=5	18.6	63.9	87.7
	δt=3	18.6	64.3	87.7
	δt=10	18.6	63.4	87.7
180°C -2 hrs	δt=5	21.0	66.7	93.2
	δt=3	21.1	67.5	93.2
	δt=10	21.0	65.7	93.2
180°C -3 hrs	δt=5	22.8	69.3	98.4
	δt=3	22.9	70.2	98.4
	δt=10	22.7	68.1	98.4
180°C -10 hrs	δt=5	29.5	80.0	129
	δt=3	29.8	81.0	129
	δt=10	29.3	78.8	129

Table 5.4.12a: The effect of varying d_2 on the prediction of the radius, the inter-precipitate spacing and width of PFZs given by combined model 1.

ageing treatment:	variable: d_2 (nm)	radius of precipitate: (nm)	inter-precipitate spacing: (nm)	width of PFZs: (nm)
160°C -0.5 hr	d_2=5	10.7	51.8	0
	d_2=1	10.7	51.8	0
	d_2=10	10.7	51.8	0
160°C -5.5 hrs	d_2=5	16.1	54.7	0
	d_2=1	16.1	54.7	0
	d_2=10	16.1	54.7	0
160°C -10.5 hrs	d_2=5	18.2	57.8	0
	d_2=1	18.2	57.8	0
	d_2=10	18.2	57.8	0
160°C -20.5 hrs	d_2=5	20.9	61.8	0
	d_2=1	20.9	61.8	0
	d_2=10	20.9	61.8	0
160°C -48 hrs	d_2=5	25.0	68.2	0
	d_2=1	25.0	68.2	0
	d_2=10	25.0	68.2	0
180°C -0.5 hr	d_2=5	16.5	63.1	0
	d_2=1	16.5	63.1	0
	d_2=10	16.5	63.1	0
180°C -1 hr	d_2=5	18.6	64.3	0
	d_2=1	18.6	64.3	0
	d_2=10	18.6	64.3	0
180°C -2 hrs	d_2=5	21.1	67.5	0
	d_2=1	21.1	67.5	0
	d_2=10	21.1	67.5	0
180°C -3 hrs	d_2=5	22.9	70.2	0
	d_2=1	22.9	70.2	0
	d_2=10	22.9	70.2	0
180°C -10 hrs	d_2=5	29.8	80.9	0
	d_2=1	29.8	80.9	0
	d_2=10	29.8	80.9	0

Table 5.4.12b: The effect of varying d_2 on the prediction of the radius, the inter-precipitate spacing and width of PFZs given by combined model 2.

ageing treatment:	variable: d_2 (nm)	radius of precipitate: (nm)	inter-precipitate spacing: (nm)	width of PFZs: (nm)
160°C -0.5 hr	d_2=5	26.5	284	5.2
	d_2=1	12.1	66.9	1.2
	d_2=10	62.7	1270	10.2
160°C -5.5 hrs	d_2=5	39.9	288	5.2
	d_2=1	17.6	69.7	1.2
	d_2=10	94.1	1280	10.2
160°C -10.5 hrs	d_2=5	44.8	292	5.2
	d_2=1	18.7	71.8	1.2
	d_2=10	106	1290	10.2
160°C -20.5 hrs	d_2=5	50.8	299	5.2
	d_2=1	19.6	73.8	1.2
	d_2=10	120	1310	10.2
160°C -48 hrs	d_2=5	59.9	309	5.2
	d_2=1	20.0	76.0	1.2
	d_2=10	143	1330	10.2
180°C -0.5 hr	d_2=5	48.7	446	5.2
	d_2=1	18.7	84.2	1.2
	d_2=10	139	2660	10.2
180°C -1 hr	d_2=5	54.8	446	5.2
	d_2=1	20.4	85.0	1.2
	d_2=10	157	2670	10.2
180°C -2 hrs	d_2=5	61.9	448	5.2
	d_2=1	21.7	86.6	1.2
	d_2=10	177	2670	10.2
180°C -3 hrs	d_2=5	66.6	450	5.2
	d_2=1	22.3	87.8	1.2
	d_2=10	191	2680	10.2
180°C -10 hrs	d_2=5	83.8	464	5.2
	d_2=1	23.8	91.8	1.2
	d_2=10	242	2710	10.2

Table 5.4.12c: The effect of varying d_2 on the prediction of the radius, the inter-precipitate spacing and width of PFZs given by combined model 3.

ageing treatment:	variable: d_2 (nm)	radius of precipitate: (nm)	inter-precipitate spacing: (nm)	width of PFZs: (nm)
160°C -0.5 hr	d_2=5	10.7	71.8	54.4
	d_2=1	10.7	51.8	54.4
	d_2=10	10.7	51.8	54.4
160°C -5.5 hrs	d_2=5	16.1	54.7	4.02
	d_2=1	16.1	54.7	4.02
	d_2=10	16.1	54.7	4.02
160°C -10.5 hrs	d_2=5	18.2	57.8	4.02
	d_2=1	18.2	57.8	4.02
	d_2=10	18.2	57.8	4.02
160°C -20.5 hrs	d_2=5	20.9	61.9	4.02
	d_2=1	20.9	61.9	4.02
	d_2=10	20.9	61.9	4.02
160°C -48 hrs	d_2=5	24.8	68.1	4.02
	d_2=1	24.8	68.1	4.02
	d_2=10	24.8	68.1	4.02
180°C -0.5 hr	d_2=5	16.5	63.1	78.0
	d_2=1	16.5	63.1	78.0
	d_2=10	16.5	63.1	78.0
180°C -1 hr	d_2=5	18.6	64.3	64.0
	d_2=1	18.6	64.3	64.0
	d_2=10	18.6	64.3	64.0
180°C -2 hrs	d_2=5	21.1	67.5	40.2
	d_2=1	21.1	67.5	4.02
	d_2=10	21.1	67.5	4.02
180°C -3 hrs	d_2=5	22.9	70.2	4.02
	d_2=1	22.9	70.2	4.02
	d_2=10	22.9	70.2	4.02
180°C -10 hrs	d_2=5	28.7	79.9	4.02
	d_2=1	28.7	79.9	4.02
	d_2=10	28.7	79.9	4.02

Table 5.4.12d: The effect of varying d_2 on the prediction of the radius, the inter-precipitate spacing and width of PFZs given by combined model 4.

ageing treatment:	variable: d_2 (nm)	radius of precipitate: (nm)	inter-precipitate spacing: (nm)	width of PFZs: (nm)
160°C -0.5 hr	d_2=5	19.5	54.9	0
	d_2=1	19.5	54.9	0
	d_2=10	19.5	54.9	0
160°C -5.5 hrs	d_2=5	63.6	134	0
	d_2=1	63.6	134	0
	d_2=10	63.6	134	0
160°C -10.5 hrs	d_2=5	97.5	199	0
	d_2=1	97.5	199	0
	d_2=10	97.5	199	0
160°C -20.5 hrs	d_2=5	157	317	0
	d_2=1	157	317	0
	d_2=10	157	317	0
160°C -48 hrs	d_2=5	291	584	0
	d_2=1	291	584	0
	d_2=10	291	584	0
180°C -0.5 hr	d_2=5	40.4	92.8	0
	d_2=1	40.4	92.8	0
	d_2=10	40.4	92.8	0
180°C -1 hr	d_2=5	58.7	126	0
	d_2=1	58.7	126	0
	d_2=10	58.7	126	0
180°C -2 hrs	d_2=5	90.1	187	0
	d_2=1	90.1	187	0
	d_2=10	90.1	187	0
180°C -3 hrs	d_2=5	118	242	0
	d_2=1	118	242	0
	d_2=10	118	242	0
180°C -10 hrs	d_2=5	279	561	0
	d_2=1	279	561	0
	d_2=10	279	561	0

Table 5.4.12e: The effect of varying d_2 on the prediction of the radius, the inter-precipitate spacing and width of PFZs given by combined model 5.

ageing treatment:	variable: d_2 (nm)	radius of precipitate: (nm)	inter-precipitate spacing: (nm)	width of PFZs: (nm)
160°C -0.5 hr	d_2=5	10.7	71.8	55.1
	d_2=1	10.7	51.8	55.1
	d_2=10	10.7	51.8	55.1
160°C -5.5 hrs	d_2=5	16.1	54.7	59.6
	d_2=1	16.1	54.7	59.6
	d_2=10	16.1	54.7	59.6
160°C -10.5 hrs	d_2=5	18.2	57.8	63.7
	d_2=1	18.2	57.8	63.7
	d_2=10	18.2	57.8	63.7
160°C -20.5 hrs	d_2=5	20.9	61.9	71.3
	d_2=1	20.9	61.9	71.3
	d_2=10	20.9	61.9	71.3
160°C -48 hrs	d_2=5	25.0	68.3	88.9
	d_2=1	25.0	68.3	88.9
	d_2=10	25.0	68.3	88.9
180°C -0.5 hr	d_2=5	16.5	63.1	84.8
	d_2=1	16.5	63.1	84.8
	d_2=10	16.5	63.1	84.8
180°C -1 hr	d_2=5	18.6	64.3	87.7
	d_2=1	18.6	64.3	87.7
	d_2=10	18.6	64.3	87.7
180°C -2 hrs	d_2=5	21.1	67.5	93.2
	d_2=1	21.1	67.5	93.2
	d_2=10	21.1	67.5	93.2
180°C -3 hrs	d_2=5	22.9	70.2	98.4
	d_2=1	22.9	70.2	98.4
	d_2=10	22.9	70.2	98.4
180°C -10 hrs	d_2=5	29.8	81.0	129
	d_2=1	29.8	81.0	129
	d_2=10	29.8	81.0	129

Table 5.4.13a: The effect of varying θ on the prediction of the radius, the inter-precipitate spacing and width of PFZs given by combined model 1.

ageing treatment:	variable: θ (s^{-1})	radius of precipitate: (nm)	inter-precipitate spacing: (nm)	width of PFZs: (nm)
160°C -0.5 hr	θ =0.1	10.7	51.8	0
	θ =1	10.7	51.8	0
	θ =0.01	10.7	51.8	0
160°C -5.5 hrs	θ =0.1	16.1	54.7	0
	θ =1	16.1	54.7	0
	θ =0.01	16.1	54.7	0
160°C -10.5 hrs	θ =0.1	18.2	57.8	0
	θ =1	18.2	57.8	0
	θ =0.01	18.2	57.8	0
160°C -20.5 hrs	θ =0.1	20.9	61.8	0
	θ =1	20.9	61.8	0
	θ =0.01	20.9	61.8	0
160°C -48 hrs	θ =0.1	25.0	68.2	0
	θ =1	25.0	68.2	0
	θ =0.01	25.0	68.2	0
180°C -0.5 hr	θ =0.1	16.5	63.1	0
	θ =1	16.5	63.1	0
	θ =0.01	16.5	63.1	0
180°C -1 hr	θ =0.1	18.6	64.3	0
	θ =1	18.6	64.3	0
	θ =0.01	18.6	64.3	0
180°C -2 hrs	θ =0.1	21.1	67.5	0
	θ =1	21.1	67.5	0
	θ =0.01	21.1	67.5	0
180°C -3 hrs	θ =0.1	22.9	70.2	0
	θ =1	22.9	70.2	0
	θ =0.01	22.9	70.2	0
180°C -10 hrs	θ =0.1	29.8	80.9	0
	θ =1	29.8	80.9	0
	θ =0.01	29.8	80.9	0

Table 5.4.13b: The effect of varying θ on the prediction of the radius, the inter-precipitate spacing and width of PFZs given by combined model 2.

ageing treatment:	variable: θ (s^{-1})	radius of precipitate: (nm)	inter-precipitate spacing: (nm)	width of PFZs: (nm)
160°C -0.5 hr	θ =0.1	10.7	51.8	1.0
	θ =1	12.1	66.9	1.2
	θ =0.01	10.7	51.8	1.0
160°C -5.5 hrs	θ =0.1	15.2	54.2	1.0
	θ =1	17.6	69.7	1.2
	θ =0.01	15.2	54.2	1.0
160°C -10.5 hrs	θ =0.1	16.0	55.9	1.0
	θ =1	18.7	71.8	1.2
	θ =0.01	16.0	55.9	1.0
160°C -20.5 hrs	θ =0.1	16.6	57.4	1.0
	θ =1	19.6	73.8	1.2
	θ =0.01	16.6	57.4	1.0
160°C -48 hrs	θ =0.1	16.7	58.9	1.0
	θ =1	20.0	76.0	1.2
	θ =0.01	16.7	58.9	1.0
180°C -0.5 hr	θ =0.1	16.3	63.1	1.0
	θ =1	18.7	84.2	1.2
	θ =0.01	16.3	63.1	1.0
180°C -1 hr	θ =0.1	17.4	63.9	1.0
	θ =1	20.4	85.0	1.2
	θ =0.01	17.4	63.9	1.0
180°C -2 hrs	θ =0.1	18.2	65.4	1.0
	θ =1	21.7	86.6	1.2
	θ =0.01	18.2	65.4	1.0
180°C -3 hrs	θ =0.1	18.6	66.4	1.0
	θ =1	22.3	87.8	1.2
	θ =0.01	18.6	66.4	1.0
180°C -10 hrs	θ =0.1	19.5	69.2	1.0
	θ =1	23.8	91.8	1.2
	θ =0.01	19.5	69.2	1.0

Table 5.4.13c: The effect of varying θ on the prediction of the radius, the inter-precipitate spacing and width of PFZs given by combined model 3.

ageing treatment:	variable: θ (s^{-1})	radius of precipitate: (nm)	inter-precpitate spacing: (nm)	width of PFZs: (nm)
160°C -0.5 hr	θ =0.1	10.7	51.8	173
	θ =1	10.7	51.8	54.4
	θ =0.01	10.7	51.8	547
160°C -5.5 hrs.	θ =0.1	16.1	54.7	171
	θ =1	16.1	54.7	4.02
	θ =0.01	16.1	54.7	547
160°C -10.5 hrs	θ =0.1	18.2	57.8	162
	θ =1	18.2	57.8	4.02
	θ =0.01	18.2	57.8	547
160°C -20.5 hrs	θ =0.1	20.9	61.9	127
	θ =1	20.9	61.9	4.02
	θ =0.01	20.9	61.9	547
160°C -48 hrs	θ =0.1	25.0	68.3	123
	θ =1	24.8	68.1	4.02
	θ =0.01	25.0	68.3	543
180°C -0.5 hr	θ =0.1	16.5	63.1	259
	θ =1	16.5	63.1	78.0
	θ =0.01	16.5	63.1	819
180°C -1 hr	θ =0.1	18.6	64.3	259
	θ =1	18.6	64.3	64.0
	θ =0.01	18.6	64.3	819
180°C -2 hrs	θ =0.1	21.1	67.5	259
	θ =1	21.1	67.5	4.02
	θ =0.01	21.1	67.5	819
180°C -3 hrs	θ =0.1	22.9	70.2	256
	θ =1	22.9	70.2	4.02
	θ =0.01	22.9	70.2	819
180°C -10 hrs	θ =0.1	29.8	81.0	202
	θ =1	28.7	79.9	4.02
	θ =0.01	29.8	81.0	819

Table 5.4.13d: The effect of varying θ on the prediction of the radius, the inter-precipitate spacing and width of PFZs given by combined model 4.

ageing treatment:	variable: θ (s^{-1})	radius of precipitate: (nm)	inter-precipitate spacing: (nm)	width of PFZs: (nm)
160°C -0.5 hr	θ =0.1	13.3	51.8	0
	θ =1	19.5	54.9	0
	θ =0.01	9.18	51.8	0
160°C -5.5 hrs	θ =0.1	34.0	79.9	0
	θ =1	63.6	134	0
	θ =0.01	20.7	59.6	0
160°C -10.5 hrs	θ =0.1	48.2	105	0
	θ =1	97.5	199	0
	θ =0.01	27.2	69.5	0
160°C -20.5 hrs	θ =0.1	72.8	152	0
	θ =1	157	317	0
	θ =0.01	37.5	86.9	0
160°C -48 hrs	θ =0.1	133	270	0
	θ =1	291	584	0
	θ =0.01	60.5	129	0
180°C -0.5 hr	θ =0.1	25.0	68.8	0
	θ =1	40.4	92.8	0
	θ =0.01	16.9	63.0	0
180°C -1 hr	θ =0.1	33.3	82.0	0
	θ =1	58.7	126	0
	θ =0.01	21.4	66.1	0
180°C -2 hrs	θ =0.1	46.8	106	0
	θ =1	90.1	187	0
	θ =0.01	27.9	75.4	0
180°C -3 hrs	θ =0.1	58.7	128	0
	θ =1	118	242	0
	θ =0.01	33.2	83.8	0
180°C -10 hrs	θ =0.1	130	266	0
	θ =1	279	561	0
	θ =0.01	61.9	134	0

Table 5.4.13e: The effect of varying θ on the prediction of the radius, the inter-precipitate spacing and width of PFZs given by combined model 5.

ageing treatment:	variable: θ (s^{-1})	radius of precipitate: (nm)	inter-precpitate spacing: (nm)	width of PFZs: (nm)
160°C -0.5 hr	θ =0.1	10.7	51.8	173
	θ =1	10.7	51.8	55.1
	θ =0.01	10.7	51.8	547
160°C -5.5 hrs	θ =0.1	16.1	54.7	174
	θ =1	16.1	54.7	59.6
	θ =0.01	16.1	54.7	547
160°C -10.5 hrs	θ =0.1	18.2	57.8	176
	θ =1	18.2	57.8	63.7
	θ =0.01	18.2	57.8	548
160°C -20.5 hrs	θ =0.1	20.9	61.9	179
	θ =1	20.9	61.9	71.3
	θ =0.01	20.9	61.9	549
160°C -48 hrs	θ =0.1	25.0	68.3	186
	θ =1	25.0	68.3	88.9
	θ =0.01	25.0	68.3	552
180°C -0.5 hr	θ =0.1	16.5	63.1	260
	θ =1	16.5	63.1	84.8
	θ =0.01	16.5	63.1	819
180°C -1 hr	θ =0.1	18.6	64.3	261
	θ =1	18.6	64.3	87.7
	θ =0.01	18.6	64.3	819
180°C -2 hrs	θ =0.1	21.1	67.5	263
	θ =1	21.1	67.5	93.2
	θ =0.01	21.1	67.5	820
180°C -3 hrs	θ =0.1	22.9	70.2	265
	θ =1	22.9	70.2	98.4
	θ =0.01	22.9	70.2	820
180°C -10 hrs	θ =0.1	29.8	81.0	277
	θ =1	29.8	81.0	129
	θ =0.01	29.8	81.0	825

Table 5.4.14a: The effect of varying ψ on the prediction of the radius, the inter-precipitate spacing and width of PFZs given by combined model 1.

ageing treatment:	variable: ψ (°)	radius of precipitate: (nm)	inter-precipitate spacing: (nm)	width of PFZs: (nm)
160°C -0.5 hr	ψ=45.0	7.72	31.3	0
	ψ=46.25	10.7	51.8	0
	ψ=47.5	15.1	88.6	0
160°C -5.5 hrs	ψ=45.0	11.5	31.5	0
	ψ=46.25	16.1	54.7	0
	ψ=47.5	22.8	93.3	0
160°C -10.5 hrs	ψ=45.0	12.9	33.5	0
	ψ=46.25	18.2	57.8	0
	ψ=47.5	25.7	97.1	0
160°C -20.5 hrs	ψ=45.0	14.8	36.7	0
	ψ=46.25	20.9	61.8	0
	ψ=47.5	29.2	102	0
160°C -48 hrs	ψ=45.0	18.0	42.2	0
	ψ=46.25	25.0	68.2	0
	ψ=47.5	34.5	110	0
180°C -0.5 hr	ψ=45.0	11.8	37.3	0
	ψ=46.25	16.5	63.1	0
	ψ=47.5	23.6	110	0
180°C -1 hr	ψ=45.0	13.2	37.5	0
	ψ=46.25	18.6	64.3	0
	ψ=47.5	26.6	111	0
180°C -2 hrs	ψ=45.0	14.9	39.5	0
	ψ=46.25	21.1	67.5	0
	ψ=47.5	30.0	115	0
180°C -3 hrs	ψ=45.0	16.2	41.7	0
	ψ=46.25	22.9	70.2	0
	ψ=47.5	32.4	118	0
180°C -10 hrs	ψ=45.0	21.6	50.9	0
	ψ=46.25	29.8	80.9	0
	ψ=47.5	41.4	131	0

Table 5.4.14b: The effect of varying ψ on the prediction of the radius, the inter-precipitate spacing and width of PFZs given by combined model 2.

ageing treatment:	variable: ψ (°)	radius of precipitate: (nm)	inter-precipitate spacing: (nm)	width of PFZs: (nm)
160°C -0.5 hr	ψ=45.2	8.61	39.5	1.2
	ψ=47.2	12.1	66.9	1.2
	ψ=49.2	17.4	117	1.2
160°C -5.5 hrs	ψ=45.2	12.4	40.0	1.2
	ψ=47.2	17.6	69.7	1.2
	ψ=49.2	25.3	122	1.2
160°C -10.5 hrs	ψ=45.2	13.1	41.1	1.2
	ψ=47.2	18.7	71.8	1.2
	ψ=49.2	26.8	125	1.2
160°C -20.5 hrs	ψ=45.2	13.7	42.3	1.2
	ψ=47.2	19.6	73.8	1.2
	ψ=49.2	28.0	128	1.2
160°C -48 hrs	ψ=45.2	14.0	43.6	1.2
	ψ=47.2	20.0	76.0	1.2
	ψ=49.2	28.6	131	1.2
180°C -0.5 hr	ψ=45.2	13.1	48.5	1.2
	ψ=47.2	18.7	84.2	1.2
	ψ=49.2	27.3	151	1.2
180°C -1 hr	ψ=45.2	14.3	48.7	1.2
	ψ=47.2	20.4	85.0	1.2
	ψ=49.2	29.8	152	1.2
180°C -2 hrs	ψ=45.2	15.2	49.5	1.2
	ψ=47.2	21.7	86.6	1.2
	ψ=49.2	31.6	154	1.2
180°C -3 hrs	ψ=45.2	15.6	50.2	1.2
	ψ=47.2	22.3	87.8	1.2
	ψ=49.2	32.4	155	1.2
180°C -10 hrs	ψ=45.2	16.6	52.7	1.2
	ψ=47.2	23.8	91.8	1.2
	ψ=49.2	34.4	161	1.2

Table 5.4.14c: The effect of varying ψ on the prediction of the radius, the inter-precipitate spacing and width of PFZs given by combined model 3.

ageing treatment:	variable: ψ (°)	radius of precipitate: (nm)	inter-precpitate spacing: (nm)	width of PFZs: (nm)
160°C -0.5 hr	ψ=45.0	7.72	31.3	54.4
	ψ=46.25	10.7	51.8	54.4
	ψ=47.5	15.1	88.6	54.4
160°C -5.5 hrs	ψ=45.0	11.5	31.5	4.02
	ψ=46.25	16.1	54.7	4.02
	ψ=47.5	22.8	93.3	4.02
160°C -10.5 hrs	ψ=45.0	12.9	33.5	4.02
	ψ=46.25	18.2	57.8	4.02
	ψ=47.5	25.7	97.2	4.02
160°C -20.5 hrs	ψ=45.0	14.9	36.8	4.02
	ψ=46.25	20.9	61.9	4.02
	ψ=47.5	29.3	102	4.02
160°C -48 hrs	ψ=45.0	17.8	41.9	4.02
	ψ=46.25	24.8	68.1	4.02
	ψ=47.5	34.2	110	4.02
180°C -0.5 hr	ψ=45.0	11.8	37.3	78.0
	ψ=46.25	16.5	63.1	78.0
	ψ=47.5	23.6	110	78.0
180°C -1 hr	ψ=45.0	13.2	37.5	64.0
	ψ=46.25	18.6	64.3	64.0
	ψ=47.5	26.6	111	64.0
180°C -2 hrs	ψ=45.0	15.0	39.6	40.2
	ψ=46.25	21.1	67.5	4.02
	ψ=47.5	30.1	115	4.02
180°C -3 hrs	ψ=45.0	16.2	41.7	4.02
	ψ=46.25	22.9	70.2	4.02
	ψ=47.5	32.5	118	4.02
180°C -10 hrs	ψ=45.0	20.8	49.7	4.02
	ψ=46.25	28.7	79.9	4.02
	ψ=47.5	40.0	130	4.02

Table 5.4.14d: The effect of varying ψ on the prediction of the radius, the inter-precipitate spacing and width of PFZs given by combined model 4.

ageing treatment:	variable: ψ (°)	radius of precipitate: (nm)	inter-precipitate spacing: (nm)	width of PFZs: (nm)
160°C -0.5 hr	ψ=45.0	14.1	33.5	0
	ψ=46.25	19.5	54.9	0
	ψ=47.5	27.5	91.6	0
160°C -5.5 hrs	ψ=45.0	53.4	109	0
	ψ=46.25	63.6	134	0
	ψ=47.5	78.9	175	0
160°C -10.5 hrs	ψ=45.0	86.9	175	0
	ψ=46.25	97.5	199	0
	ψ=47.5	114	242	0
160°C -20.5 hrs	ψ=45.0	147	295	0
	ψ=46.25	157	317	0
	ψ=47.5	175	358	0
160°C -48 hrs	ψ=45.0	285	571	0
	ψ=46.25	291	584	0
	ψ=47.5	306	618	0
180°C -0.5 hr	ψ=45.0	31.0	65.8	0
	ψ=46.25	40.4	92.8	0
	ψ=47.5	54.6	138	0
180°C -1 hr	ψ=45.0	47.8	98.3	0
	ψ=46.25	58.7	126	0
	ψ=47.5	75.5	174	0
180°C -2 hrs	ψ=45.0	78.3	158	0
	ψ=46.25	90.1	187	0
	ψ=47.5	109	236	0
180°C -3 hrs	ψ=45.0	107	214	0
	ψ=46.25	118	242	0
	ψ=47.5	139	292	0
180°C -10 hrs	ψ=45.0	271	542	0
	ψ=46.25	279	561	0
	ψ=47.5	299	606	0

Table 5.4.14e: The effect of varying ψ on the prediction of the radius, the inter-precipitate spacing and width of PFZs given by combined model 5.

ageing treatment:	variable: ψ (°)	radius of precipitate: (nm)	inter-precpitate spacing: (nm)	width of PFZs: (nm)
160°C -0.5 hr	ψ=45.0	7.72	31.3	55.1
	ψ=46.25	10.7	51.8	55.1
	ψ=47.5	15.1	88.6	55.1
160°C -5.5 hrs	ψ=45.0	11.5	31.5	59.6
	ψ=46.25	16.1	54.7	59.6
	ψ=47.5	22.8	93.3	59.6
160°C -10.5 hrs	ψ=45.0	12.9	33.5	63.7
	ψ=46.25	18.2	57.8	63.7
	ψ=47.5	25.7	97.2	63.7
160°C -20.5 hrs	ψ=45.0	14.9	36.8	71.3
	ψ=46.25	20.9	61.9	71.3
	ψ=47.5	29.3	102	71.3
160°C -48 hrs	ψ=45.0	18.0	42.3	88.9
	ψ=46.25	25.0	68.3	88.9
	ψ=47.5	34.6	110	88.9
180°C -0.5 hr	ψ=45.0	11.8	37.3	84.8
	ψ=46.25	16.5	63.1	84.8
	ψ=47.5	23.6	110	84.8
180°C -1 hr	ψ=45.0	13.2	37.5	87.7
	ψ=46.25	18.6	64.3	87.7
	ψ=47.5	26.6	111	87.7
180°C -2 hrs	ψ=45.0	15.0	39.6	93.2
	ψ=46.25	21.1	67.5	93.2
	ψ=47.5	30.1	115	93.2
180°C -3 hrs	ψ=45.0	16.2	41.7	98.4
	ψ=46.25	22.9	70.2	98.4
	ψ=47.5	32.5	118	98.4
180°C -10 hrs	ψ=45.0	21.6	51.0	129
	ψ=46.25	29.8	81.0	129
	ψ=47.5	41.5	131	129

Table 5.4.15a: The effect of varying T_i on the prediction of the radius, the inter-precipitate spacing and width of PFZs given by combined model 1.

ageing treatment:	variable: T_i (nm)	radius of precipitate: (nm)	inter-precipitate spacing: (nm)	width of PFZs: (nm)
160°C -0.5 hr	T_i=763	15.3	104	0
	T_i=748	10.7	51.8	0
	T_i=733	8.11	29.5	0
160°C -5.5 hrs	T_i=763	22.9	107	0
	T_i=748	16.1	54.7	0
	T_i=733	12.4	33.4	0
160°C -10.5 hrs	T_i=763	25.7	110	0
	T_i=748	18.2	57.8	0
	T_i=733	14.4	36.6	0
160°C -20.5 hrs	T_i=763	29.1	114	0
	T_i=748	20.9	61.8	0
	T_i=733	17.0	40.9	0
160°C -48 hrs	T_i=763	34.1	121	0
	T_i=748	25.0	68.2	0
	T_i=733	21.1	48.4	0
180°C -0.5 hr	T_i=763	25.2	139	0
	T_i=748	16.5	63.1	0
	T_i=733	12.0	34.1	0
180°C -1 hr	T_i=763	28.3	140	0
	T_i=748	18.6	64.3	0
	T_i=733	13.7	36.6	0
180°C -2 hrs	T_i=763	31.9	142	0
	T_i=748	21.1	67.5	0
	T_i=733	15.9	40.3	0
180°C -3 hrs	T_i=763	34.2	144	0
	T_i=748	22.9	70.2	0
	T_i=733	17.6	43.1	0
180°C -10 hrs	T_i=763	42.9	155	0
	T_i=748	29.8	80.9	0
	T_i=733	23.9	54.7	0

Table 5.4.15b: The effect of varying T_i on the prediction of the radius, the inter-precipitate spacing and width of PFZs given by combined model 2.

ageing treatment:	variable: T_i (nm)	radius of precipitate: (nm)	inter-precipitate spacing: (nm)	width of PFZs: (nm)
160°C -0.5 hr	T_i=763	15.3	104	1.2
	T_i=748	12.1	66.9	1.2
	T_i=733	9.51	40.9	1.2
160°C -5.5 hrs	T_i=763	21.7	106	1.2
	T_i=748	17.6	69.7	1.2
	T_i=733	13.7	44.3	1.2
160°C -10.5 hrs	T_i=763	22.7	108	1.2
	T_i=748	18.7	71.8	1.2
	T_i=733	14.5	46.0	1.2
160°C -20.5 hrs	T_i=763	23.5	111	1.2
	T_i=748	19.6	73.8	1.2
	T_i=733	15.0	47.3	1.2
160°C -48 hrs	T_i=763	23.5	113	1.2
	T_i=748	20.0	76.0	1.2
	T_i=733	15.0	48.3	1.2
180°C -0.5 hr	T_i=763	24.9	139	1.2
	T_i=748	18.7	84.2	1.2
	T_i=733	14.3	48.8	1.2
180°C -1 hr	T_i=763	26.6	140	1.2
	T_i=748	20.4	85.0	1.2
	T_i=733	15.3	50.1	1.2
180°C -2 hrs	T_i=763	27.7	141	1.2
	T_i=748	21.7	86.6	1.2
	T_i=733	16.2	51.9	1.2
180°C -3 hrs	T_i=763	28.2	142	1.2
	T_i=748	22.3	87.8	1.2
	T_i=733	16.4	53.0	1.2
180°C -10 hrs	T_i=763	29.2	146	1.2
	T_i=748	23.8	91.8	1.2
	T_i=733	17.1	55.2	1.2

Table 5.4.15c: The effect of varying T_i on the prediction of the radius, the inter-precipitate spacing and width of PFZs given by combined model 3.

ageing treatment:	variable: T_i (nm)	radius of precipitate: (nm)	inter-precipitate spacing: (nm)	width of PFZs: (nm)
160°C -0.5 hr	T_i=763	15.3	104	44.9
	T_i=748	10.7	51.8	54.4
	T_i=733	8.11	29.5	65.2
160°C -5.5 hrs	T_i=763	22.9	107	4.46
	T_i=748	16.1	54.7	4.02
	T_i=733	12.4	33.4	3.64
160°C -10.5 hrs	T_i=763	25.7	110	4.46
	T_i=748	18.2	57.8	4.02
	T_i=733	14.4	36.6	3.64
160°C -20.5 hrs	T_i=763	29.1	114	4.46
	T_i=748	20.9	61.9	4.02
	T_i=733	17.0	40.9	3.64
160°C -48 hrs	T_i=763	34.1	121	4.46
	T_i=748	24.8	68.1	4.02
	T_i=733	21.1	48.4	3.64
180°C -0.5 hr	T_i=763	25.2	139	60.5
	T_i=748	16.5	63.1	78.0
	T_i=733	12.0	34.1	96.4
180°C -1 hr	T_i=763	28.3	140	32.5
	T_i=748	18.6	64.3	64.0
	T_i=733	13.7	36.6	88.4
180°C -2 hrs	T_i=763	31.9	142	4.46
	T_i=748	21.1	67.5	4.02
	T_i=733	15.9	40.3	55.6
180°C -3 hrs	T_i=763	34.2	144	4.46
	T_i=748	22.9	70.2	4.02
	T_i=733	17.6	43.1	3.64
180°C -10 hrs	T_i=763	42.9	155	4.46
	T_i=748	28.7	79.9	4.02
	T_i=733	23.9	54.7	3.64

Table 5.4.15d: The effect of varying T_i on the prediction of the radius, the inter-precipitate spacing and width of PFZs given by combined model 4.

ageing treatment:	variable: T_i (nm)	radius of precipitate: (nm)	inter-precipitate spacing: (nm)	width of PFZs: (nm)
160°C -0.5 hr	T_i=763	29.4	106	0
	T_i=748	19.5	54.9	0
	T_i=733	14.0	33.9	0
160°C -5.5 hrs	T_i=763	78.8	181	0
	T_i=748	63.6	134	0
	T_i=733	56.0	114	0
160°C -10.5 hrs	T_i=763	111	239	0
	T_i=748	97.5	199	0
	T_i=733	92.3	186	0
160°C -20.5 hrs	T_i=763	162	336	0
	T_i=748	157	317	0
	T_i=733	159	319	0
160°C -48 hrs	T_i=763	268	544	0
	T_i=748	291	584	0
	T_i=733	317	635	0
180°C -0.5 hr	T_i=763	59.7	162	0
	T_i=748	40.4	92.8	0
	T_i=733	31.0	65.5	0
180°C -1 hr	T_i=763	80.2	192	0
	T_i=748	58.7	126	0
	T_i=733	48.7	100	0
180°C -2 hrs	T_i=763	112	251	0
	T_i=748	90.1	187	0
	T_i=733	81.6	165	0
180°C -3 hrs	T_i=763	138	300	0
	T_i=748	118	242	0
	T_i=733	112	226	0
180°C -10 hrs	T_i=763	272	558	0
	T_i=748	279	561	0
	T_i=733	299	599	0

Table 5.4.15e: The effect of varying T_i on the prediction of the radius, the inter-precipitate spacing and width of PFZs given by combined model 5.

ageing treatment:	variable: T_i (nm)	radius of precipitate: (nm)	inter-precipitate spacing: (nm)	width of PFZs: (nm)
160°C -0.5 hr	T_i=763	15.3	104	46.5
	T_i=748	10.7	51.8	55.1
	T_i=733	8.11	29.5	65.4
160°C -5.5 hrs	T_i=763	22.9	107	52.0
	T_i=748	16.1	54.7	59.6
	T_i=733	12.4	33.4	69.1
160°C -10.5 hrs	T_i=763	25.7	110	56.9
	T_i=748	18.2	57.8	63.7
	T_i=733	14.4	36.6	72.6
160°C -20.5 hrs	T_i=763	29.1	114	65.7
	T_i=748	20.9	61.8	71.3
	T_i=733	17.0	40.9	79.1
160°C -48 hrs	T_i=763	34.1	121	85.3
	T_i=748	25.0	68.2	88.9
	T_i=733	21.1	48.4	94.7
180°C -0.5 hr	T_i=763	25.2	139	71.8
	T_i=748	16.5	63.1	84.8
	T_i=733	12.0	34.1	100
180°C -1 hr	T_i=763	28.3	140	75.4
	T_i=748	18.6	64.3	87.7
	T_i=733	13.7	36.6	103
180°C -2 hrs	T_i=763	31.9	142	81.9
	T_i=748	21.1	67.5	93.2
	T_i=733	15.9	40.3	107
180°C -3 hrs	T_i=763	34.2	144	88.0
	T_i=748	22.9	70.2	98.4
	T_i=733	17.6	43.1	112
180°C -10 hrs	T_i=763	42.9	155	122
	T_i=748	29.8	80.9	129
	T_i=733	23.9	54.7	139

Chapter Six

Discussion

6.1 *The parameters needed for prediction*

The parameters that the combined models need to predict the size, the distribution of the grain boundary precipitates and the widths of the precipitate-free zones as a function of heat-treatment are listed as follows:

a: lattice parameter of matrix phase,

a_b: entropy term for the calculation of the grain-boundary diffusion coefficient of the solute element,

a_c: entropy term for the calculation of the diffusion coefficient of the impurity-vacancy complexes,

a_I: entropy term for the calculation of the volume diffusion coefficient of the solute element,

c: entropy-connected term of solute in the solubility product equation,

C_c: concentration of the non-rate controlling element (in this case is Zn) participating in the precipitation reaction,

C_g: concentration of the impurity in the matrix phase (in this case is Mg)

d: mean diameter of the grains, d = 5000 nm,

d_0: width of grain boundary within which the solute diffusion is interfacial diffusion controlling, d_0=0.1 nm,

d_1: the width of the boundary, d_1=0.25 nm,

E_b: vacancy-impurity binding energy,

E_f: energy needed to form a vacancy,

Q_b: activation energy term for the calculation of the grain-boundary diffusion coefficient of the solute element,

Q_c: activation energy term for the calculation of the diffusion coefficient of the impurity-vacancy complex,

Q_I: activation energy term for the calculation of the volume diffusion coefficient of the solute element,

r: radius of the curvature of the precipitate at the advancing interface,

T: ageing treatment temperature,

T_i: solution treatment temperature,

T_m: melting temperature of the alloy,

T_{mp}: the temperature at which most segregation will have been completed, $T_{mp} = 0.6T_m$,

T_{nuc}: temperature of the environment where nucleation takes place,

V_θ: molar volume of the precipitate phase,

δt: time interval,

Δ: effective time interval,

ΔH: enthalpy term of solute in the solubility product equation,

d_2: width of solute concentrated layer given by Xu & Song's non-equilibrium segregation model,

θ: the cooling rate parameter,

ρ_α: molar density of matrix phase,

ρ_θ: molar density of precipitate phase,

$\sigma_{\alpha\alpha}$: grain boundary energy,

$\sigma_{\alpha\theta}$: matrix/nucleus interfacial energy,

Ω: molar volume of the matrix phase,

ψ: the angle where $\cos\psi = \sigma_{\alpha\alpha} / 2\sigma_{\alpha\theta}$,

ς: numerical factor.

Except for T_{nuc} and T, the data of these parameters and the corresponding references have been given in Table 5.1.1, in chapter 5.

d_0 is the thickness of the grain boundary within which the diffusion of the solute atoms is grain boundary diffusion controlling. Normally it is taken as 0.1 nm.

Q_b is the diffusion activation energy of the solute atoms at grain boundaries. Q_b is assumed as having a value $Q_b = \frac{2Q_I}{3}$ where Q_I is the activation energy term for the calculation of the volume diffusion coefficient of solute atoms.

a_b is the entropy term for the calculation of the grain-boundary diffusion coefficient of the solute element. a_b is assumed to be the same as a_s, the entropy term for the calculation of the self-diffusion coefficient of the matrix atom in matrix phase.

r is the radius of the curvature of the precipitate at the advancing interface. r is assumed having a value of 10^{-5} m. This is because r has little influence on the modelling results unless $r \leq 10^{-7} m$.

T_{mp} is the temperature at which most segregation have been completed, $T_{mp} = 0.6T_m$ where T_m is the melting point of the alloy. The temperature, T_{mp}, is chosen in this way because it is assumed that very little diffusion will occur below T_{mp}.

d_2 is the width of the solute concentrated layer and d_2 is taken as 1 nm according to Xu and Song's work[71].

δt is the time interval, by bringing in it into the modelling, the solute concentration term, the mean collector plate area and the mean radius of the precipitate so on change with time in increments of δt. The smaller δt is, the closer of the change along the stepped curves to real situation of the continual change with time but the longer the time needed for running the computer programme.

The vibration entropy, a_c and the activation energy, Q_c for the calculation of the diffusion coefficient of the vacancy-impurity complex are taken from reference[102]. Further analysis reveals that the activation energy for the diffusion of the vacancy-impurity complex has a value which is the activation energy for the diffusion of the impurity *minus* the binding energy between the impurity and the vacancy. The vibration entropy remains the same as that for the diffusion of the impurity. By combining with vacancies to form vacancy-impurity complexes, the impurity atoms are dragged by the vacancies during diffusion and the diffusion of the impurity atoms becomes easier. Such effect could be presented as the reduction in the diffusion activation energy by a value of binding energy.

c is the entropy-connected term of the solute in the solubility product equation. The derivation of c is as follows.

At solvus temperature of η' phase, T_s=250°C, we have

$$\ln[(C_g)^{\ddagger}\cdot(C_c)]=-\frac{\Delta H}{RT_s}+\frac{\Delta S}{R} \qquad (6.1.1)$$

$$c=\frac{\Delta S}{R}=\ln[(C_g)^{\ddagger}\cdot(C_c)]+\frac{\Delta H}{RT_s} \qquad (6.1.2)$$

inserting the data for C_g, C_c, ΔH and T_s gives c = -1.365

Finding the data for $\sigma_{\alpha\alpha}$ and ψ is normally difficult. In this work ψ is based on the experimental observation. The sensitivity analysis of the combined models shows that ψ is a very sensitive factor to the combined models. 3% variation of ψ will cause the prediction of the grain boundary precipitate size and distribution to change about 25%.

T, the ageing treatment temperature; T_i, the solution treatment temperature and T_{nuc}, the temperature of the environment where nucleation takes place, depend on the heat treatment conditions. In this work all the samples are subjected to the solution treatment on 475±5 °C for 20 - 30 minutes, cold water quenching to room temperature, followed by ageing treatment at a chosen ageing temperature. It is assumed that the quenching is so fast that no nucleation of the precipitates occurs at the grain boundary and nucleation only takes place at the ageing temperature, $T_{nuc} = T$.

6.2 *Combined models and their limitations*

Before combined models, simple precipitation models were developed by other people[94-99]. From the modelling of the precipitation behaviour of $AlCu_2$ in Al-Cu alloy carried by Aaron and Aaronson in 1969[98] to the modelling of carbide precipitation in steel by Carolan and Faulkner in 1981[99], the simple precipitation kinetics has been well developed. Carolan and Faulkner's model has been used in predicting the precipitation behaviour of $MgZn_2$ in 7xxx aluminium alloys. Very bad predictions were given. The predicted precipitate growth rate was much smaller than the experimental results[101]. The fact of the failure of the simple precipitation model in this case led the modelling work to the direction of the construction of a combined model in which the segregation influence on the precipitate nucleation and growth is taken into account. This is because the accumulation of the solute atoms caused by segregation influences precipitation nucleation by altering the driving force for the nucleation. The nucleation has a strong effect on the density of grain boundary precipitates. Besides, such accumulation of the solute atoms can affect the precipitate growth rate by introducing an additional flux of solute atoms.

The combined model is created in which the kinetics of the segregation of the solute atoms, the nucleation of the grain boundary precipitates, the precipitate growth and coarsening are taken into account and the model will predict the state of the grain boundary and its environment as a function of heat treatment. In **chapter 3** the details of the combined model are given. Five combined models have been created. Among them the combined models 1, 2, 3 and 5 are generated by combining precipitate nucleation and growth with the segregation described by four different segregation models. Combined model 4 is created by using the same segregation model as that for combined model 1 but with a different analysis approach. The comparisons of the theoretical predictions with the experimental results of $MgZn_2$ grain boundary precipitation and widths of precipitate-free zones in 7150 aluminium alloy after water quenching from solution treatment temperature to room temperature then ageing at 160°C or 180°C are given in Chapter 5.

In Chapter 5, Figs .5.3.1a, c, e and 5.3.2a, c, e show that the combined models 1, 3 and 5 give the predictions of the radius and the inter-precipitate spacing of grain boundary precipitates as a function of ageing time for ageing temperatures 160°C and 180°C; the predictions are well in line with the experimental results. In Figs. 5.3.3a.-5.3.3e only the curve "WPFZ-model3" shows that the trend of the change of width PFZs with ageing time is in good agreement with that of the experimental results. The experimental results and the predictions given by combined model 3 present that the widths of PFZs decrease with the increase in ageing time. Among these five combined models, therefore, combined model 3 is the best one. Combined models 2 and 4 give the predictions which do not agree with the experimental results. The reason for the failure of the models in prediction may be brought about by the limitations of the models which are the combined effects of the limitations in various components such as segregation, precipitate nucleation and growth, and precipitate-free zone formation.

6.2.1 *The component of segregation*

The discussion starts from combined model 4. In combined model 4, the segregation is described by Faulkner's segregation model[70] and the relationship of the segregation concentration is given by Equation (2.1.15) for the segregation process and Equation (2.1.17) for de-segregation process respectively. From further study we have found that although the relationship described by Equation (2.1.15) gives a good description of the trend in which solute atoms are drawn to and concentrated at the grain boundary and the area adjacent to the grain boundary, it does not represent the real kinetic relation during the segregation process of non-equilibrium segregation. According to this relationship, the average concentration of the solute in the whole area of the grain becomes bigger than that decided by the composition of the alloy during the whole segregation process. This is unreasonable. Consequently, combined model 4 is not suitable for predicting the precipitate growth and width of PFZs.

Good predictions of the precipitate growth and inter-particle spacing are given by combined model 1 which uses the same segregation model as that used by combined model 4. In the combined model 1, the solute concentration term used for the calculation of the growth rate of the precipitates is taken as the average concentration of the solute within the area from the boundary to a mean diffusion distance given by $\sqrt{2D_l t}$. For the material and heat-treatment conditions used in this work, $\sqrt{2D_l t} << 2\sqrt{D_{ci} t_{eff}}$. According to Equation (2.1.15), in the area very close to the boundary, for instance, $\delta l << 2\sqrt{D_{ci} t_{eff}}$ the concentration given by such relationship is approximately equal to the maximum segregation concentration given by the thermodynamic relationship of the segregation (see Equation 2.1.8). Therefore, the concentration term calculated by using the concentration profile described by Faulkner's model could be very close to the real situation and this

could explain why combined model 1 gives a good prediction of precipitate growth for this work.

In combined model 2, the segregation component is described by Xu & Song's segregation model[71] and the relationship of the segregation concentration is given by Equations (2.1.18) and (2.1.24). In combined model 2, d_2 which is the width of the solute concentrated layer, is an important and sensitive factor for predicting the growth of the precipitates and the width of PFZs. A different d_2 gives a different concentration profile and this in turn affects the grain boundary precipitate nucleation and growth. In Xu and Song's treatment, d_2 is assumed to be the width of 3 atomic layers. This assumption may not agree with the real situation as the spatial extent of the segregate redistribution may extend to hundreds of atomic layers for non-equilibrium segregation depending on heat treatment conditions. A real value for d_2 can be obtained from the experimental measurement. But such measurement needs very high technology and may be very difficult and inaccurate. As a result, combined model 2 can not give good predictions of the precipitate growth and PFZ width.

In combined model 5, the segregation component is given by the new generated numerical segregation model described in **Section 3.1.1.** This model gives a time-dependence of the width of the solute concentrated layer (SCL) where the solute concentration is C_b given by Equation (2.1.8). In terms of this model, in the solute depleted layer (SDL), which is the area adjacent to the solute concentrated layer, the concentration is linear with the distance from the SCL/SDL interface. The width of this layer and the slope of concentration-distance line both are time-dependent. Using this segregation model, combined model 5 gives a good prediction of the grain boundary precipitate growth but it fails to predict the width of PFZs. Further study of this segregation model shows that this segregation model may not be suitable for the case in which the materials are aged at a temperature

lower than t_{mp} after being quenched from solution treatment temperature. This is because the thermodynamic relationship of segregation (see Equation 2.1.8) may become unsuitable in this case even before the critical time when de-segregation begins. In fact, during ageing at a temperature lower than t_{mp}, the width of the SCL will stop increasing with ageing time. The diffusion of impurity-vacancy complexes down the concentration gradients between the grain centre and the SCL/SDL interface created during quench brings the solute atoms towards the grain boundaries. Such arriving solute atoms from the grain centre will stay in the vicinity of the SCL to relieve the depletion situation of the solute in this area. Consequently, the unsuitability of the segregation model used by combined model 5 for ageing at a temperature lower than t_{mp} is a major reason for the failure in predicting the width of PFZs.

In combined model 3, the segregation component is given by the new generated numerical-analytical segregation model described in **Section 3.1.2.** This segregation model is established by artificially distinguishing the situation during ageing from that during quenching and predicts the solute concentration profile during the quenching and during ageing separately. The reason for this is that the thermodynamic relationship of segregation (see Equation 2.1.8) may become unsuitable when the material is aged at a temperature lower than t_{mp} after being quenched from solution treatment temperature. During ageing, instead of supporting the increase in the width of the solute concentrated layer, the solute atoms brought towards grain boundaries by the diffusion of impurity-vacancy complexes stay in the vicinity of the SCL to relieve the depletion situation of the solute in this area. Thus combined model 3 can be only suitable for the situation in which the samples are aged at a temperature lower than t_{mp} after being quenched from solution treatment temperature. Good predictions of the size and the inter-particle spacing of $MgZn_2$ grain boundary precipitate in 7150 aluminium alloy as a function of ageing time for ageing temperature 160^{o}C or 180^{o}C after being water

quenched from solution treatment temperature are given by combined model 3. Combined model 3 predicts that the widths of precipitate-free zones decrease with ageing time. This trend agrees with the experimental results.

6.2.2 *The component of precipitation nucleation*

The component of precipitation nucleation plays an important role in determining the collector plate area which directly affects the growth rate of the precipitates. In the combined analysis, the mean collector plate size is defined as the inverse of the number of the equilibrium precipitate nuclei per unit grain boundary area. The mean collector plate area strongly depends on the nucleation conditions such as the temperature at which the nucleation takes place, the grain boundary structure and the solute concentration at the grain boundary.

In modelling, we consider that the quench is so fast that no nucleation happens during quenching and nucleation takes place at the ageing temperature. This assumption is proved to be acceptable by the fact that no precipitate is observed by TEM for the sample in the as-quenched condition.

The mean size of collector plates is rather sensitive to ψ, which is a parameter depending on the grain boundary structure. ψ can be calculated from Equation (3.2.5) but this is very difficult because of the shortage of data on the precipitate/matrix interface energy and the grain boundary energy. In this work, ψ is obtained from the experimental measurement for one heat-treatment condition and then used for other heat-treatment conditions.

The solute concentration at the grain boundary is determined by the segregation. The limitations of the segregation model used will strongly affect the value of this concentration.

There is a statistical distribution of the collector plates. The distribution probability density function of the collector plates is assumed to be in the form of a normal probability density function in terms of the collector plate size. For this normal probability density function, the mean is the mean size of the collector plates, the standard deviation is one third of the difference between the mean size and the mean diffusion area at the grain boundary during the incubation period of the grain boundary precipitate nucleation. Such a mean diffusion area is determined by the grain boundary diffusion coefficient and the nucleation time at the nucleation temperature.

In modelling, the nucleation time is taken as the incubation time according to Russell's theory. Only coherent precipitates were involved in Russell's work. The solute transfer is volume diffusion controlling in the nucleation kinetics of Russell's treatment. Such a treatment works very well for carbide precipitation and nucleation in steels but not for $MgZn_2$ precipitation in 7150 aluminium alloy. An abnormally high nucleation time is predicted. This kind of precipitate is semicoherent, which means that solute transfer across the nucleus surface from the matrix is difficult compared with that for coherent precipitates. As a modification, grain boundary or interface diffusion control of the nucleation kinetics is adopted in the modelling. The results from the modified equation of the incubation time are more acceptable.

By using the normal probability density function of the collector plate size to describe the statistical distribution of the collector plates, the models can predict the variation of the mean collector plate size with time, caused by coalescence, during the growth of the precipitates in ageing treatment.

6.2.3 *The growth component of the precipitates*

In the precipitate growth component of the combined models, Faulkner & Carolan's precipitate growth model for constant square collector plate growth control is adopted. Faulkner & Carolan's precipitate growth model for variable circular collector plate growth control is not adopted because an abnormally fast precipitate growth prediction for $MgZn_2$ precipitation in 7150 aluminium alloy would be given by such model. This is because, for $MgZn_2$ precipitation in 7150 aluminium alloy, the variable circular collector plate size defined by $\pi(2\sqrt{D_b t})^2$ which is determined by the mean boundary diffusion distance, is much larger than the collector plate size defined by either the measured inter-particle spacing or the collector plate area defined by Equation (3.5.22). Unrealistically large collector plate size defined by the mean boundary diffusion distance may explain the abnormally high precipitate growth rate.

The combined models give the predictions of the mean size of the precipitates as a function of ageing time during ageing treatment. In modelling, because of very fast diffusion at the grain boundary, solute atoms arriving at the grain boundary from the regions beyond it by volume diffusion have equal chance to be captured by any one of the precipitate sites. Thus the growth rates of radius of precipitate of all the precipitates at a grain boundary can be considered as the same. Precipitates of different sizes at the same boundary face are caused by coalescence.

When coalescence happens, the number of precipitates at the grain boundary decreases. This provides extra solute supply to every precipitate site left. Such extra solute supply compensates partly the reduction in the number of solute atoms diffusing to the boundary from the areas adjacent to it.

The combined models predict that the changes of the mean size and the mean inter-particle spacing of the grain boundary precipitates arise from the coalescence instead of the coarsening during the heat treatments chosen for this work. This is

because the growth of the precipitates from supersaturated solid solution is not complete for the heat treatment conditions used and the whole process is still growth controlling.

The critical time for the onset of coarsening is taken as the time when there exits no longer supersaturation of solute in the areas adjacent to the grain boundaries and hence no flux of solute to the grain boundary appears; i.e., when the average solute concentration in the region from the grain boundary to a distance δl becomes equal to or less than $x_{\alpha T}^{\alpha\theta}$. δl is the diffusion distance of the solute in the matrix within this time, and $x_{\alpha T}^{\alpha\theta}$ is the solute equilibrium concentration of the nucleated precipitate phase/matrix interface at this temperature.

Further ageing after the critical time leads to precipitate coarsening driven by the interfacial free energy between the precipitate and the matrix - the process known as Ostwald ripening. The physical process by which the microstructure coarsens and releases its excess surface energy is due to the higher solubility of small particles, since these have a larger ratio of surface area to volume. The larger particles thus grow at the expense of the smaller ones. The relationship of the mean radius of the grain boundary precipitate with ageing time during coarsening follows Kirchner's theory[100], which shows that the mean radius of precipitate is proportional to $(\text{time})^{1/4}$.

The experimental results of this work show that the mean size of the grain boundary precipitates is not proportional to $(\text{time})^{1/4}$. Therefore, the process is not coarsening but growth controlling.

6.2.4 *The component of width of PFZs*

In the modelling, only solute depletion in the area adjacent to the grain boundary is taken into account in the consideration of the reason of the formation of precipitate-free zones. The depletion of the solute in this kind of area is caused mainly by non-equilibrium segregation during quenching from high temperature to a lower temperature and by precipitate growth. Because of the limitations of the segregation models, only combined model 3 gives the prediction which has similar trends to that given by experimental measurements which indicates that the width of PFZs decreases with ageing time (see Fig. 5.3.3c). However, the result of the theoretical prediction is not very consistent with the experimental measurements. The results obtained from combined model 3 show that the width of PFZs for ageing at a temperature of $180°C$ is greater than that for ageing at a temperature of $160°C$ while the experimental results do not give too much difference. This is because only the influence of the solute depletion in the area adjacent to the grain boundary on PFZs is taken into account in the modelling. In the real situation, the vacancy also plays an important role in determining the width of PFZs, especially when the sample is subjected to an ageing treatment at a temperature above the solvus temperature of GP zones, which is the case the heat-treatment employed in this work. The higher the ageing temperature is, the higher the vacancy concentration and then the easier the formation of the precipitate nuclei. Owing to the above reasons, there appears little difference between the widths of PFZs for these two temperatures. There is still a lot of work to do before we can have a better understanding of the origin of PFZs.

6.3 *Sensitivity analysis*

Table 5.4.1a-e and Table 5.4.15a-e show the effects of varying a_c, a_I, C_c, C_g, E_b, Q_{bnuc}, Q_c, Q_I, r, T_{mp}, δt, d_2, θ, ψ, T_i on the predictions of the precipitate size, inter-precipitate spacing and width of precipitate-free zones as a function of ageing time

for ageing temperatures of 160 $°C$ and 180$°C$. The sensitivity of the models to these parameters in decreasing order is tabulated as shown in Tables 6.3.1-6.3.5.

Table6.3.1: The results of the sensitivity analysis of combined model 1.

Sensitivity (in decreasing order)	For the prediction of the size of GB precipitate	For the prediction of inter-particle spacing	For the prediction of the width of PFZs
1.	T_{mD}	T_{mD}	-
2.	C_c	C_c	-
3.	Q_I, C_g, ψ, T_i	C_g, T_i	-
4.	E_b, a_I, r	ψ	-
5.	Q_c, a_c	a_I, Q_I	-
6.	δt, θ	E_b, r	-
7.	Q_{bnuc}, d_2	Q_c, a_c	-
8.	-	δt, θ	-
9.	-	Q_{bnuc}, d_2	-

Table6.3.2: The results of the sensitivity analysis of combined model 2.

Sensitivity (in decreasing order)	For the prediction of the size of GB precipitate	For the prediction of inter-particle spacing	For the prediction of the width of PFZs
1.	T_{mD}	T_{mD}	d_2
2.	C_c, d_2	C_c, d_2	θ, T_{mD}, Q_c, a_c
3.	C_g	C_g, Q_c, a_c, ψ,θ, T_i	C_c, C_g, E_b, r
4.	Q_I, T_i	r	ψ, a_I, Q_I, T_i
5.	θ, ψ, a_I, Q_c, a_c	E_b	δt, Q_{bnuc}
6.	E_b, r	a_I, Q_I	-
7.	δt	δt	-
8.	Q_{bnuc}	Q_{bnuc}	-

Table6.3.3: The results of the sensitivity analysis of combined model 3.

Sensitivity (in decreasing order)	For the prediction of the size of GB precipitate	For the prediction of inter-particle spacing	For the prediction of the width of PFZs
1.	T_{mD}	T_{mD}	θ
2.	C_c	C_c	Q_c, C_c
3.	Q_I, C_g, ψ, T_i	C_g, T_i	C_g, T_i
4.	a_I	ψ	a_c
5.	E_b, r, Q_c, a_c	E_b, r, Q_I	E_b, r, T_{mD}, T_i
6.	δt, θ	Q_c, a_I, a_c	ψ,d_2, a_I,Q_I,δt,Q_{bnuc}
7.	Q_{bnuc}, d_2	δt, θ	-
8.	-	Q_{bnuc}, d_2	

Table6.3.4: The results of the sensitivity analysis of combined model 4.

Sensitivity (in decreasing order)	For the prediction of the size of GB precipitate	For the prediction of inter-particle spacing	For the prediction of the width of PFZs
1.	T_{mp}	T_{mp}	-
2.	C_c, Q_c, θ	C_c	-
3.	C_g, ψ, a_c, T_i	C_g	-
4.	E_b	ψ, Q_c, T_i	-
5.	r, Q_I, a_I	E_b, r, a_c, θ	-
6.	δt	Q_I, a_I	-
7.	Q_{bnuc}, d_2	δt	-
8.	-	Q_{bnuc}, d_2	-

Table6.3.5: The results of the sensitivity analysis of combined model 5.

Sensitivity (in decreasing order)	For the prediction of the size of GB precipitate	For the prediction of inter-particle spacing	For the prediction of the width of PFZs
1.	T_{mp}	T_{mp}	θ, Q_c, C_c, a_c
2.	C_c	C_c	C_g
3.	Q_I, C_g, ψ, T_i	C_g, ψ, T_i	E_b, r, T_{mp}
4.	a_I	E_b, r, Q_I	ψ,d_2, a_I,Q_I,δt,Q_{bnuc}
5.	E_b, r, Q_c, a_c	Q_c, a_I, a_c	-
6.	δt, θ	δt, θ	-
7.	Q_{bnuc}, d_2	Q_{bnuc}, d_2	-

The combined models are very sensitive to C_c and C_g, the concentrations of non-rate controlling and rate controlling elements participating in the precipitation reaction. In this work, the non-rate controlling element is Zn and the rate controlling element is Mg. The combined models predict that for 7150 aluminium alloy, the higher the concentrations of Zn and Mg are, the smaller and closer separated the $MgZn_2$ grain boundary precipitates and the smaller the width of PFZs (see Tables 5.4.3a-e - 5.4.4a-e). This is because the higher the concentrations of Zn and Mg in the alloy are, the lower the equilibrium solute concentration at the precipitate/matrix interface at a given temperature (see Equation (3.2.7)) and the higher the solute concentration at a grain boundary caused by non-equilibrium segregation during the segregation process (see Equation (2.1.8)). This results in the increase in the driving force for precipitate nucleation at a grain boundary so

that the critical energy required for the formation of the precipitate nuclei decreases and more precipitate nuclei form in a unit grain boundary area. The increase in the number of precipitate nucleus per unit grain boundary area decreases the inter-precipitate spacing and overall decreases the growth rate of the precipitates.

As a characteristic of the alloy, increasing additions of both zinc and magnesium decreases the overall corrosion resistance and the resistance to stress corrosion cracking[12]. From the prediction given by the combined models, the decrease in the resistance to SCC with the increase in the concentrations of Mg and Zn may be explained by the high density and the small size grain boundary precipitates. This prediction supports the results from other researchers' work[6,11,15-23,27,28,50,51] which demonstrate that stress corrosion cracks form due to the electrochemical dissolution of anodic grain boundary precipitates and then propagate along the GB due to the presence of stress concentrations at GBs. The crack propagation between anodic precipitates at GBs is brittle in nature and thus occurs very quickly. The brittle fracture is caused by the collapse of microvoids created during the plastic deformation. The stress crack propagation along the GB is delayed by the increase in inter-particle spacing at GB that occurs during ageing, which renders the alloys more resistant to stress corrosion attack[6,11,15-23,27,28,50,51]. The decrease in the inter-particle spacing of grain boundary precipitates promotes the propagation speed of SCC along the GBs, which gives rise to the decrease in the resistance to stress corrosion cracking.

The width of PFZ predicted by the combined models is very sensitive to θ, the cooling rate parameter. The slower the materials are cooled from solution treatment temperature, the smaller the θ and the greater the width of PFZ. This result agrees with the experimental measurements reported by other researchers[38-40] whose results indicate that the width of PFZ is related to the vacancy concentration profile in the area adjacent to the grain boundary. However, here the increase in the width

of PFZ with the decrease in quench rate is due to the increase in the widths of both solute concentrated and depleted layers caused by non-equilibrium segregation.

According to combined model 5, the slower the quench rate and the longer the ageing time at an ageing temperature, T, where $T \geq T_{mp}$, the greater are the widths of both the solute concentrated and depleted layers caused by non-equilibrium segregation. This is the situation of the white zones, which are areas adjacent to weld pools in Al-Zn-Mg alloys. Broad magnesium and zinc segregation profile, few precipitates and marked GB migration are found in the white zones[73-76]. In this condition, the segregation of magnesium and zinc makes these zones highly reactive and promotes the localised production and diffusion of hydrogen to these areas. Magnesium hydride formation takes place selectively on the incoherent interfaces of grain boundary precipitates (η phase precipitates formed in rather high temperature range during slow cooling) and facilitates crack nucleation at these sites. Thus these areas become very sensitive to SCC[77-79].

6.4 *Error of experimental measurements*

The measurement of the size of the grain boundary precipitate is taken as the length of the line linking two ends of a precipitate particle along the grain boundary direction; the inter-particle spacing is taken as the length of the line linking the centres of two particles next to each other along the boundary; the width of PFZs is taken as the length of the line crossing the PFZ from one side of the grain boundary perpendicularly to another side. The error of the experimental measurements arises mainly from the calibration of the magnification, drawing lines by hand, the estimations made for distinguishing the overlapped precipitates, identifying precipitates which are the neighbouring particles to each other, and the determination of the edge of the PFZ. The margin of error encountered by either the

calibration of magnification or drawing lines is approximately of the order 15% ~20%. The margin of error encountered by the estimation is of the order 0~33%.

Since a TEM micrograph is a projective image of the observation field of the foil sample in the direction of incident electron beam, the precipitates overlapping on the TEM micrographs is rarely avoided. In order to separate two overlapping particles, an estimation is used to measure the individual precipitate dimensions. For the measurement of the inter-particle spacing, because of the same reason as above an estimation is also used in order to group neighbouring particles. Even though the error encountered by the estimation for the measurement of the size of the precipitate may be minimised by ignoring the overlapping and unclear particles, it is hard to reduce the error encountered by the estimation for the measurement of inter-particle spacing.

For the measurement of the width of PFZs, the accuracy of the measurement is very sensitive to how far the boundary face is tilted from the direction of incident electron beam. This influence becomes less significant if we are only interested in comparing the results of PFZs from different heat-treatments.

6.5 *Future work*

(I). The development of the models

For all the combined models presented above, the utility of them is limited by the limitations of the segregation models used and the understanding of the origin of precipitate-free zone. For segregation, the non-equilibrium segregation models used for combined modelling are based on the idea of critical time and the modelling is done separately for segregation and de-segregation processes. In real situations, both segregation and de-segregation occur simultaneously with one of

them dominant during a heat-treatment. Karlsson[106] has developed a segregation model in which the diffusion of vacancies, impurity atoms and impurity-vacancy complexes is analysed simultaneously during a heat treatment. This model gives the predictions of the concentrations of vacancies, impurity atoms and impurity-vacancy complexes as a function of a heat treatment. Unfortunately, much data needed by this model is assumed, which limits the utility of the model. More work is needed to develop a better non-equilibrium segregation model. For precipitate-free zones, a better model is required in which the influence of the depletion of vacancies and solute atoms, and the nucleation time should be considered since they all are important to the formation of precipitate nuclei.

Apart from developing better segregation and precipitate-free zone models, the combined models need to be further developed for multi-stage ageing treatment. The work of the modelling for two stage ageing treatment has started through the modification of the existing combined models for one stage ageing treatment conditions. The further work will be concerned with the programming and the comparison of the prediction with experimental work.

(II). Application of the combined models

Further work could be directed at establishing a correlation between the microstructural features predicted by the combined model and the properties of the materials. Based on this, the thermal process modelling may be realised. This work needs a good understanding of the mechanisms of the SCC of the materials and mechanical strengthening.

Chapter Seven

Conclusions

1. Two new kinetic models of non-equilibrium segregation for the segregation process have been constructed by using both numerical and analytical approaches. The models are named the numerical-analytical non-equilibrium segregation model and the numerical non-equilibrium segregation model. The details of the numerical-analytical non-equilibrium segregation model are given in **Section 3.1.2.** It is produced by artificially distinguishing the situation during ageing from that during quenching, and predicts the solute concentration profile during the quenching and ageing respectively. This segregation model depicts the segregation kinetics for the heat treatments in which ageing temperatures are lower than T_{mp}, which is the temperature at which most of the segregation concerned is completed. The model predicts that the width of solute concentrated layer depends on the quenching process and it does not change with time during the ageing process.

   The details of the numerical non-equilibrium segregation model are given in **Section 3.1.1.** The model gives the time-dependence widths of both the solute concentrated and depleted layers. As an approximation, in the solute depleted layer, which is the area adjacent to the solute concentrated layer, the concentration is linear with the distance from the interface between solute concentrated and solute depleted layers. The slope of concentration-distance line is time-dependent as well. This segregation model describes the segregation kinetics for the heat treatments in which ageing temperatures are higher than T_{mp}.

2. New methods have been developed to predict the effect of heat treatment on combined grain boundary segregation, precipitation and the width of precipitate-

free zone in high strength aluminium alloys. Five models have been put forward for predicting the size and inter-particle spacing of the grain boundary precipitates and the width of precipitate-free zone as a function of heat treatment. The models are summarised as follows.

(i) Combined model 1 - the model generated by combining precipitate nucleation and growth with the segregation described by Faulkner's segregation model in combined analysis.

(ii) Combined model 2 - the model generated by combining precipitate nucleation and growth with the segregation described by Xu & Song's segregation model in combined analysis.

(iii) Combined model 3 - the model generated by combining precipitate nucleation and growth with the segregation described by newly generated numerical-analytical segregation model in combined analysis.

(iv) Combined model 4 - the model generated by combining precipitate nucleation and growth with the segregation described by the same segregation model as that for combined model 1 but with a different combined analysis approach.

(v) Combined model 5 - the model generated by combining precipitate nucleation and growth with the segregation described by newly generated numerical segregation model in combined analysis.

The combined models listed above were used to predict the size and the inter-particle spacing of $MgZn_2$ grain boundary precipitates, and the widths of precipitate-free zones in 7150 aluminium alloy as a function of heat treatment.

The results of the theoretical prediction were compared with the experimental measurements. The comparison shows that both combined models 3 and 5 make the predictions which are well in line with experimental data. In the situation that the materials are subjected to an ageing treatment at temperatures lower than T_{mp}, combined model 3 is more suitable and it predicts that the width of PFZ decreases with the increase in ageing time and this prediction is in agreement with the experimental results.

3. The combined models predicts that the increase in the grain boundary precipitate size with the increase in ageing time is growth kinetics controlled. This conclusion is proved by the experimental results that the mean radius is not proportional to $(\text{time})^{1/4}$. The higher the ageing temperature is, the faster the growth rate. The growth rate is very sensitive to the mean collector plate area, and the volume diffusion coefficient of the solute in the matrix. In the modelling, Carolan & Faulkner's variable circular collector plate precipitate growth model is not adopted because the collector plate size, calculated by the formula for mean boundary diffusion distance, is too large compared with that experimentally observed.

4. Precipitates with different sizes have been found at the same grain boundary. Such phenomenon is caused by coalescence.

5. The collector plate area before the growth of the precipitates begins depends on the density of the precipitate nuclei, which is strongly dependant on the solute concentration at the grain boundary, nucleation temperature and grain boundary structures. The mean collector plate area is very sensitive to T_{mp}, the concentration of Zn and Mg of the alloy, the precipitate nucleation temperature, and the factor $s(\psi)$. Within the temperature range of interest here, the higher the temperature and/or, the lower the concentrations of Zn and Mg and/or the bigger

the ψ, the fewer the equilibrium precipitate nuclei and the bigger the mean collector plate area. The nucleation kinetics of $MgZn_2$ precipitates at the grain boundaries is boundary diffusion controlled due to the semicoherent nature of the precipitates.

6. There is no coarsening within the time range considered. The mean collector plate area changing with time is caused by the coalescence of the precipitates at the grain boundaries. When coalescence happens, the number of precipitates on the grain boundary decreases. The distribution of the precipitate becomes more scattered. Thus the mean collector plate area, or, the inter-particle spacing increases.

7. The width of the precipitate free zone is very sensitive to the quenching rate, the diffusion coefficient of the impurity-vacancy complexes and the ageing temperature. The combined model 3 predicts that, when the materials are subjected to an ageing treatment at temperatures lower than T_{mp}, the width of PFZ decreases with the increase in ageing time and this prediction is in agreement with the experimental results.

8. In the situation where both segregation and precipitation take place, the SCC susceptibility is mainly controlled by the inter-particle spacing of the grain boundary precipitates. The decrease in the inter-particle spacing of grain boundary precipitates promotes the propagation speed of SCC along the GBs, and this induces the decrease in the resistance to stress corrosion cracking[6,11,15-23,27,28,50,51].

9. The slower the quench rate and/or the longer the ageing time at an ageing temperature, T, where $T \geq T_{mp}$, the greater are the widths of both solute concentrated and depleted layers caused by non-equilibrium segregation and the

bigger but the fewer incoherent precipitates (η phase). The white zones of welds of Al-Zn-Mg alloy satisfy the above condition. Under such condition, the segregation of magnesium and zinc makes these zones highly reactive and promotes the localised production and diffusion of hydrogen into these areas. Magnesium hydride formation takes place selectively on the incoherent interfaces of grain boundary precipitates and facilitates crack nucleation at these sites. Thus these areas become very sensitive to SCC[77-79].

10. Successful strategies for effectively using the image analysis system in analysing TEM micrographs have been developed.

References

1. Kent, R., Van Horn, *"Aluminium Volume 1, Properties, Physical Metallurgy And Phase Diagrams"* 1967, American Society for Metals.
2. Martin, J.W., *"Precipitation hardening"* 1968, Pergamon Press Ltd.
3. King, F., *"Aluminium And Its Alloys"* 1987, Ellis Horwood Limited Publers, Chichester, England.
4. *Aerospace Engineering* 1991, Sept., 21.
5. Lukasak, D. A. and Hart, R. M. *Adv. Mater. Proc.* 1991, Oct., 46.
6. Pow, E.C.H. *Diss. Abstr. Int.* 1983, 172.
7. Prasad, A., D'Antonio, C. and Mukherjee, K. paper from *Conf. Thermomechanical processing of Aluminium Alloys*, St. Louis, 1978, 195-209.
8. Rajan, K., Wallace, W. and Beddoes, J.C. *J. Mater. Sci.* 1982, Vol. 17, 2817.
9. Danh, N.C., Rajan, K. and Wallace, W. *Met. Trans. A* 1983, Vol. 14A, 1843.
10. Polmear, I. J. *Chapter 3.5.4-3.5.5, "Light Alloys"* 1981, Edward Arnold Ltd, 83.
11. Lorimer, G.W. *Proc. AIME Conf. Precipitation Process in Solids* 1976, 87.
12. *"Aluminium Properties And Physical Metallurgy"* edited by Hatch, J. E. 1984, Chapter 6.
13. Zakharrov, A.M. *Tsvet. Metally* 1961 (1), 124.
14. Sander, T.H. and Starke, E.A. *Met Trans* 1976, Vol. 7A, 1407.
15. Burmistrova, O.K. and Polyanskii, V.M. *Sov. Mater. Sci.* 1983, 19, (5), 418.
16. Asahi, T., Yabusaki, F., Osamura, K. and Murakami, Y. *paper from "Proc. 6th Int. Conf. on Light Metals"* 1975, 64.
17. Murakami, Yotaro, Miyamoto and Mababu *paper from "Metall. Abstr. on Light Metals and Alloya"* 1972, Vol. 7, 16.

18. Watkinson, F.E. and Scully, J.C. *Corros. Sci.* 1972, **12, (12)**, 905.

19. Kent, K.G. *J. Inst. Metals* 1969, **97**, 127.

20. Kent, K.G. *J. Austral. Inst. Metals* 1970, **15(3)**, 171.

21. Unwin, P.N.T. and Nicholson, R.B. *Acta. Metall.* 1969, **17**,1379.

22. Adler, P.N., DeIasi, R. and Gechwind, G. *Metall. Trans.* 1972, **3(12)**, 3191.

23. Gruhl, W. *paper from Int. Congr. on Aluminium Alloys in Aircraft Ind., Turin* 1978, 171-174.

24. Peel, C.J., Clark, D., Poole, P. and Farra, R.A. *Technical Report 78110, Royal Aircraft Establishment* 1978, **Sept.**

25. European Patent Specification (0020505).

26. Kim, Y.S. and Pyum, S. *Br. Corros. J.* 1983, **Vol. 18**, No.2, 71.

27. Jacobs, A.J. *Trans, ASM* 1965, **58**, 579.

28. Jacobs, A.J. *Proc. Conf. Fund. Aspects SCC* 1969, 530.

29. Gruhl, W. and Brungs, D. *Metall* 1969, **23(10)**, 1020.

30. Brungs, D. and Gruhl, W. *ibid* 1970, **24(3)**, 217.

31. Gerberich, W.W. and Wood, W.E. *Metall. Trans.* 1974, **5(6)**, 1295.

32. Polmear, I. J. *Chapter 2.1.3, "Light Alloys", by Edward Arnold Ltd,* 1981, 19.

33. Sperry, P.R. *Met. Trans.* 1970, **1**, 2650.

34. Smith, W.F.and Grant, N.J. *ASM Trans. Quart.* 1969, **62(3)**, 724.

35. Unwin, P.N., Lorimer, G.W.and Nicholson, R.B. *Acta. Met.* 1969, **17(11)**, 1363.

36. Shastry, C.R.and Judd, G. *Met. Trans.* 1971, **2(12)**, 3283.

37. Starke, Edgar, A., Jr, *J. Metals* 1970, **22(1)**, 54.

38. Yannacopoulos, S. *Diss. Abstr. Int.* 1986, **47(4)**.

39. Fujikawa, S., Akutsu, Y. and Hirano, K. *Mater. Sci. Forum* 1987, **13-14**, 505.

40. Chang, S. and Morral, J.E. *Acta. Metall.* 1975, **23(6)**, 685.

41. Ryu, J.S. and Kim, I.S. *Taehan Kumsok Hakheo Chi.* 1981, **19(4)**, 310.

42. Thomas, G. and Nutting, J, *J. Inst. Metals* 1959-60, **88**, 81.

43. Sedrike, A.J., Slattery, P.W. and Pugh, E.N. *Trans, ASM* 1969, **62**, 238.

44. Sedrike, A.J., Slattery, P.W. and Pugh, E.N. *ibid* 1969, **62**, 815.

45. Doig, P. and Edington, J.W. *Corrosion* 1975, **31(10)**, 347.

46. Miyagi, Y. and Hirano, M. *Kobelco Tech. Bull.* 1980, 8.

47. Vrankovic, A. and Jaric, M. *Aluminium* 1981, **57(5)**, 335.

48. "High-strength Aluminium Alloy" JAJ80110745, Japan, 21st, Feb.1979.

49. Miyagi, Y. and Hirano, K., *Kobe Steel Eng. Rep (R&D)* 1978, **28(1)**, 73.

50. Pyun, S.I., Suh, T.S. and Kim, H.P. *Werkst. Korros.* 1987, **38(3)**, 129.

51. De-Ardo, A.J., Jr, & Townsend, R.D. *Metall. Trans.* 1970, **1(9)**, 2573.

52. Speidel, M.O. *Metall. Trans.* 1975, **6A(4)**, 631.

53. Swanson, R.E. *Diss. Abstr. Int.* 1984, **45 (3)**, 174.

54. Richter, J., Hornig, W. and Kaesche, H. *Wekst. Korros.* 1984, **35 (1)**, 23.

55. Richter, J., Hornig, W. and Kaesche, H. *Wekst. Korros.* 1981, **32 (7)**, 289.

56. Montgrain, L. and Swann, P.R. *paper from "Hydrogen in Metals" ASM, Metals Park, Ohio.* 1974, 575.

57. Thompson, A.W. and Bernstain, I.M. in *"Adv. Corros. Sci. Tech."* 1980, **Vol. 7**, 53.

58. Gruhl W. *Z. Metallkunde* 1963, **54(3)**, 86.

59. Gruhl, W. *Metall.* 1965, **19(3)**, 206.

60. Brungs, D. and Gruhl, W. *Wekst. Korros.* 1969, **20 (4)**, 314.

61. Gest, R.J. and Troiano, A.R. *Corrosion* 1974, **30(8)**, 274.

62. Yoshino, K. and McMahon, C.J., Jr., *Metall. Trans.* 1974, **5(2)**, 363.

63. Gibbs, J.W. *Scientific Papers, Vol. (I) (Thermodynamica)* 1906, 219.

64. McLean, D. *"Grain boundaries in Metals"* 1975, Oxford Univ. Press.

65. Hondros, E.D. and Seah, M.P. *Int. Met. Rev.* 1977, **22**, 262.

66. Hondro, E.D. Seah, M.P. and Cahn, R.W., *"Physical Metallurgy"*, North Holland Physics Publisher, 1983, 855.

67. Westbrooke, J.H. *Metall. Rev.* 1964, **9**, 415.

68. Aust, K.T. and Westbrooke, J.H. *Met. Sci.* Jan. 9, 1976.

69. Anthony, T.R. *Acta. Metall.* 1970, **18**, 307.

70. Faulkner, R.G. *J. Mater. Sci.* 1981, **16**, 373.

71. Xu, T. and Song, S. *Acta. Metall.* 1989, **37(9)**, 2499.

72. Faulkner, R.G. *Mater. Sci. & Tech.* 1985, **Vol. 1**, 442.

73. Scamans, G.M., Holroyd, N.J.H. and Tuck, C.D.S. *Corros. Sci.* 1987, **Vol. 27**, No.4, 329.

74. Rahman, G.S., Cordier, H. and Polmear, I. *Z. Metall.* 1982, **73**, 589.

75. Cordier, H., Schippers, M. and Polmear, I. *Z. Metall.* 1977, **68**, 280.

76. Kent, K.G. *Met. Rev.* 1970, **147**, 135.

77. Viswanadham, R.K., Sun, T.S. and Green, A.S. *Met. Trans.* 1980, **11A**, 85.

78. Scamans, G.M. and Rehal, A. *J. Mat. Sci.* 1979, **14**, 2459.

79. Tuck, C.D.S. and Scamans, G.M. *Second Int. Cong. on Hydrogen in Metals* 1977, 4A.

80. Tuck, C.D.S. *Third Int. Conf. on the Effect of Hydrogen on the Behavoiour of Materials*, 1980, TMA-AIME, Wyoming, 503.

81. Polmear, I. J. *Chapter 2.4.4, "Light Alloys", by Edward Arnold Ltd,* 1981, 42.

82. Sherc liff, H.R. and Ashby, M.F. *Acta. Met.* 1990, **38**, 1789.

83. Doig, P. and Flewitt, P.E.J. *Metall. Trans. A* 1987, **18A**, 399.

84. Russell, K.C. *"Phase Transformations", Metals Park, OH, ASM,* 1970, 219.

85. Aaronson, H.I. and Lee, J.K. *in "Lectures on the theory of phase transformations", New York, AIMMPE,* 1975, 83.

86. Russell, K.C. *Adv. Collod Interface Sci.* 1980, **13**, 205.

87. Fontaine, D.DE *in "Metall. Treatises", (er. Aaronson et al), Metallurgical Society of AIME,* 1981, 371.

88. Aaronson, H.I. and Russell, K.C. *in "Proc. of Int. Conf. on Solid-Solid Phase Transformations", Warrendale, PA, Metallurgical Society of AIME,* 1983, 371.

89. Lange, W.F., Enomoto, III.M. and Aaronson, H.I. *Int. Mater. Rev.*, 1989, **34(3)**, 125.

90. Russell, K.C. *Acta. Metall.* 1969, **17**, 1123.

91. Johnson, W.C., White, C.L., Marth, P.E., Ruf, P.K., Tuominen, S.M., Wade, K.D., Russell, K.C. and Aaronson, H.I. *Met. Trans. A* 1975, **6A**, 911.

92. Vander Velde, G., Velasco, J.A., Russell, K.C. and Aaronson, H.I. *Metall. Trans.* 1976, **7A**, 1472.

93. Russell, K.C. *Acta. Metall.* 1968, **16**, 761.

94. Zener, C. J. Appl. Phys., 1949, **20**, 950

95. Hillert, M. *Jernkontorets Ann.* 1957, **141**, 757.

96. Horvay, G. and Cahn, J.W. *Acta, Metall.* 1961, **9**, 695.

97. Faulkner, R.G. and Caisley, J. *Metal Sci.* 1977, **11**, 200.

98. Aaron, H.B. and Aaronson, H.I. *Acta. Metall.* 1968, **16**, 789.

99. Carolan, R.A. and Faulkner, R.G. *Acta Metall.* 1988, **36**, 257.

100. Kirchner, H.P.K. *Met. Trans.* 1971, **2**, 2861.

101. Faulkner, R.G. and Jiang, H. *Mater. Sci. & Tech.* 1993, **9**, 665.

102. Monodolfo, L.F. in *"Aluminium Alloys: Structure And Properties", Butterworth*, 1976, 26.

103. Lundy, T.S. and Murdock, J.F. *J. Appl. Phys.* 1962, **33**, 1671.

104. Zakharrov, A.M. *Tsvet. Metally* 1961.

105. Holroyd, N.J.H. *Mater. Sci. Eng. A* 1990, **A123**, 219.

106. Karlsson, L. *Acta Metall.* 1988, **vol. 36**, 13.

Appendix 1: computer programmes for combined model 1

```
c model:        combined model 1
c segregation:  Faulkner's model
c function:     predict radius and inter-particle spacing, width of PFZ
c               as a function of geing time (for one stage ageing)

      dimension te(700000),s1(700000),s2(700000),s(700000),
     3w1(700000),xc(700000),xa2(700000),spp(700000),sspp(700000)
     4,raa(20),sl2(700000),tef(700000),sl1(700000)
      common erfc
      call get(rad)
      call get(roef)
      call get(dt)
      call get(xa)
      call get(cb)
      call get(qa)
      call get(qab)
      call get(ra)
      call get(ao)
      call get(ab)
      call get( av)
      call get( ap)
      call get( qp)
      call get( cooli)
      call get( eb)
      call get (tmp)
      call get (tt)
      call get (tt0)
      aa=4.04e-10
      ea=4.3101e-5*qp
      ef=1.25
      c=-1.365
      gs=5.e-6
      delta=0.05
      gamma=0.3
      omega=9.94e-6
      xt=0.333
      xe=2.
      ti=748.
      tt=1800.
      qb=4200.
      r=0.01
      wh=1.e-10
      xe1=1./xe
      u=2./3.
      v=1./3.
      tm=qb/(2.*(c-alog((xa**xe1)*cb)))
      g=(eb-ef)/(8.6e-5*ti)
      p=(eb-ef)/(8.6e-5*tmp)
      g1=(exp(g-p)*eb)/ef
      cb5=g1*xa
      write(*,5)


      tq=0
      i1=1000.*alog((ti-300.)/(tmp-300))/cooli
```

```
      do 710 i=1,i1
      tqt=(ti-300)*exp(-0.001*i*cooli)+300
      tq=tq+0.001*exp(-ea*(ti-tqt)/(8.6e-5*ti*tqt))
  710 continue

      dv1=ap*exp((-qp)/(2.*ti))

      ag1=xt/(6.02*1.e28*wh)
      co1=cos(rad*3.14159/180.)
      si=sin(rad*3.14159/180.)
      ag=16.*3.14*gamma**3.*(2.-3.*co1+co1**3.)/6.

      do 610 n=1,2
      t0=ttt0+20.*(n-1)
      xa1=((exp(((-qb)/(2.*t0))+c))/cb)**xe
      d11=exp((2.*gamma*omega)/(8.31*t0*ra))
      xa1=xa1*d11
      dgv=0.5*8.31*t0*alog(cb5/xa1)/omega
      dg3=ag/dgv**2.
      sp=sqrt(ag1*(exp(dg3/(1.38*1.e-23*t0))))
      ssp=1./sp**2.
      write(*,19)sp,cb6
   19 format(e10.3,2x,e10.3,2x,e10.3,2x,e10.3)

      a9=u-u*co1
      so=2.*gamma/dgv*si
      f9=3.14*(so)**2./sp**2
      b9=0.5*alog(1./f9)
      fchi=ag*2./(16.*3.14*gamma**3.)/si**3.

      dvb1=ab*exp((-qab)/(2.*t0))
      tn11=(32*1.38*6.02**2*t0*gamma**2)/(si*cb5)
      tn33=(1.e23*aa**2.)*(aa**2./(dvb1*wh))/(omega**2.*dgv**3.)
      tn0=tn11*tn33
      av1=16.*dvb1*tn0
      eta=(av1-sp**2.)**2./9.
  939 wa=roef/2.

      tu=ttt+20.*(n-1)
      dv=ao*exp((-qa)/(2.*tu))
      dvb=ab*exp((-qab)/(2.*tu))
      dp=ap*exp((-qp)/(2.*tu))
      xaa=((exp(((-qb)/(2.*tu))+c))/cb)**xe
      d=exp((2.*gamma*omega)/(8.31*tu*ra))
      xaa=xaa*d
      xb=xt-xaa
      ma=7
      m=1

      do 12 j=1,700000
      if(tu.lt.453)goto 331
      if(m.ge.ma)goto 30
      raa(m)=tt*m
      taget=raa(m)
      go to 333
   30 taget=36000.
      go to 333
  331 if(m.ge.ma)goto 33
```

```
      raa(m)=tt*(1+(m-1)*10.)
      taget=raa(m)
      go to 333
   33 taget=172800.
  333 l=taget/dt
      pfz=0

  202 te(j)=dt*(j)
      tef(j)=tq+te(j)*exp(-ea*(ti-tu)/(8.6e-5*ti*tu))
      sl2(j)=sqrt(2.*dv*te(j))
      sl1(j)=2.*sqrt(dv1*tef(j))
      kds1=sl2(j)*1.e10
      fs=0
      do 404 kd=1,kds1
      kds=kd*1.e-10
      dsl=kds/sl1(j)
      call erfx(dsl)
      erfc=1.-erfc
      ffs=(cb5-xa)*erfc+xa
      fs=fs+ffs
  404 continue
      if(j-1)49,49,18
   49 dw=0
      avm=sp**2.
      go to 28
   18 dw=w1(j-1)
      avm=spp(j-1)**2.
   28 xa2(j)=(fs*avm-dw)/(avm*sl2(j))
      if(xa2(j).ge.xaa)go to 8
      go to 79
    8 xc(j)=xa2(j)-xaa
      if(j-1)80,80,82
   80 s1(j)=xc(j)
      s3=2*sqrt(te(j))
      s4=3.14159**1.5*xb*fchi
      s2(j)=sqrt(dv)
      s5=sp**2.
      s(j)=(s1(j)*s3/s4*s5*s2(j))**v
      w1(j)=(s(j)**3)*3.14*xb*fchi
      sss=(s(j)**2.)*4.
      if (sss.ge.av1)goto 301
      spp(j)=sp
      sspp(j)=ssp
      spo=spp(j)
      so=s(j)
      f9=3.14*so**2./spo**2.
      b9=0.5*alog(1./f9)
      go to 11
  301 ba1=(sp**2.-sss)/(sqrt(2.*eta))
      ba2=(sp**2.-av1)/sqrt(2*eta)
      ba3=3./2.**0.5
      call erfx(ba1)
      bc1=erfc
      call erfx(ba2)
      bc2=erfc
      call erfx(ba3)
      bc3=erfc
      sspp(j)=ssp*(0.5*(bc2-bc1)/bc3)
```

```
      sspp(j)=ssp-sspp(j)**2./ssp
      spp(j)=sqrt(1/sspp(j))
      spo=spp(j)
      so=s(j)
      f9=3.14*so**2./spo**2.
      b9=0.5*alog(1./f9)
      go to 11

   82 s1(j)=xc(j)
      s3=2*(sqrt(te(j))-sqrt(te(j-1)))
      s4=3.14159**1.5*xb*fchi
      s5=spp(j-1)**2.
      s2(j)=sqrt(dv)
      s(j)=(s1(j)*s3/s4*s2(j)*s5+s(j-1)**3.)**v
      w1(j)=(s(j)**3.)*3.14*xb*fchi
      sss=(s(j)**2.*4.)
      if (sss.ge.av1)goto 302
      spp(j)=spp(j-1)
      sspp(j)=sspp(j-1)
      so=s(j)
      spo=spp(j)
      f9=3.14*so**2./spo**2.
      b9=0.5*alog(1./f9)
      go to 11
  302 ba1=(spp(j-1)**2.-sss)/(sqrt(2.*eta))
      ba2=(spp(j-1)-av1)/(sqrt(2.*eta))
      call erfx(ba1)
      bc1=erfc
      call erfx(ba2)
      bc2=erfc
      ba3=sqrt(3./2.**0.5)
      call erfx(ba3)
      bc3=erfc
      sspp(j)=sspp(j-1)*(0.5*(bc2-bc1)/bc3)
      sspp(j)=sspp(j-1)-sspp(j)**2./sspp(j-1)
      spp(j)=sqrt(1/sspp(j))
      spo=spp(j)
      so=s(j)
      f9=3.14*so**2./spo**2.
      b9=0.5*alog(1./f9)
   11 if(te(j)-taget)12,14,14
   14 ss=s(j)*1.e10
      spo1=spp(j)*1.e10
      ti1=-7
      go to 73
   79 s1(j)=9.*wh*dvb*xaa*gamma*(taget-te(j))*omega
      s2(j)=32*8.31*tu*b9*a9
      s(j)=s1(j)/s2(j)+(so)**4.
      s(j)=s(j)**0.25
      if(j-1)303,303,304
  303 spp(j)=sp*(s(j)/so)
      go to 305
  304 spp(j)=spp(j-1)*(s(j)/(so))
  305 ti1=te(j)/3600
      ss=s(j)*1.e10
   77 spo1=spp(j)*1.e10
   73 t1=taget/3600
      tu1=tu-273.
```

```
      write(*,3) tu1,t1,ss,spo1,we,wpfz
      if(m.lt.ma)goto 919
      go to 610
919 m=m+1
 12  continue
610 continue
    1format(i2)
    3format(e10.3,3x,e10.3,3x,e10.3,3x,e10.3,3x,e10.3,3x,e10.3)
    5format(10hage temp c,3x,10hage time h,4x,8hradius A,5x
    1,10hint spac A,3x,10hwid conl A,3x,10hwidt pfz A)
     stop
     end



     subroutine erfx(x111)
     common erfc
     if (x111.ge.9.) go to 21
     if (x111.lt.-10.) go to 22
     if (x111.gt.1.5) go to 4
     if (x111.lt.-1.5) go to 4
     y=x111+((x111**5)/10.)+((x111**9)/216.)+((x111**13.)/9350.)
     z=((x111**3)/3.)+((x111**7)/42.)+((x111**11)/1320.)
    1+((x111**15)/75500.)
     erfc=(y-z)*2./sqrt(3.14159)
     go to 45
  4 erfc=1.-(1./(sqrt(3.14159)*x111*exp(x111**2)))
     go to 45
 21 erfc=1.
     go to 45
 22 erfc=-1.
 45 return
     end

     subroutine get(x)
     read(*,*,iostat=ios)x
     if(ios.eq.0)then
        print *,x
     else
        print '(a)','End of file'
        stop
     endif
     return
     end
```

Appendix 2: computer programmes for combined model 2

```
c model:        combined model 2
c segregation:  Xu & Song's  model
c function:     predict radius and inter-particle spacing, width of PFZ
c               as a function of geing time (for one stage ageing)

      dimension te(700000),s1(700000),s2(700000),s(700000),
     3w1(700000),xc(700000),xa2(700000),spp(700000),sspp(700000)
     4,raa(20),sl1(700000),sl2(700000),tef(700000)
      common erfc
      call get(rad)
      call get(roef)
      call get(dt)
      call get(xa)
      call get(cb)
      call get(qa)
      call get(qab)
      call get(ra)
      call get(ao)
      call get(ab)
      call get( av)
      call get( ap)
      call get( qp)
      call get( cooli)
      call get( eb)
      call get (tmp)
      call get (tt)
      call get (ttt0)
      aa=4.04e-10
      ea=4.3103e-5*qp
      ef=1.25
      c=-1.365
      gs=5.e-6
      delta=0.05
      gamma=0.3
      omega=9.94e-6
      xt=0.333
      xe=2.
      ti=748.
      tt=1800.
      qb=4200.
      r=0.01
      wh=1.e-10
      xe1=1./xe
      u=2./3.
      v=1./3.
      tm=qb/(2.*(c-alog((xa**xe1)*cb)))
      g=(eb-ef)/(8.6e-5*ti)
      p=(eb-ef)/(8.6e-5*tmp)
      g1=(exp(g-p)*eb)/ef
      cb5=g1*xa
      write(*,5)


      tq=0
      i1=1000.*alog((ti-300.)/(tmp-300))/cooli
```

```
      do 710 i=1,i1
      tqt=(ti-300)*exp(-0.001*i*cooli)+300
      tq=tq+0.001*exp(-ea*(ti-tqt)/(8.6e-5*ti*tqt))
  710 continue

      dv1=ap*exp((-qp)/(2.*ti))
      ern=2.*sqrt(dv1*tq)/(g1*roef)
      call erfx(ern)
      refc=1-erfc
      if(refc.le.1.e-39)goto 29
      cb6=cb5-xa*(g1-1)*exp(ern**2.)*refc
      go to 23
   29 cb6=cb5
   23 continue

      ag1=xt/(6.02*1.e28*wh)
      co1=cos(rad*3.14159/180.)
      si=sin(rad*3.14159/180.)
      ag=16.*3.14*gamma**3.*(2.-3.*co1+co1**3.)/6.

      do 610 n=1,2
      t0=ttt0+20.*(n-1)
      xa1=((exp(((-qb)/(2.*t0))+c))/cb)**xe
      d11=exp((2.*gamma*omega)/(8.31*t0*ra))
      xa1=xa1*d11
      dgv=0.5*8.31*t0*alog(cb6/xa1)/omega
      dg3=ag/dgv**2.
      sp=sqrt(ag1*(exp(dg3/(1.38*1.e-23*t0))))
      ssp=1./sp**2.
      write(*,39)sp,cb6
   39 format(e10.3,2x,e10.3,2x,e10.3,2x,e10.3)

      a9=u-u*co1
      so=2.*gamma/dgv*si
      f9=3.14*(so)**2./sp**2
      b9=0.5*alog(1./f9)
      fchi=ag*2./(16.*3.14*gamma**3.)/si**3.

      dvb1=ab*exp((-qab)/(2.*t0))
      tn11=(32*1.38*6.02**2*t0*gamma**2)/(si*cb5)
      tn33=(1.e23*aa**2.)*(aa**2./(dvb1*wh))/(omega**2.*dgv**3.)
      tn0=tn11*tn33
      av1=16.*dvb1*tn0
      eta=(av1-sp**2.)**2./9
  939 wa=roef/2.

      tu=ttt+20.*(n-1)
      dv=ao*exp((-qa)/(2.*tu))
      dvb=ab*exp((-qab)/(2.*tu))
      dp=ap*exp((-qp)/(2.*tu))
      xaa=((exp(((-qb)/(2.*tu))+c))/cb)**xe
      d=exp((2.*gamma*omega)/(8.31*tu*ra))
      xaa=xaa*d
      xb=xt-xaa
      ma=7
      m=1

      do 12 j=1,700000
```

```
      if(tu.lt.453)goto 331
      if(m.ge.ma)goto 30
      raa(m)=tt*m
      taget=raa(m)
      go to 333
 30   taget=36000.
      go to 333
 331  if(m.ge.ma)goto 33
      raa(m)=tt*(1+(m-1)*10.)
      taget=raa(m)
      go to 333
  33  taget=172800.
 333  l=taget/dt

 202  te(j)=dt*(j)
      tef(j)=tq+te(j)*exp(-ea*(ti-tu)/(8.6e-5*ti*tu))
      sl2(j)=sqrt(2.*dv*te(j))
      sl1(j)=2.*sqrt(dv1*tef(j))
      ern1=sl1(j)/(g1*wa*2)
      call erfx(ern1)
      refc=1.-erfc
      if(refc.le.1.e-39)goto 19
      cbb=cb5-xa*(g1-1)*exp(ern1**2.)*refc
      if(sl2(j).gt.wa)goto 17
      ffs=cbb
      fs=ffs*sl2(j)
      go to 41
 17   fs=0
      kds1=(sl2(j)-wa)*1.e10

      do 404 kd=1,kds1
      ernk=kd/sl1(j)+ern1
      call erfx(ernk)
      erfc=1.-erfc
      ffs=xa-xa*(1-1./g1)*exp(2*kd/(g1*2.*wa)+ern1**2.)*erfc
      fs=fs+ffs
 404  continue
      fs=fs+cbb*wa
      go to 41
  19  cbb=cb5
      if(sl2(j).gt.wa)goto 87
      ffs=cbb
      fs=ffs*sl2(j)
      go to 41
  87  ern3=xa*(sl2(j)-wa)

  41  continue
      if(j-1)49,49,18
  49  dw=0
      avm=sp**2.
      go to 28
  18  dw=w1(j-1)
      avm=spp(j-1)**2.
  28  xa2(j)=(fs*avm-dw)/(avm*sl2(j))
      if(xa2(j).ge.xaa)go to 8
      go to 79
   8  xc(j)=xa2(j)-xaa
      if(j-1)80,80,82
```

```
80 s1(j)=xc(j)
   s3=2*sqrt(te(j))
   s4=3.14159**1.5*xb*fchi
   s2(j)=sqrt(dv)
   s5=sp**2.
   s(j)=(s1(j)*s3/s4*s5*s2(j))**v
   w1(j)=(s(j)**3)*3.14*xb*fchi
   sss=(s(j)**2.)*4.
   if (sss.ge.av1)goto 301
   spp(j)=sp
   sspp(j)=ssp
   spo=spp(j)
   so=s(j)
   f9=3.14*so**2./spo**2.
   b9=0.5*alog(1./f9)
   go to 11
301 ba1=(sp**2.-sss)/(sqrt(2.*eta))
   ba2=(sp**2.-av1)/sqrt(2*eta)
   ba3=3./2.**0.5
   call erfx(ba1)
   bc1=erfc
   call erfx(ba2)
   bc2=erfc
   call erfx(ba3)
   bc3=erfc
   sspp(j)=ssp*(0.5*(bc2-bc1)/bc3)
   sspp(j)=ssp-sspp(j)**2./ssp
   spp(j)=sqrt(1/sspp(j))
   spo=spp(j)
   so=s(j)
   f9=3.14*so**2./spo**2.
   b9=0.5*alog(1./f9)
   go to 11

82 s1(j)=xc(j)
   s3=2*(sqrt(te(j))-sqrt(te(j-1)))
   s4=3.14159**1.5*xb*fchi
   s5=spp(j-1)**2.
   s2(j)=sqrt(dv)
   s(j)=(s1(j)*s3/s4*s2(j)*s5+s(j-1)**3.)**v
   w1(j)=(s(j)**3.)*3.14*xb*fchi
   sss=(s(j)**2.*4.)
   if (sss.ge.av1)goto 302
   spp(j)=spp(j-1)
   sspp(j)=sspp(j-1)
   so=s(j)
   spo=spp(j)
   f9=3.14*so**2./spo**2.
   b9=0.5*alog(1./f9)
   go to 11
302 ba1=(spp(j-1)**2.-sss)/(sqrt(2.*eta))
   ba2=(spp(j-1)-av1)/(sqrt(2.*eta))
   call erfx(ba1)
   bc1=erfc
   call erfx(ba2)
   bc2=erfc
   ba3=sqrt(3./2.**0.5)
   call erfx(ba3)
```

```
      bc3=erfc
      sspp(j)=sspp(j-1)*(0.5*(bc2-bc1)/bc3)
      sspp(j)=sspp(j-1)-sspp(j)**2./sspp(j-1)
      spp(j)=sqrt(1/sspp(j))
      spo=spp(j)
      so=s(j)
      f9=3.14*so**2./spo**2.
      b9=0.5*alog(1./f9)
   11 if(te(j)-taget)12,14,14
   14 ss=s(j)*1.e10
      spo1=spp(j)*1.e10
      we=2.*wa*1.e10
      ti1=-7
      kk1=0.5*gs*1.e10
      do 42 k=1,kk1
      ern0=k*1.e-10
      ern4=ern0/sl1(j)+ern1
      call erfx(ern4)
      erfc=1.-erfc
      ffs=xa-xa*(1-1./g1)*exp(ern0/(g1*wa)+ern1**2.)*erfc
      if(ffs.lt.xaa)goto 42
      pfz=ern0*2.
      go to 730
   42 continue
      go to 730
   79 s1(j)=9.*wh*dvb*xaa*gamma*(taget-te(j))*omega
      s2(j)=32*8.31*tu*b9*a9
      s(j)=s1(j)/s2(j)+(so)**4.
      s(j)=s(j)**0.25
      if(j-1)303,303,304
  303 spp(j)=sp*(s(j)/so)
      go to 305
  304 spp(j)=spp(j-1)*(s(j)/(so))
  305 ti1=te(j)/3600
      ss=s(j)*1.e10
   77 spo1=spp(j)*1.e10
  730 t1=taget/3600
      wpfz=(wa*2.+pfz)*1.e10
      tu1=tu-273.
      eta2=(eta)**0.25*1.e10
      write(*,3) tu1,t1,ss,spo1,we,wpfz
      if(m.lt.ma)goto 919
      go to 610
  919 m=m+1
   12 continue
  610 continue
      1 format(i2)
      3 format(e10.3,3x,e10.3,3x,e10.3,3x,e10.3,3x,e10.3,3x,e10.3)
      5 format(10hage temp c,3x,10hage time h,4x,8hradius A,5x
     1,10hint spac A,3x,10hwid con1 A,3x,10hwidt pfz A)
      stop
      end


      subroutine erfx(x111)
      common erfc
      if (x111.ge.9.) go to 21
      if (x111.lt.-10.) go to 22
```

```
      if (x111.gt.1.5) go to 4
      if (x111.lt.-1.5) go to 4
      y=x111+((x111**5)/10.)+((x111**9)/216.)+((x111**13.)/9350.)
      z=((x111**3)/3.)+((x111**7)/42.)+((x111**11)/1320.)
     1+((x111**15)/75500.)
      erfc=(y-z)*2./sqrt(3.14159)
      go to 45
    4 erfc=1.-(1./(sqrt(3.14159)*x111*exp(x111**2)))
      go to 45
   21 erfc=1.
      go to 45
   22 erfc=-1.
   45 return
      end

      subroutine get(x)
      read(*,*,iostat=ios)x
      if(ios.eq.0)then
         print *,x
      else
         print '(a)','End of file'
         stop
      endif
      return
      end
```

Appendix 3: computer programmes for combined model 3

```
c model:        combined model 3
c segregation:  new generated numerical-analytical model
c function:     predict radius and inter-particle spacing, width of PFZ
c               as a function of geing time (for one stage ageing)

      dimension te(700000),s1(700000),s2(700000),s(700000)
     3,w1(700000),xc(700000),xa2(700000),spp(700000),sspp(700000)
     4,raa(20),sl(70000),sl1(70000),sl2(700000),tii(70000)
      common erfc,ffs,cfs,dt,dv1,xa,cb5
      call get(rad)
      call get(roef)
      call get(dt)
      call get(xa)
      call get(cb)
      call get(qa)
      call get(qab)
      call get(ra)
      call get(ao)
      call get(ab)
      call get( av)
      call get( ap)
      call get( qp)
      call get( cooli)
      call get( eb)
      call get (tmp)
      call get (tt)
      call get (ttt0)
      aa=4.04e-10
      ea=4.3103e-5*qp
      ef=1.25
      c=-1.365
      gs=1.e-6
      delta=0.05
      gamma=0.3
      omega=9.94e-6
      xt=0.333
      xe=2.
      ti=748.
      tt=1800.
      qb=4200.
      r=0.01
      wh=1.e-10
      xe1=1./xe
      u=2./3.
      v=1./3.
      tm=qb/(2.*(c-alog((xa**xe1)*cb)))
      g=(eb-ef)/(8.6e-5*ti)
      p=(eb-ef)/(8.6e-5*tmp)
      g1=(exp(g-p)*eb)/ef
      cb5=g1*xa
      write(*,5)

      dv1=ap*exp((-qp)/(2.*ti))
```

```
      i1=100*(ti-tmp)
      do 50 i=1,i1
      if(i-1)511,511,512
  511 wa=0
      wb=0
      wc=0
      tq=0
      ti0=ti
      go to 513
  512 wa=wa
      wb=wb
      tq=tq
      ti0=tii(i-1)
  513 tii(i)=ti-0.01*i
      tqt=alog((ti0-300)/(tii(i)-300))/cooli
      tqtq=tqt*exp(-ea*(ti-tii(i))/(8.6e-5*ti*tii(i)))
      tq=tq+tqtq
      sl(i)=sqrt(dv1*2*tqtq)
      if(sl(i).le.wb)goto 52
      ds=0.5*wb*xa+(sl(i)-wb)*xa
      go to 53
   52 ds=0.5*sl(i)**2.*xa/wb
   53 wa=wa+ds/cb5
      wb=2.*wa*cb5/xa
   50 continue
      w=wb
      ag1=xt/(6.02*1.e28*wh)
      co1=cos(rad*3.14159/180.)
      si=sin(rad*3.14159/180.)
      ag=16.*3.14*gamma**3.*(2.-3.*co1+co1**3.)/6.

      do 610 n=1,2
      t0=ttt0+20.*(n-1)
      xa1=((exp(((-qb)/(2.*t0))+c))/cb)**xe
      d11=exp((2.*gamma*omega)/(8.31*t0*ra))
      xa1=xa1*d11
      dgv=0.5*8.31*t0*alog(cb5/xa1)/omega
      dg3=ag/dgv**2.
      sp=sqrt(ag1*(exp(dg3/(1.38*1.e-23*t0))))
      ssp=1./sp**2.

      a9=u-u*co1
      so=2.*gamma/dgv*si
      f9=3.14*(so)**2./sp**2
      b9=0.5*alog(1./f9)
      fchi=ag*2./(16.*3.14*gamma**3.)/si**3.

      dvb1=ab*exp((-qab)/(2.*t0))
      tn11=(32*1.38*6.02**2*t0*gamma**2)/(si*cb5)
      tn33=(1.e23*aa**2.)*(aa**2./(dvb1*wh))/(omega**2.*dgv**3.)
      tn0=tn11*tn33
      av1=16.*dvb1*tn0
      eta=(av1-sp**2.)**2./9.

      write(*,19)sp,tq
   19 format(e10.3,2x,e10.3,2x,e10.3,2x,e10.3)

      tu=ttt+20.*(n-1)
```

```
      dv=ao*exp((-qa)/(2.*tu))
      dvb=ab*exp((-qab)/(2.*tu))
      dp=ap*exp((-qp)/(2.*tu))
      xaa=((exp(((-qb)/(2.*tu))+c))/cb)**xe
      d=exp((2.*gamma*omega)/(8.31*tu*ra))
      xaa=xaa*d
      xaaf=xaaf*df
      xb=xt-xaa
      ma=7
      m=1

      do 12 j=1,700000
      if(tu.lt.453)goto 331
      if(m.ge.ma)goto 30
      raa(m)=tt*m
      taget=raa(m)
      go to 333
   30 raa(m)=36000
      taget=36000.
      go to 333
  331 if(m.ge.ma)goto 33
      raa(m)=tt*(1+(m-1)*10.)
      taget=raa(m)
      go to 333
   33 raa(m)=172800.
      taget=172800.
  333 l=taget/dt

  202 te(j)=dt*(j)
      sl2(j)=sqrt(2.*dv*te(j))
      sl1(j)=2.*sqrt(dp*te(j))
      if(sl2(j).gt.wa)goto 17
      ffs=cb5
      fs=ffs*sl2(j)
      go to 41
   17 ern0=sl2(j)-wa
      ern2=w/sl1(j)
      ern22=(ern0+w)/sl1(j)
      ern21=(ern0-w)/sl1(j)
      ern20=ern0/sl1(j)
      call erfx(ern20)
      erfc0=erfc
      call erfx(ern22)
      erfc2=erfc
      call erfx(ern21)
      erfc1=erfc
      call erfx(ern2)
      ern3=xa*ern0/2.*(2.-erfc2*(1+ern0/(2.*w))-erfc1*
     2(1-ern0/(2.*w)))+sl1(j)**2.*xa/(2.*w)*(erfc0-0.5
     1*(erfc1+erfc2))
      fs=ern3+cb5*wa
   41 if(j-1)49,49,18
   49 dw=0
      avm=sp**2.
      go to 28
   18 dw=w1(j-1)
      avm=spp(j-1)**2.
   28 xa2(j)=(fs*avm-dw)/(avm*sl2(j))
```

```
      if(xa2(j).ge.xaa)go to 8
      go to 79
    8 xc(j)=xa2(j)-xaa
      if(j-1)80,80,82
   80 s1(j)=xc(j)
      s3=2*sqrt(te(j))
      s4=3.14159**1.5*xb*fchi
      s2(j)=sqrt(dv)
      s5=sp**2.
      s(j)=(s1(j)*s3/s4*s5*s2(j))**v
      w1(j)=(s(j)**3)*3.14*xb*fchi
      sss=(s(j)**2.)*4.
      if (sss.ge.av1)goto 301
      spp(j)=sp
      sspp(j)=ssp
      spo=spp(j)
      so=s(j)
      f9=3.14*so**2./spo**2.
      b9=0.5*alog(1./f9)
      go to 11
  301 ba1=(sp**2.-sss)/(sqrt(2.*eta))
      ba2=(sp**2.-av1)/sqrt(2*eta)
      ba3=3./2.**0.5
      call erfx(ba1)
      bc1=erfc
      call erfx(ba2)
      bc2=erfc
      call erfx(ba3)
      bc3=erfc
      sspp(j)=ssp*(0.5*(bc2-bc1)/bc3)
      sspp(j)=ssp-sspp(j)**2./ssp
      spp(j)=sqrt(3.*sqrt(eta)+sss)
      spp(j)=sqrt(1/sspp(j))
      spo=spp(j)
      so=s(j)
      f9=3.14*so**2./spo**2.
      b9=0.5*alog(1./f9)

      go to 11
   82 s1(j)=xc(j)
      s3=2*(sqrt(te(j))-sqrt(te(j-1)))
      s4=3.14159**1.5*xb*fchi
      s5=spp(j-1)**2.
      s2(j)=sqrt(dv)
      s(j)=(s1(j)*s3/s4*s2(j)*s5+s(j-1)**3.)**v
      w1(j)=(s(j)**3.)*3.14*xb*fchi
      sss=(s(j)**2.*4.)
      if (sss.ge.av1)goto 302
      spp(j)=spp(j-1)
      sspp(j)=sspp(j-1)
      so=s(j)
      spo=spp(j)
      f9=3.14*so**2./spo**2.
      b9=0.5*alog(1./f9)
      go to 11
  302 ba1=(spp(j-1)**2.-sss)/(sqrt(2.*eta))
      ba2=(spp(j-1)-av1)/(sqrt(2.*eta))
      call erfx(ba1)
```

```
      bc1=erfc
      call erfx(ba2)
      bc2=erfc
      ba3=sqrt(3./2.**0.5)
      call erfx(ba3)
      bc3=erfc
      sspp(j)=sspp(j-1)*(0.5*(bc2-bc1)/bc3)
      sspp(j)=sspp(j-1)-sspp(j)**2./sspp(j-1)
      spp(j)=sqrt(3.*sqrt(eta)+sss)
      spp(j)=sqrt(1/sspp(j))
      spo=spp(j)
      so=s(j)
      f9=3.14*so**2./spo**2.
      b9=0.5*alog(1./f9)
   11 if(te(j)-taget)12,14,14
   14 ss=s(j)*1.e10
      spo1=spp(j)*1.e10
      ti1=-7
      kk1=0.5*gs*1.e10
      do 42 k=1,kk1
      ern=k*1.e-10
      ern4=ern/sl1(j)
      ern41=(w-ern)/sl1(j)
      ern42=(w+ern)/sl1(j)
      call erfx(ern4)
      erf0=erfc
      call erfx(ern41)
      erf1=erfc
      call erfx(ern42)
      erf2=erfc
      ffs1=xa*(1.-0.5*(erf1+erf2))
      ffs2=sl1(j)*xa/(sqrt(3.14)*w)*(exp(-ern4**2.)-0.5
     1*(exp(-ern41**2.)+exp(-ern42**2.)))
      ffs3=ern*xa/w*(erf0-0.5*(erf2-erf1))
      ffs=ffs1+ffs2+ffs3
      if(ffs.lt.xaa)goto 42
   73 pfz=ern*2.
      go to 730
   42 continue
      go to 730
   79 s1(j)=9.*wh*dvb*xaa*gamma*(taget-te(j))*omega
      s2(j)=32*8.31*tu*b9*a9
      s(j)=s1(j)/s2(j)+(so)**4.
      s(j)=s(j)**0.25
      if(j-1)303,303,304
  303 spp(j)=sp*(s(j)/so)
      go to 305
  304 spp(j)=spp(j-1)*(s(j)/(so))
  305 ti1=te(j)/3600
      ss=s(j)*1.e10
   77 spo1=spp(j)*1.e10
  730 t1=taget/3600
      wpfz=(wa*2.+pfz)*1.e10
      we=2.*wa*1.e10
      tu1=tu-273.
      write(*,3) tu1,t1,ss,spo1,we,wpfz
      if(m.lt.ma)goto 919
      go to 610
```

```
919 m=m+1
 12 continue
610 continue
    1 format(i2)
    3 format(e10.3,3x,e10.3,3x,e10.3,3x,e10.3,3x,e10.3,3x,e10.3)
    5 format(10hage temp c,3x,10hage time h,4x,8hradius A,5x
     1,10hint spac A,3x,10hwid conl A,3x,10hwidt pfz A)
      stop
      end


      subroutine erfx(x111)
      common erfc,ffs
      if (x111.ge.9.) go to 21
      if (x111.lt.-10.) go to 22
      if (x111.gt.1.5) go to 4
      if (x111.lt.-1.5) go to 4
      y=x111+((x111**5)/10.)+((x111**9)/216.)+((x111**13.)/9350.)
      z=((x111**3)/3.)+((x111**7)/42.)+((x111**11)/1320.)
     1+((x111**15)/75500.)
      erfc=(y-z)*2./sqrt(3.14159)
      go to 45
  4 erfc=1.-(1./(sqrt(3.14159)*x111*exp(x111**2)))
      go to 45
 21 erfc=1.
      go to 45
 22 erfc=-1.
 45 return
      end

      subroutine get(x)
      read(*,*,iostat=ios)x
      if(ios.eq.0)then
         print *,x
      else
         print '(a)','End of file'
         stop
      endif
      return
      end
```

Appendix 4: computer programmes for combined model 4

```
c model:        combined model 4
c segregation:  Faulkner's model (by analytical approach)
c function:     predict radius and inter-particle spacing, width of PFZ
c               as a function of geing time (for one stage ageing)

      dimension te(700000),s1(700000),s2(700000),s(700000),
     3spp(700000),sspp(700000),raa(20),tef(700000)
     5,sl1(700000),sl2(700000)
      character*32 ititle
      common erfc
      call get(rad)
      call get(roef)
      call get(dt)
      call get(xa)
      call get(cb)
      call get(qa)
      call get(qab)
      call get(ra)
      call get(ao)
      call get(ab)
      call get( av)
      call get( ap)
      call get( qp)
     call get( cooli)
     call get( eb)
      call get (tmp)
      call get (ttt)
      call get (ttt0)
      read(*,67) ititle
  67 format(a)
      aa=4.04e-10
      ea=4.3103e-5*qp
      ef=1.25
      c=-1.365
      gs=1.e-6
      delta=0.05
      gamma=0.3
      omega=9.94e-6
      xt=0.333
      xe=2.
      ti=748.
      tt=1800.
     qb=4200.
     r=0.01
     wh=1.e-10
     xe1=1./xe
     u=2./3.
     v=1./3.
     tm=qb/(2.*(c-alog((xa**xe1)*cb)))
     g=(eb-ef)/(8.6e-5*ti)
     p=(eb-ef)/(8.6e-5*tmp)
     g1=(exp(g-p)*eb)/ef
     cb5=g1*xa
     write(*,5)
```

```
      tq=0
      i1=1000.*alog((ti-300.)/(tmp-300))/cooli
      do 710 i=1,i1
      tqt=(ti-300)*exp(-0.001*i*cooli)+300
      tq=tq+0.001*exp(-ea*(ti-tqt)/(8.6e-5*ti*tqt))
710 continue

      dv1=ap*exp((-qp)/(2.*ti))

      ag1=xt/(6.02*1.e28*wh)
      co1=cos(rad*3.14159/180.)
      si=sin(rad*3.14159/180.)
      ag=16.*3.14*gamma**3.*(2.-3.*co1+co1**3.)/6.

      do 610 n=1,2
      t0=ttt0+20.*(n-1)
      xa1=((exp(((-qb)/(2.*t0))+c))/cb)**xe
      d11=exp((2.*gamma*omega)/(8.31*t0*ra))
      xa1=xa1*d11
      dgv=0.5*8.31*t0*alog(cb5/xa1)/omega
      dg3=ag/dgv**2.
      sp=sqrt(ag1*(exp(dg3/(1.38*1.e-23*t0))))
      ssp=1./sp**2.
      write(*,19)sp,cb6
19    format(e10.3,2x,e10.3,2x,e10.3,2x,e10.3)

      a9=u-u*co1
      so=2.*gamma/dgv*si
      f9=3.14*(so)**2./sp**2
      b9=0.5*alog(1./f9)
      fchi=ag*2./(16.*3.14*gamma**3.)/si**3.

      dvb1=ab*exp((-qab)/(2.*t0))
      tn11=(32*1.38*6.02**2*t0*gamma**2)/(si*cb5)
      tn33=(1.e23*aa**2.)*(aa**2./(dvb1*wh))/(omega**2.*dgv**3.)
      tn0=tn11*tn33
      av1=16.*dvb1*tn0
      eta=(av1-sp**2.)**2./9.
939   wa=roef/2.

      tu=ttt+20.*(n-1)
      dv0=ap*exp((-qp)/(2.*tu))
      dv=ao*exp((-qa)/(2.*tu))
      dvb=ab*exp((-qab)/(2.*tu))
      dp=ap*exp((-qp)/(2.*tu))
      xaa=((exp(((-qb)/(2.*tu))+c))/cb)**xe
      d=exp((2.*gamma*omega)/(8.31*tu*ra))
      xaa=xaa*d
      xb=xt-xaa
      ma=7
      m=1

      do 12 j=1,700000

      if(tu.lt.453)goto 331
      if(m.ge.ma)goto 30
      raa(m)=tt*m
```

```
      go to 202
 30   raa(m)=36000.
      go to 202
 331  if(m.ge.ma)goto 33
      raa(m)=tt*(1+(m-1)*10.)
      go to 202
 33   raa(m)=172800.

 202  te(j)=dt*(j)
      tef(j)=tq+te(j)*exp(-ea*(ti-tu)/(8.6e-5*ti*tu))
      s4=3.14159**1.5*xb*fchi
      s3=exp(-ea*(ti-tu)/(8.6*1.e-5*ti*tu))
      s6=(cb5-xa)/s4
      s7=(xa-xaa)/s4
      if(j-1)49,49,18
 49   s5=sp**2.
      sl1(j)=2.*sqrt(te(j)*dv)
      sl2(j)=2.*(sqrt(tef(j)*dv1)-sqrt(tq*dv1))
      go to 28
 18   s5=spp(j-1)**2.
      sl1(j)=2.*(sqrt(te(j)*dv)-sqrt(te(j-1)*dv))
      sl2(j)=2.*(sqrt(tef(j)*dv1)-sqrt(tef(j-1)*dv1))
 28   if(j-1)80,80,82
 80   s1(j)=s5*sl1(j)*s7
      s2(j)=s5*sl2(j)*s6
      s(j)=(s1(j)+s2(j))**v
      sss=(s(j)**2.)*4.
      if (sss.ge.av1)goto 301
      spp(j)=sp
      sspp(j)=ssp
      go to 11

 301  ba1=(sp**2.-sss)/(sqrt(2.*eta))
      ba2=(sp**2.-av1)/sqrt(2*eta)
      ba3=3./2.**0.5
      call erfx(ba1)
      bc1=erfc
      call erfx(ba2)
      bc2=erfc
      call erfx(ba3)
      bc3=erfc
      sspp(j)=ssp*(0.5*(bc2-bc1)/bc3)
      sspp(j)=ssp-sspp(j)**2./ssp
      spp(j)=sqrt(1/sspp(j))
      go to 11

 82   s1(j)=s5*sl1(j)*s7
      s2(j)=s5*sl2(j)*s6
      s(j)=(s1(j)+s2(j)+s(j-1)**3.)**v
      sss=(s(j)**2.*4.)
      if (sss.ge.av1)goto 302
      spp(j)=spp(j-1)
      sspp(j)=sspp(j-1)
      go to 11
 302  ba1=(spp(j-1)**2.-sss)/(sqrt(2.*eta))
      ba2=(spp(j-1)-av1)/(sqrt(2.*eta))
      call erfx(ba1)
      bc1=erfc
```

```
call erfx(ba2)
bc2=erfc
ba3=sqrt(3./2.**0.5)
call erfx(ba3)
bc3=erfc
sspp(j)=sspp(j-1)*(0.5*(bc2-bc1)/bc3)
sspp(j)=sspp(j-1)-sspp(j)**2./sspp(j-1)
   spp(j)=sqrt(1/sspp(j))
11 if(te(j)-raa(m))12,14,14
14 ss=s(j)*1.e10
   spo1=spp(j)*1.e10
   ti1=-7

73 t1=raa(m)/3600
   tu1=tu-273.
   write(*,3) tu1,t1,ss,spo1,s1(j),s2(j)
   if(m.lt.ma)goto 919
   go to 610
919 m=m+1
 12 continue
610 continue
 1 format(i2)
 3 format(e10.3,3x,e10.3,3x,e10.3,3x,e10.3,3x,e10.3,3x,e10.3)
 5 format(10hage temp c,3x,10hage time h,4x,8hradius A,5x
  1,10hint spac A,3x,10hwid conl A,3x,10hwidt pfz A)
  stop
  end


  subroutine erfx(x111)
  common erfc
  if (x111.ge.9.) go to 21
  if (x111.lt.-10.) go to 22
  if (x111.gt.1.5) go to 4
  if (x111.lt.-1.5) go to 4
    y=x111+((x111**5)/10.)+((x111**9)/216.)+((x111**13.)/9350.)
    z=((x111**3)/3.)+((x111**7)/42.)+((x111**11)/1320.)
   1+((x111**15)/75500.)
    erfc=(y-z)*2./sqrt(3.14159)
    go to 45
  4 erfc=1.-(1./(sqrt(3.14159)*x111*exp(x111**2)))
    go to 45
 21 erfc=1.
    go to 45
 22 erfc=-1.
 45 return
    end


subroutine get(x)
read(*,*,iostat=ios)x
if(ios.eq.0)then
   print *,x
else
   print '(a)','End of file'
   stop
endif
return
```

end

Appendix 5: computer programmes for combined model 5

```
c model:        combined model 5
c segregation:  new generated numerical model
c function:     predict radius and inter-particle spacing, width of PFZ
c               as a function of geing time (for one stage ageing)

      dimension te(700000),s1(700000),s2(700000),s(700000),ww(700000)
     3,w1(700000),xc(700000),xa2(700000),spp(700000),sspp(700000)
     4,raa(20),sl(70000),w0(700000),w(700000)
     6,dss(700000),wl(700000),sl2(700000),tii(70000)
      common erfc,ffs,cfs,dt,dv1,xa,cb5
      call get(rad)
      call get(roef)
      call get(dt)
      call get(xa)
      call get(cb)
      call get(qa)
      call get(qab)
      call get(ra)
      call get(ao)
      call get(ab)
      call get( av)
      call get( ap)
      call get( qp)
      call get( cooli)
      call get( eb)
      call get (tmp)
      call get (ttt)
      call get (ttt0)
      aa=4.04e-10
      ea=4.3103e-5*qp
      ef=1.25
      c=-1.365
      gs=1.e-6
      delta=0.05
      gamma=0.3
      omega=9.94e-6
      xt=0.333
      xe=2.
      ti=748.
      tt=1800.
      qb=4200.
      r=0.01
      wh=1.e-10
      xe1=1./xe
      u=2./3.
      v=1./3.
      tm=qb/(2.*(c-alog((xa**xe1)*cb)))
      g=(eb-ef)/(8.6e-5*ti)
      p=(eb-ef)/(8.6e-5*tmp)
      g1=(exp(g-p)*eb)/ef
      cb5=g1*xa
      write(*,5)

      dv1=ap*exp((-qp)/(2.*ti))
```

```
      i1=100*(ti-tmp)
      do 50 i=1,i1
      if(i-1)511,511,512
  511 wa=0
      wb=0
      wc=0
      tq=0
      ti0=ti
      go to 513
  512 wa=wa
      wb=wb
      tq=tq
      ti0=tii(i-1)
  513 tii(i)=ti-0.01*i
      tqt=alog((ti0-300)/(tii(i)-300))/cooli
      tqtq=tqt*exp(-ea*(ti-tii(i))/(8.6e-5*ti*tii(i)))
      tq=tq+tqtq
      sl(i)=sqrt(dv1*2*tqtq)
      if(sl(i).le.wb)goto 52
      ds=0.5*wb*xa+(sl(i)-wb)*xa
      go to 53
   52 ds=0.5*sl(i)**2.*xa/wb
   53 wa=wa+ds/cb5
      wb=2.*wa*cb5/xa
   50 continue

      ag1=xt/(6.02*1.e28*wh)
      co1=cos(rad*3.14159/180.)
      si=sin(rad*3.14159/180.)
      ag=16.*3.14*gamma**3.*(2.-3.*co1+co1**3.)/6.

      do 60 n=1,2
      t0=ttt0+20.*(n-1)
      xa1=((exp(((-qb)/(2.*t0))+c))/cb)**xe
      d11=exp((2.*gamma*omega)/(8.31*t0*ra))
      xa1=xa1*d11
      dgv=0.5*8.31*t0*alog(cb5/xa1)/omega
      dg3=ag/dgv**2.
      sp=sqrt(ag1*(exp(dg3/(1.38*1.e-23*t0))))
      ssp=1./sp**2.
      write(*,61)sp,cb6
   61 format(e10.3,2x,e10.3,2x,e10.3,2x,e10.3)

      a9=u-u*co1
      so=2.*gamma/dgv*si
      f9=3.14*(so)**2./sp**2
      b9=0.5*alog(1./f9)
      fchi=ag*2./(16.*3.14*gamma**3.)/si**3.

      dvb1=ab*exp((-qab)/(2.*t0))
      tn11=(32*1.38*6.02**2*t0*gamma**2)/(si*cb5)
      tn33=(1.e23*aa**2.)*(aa**2./(dvb1*wh))/(omega**2.*dgv**3.)
      tn0=tn11*tn33
      av1=16.*dvb1*tn0
      eta=(av1-sp**2.)**2./9.

      tu=ttt+20.*(n-1)
```

```
      dv=ao*exp((-qa)/(2.*tu))
      dvb=ab*exp((-qab)/(2.*tu))
      dp=ap*exp((-qp)/(2.*tu))
      xaa=((exp(((-qb)/(2.*tu))+c))/cb)**xe
      d=exp((2.*gamma*omega)/(8.31*tu*ra))
      xaa=xaa*d
      xb=xt-xaa
      ma=7
      m=1


      do 12 j=1,700000
      if(tu.lt.453)goto 71
      if(m.ge.ma)goto 72
      raa(m)=tt*m
      taget=raa(m)
      go to 74
   72 raa(m)=36000
      taget=36000.
      go to 74
   71 if(m.ge.ma)goto 75
      raa(m)=tt*(1+(m-1)*10.)
      taget=raa(m)
      go to 74
   75 raa(m)=172800
      taget=172800.
   74 l=taget/dt

  202 te(j)=dt*(j)
      tef=dt*exp(-ea*(ti-tu)/(8.6e-5*ti*tu))
      sl1=sqrt(2.*tef*dv1)
      sl2(j)=sqrt(2.*te(j)*dv)
      if(j-1)49,49,18
   49 sppp=sp
      w0(j)=wa
      w(j)=wb
      wl(j)=0
      go to 28
   18 sppp=spp(j-1)
      w0(j)=w0(j-1)
      w(j)=w(j-1)
      wl(j)=w1(j-1)

   28 if(sl1.le.w(j))goto 21
      dss(j)=0.5*w(j)*xa+(sl1-w(j))*xa
      go to 22
   21 dss(j)=0.5*sl1**2.*xa/w(j)
   22 w0(j)=w0(j)+dss(j)/cb5
      w(j)=2.*w0(j)*cb5/xa
      ww(j)=w0(j)+w(j)

      if(sl2(j).le.w0(j))goto 30
      if(sl2(j).le.ww(j))goto 31
      xa2(j)=w0(j)*cb5+0.5*xa*w(j)+(sl2(j)-ww(j))*xa
      go to 32
   30 xa2(j)=sl2(j)*cb5
      go to 32
   31 xa2(j)=w0(j)*cb5+0.5*(sl2(j)-w0(j))**2.*xa/w(j)
```

```
32  xa2(j)=(xa2(j)*sppp**2.-w1(j))/(sppp**2.*sl2(j))

    if(xa2(j).ge.xaa)go to 8
    go to 79
 8  xc(j)=xa2(j)-xaa
    if(j-1)80,80,82
80  s1(j)=xc(j)
    s3=2*sqrt(te(j))
    s4=3.14159**1.5*xb*fchi
    s2(j)=sqrt(dv)
    s5=sp**2.
    s(j)=(s1(j)*s3/s4*s5*s2(j))**v
    w1(j)=(s(j)**3)*3.14*xb*fchi
    sss=(s(j)**2.)*4.
    if (sss.ge.av1)goto 301
    spp(j)=sp
    sspp(j)=ssp
    spo=spp(j)
    so=s(j)
    f9=3.14*so**2./spo**2.
    b9=0.5*alog(1./f9)
    go to 11
301 ba1=(sp**2.-sss)/(sqrt(2.*eta))
    ba2=(sp**2.-av1)/sqrt(2*eta)
    ba3=3./2.**0.5
    call erfx(ba1)
    bc1=erfc
    call erfx(ba2)
    bc2=erfc
    call erfx(ba3)
    bc3=erfc
    sspp(j)=ssp*(0.5*(bc2-bc1)/bc3)
    sspp(j)=ssp-sspp(j)**2./ssp
    spp(j)=sqrt(1/sspp(j))
    spo=spp(j)
    so=s(j)
    f9=3.14*so**2./spo**2.
    b9=0.5*alog(1./f9)
    go to 11

82  s1(j)=xc(j)
    s3=2*(sqrt(te(j))-sqrt(te(j-1)))
    s4=3.14159**1.5*xb*fchi
    s5=spp(j-1)**2.
    s2(j)=sqrt(dv)
    s(j)=(s1(j)*s3/s4*s2(j)*s5+s(j-1)**3.)**v
    w1(j)=(s(j)**3.)*3.14*xb*fchi
    sss=(s(j)**2.*4.)
    if (sss.ge.av1)goto 302
    spp(j)=spp(j-1)
    sspp(j)=sspp(j-1)
    so=s(j)
    spo=spp(j)
    f9=3.14*so**2./spo**2.
    b9=0.5*alog(1./f9)
    go to 11
302 ba1=(spp(j-1)**2.-sss)/(sqrt(2.*eta))
    ba2=(spp(j-1)-av1)/(sqrt(2.*eta))
```

```
      call erfx(ba1)
      bc1=erfc
      call erfx(ba2)
      bc2=erfc
      ba3=sqrt(3./2.**0.5)
      call erfx(ba3)
      bc3=erfc
      sspp(j)=sspp(j-1)*(0.5*(bc2-bc1)/bc3)
      sspp(j)=sspp(j-1)-sspp(j)**2./sspp(j-1)
      spp(j)=sqrt(1/sspp(j))
      spo=spp(j)
      so=s(j)
      f9=3.14*so**2./spo**2.
      b9=0.5*alog(1./f9)
   11 if(te(j)-raa(m))12,14,14
   14 ss=s(j)*1.e10
      spo1=spp(j)*1.e10
      wc=w0(j)*2.e10
      wd=w(j)*1.e10
      wpfz=(xaa*w(j)/xa+w0(j))*2.e10
      ti1=-7
      go to 730
   79 s1(j)=9.*wh*dvb*xaa*gamma*(taget-te(j))*omega
      s2(j)=32*8.31*tu*b9*a9
      s(j)=s1(j)/s2(j)+(so)**4.
      s(j)=s(j)**0.25
      if(j-1)303,303,304
  303 spp(j)=sp*(s(j)/so)
      go to 305
  304 spp(j)=spp(j-1)*(s(j)/(so))
  305 ti1=te(j)/3600
      ss=s(j)*1.e10
   77 spo1=spp(j)*1.e10
  730 t1=raa(m)/3600
      tu1=tu-273.
      write(*,3) tu1,t1,ss,spo1,wc,wpfz
      if(m.lt.ma)goto 70
      go to 60
   70 m=m+1
   12 continue
   60 continue
    1 format(i2)
    3 format(e10.3,3x,e10.3,3x,e10.3,3x,e10.3,3x,e10.3,3x,e10.3)
    5 format(10hage temp c,3x,10hage time h,4x,8hradius A,5x
     1,10hint spac A,3x,10hwid con1 A,3x,10hwidt pfz A)
      stop
      end
```

```
      subroutine erfx(x111)
      common erfc,ffs
      if (x111.ge.9.) go to 21
      if (x111.lt.-10.) go to 22
      if (x111.gt.1.5) go to 4
      if (x111.lt.-1.5) go to 4
      y=x111+((x111**5)/10.)+((x111**9)/216.)+((x111**13.)/9350.)
      z=((x111**3)/3.)+((x111**7)/42.)+((x111**11)/1320.)
```

```
    1+((x111**15)/75500.)
     erfc=(y-z)*2./sqrt(3.14159)
     go to 45
  4 erfc=1.-(1./(sqrt(3.14159)*x111*exp(x111**2)))
     go to 45
 21 erfc=1.
     go to 45
 22 erfc=-1.
 45 return
     end
```

```
subroutine get(x)
read(*,*,iostat=ios)x
if(ios.eq.0)then
   print *,x
else
   print '(a)','End of file'
   stop
endif
return
end
```